A THEORETICAL STUDY OF RECOMBINATION AT GRAIN BOUNDARIES AND SURFACES IN SOLAR CELLS AND QUANTUM WELL LASERS

by

Martin Stuart Abrahams,

Faculty of Mathematical Studies,

University of Southampton.

Thesis submitted for the degree of

Doctor of Philosophy

University of Southampton, September 1984.

CONTENTS

UNIVERSITY OF SOUTHAMPTON

ABSTRACT

FACULTY OF MATHEMATICAL STUDIES

MATHEMATICS

Doctor of Philosophy

A THEORETICAL STUDY OF RECOMBINATION AT GRAIN BOUNDARIES AND SURFACES IN SOLAR CELLS AND QUANTUM WELL LASERS

by Martin Stuart Abrahams

The Shockley-Read recombination statistics was recently generalised to include the effects of a finite relaxation time of the captured carrier as it settles into the ground energy state of the trap, Auger effects and the so-called extra carriers supplied by the neighbouring material. The combined result of these effects is studied here theoretically at a surface together with consideration of a single trap energy level and a simple trap spectrum. This model of surface trap occupation is utilised in calculations of the potential barriers at grain boundaries in polycrystalline semiconductors and these calculations are compared with some recent experimental results. The recombination rate at a grain boundary, resistivity and capacitance of polycrystalline semiconductors are studied.

Another problem concerning the recombination of electrons and holes is found in quantum well laser diodes. It is suggested that the processes giving rise to radiation in quantum well heterostructures can be described by a no k-selection model for the electronic transition. The reason is contained in the similarity of experimental gain curves and those obtained using the no k-selection model.

For lifetime measurements in solar cells, the minority carrier diffusion equation is solved. Results are given of treatments by Sturm-Liouville transform and Green's function for the excess minority carrier concentration in photovoltage decay and in the steady-state in monocrystalline and polycrystalline semiconductors. The effects of surface recombination and grain boundary recombination on lifetimes in solar cells are examined using this theory.

ACKNOWLEDGEMENTS

I would like to thank Professor P.T.Landsberg for his unfailing direction throughout the period of research which led to this thesis. I am also very grateful to Drs. T.Cumberbatch, T. Sluckin and M. Osiński for their help during the time of the Professor's absences. I would like to thank Mrs. Hazel Paul for her assistance with the typing of this work.

Financial support for the project was provided jointly by the Science and Engineering Research Council and Thorn-EMI Central Research Laboratories through a C.A.S.E. studentship.

CHAPTER 1

A BRIEF SURVEY OF RECOMBINATION IN SOLAR CELLS AND QUANTUM WELL LASERS

A semiconductor solar cell is a device which directly converts energy radiated by the sun into electrical current. The main assets of solar cells are that there are no running costs after the initial production expense and the only waste product is heat. Solar cells have been used extensively in space satellites because they are an inexhaustible supply of energy. In space, the weight of a solar cell array is of prime importance, and for this reason high efficiency designs have been made. However, the cost of making solar cells is so high as to make them unattractive for widescale power generation on earth. A possible way of making solar cells attractive for earth use is to trade-off a little of the efficiency of power generation for much cheaper production costs. One method of doing this is to use polycrystalline silicon or cadmium sulphide to construct all or part of the device. In this work, some of the problems associated with polycrystalline solar cells are studied theoretically.

There is a variety of mechanisms by which incident photons never enter the solar cell. For example, some photons are reflected by the top surface, and the top contact shades a portion of the front of the cell from incident photons. Since antireflective coatings for the front surface and small area top contact are well-known (Hovel, 1975), these effects are not studied here. It is the loss of photogenerated electrons and holes by recombination inside the solar cell which is examined in Part A of this work.

Ideally, when a photon penetrates the solar cell and with energy greater than the semiconductor band-gap, it is absorbed, promoting an

electron into the conduction band. An empty state, known as a hole, is left behind in the valence band. The electron and hole diffuse in opposite directions to be collected at the external contacts to the solar cell and then they generate photocurrent into a load. Before reaching the contact, some of the photogenerated electrons fall back into vacant states in the valence band by processes known collectively as recombination of electrons and holes.

Recombination occurs either by an electron making a direct transition from the conduction band into the valence band or by an electron falling into an empty defect level in the energy gap and from there the electron falls in a second step into the valence band. The first process is known as band-to-band recombination and is unavoidable once the semiconductor material for the device is chosen. The second process is called band-to-trap recombination and may be avoided by reducing the number of defect levels in the energy-gap. A trap is an isolated energy level in the energy-gap brought about by a random impurity or by lattice damage for example.

There are three electronic transitions considered in this work. Either a single electron transition is involved in the recombination process or an Auger electron (Evans and Landsberg, 1963) or Auger hole takes up the energy released in the electron transition by moving deeper into its own energy band. A model of recombination in the bulk of a semiconductor device was presented over thirty years ago (Shockley and Read, 1952) and has been generalized since to include Auger effects (Landsberg, 1982a) and the finite relaxation times of traps immediately after the capture of an electron or hole (Dhariwal, Kothari and Jain, 1981). In Chapter 2, this work is extended to a distribution of trap levels in the energy-gap at a simple surface. The concentration of traps is larger at a surface than in the bulk material because the

discontinuity of the lattice at the surface gives rise to surface traps and because chemical residues tend to collect at the surface causing isolated defect levels.

The steady-state recombination of electrons with holes involving donor or acceptor-like surface states leads to a net charge on the surface. The surface state charge is balanced by an equal and opposite charge in the neighbouring bulk semiconductor. This accumulation of space-charge near the surface causes a potential barrier to form in the region. The potential barrier impedes the transport of electrons and holes over it. The barrier height also affects the carrier (electron and hole) concentrations at the surface and hence alters the surface recombination rate. These effects amongst others are considered in Chapter 3 where a model of the potential barrier and recombination rate at a grain boundary in polycrystalline silicon or in cadmium sulphide is given. This model uses the surface recombination statistics given in Chapter 2 and applies with minor alterations to other surfaces in semiconductor devices.

Unlike a solar cell, in which recombination has to be avoided for high efficiency, recombination involving the stimulated emission of a photon is encouraged in a laser diode. The radiative recombination process in a quantum-well laser diode is also studied here. The object of a laser is to provide a source of light with a narrow range of wavelength. Large electron and hole concentrations are created in the laser diode by passing an electrical current through it. In an active region with narrower band-gap than the surrounding semiconductor, the carrier concentrations are especially large and radiative recombination preferentially takes place. The active layer in a quantum-well laser diode is so narrow that the energy levels in the conduction and valence

bands become a series of two-dimensional sub-bands. The advantage of the quantum well structure lies in the laser possessing fewer longitudinal modes in operation. The theoretical energy and wavevector ($\underset{\sim}{k}$) dependence of radiative recombination in quantum well structures are compared with experimental results (Dutta et al., 1983, Kobayashi et al., 1983) obtained recently. Thereby evidence is presented for no conservation of the electronic wavevector in the radiative recombination process because good agreement is obtained with experiments using this premiss.

In Part B of this work, the effects of recombination at the front and back surfaces and at grain boundaries on the carrier concentrations of a solar cell are treated. In Chapter 5, the electron and hole transport and continuity equations are explained and their steady-state solution with low injection of excess carriers is presented. The low injection condition is the main restriction on the validity of the solutions presented in Chapters 5 to 8, but Hovel (1975) has shown that this condition is appropriate for up to twenty times the illumination intensity of the sun. The surface recombination statistics of Chapter 2 is used to yield a simple boundary condition in low injection conditions at a surface.

Accurate representation of the solar spectrum under different meteorological conditions by mathematical functions is quite difficult. In this work, the carrier transport equations are solved with a general photogeneration rate. One is then able to solve the electron diffusion equation with a new mathematical representation (Hsieh, Hu and Drowley, 1980) of the sun's spectrum and this is done in Chapter 6.

New methods of lifetime measurement in solar cells have been given recently which utilize the transient decay of photovoltage from the steady-state (Sharma and Tewary, 1982) and following a short-pulse of

light. Solutions of the electron diffusion equation for these methods are shown in Chapter 7.

In recent years, there has been much interest in polycrystalline semiconductors for use in low cost solar cells, thin-film resistors and polycrystalline emitter transistors. A theoretical understanding of the ways in which polycrystalline semiconductors differ from single crystal semiconductors is desirable. A step towards this better understanding is made in Chapter 3 where a simple model of the barrier height and recombination rate at a grain boundary is presented. Also, in Chapter 8 the effects of surface recombination velocity at a grain boundary (using the work of Chapter 3) and grain size on the current-voltage relationship of a polycrystalline solar cell are examined.

The conclusions of this study are summarized in Chapter 9 where a few suggestions for future research are made. These future topics involve both theoretical and experimental points of interest. Detailed conclusions and reviews of previous work are presented in the appropriate chapters.

Although the functions and parameters are defined in the text as they are introduced, it may be helpful to have a list of the basic parameters on hand and this is done in Table 1.1. Further parameters are defined from those of Table 1.1 in the text as they are required and so Table 1.1 should not be regarded as a comprehensive list of the parameters used here.

Table 1.1 Notation of the Basic Parameters

D	Diffusion coefficient of electrons.
D(E)	Density of states as a function of energy in the band-gap.
d	Width of the base of the solar cell in Figure 5.1.
E	Energy.
$\underset{\sim}{E}$	Electric field.
E_A, E_{AS}	Energy levels of acceptors in the bulk and at a surface respectively.
E_c	Conduction band edge energy.
E_D, E_{DS}	Energy levels of donors in the bulk and at a surface respectively.
E_v	Valence band edge energy.
e	Modulus of the electronic charge.
F_e	Electron quasi-Fermi level.
F_h	Hole quasi-Fermi level.
F_o	Fermi level of electrons in equilibrium.
$\underset{\sim}{f}$	$e\underset{\sim}{E}/2k_BT$.
f	Probability of occupation of a trap level in the energy gap.
f_c	Fermi-Dirac probability for electrons in the conduction band.
f_v	Fermi-Dirac probability for electrons in the valence band.
G	Electron (band-to-trap) capture coefficient.
g(x)	Photo-generation rate of electrons and holes.
H	Hole (band-to-trap) capture coefficient.
h	Planck's constant (also $\hbar \equiv h/2\pi$) .
J	Current density.
J_o	Dark current of a solar cell.
J_L	Light generated current of a solar cell (sometimes called J_{sc} or short-circuit current).
$\underset{\sim}{k}$	Electron wavevector.
k_B	Boltzmann's constant.

L	Diffusion length in a solar cell $(\sqrt{D\tau})$.
L_z	Width of active layer in a quantum well laser diode.
$\underset{\sim}{L}$	Self-adjoint operator.
m	Effective mass.
m_c	Conduction band effective mass.
m_v^h	Heavy-hole valence band effective mass.
m_v^ℓ	Light-hole valence band effective mass.
m_o	Free electron rest mass.
N_A, N_{AS}	Concentration of acceptors in the bulk or at a surface respectively.
N_c	Effective density of states in the conduction band.
N_D, N_{DS}	Concentration of donors in the bulk or at surface respectively
N_v	Effective density of states in the valence band.
N_o	Flux of incident photons in a solar cell.
N_t	Concentration of traps.
n, n_o, n_e, n_1	Electron concentration (with appropriate suffices to denote equilibrium (0), in excess (e) and when the Fermi level is at a trap level (1)).
p, p_0, p_1	Hole concentration (with suffices as above).
R	Reflectivity of the end mirrors in a laser diode.
r	Radial coordinate.
$r_{stim}(E)$	Rate of stimulated emission from a laser diode.
s, s_o, s_n, s_p, s_{gb}	Surface recombination velocity (with suffices to indicate for equilibrium (o), electrons (n), holes (p) and at a grain boundary (gb)).
T	Temperature.
T_1^s, T_2^s, T_1, T_2, T_3, T_4	Trap single electron and Auger capture coefficients of Figure 2.1.

t	Time.
t_1	Duration of short pulse.
U	Recombination rate.
V	Voltage across solar cell p-n junction.
v_d, v_D, v_R	Drift (d), diffusion (D) and recombination (R) velocities.
w, w_1, w_2	Widths of one side of grain boundary space-charge region.
x	Spatial coordinate.
y	Spatial coordinate.
Z	Canonical partition function.
z	Spatial coordinate.

Greek Alphabet

α	Absorption coefficient.
Γ	Optical confinement factor in a laser diode.
γ	With appropriate suffices, Fermi levels (F) divided by k_BT.
ε	Relative dielectric constant of bulk semiconductor.
ε_o	Permittivity of free space.
η	With appropriate suffices, Energy levels (E) divided by k_BT.
λ	Wavelength.
μ	Effective diffusion length (see Chapter 5).
ν	Frequency.
ρ	Resistivity.
$\rho_c(E)$, $\rho_v(E)$	Density of states in the conduction and valence bands.
σ	Conductivity.
τ	Lifetime in a semiconductor.
υ	Mobility.
$\phi(x)$	Electrostatic potential.
ϕ_B	Potential barrier height.
ψ	Electronic wavefunction.

PART A

RECOMBINATION OF ELECTRONS AND HOLES AT SEMICONDUCTOR SURFACES AND IN QUANTUM WELLS

CHAPTER 2

RECOMBINATION STATISTICS FOR SURFACE TRAPS

2.1 Introduction

The widely occurring recombination via traps in semiconductor devices has rendered the Shockley-Read-Hall recombination statistics of considerable importance. It has been extended in a number of ways in the thirty or so years that have elapsed since it was proposed.

(a) Some effects of Fermi degeneracy have been included (Landsberg, 1957 and Von Roos, 1978). This effect is not treated here.

(b) The possibility of more than two charge states, and of excited states of the traps has been incorporated (Landsberg, 1956; Landsberg, 1960; and Sah and Shockley, 1958). In this work only two charge states and two excited states were considered theoretically.

(c) The effect of Auger transitions has been studied (Evans and Landsberg, 1963).

In recent papers, two new effects have been added to this list:

(d) The effect of finite relaxation times of the traps immediately after capture of an electron or hole (Dhariwal, Kothari and Jain, 1981; Agarwal, Jain and Harsh, 1982). It has been suggested that this leads to an increase of the minority carrier lifetime with injection. The reason is that injection, by saturating the traps, leaves a smaller number of them available to mediate the electron-hole recombination traffic.

(e) The effect of extra carriers entering the semiconductor from neighbouring material or leaving to neighbouring material (Landsberg, 1982a). The result of this effect can also act to either increase or decrease the recombination rate. This effect is of importance in for

example MIS structures and Cu_xS-CdS heterojunction interfaces by adding additional recombination traffic.

Recent reviews of several of the effects have been given by Look (1981), Landsberg (1982b) and Nimtz (1980).

In this work, a single discussion incorporates the effects (c) to (e). Effect (b) could readily be incorporated but it would make the discussion algebraically rather heavy. By dropping effect (a), an essential simplification is gained: one is able to use the normal mass action laws in the formulation of the rate equations and this is done in the theory presented in Section 2.

The effect on the recombination rate of variation in the Fermi level and of variation in the excess carrier density is considered. In each case, we also contrast the case of N_t traps at a single level with the case when these N_t traps are uniformly distributed over a range of levels. The latter case tends to produce the bigger changes.

The work is presented in the language of surface recombination. If the trap concentration N_t has dimension L^{-a}, where $a = 2$ (or 3), it can also be regarded as taken per unit area (or per unit volume). Then the dimension of U, the recombination rate is $L^{-a}T^{-1}$. i.e. it is a recombination rate per unit area (or per unit volume). In this way, the recombination formula is applicable to surfaces: all one needs is to interpret N_t as a trap concentration per unit area (instead of volume). The amendments needed to apply the work to bulk recombination are indicated throughout. The surface recombination language is advantageous because one can use it to treat recombination at grain boundaries in polycrystalline material and this is done in Chapters 3 and 8.

2.2 *General Theory*

A small range of energies $(E_{1g}, E_{1g} + dE_{1g})$ will be considered for the occupied traps in their ground states. This will imply an appropriate, but different, small range of energy for the empty traps in their ground state. Similarly, it will imply other small, and different, ranges of energies for the empty traps in their first excited state and the full traps in their first excited state. It is of course necessary for these three energy ranges to go to zero with dE_{1g}, but they need not be specified in any other way at this stage. The following notation will be adopted:

(i) dn_{tg}, the number of occupied traps per unit area which lie in the energy range $(E_{1g}, E_{1g} + dE_{1g})$ and are in the ground state;

(ii) dp_{tg}, the number of empty traps per unit area which lie in the energy range corresponding to (i) and are in their ground state;

(iii) dn_{te}, the number of occupied traps per unit area which lie in the energy range corresponding to (i) and are in their first excited state;

(iv) dp_{te}, the number of empty traps per unit area which lie in the energy range corresponding to (i) and are in their first excited state.

It is assumed that the capture of an electron by an empty trap in its ground state, Og, leaves it in its first excited state, 1e, and that the electron, e, comes from the conduction band. There can then be a relaxation of the trap into its ground state, 1g, and thermal excitation from the ground state is also possible. These processes can be represented by the reactions

$$Og + e \rightleftharpoons 1e \,, \tag{2.1}$$

$$1e \rightleftharpoons 1g \,. \tag{2.2}$$

Similarly, the capture of a hole, h , by a full trap in its ground state 1g leaves it in its first excited state, 0e , and it is assumed that the hole comes from the valence band. Also, the empty excited trap can relax into its ground state or be thermally excited into its first excited state:

$$1g + h \rightleftharpoons 0e \ , \tag{2.3}$$

$$0e \rightleftharpoons 0g \ . \tag{2.4}$$

In this model, inter-trap transfers and the contributions of higher excited states are regarded as negligible.

The rate of change in the number of occupied traps in the first excited state can be written as:

$$dn_{te} = G\left[ndp_{tg} - n_2 dn_{te}\right] - \left[\frac{1}{t_n} dn_{te} - \frac{1}{t'_n} dn_{tg}\right] \ . \tag{2.5}$$

The first bracket takes account of the reaction given in (2.1), G being the reaction constant for the forward reaction and Gn_2 for the reverse reaction. The second bracket describes the reaction (2.2) where t_n and t'_n are the mean times for the decay of the excited state into the ground state and for the reverse thermal excitation process. The quantity G takes into account the three processes shown in Figure 2.1: (i) The direct capture by a single-electron process with reaction constant T_1^s . (ii) The capture by an Auger process in which a second conduction band electron absorbs the energy released. This has reaction constant, say T_1 , so that the reaction proceeds at a rate $T_1 n^2 dp_{tg}$. This process contributes an additional term $T_1 n$ to G . (iii) The capture by an Auger process in which a valence band hole takes up the energy and moves deeper into the valence band. This reaction contributes an additional term, $T_2 p$ to G , so that:

$$G = T_1^s + T_1 n + T_2 p \quad . \tag{2.6}$$

By similar arguments, and in an analogous notation, the capture rate into the first excited empty state of the trap is

$$\dot{dp}_{te} = H(pdn_{tg} - p_2 dp_{te}) - \left(\frac{1}{t_p} dp_{te} - \frac{1}{t_p'} dp_{tg} \right) \quad . \tag{2.7}$$

Here the hole capture in the forward reaction (2.3) incorporates a single-electron transition (T_2^s) and two Auger processes (Figure 2.1). The first Auger process adds an extra capture rate $T_3 npdn_{tg}$ and the second process adds an additional capture rate $T_4 p^2 dn_{tg}$, thus

$$H \equiv T_2^s + T_3 n + T_4 p \quad . \tag{2.8}$$

Hp_2 is the reaction constant for the reverse process in (2.3). Also t_p and t_p' are the mean lifetimes for the ground state and for the reverse thermal excitation process.

The rate at which the concentration of occupied ground state traps increases is

$$\dot{dn}_{tg} = \frac{1}{t_n} dn_{te} - \frac{1}{t_n'} dn_{tg} - H(pdn_{tg} - p_2 dp_{te}) \quad , \tag{2.9}$$

and one also finds the capture rate into the empty ground state of the traps is

$$\dot{dp}_{tg} = \frac{1}{t_p} dp_{te} - \frac{1}{t_p'} dp_{tg} - G(ndp_{tg} - n_2 dp_{te}) \tag{2.10}$$

by taking the appropriate terms from (2.5) and (2.7).

One now imposes the steady state condition by requiring the four time derivatives to vanish. Any three of the four conditions (2.5, 2.7, 2.9, 2.10) can then be used to deduce the fourth by addition. Therefore, one has only three independent equations for the four

unknowns, namely dp_{te}, dn_{te}, dp_{tg}, dn_{tg} . The fourth condition presumes that the number of traps is fixed

$$d(n_{tg} + n_{te} + p_{tg} + p_{te}) = D(E_{1g})dE_{1g} \ . \qquad (2.11)$$

Here, $D(E_{1g})$ is the total number of traps per unit area whose occupied ground states lie in the energy range $(E_{1g}, E_{1g} + dE_{1g})$. These equations will now be solved.

Taking three of equations (2.5, 2.7, 2.9, 2.10) and equation (2.11), writing these in matrix form one has

$$Ax = y \ ,$$

where,

$$A = \begin{Bmatrix} 1 & 1 & 1 & 1 \\ -Gn_2 - 1/t_n & 1/t'_n & 0 & Gn \\ 1/t_n & -1/t'_n - Hp & Hp_2 & 0 \\ 0 & Hp & -Hp_2 - 1/t'_p & 1/t'_p \end{Bmatrix} \ ,$$

$$x = \begin{Bmatrix} dn_{te} \\ dn_{tg} \\ dp_{te} \\ dp_{tg} \end{Bmatrix} \quad \text{and} \quad y = \begin{Bmatrix} D(E_{1g})dE_{1g} \\ 0 \\ 0 \\ 0 \end{Bmatrix}$$

Since,

$$x = A^{-1}y$$

one can solve these equations by finding the inverse matrix of A. The inverse of A is given by (Lennox and Chadwick, 1970)

$$A^{-1} = \frac{1}{|A|} \text{ adj } A \ ,$$

where the adjoint of A is the transposed matrix of cofactors of A.

A cofactor A_{ij} of the matrix A is the signed minor of the element a_{ij} of A. The minor corresponding to a_{ij} is the determinant of the submatrix constructed by leaving out the ith row and jth column (Lennox and Chadwick, 1970). Thus,

$$\begin{pmatrix} dn_{te} \\ dn_{tg} \\ dp_{te} \\ dp_{tg} \end{pmatrix} = \frac{1}{|A|} \begin{pmatrix} A_{11} & A_{21} & A_{31} & A_{41} \\ A_{12} & A_{22} & A_{32} & A_{42} \\ A_{13} & A_{23} & A_{33} & A_{43} \\ A_{14} & A_{24} & A_{34} & A_{44} \end{pmatrix} \begin{pmatrix} D(E_{1g})dE_{1g} \\ 0 \\ 0 \\ 0 \end{pmatrix} .$$

Because the first term of y is its only non-zero term, one need only find the co-factors $(A_{11}, A_{12}, A_{13}, A_{14})$ and the determinant of A, which is

$$|A| = A_{11} + A_{12} + A_{13} + A_{14} .$$

These co-factors are

$$A_{11} = 1/t'_n(Hp_2/t'_p) + G_n[(1/t'_n+Hp)(1/t_p+Hp_2) - Hp_2Hp] ,$$

$$A_{12} = (Gn_2 + 1/t_n)Hp_2/t'_p + (Hp_2/t_n+1/t_nt_p)Gn ,$$

$$A_{13} = (Gn_2+1/t_n)(Hp+1/t'_n)1/t'_p - 1/t_nt'_nt_p + GHnp/t_n ,$$

and

$$A_{14} = (Gn_2+1/t_n)\{(Hp_2+1/t_p)(Hp+1/t'_n)-Hp_2Hp\} - (Hp_2+1/t_p)1/t_nt'_n .$$

The determinant of A is

$$\begin{aligned} |A| = 1/t_nt_p[GH\{np(t_n+t_p)+bnp_2t_p+an_2pt_n+n_2p_2t_nt_p(1/t'_n+1/t'_p)\} \\ + H(ap+bp_2t_p/t'_p) + G(bn+an_2t_n/t'_n)] \end{aligned}$$

where $a = 1+t_p/t'_p$, and $b = 1 + t_n/t'_n$. It therefore follows that

$$\begin{pmatrix} dn_{te} \\ dn_{tg} \\ dp_{te} \\ dp_{tg} \end{pmatrix} = \frac{D(E_{1g})dE_{1g}}{|A|} \begin{pmatrix} A_{11} \\ A_{12} \\ A_{13} \\ A_{14} \end{pmatrix}$$

and so using the expression for the determinant and the co-factors,

$$dn_{te} = \frac{\{GH(npt_n+np_2t_nt_p/t'_n)+Hp_2t_nt_p/t'_nt'_p+Gnt_n/t'_n\}D(E_{1g})dE_{1g}}{|A|}$$

$$dn_{tg} = \frac{\{GH(n_2p_2t_nt_p/t'_p+np_2t_p)+Hp_2t_p/t'_p+Gn\}D(E_{1g})dE_{1g}}{|A|}$$

$$dp_{te} = \frac{\{GH(npt_p+n_2pt_nt_p/t'_p)+Hpt_p/t'_p+Gn_2t_nt_p/t'_nt'_p\}D(E_{1g})dE_{1g}}{|A|}$$

and

$$dp_{tg} = \frac{\{GH(n_2p_2t_nt_p/t'_n+n_2pt'_n)+Hp+Gn_2t_n/t'_n\}D(E_{1g})dE_{1g}}{|A|} \quad .$$

In the steady-state, the bracketed terms of (2.5), (2.7), (2.9) and (2.10) are all equal to the steady-state recombination rate, dU, of electrons in the conduction band or holes in the valence band. The steady-state recombination rate is by (2.9)

$$dU = \frac{1}{t_n} dn_{te} - \frac{1}{t'_n} dn_{tg} ,$$

that is

$$dU = \frac{GH(np-n_2p_2t_nt_p/t'_nt'_p)D(E_{1g})dE_{1g}}{GH\{np(t_n+t_p)+bnp_2t_p+an_2pt_n+n_2p_2t_nt_p(1/t'_n+1/t'_p)\}+H(ap+bp_2t_p/t'_p)+G(bn+an_2t_n/t'_n)} \qquad (2.12)$$

The statistics of charged centres by the grand canonical ensemble shows the number of electrons in centres with energy state, ℓ, which have captured r-electrons is given by (Landsberg, 1982b)

$$\nu_{\ell,r} = Np(\ell,r) = N\lambda^{r}\exp\left(-E(\ell,r)/k_{B}T\right) \sum_{s=0}^{M} \lambda^{s}Z_{s} \qquad (2.13)$$

where

$$\lambda = \exp(F/k_{B}T)$$

and the partition function is

$$Z_{r} = \sum_{\ell} \exp\left(-E(\ell,r).k_{B}T\right) \qquad (2.15)$$

with F the Fermi level, k_{B}, Boltzmann's constant, T, the temperature and N is the number of centres. In the present case $(\ell,r) = (0 \text{ or } 1)$. Hence the difference between the trap quasi-Fermi level and the equilibrium Fermi level may be expected to be the main parameter for the left hand side of the following equation and this is why it is useful. One has

$$\frac{dp_{tg}}{dn_{tg}} = \frac{GH(n_{2}p_{2}t_{n}t_{p}/t'_{p}+n_{2}pt_{n})+Hp+Gn_{2}t_{n}/t'_{n}}{GH(n_{2}p_{2}t_{n}t_{p}/t'_{p}+np_{2}t_{p})+Hp_{2}t_{p}/t'_{p}+Gn}. \qquad (2.16)$$

From (2.5) using detailed balance in equilibrium

$$n_{2} = \left(n\,\frac{dp_{tg}}{dn_{te}}\right)_{o}$$

and

$$\left(\frac{dn_{te}}{dn_{tg}}\right)_{o} = \frac{t_{n}}{t'_{n}} \quad .$$

Thus,

$$n_2 = n_o \frac{t'_n}{t_n} \left(\frac{dp_{tg}}{dn_{tg}}\right)_o \qquad (2.17)$$

and likewise from (2.7),

$$p_2 = p_o \frac{t'_p}{t_p} \left(\frac{dn_{tg}}{dp_{tg}}\right)_o \quad . \qquad (2.18)$$

Using (2.16), (2.17) and (2.18),

$$\left(\frac{dp_{tg}}{dn_{tg}}\right)\left(\frac{dn_{tg}}{dp_{tg}}\right)_o = \frac{GH\{n_o p_2 t_p + n_2 p_2 t_n t_p / t'_p (p/p_o)\} + Hp_2 t_p / t'_p (p/p_o) + Gn_o}{GH\{np_2 t_p + n_2 p_2 t_n t_p / t'_p\} + Hp_2 t_p / t'_p + Gn} \quad . \qquad (2.19)$$

The steady-occupation of the traps in a given range of energy is determined by this relation relative to the equilibrium occupation [see also (2.28) below].

The four distinct brackets (2.5, 2.7, 2.9, 2.10) introduce six "reaction constants" $(n_2, p_2, t'_n, t'_p, t_n, t_p)$ of which only the last two will be taken as independent, the other four being determined by the four conditions of detailed balance.

Although the argument has been in terms of the quantities introduced at the beginning of the section, i.e. per unit area, the whole treatment stands unchanged for volume recombination. In all cases G and H are of dimension L^3T^{-1}, so that Gn, Hp, Gn_2 and Hp_2 are all of dimension T^{-1}. Thus equations such as (2.9) are dimensionally homogeneous provided only the variables dn_{tg}, dp_{tg}, dn_{te} and dp_{te} are all of the same dimensions: all per unit volume or per unit area. For a surface, $D(E_{1g})dE_{1g}$ is the density of trapping states per unit area in the energy range $(E_{1g}, E_{1g}+dE_{1g})$, in

which case dU is the recombination rate per unit area. However, for volume recombination in the bulk, $D(E_{1g})dE_{1g}$ is the density of states per unit volume and the recombination rate, dU, is per unit volume.

2.3 Analogies with the Shockley-Read-Hall Statistics

The notation of (Landsberg, 1982b) will be used with appropriate suffices, γ for Fermi levels divided by k_BT and η for energies divided by k_BT. The four energy levels required for the theory of Section 2 are r and $r+1$ electron energies, where r is the minimum number of electrons in the system. To represent these energies on an energy band diagram, which is made up of single electron energies, we find three independent energy differences which will be taken to be

$$\eta_t \equiv \eta_{1g} - \eta_{og} , \quad \delta_p \equiv \eta_{oe} - \eta_{og} , \quad \delta_n \equiv \eta_{1e} - \eta_{1g} . \qquad (2.20)$$

This preserves some analogy with the notation of (Dhariwal, Kothari and Jain, 1981). The energy levels E_{1g} of an $r+1$-electron centre and E_{og} of an r-electron centre cannot be shown on a single-electron energy diagram, as is usually employed for semiconductor bands. Also their energy zeros are different. However, the difference E_t between them, although still referred to a general zero, can be shown as is done here in Figure 2.1. For donor-like traps it is appropriate to take the energy zero at the edge of the conduction band and for acceptor-like traps the energy zero is at the edge of the valence band. These are the analogues of the vacuum level for the free atom, and the ionization energies are either E_c-E_t for a donor or E_t-E_v for an acceptor.

Two possible arrangements of the r and r+1 electron energy levels are shown in Figure 2.2(a) for donors and (b) acceptors. Examples of Phosphorous (Martin, 1959) and Boron (Lineberger, 1976) which occur in silicon are given. These translate into the single electron energies of Figure 2.2 (c) and (d), where one remembers to divide the energy levels in a vacuum by the relative dielectric constant squared (see for example Landsberg, 1969). Thus, for phosphorous in Si (where $\varepsilon = 11.9$),

$k_B T = 0.026$ eV , $k_B T\delta_n = 0.010$ eV , $k_B T\delta_p = 0.007$ eV , $E_c - E_t = 0.074$ eV ,

at normal room temperature of 300 K.

From the first bracket of (2.5) using detailed balance in equilibrium

$$n_2 = \left(\frac{ndp_{tg}}{dn_{te}}\right)_o ,$$

expanding the contents of the bracket

$$n_2 = n_o \left(\frac{dp_{tg}}{dn_{tg}} \frac{dn_{tg}}{dn_{te}}\right)_o .$$

Using the statistics of charged centres (Landsberg, 1982b) and equations (2.13) to (2.15),

$$n_2 = n_o \left(e^{\eta_t - \gamma_o} e^{\delta_n}\right)_o .$$

It is useful to define

$$\nu_1 \equiv n_o e^{\eta_t - \gamma_o} \qquad (2.21)$$

to maintain the analogy with n_1 of Shockley-Read-Hall statistics.

Likewise from the first bracket of (2.7),

$$p_2 = p\left(\frac{dn_{tg}}{dp_{tg}}\,\frac{dp_{tg}}{dp_{te}}\right)_o = p_o e^{\gamma_o - \eta_{te}\,\delta_p} \equiv \pi_1 e^{\delta_p} \,. \qquad (2.22)$$

That ν_1 and π_1 are not the same as the familiar n_1 and p_1 may be seen as follows. The general expression for n_1 in this statistics, if the centre can be in two states of charge is obtainable from the canonical partition functions Z_o and Z_1 for empty and occupied centres respectively [Landsberg, 1982b, e.g. (15.13)].

Hence, from equation (2.15)

$$Z_o = e^{\eta_{og}} + e^{\eta_{oe}} \,,$$

$$Z_1 = e^{\eta_{1g}} + e^{\eta_{1e}} \,,$$

and by definition, the Shockley-Read parameter n_1 is

$$n_1 \equiv (Z_o/Z_1)ne^{-\gamma_e} \,,$$

hence, using the above expressions for Z_o and Z_1, in equilibrium

$$n_1 = \left(\frac{1+e^{-\delta_p}}{1+e^{-\delta_n}}\right) \times e^{\eta_t} \times n_o e^{-\gamma_o} \,,$$

so that the new parameter ν_1 (2.21) yields

$$\nu_1 = \left(\frac{1+e^{-\delta_n}}{1+e^{-\delta_p}}\right) n_1 \,. \qquad (2.23)$$

$$p_1 = (Z_1/Z_o)pe^{\gamma_h} \,,$$

hence, using the expressions for Z_o and Z_1, in equilibrium

$$p_1 = \frac{1+e^{-\delta_n}}{1+e^{-\delta_p}} e^{-\eta_t} p_o e^{\gamma_o} ,$$

so that the new parameter π_1 yields

$$\pi_1 = \frac{1+\exp(-\delta_p)}{1+\exp(-\delta_n)} p_1 . \qquad (2.24)$$

One sees that the product $\nu_1\pi_1 = n_1p_1 = n_i^2$, but ν_1 and n_1, π_1 and p_1 may be identified only if $\delta_n = \delta_p$, in which case both

$$\nu_1 = n_1 , \quad \pi_1 = p_1$$

In passing, note that the fraction of traps filled can be calculated from (2.13) and in the steady-state this is

$$\frac{\lambda Z_1}{Z_0+\lambda Z_1} = \frac{1}{1+X}$$

where

$$X = \lambda^{-1}Z_o/Z_1 = \left(\frac{1+e^{-\delta_p}}{1+e^{-\delta_n}}\right) e^{\eta_t-\gamma_t} . \qquad (2.25)$$

Note here the analogous form of (2.25) to the Fermi-Dirac probability of occupation of the trap which is $(1+X)^{-1}$, where

$$X = e^{\eta_t-\gamma_t} .$$

Hence, if $\delta_n = \delta_p$ or if δ_n and δ_p tend to infinity one recovers the Fermi-Dirac form of the occupation probability in equilibrium. Otherwise, the addition of the trap excited states gives rise to an additional factor

$$\frac{1+\exp(-\delta_p)}{1+\exp(-\delta_n)}$$

which has an effect not unlike a shift of the trap level to a new position

$$E_t^* = E_t + k_B T \ln\left(\frac{1+e^{-\delta_p}}{1+e^{-\delta_n}}\right) \quad .$$

In addition, the latter bracketed terms of equations (2.5) and (2.7) give, using detailed balance together with equations (2.20) and (2.13),

$$\left(\frac{dn_{tg}}{dn_{te}}\right)_o = \frac{t'_n}{t_n} = e^{\delta_n} \quad , \tag{2.26}$$

$$\left(\frac{dp_{tg}}{dp_{te}}\right)_o = \frac{t'_p}{t_p} = e^{\delta p} \quad .$$

Hence, the shifted trap level in equilibrium is given by

$$E_t^* = E_t + k_B T \ln(a/b) \quad .$$

Given the energy level system, as for example in Figure 2.2, these relations determine the excitation times t'_n, t'_p in terms of the relaxation times t_n, t_p . Thus, from (2.21) and (2.22)

$$\nu_1 = n_2 \, t_n/t'_n$$

and

$$\pi_1 = p_2 \, t_p/t'_p \quad .$$

Putting these expressions into (2.12),

$$dU = \frac{GH(np-\nu_1\pi_1)D(E_{1g})dE_{1g}}{\{GH[np(t_n+t_p)+a\nu_1 pt'_n+b\pi_1 nt'_p+\nu_1\pi_1(t'_n+t'_p)]+H(ap+b\pi_1)+G(bn+a\nu_1)\}}$$

which can be written as

$$dU = \frac{GH(np-\nu_1\pi_1)D(E_{1g})dE_{1g}}{GH(np-\nu_1\pi_1)(t_n+t_p)+H(ap+b\pi_1)(1+G\nu_1 t_n')+G(bn+a\nu_1)(H\pi_1 t_p'+1)} . \quad (2.27)$$

Also, from (2.19) and (2.13),

$$\left(\frac{dp_{tg}}{dn_{tg}}\right)\left(\frac{dn_{tg}}{dp_{tg}}\right)_o = \exp(\gamma_o-\gamma_t)$$

$$= \frac{GH\{n_o\pi_1 t_p'+\nu_1\pi_1 t_n'(p/p_o)\}+H\pi_1(p/p_0)+Gn_o}{GH(n\pi_1 t_p'+\nu_1\pi_1 t_n')+H\pi_1+Gn} . \quad (2.28)$$

These relations give the steady-state recombination rate per unit area and the energy difference of the equilibrium Fermi level and the steady-state trap quasi-Fermi level. The fraction of traps filled in the non-equilibrium steady-state and whose energy of the occupied ground state lies in the energy range E_{1g} to $E_{1g} + dE_{1g}$ is given by $(1+X)^{-1}$ where

$$X = \frac{dp_{te}+dp_{tg}}{dn_{te}+dn_{tg}} .$$

Using the results for dn_{te}, dn_{tg}, dp_{te}, dp_{tg} given in Section 2, X can be put in the form

$$X = e^{\eta_t-\gamma_o}\frac{a}{b}\left\{\frac{GH[(np-\nu_1\pi_1)(t_p/a+\nu_1\pi_1 t_p'+\nu_1 p t_n']+G\nu_1+Hp}{GH[(np-\nu_1\pi_1)(t_n/b)e^{\eta_t-\gamma_o}+np_o t_p'+\nu_1 p_o t_n']+Gne^{\eta_t-\gamma_o}+Hp_o}\right\}$$

for the steady-state. In equilibrium, the braced term equals unity,

$$X_o = e^{\eta_t-\gamma_o}\frac{a}{b}$$

as before, since $n_o p_o = \nu_1\pi_1 = n_i^2$.

For ordinary bulk recombination per unit volume one can make the replacements

$$dU \to U \ , \quad D(E_{1g})dE_{1g} \to N_t \tag{2.29}$$

where U is a recombination rate per unit volume and N_t is a trap concentration per unit volume. One can regain the structure of the Shockley-Read-Hall recombination rate from (2.27) (Landsberg 1982a, equation (11)):

$$U = \frac{GHN_t(np-n_1p_1)}{G(n+n_1)+H(p+p_1)} \tag{2.30}$$

where $n_1 = n_o e^{\eta_t - \gamma_o}$, $p_1 = p_o e^{\gamma_o - \eta_t}$. It is necessary in addition to (2.29) that the excited states become far removed from their ground states at the temperature considered while the excitation and relaxation times go to zero:

$$\delta_n, \delta_p \to \infty \ , \ \{t_n, t_p, t_n e^{\delta_n} = t_n' \ , \quad t_p e^{\delta_p} = t_p'\} \to 0 \ .$$

The Shockley-Read probability of finding a trap at energy E_t occupied is then given by $(1+X)^{-1}$ where

$$X = \frac{Gn_1+Hp}{Gn+Hp_1} \ ,$$

multiplying X by $e^{\eta_t - \gamma_h}$ in the denominator yields

$$X = e^{\eta_t - \gamma_h} \left(\frac{Gn_1+Hp}{Gn_1 e^{\gamma_e - \gamma_h} + Hp} \right) \tag{2.31}$$

In equilibrium, $(\gamma_e = \gamma_h = \gamma_o)$ X reduces to the Fermi-Dirac probability x , i.e.

$$X = e^{\eta_t - \gamma_o}$$

Thus, in some sense the Fermi-Dirac statistics are a special case where the Shockley-Read statistics for steady-state are applied to equilibrium conditions.

2.4 Extension and Special Cases

(a) The Effect of Extra Carriers

The effect of extra carriers supplied by the neighbouring material on the recombination rate was proposed by Landsberg (1982a), and can be easily incorporated in the preceding theory. This technique may be useful when recombination is modelled at the interface between two dissimilar materials, e.g. the interface between insulator and semiconductor in an MIS structure or at the interface between Cu_xS and CdS layers in a heterojunction solar cell. In both cases, the tunnelling of electrons and holes to the interface through potential barriers is important. The first brackets in (2.5), (2.7), (2.9) and (2.10) are all affected by the extra capture rates and emission rates. Attention will be confined to the first brackets in (2.5) and (2.7). These terms become

$$G[(n+\alpha_n/G)dp_{tg}-(n_2+\beta_n/G)dn_{te}]$$

and

$$H[(p+\alpha_p/H)dn_{tg}-(p_2+\beta_p/H)dp_{te}] \quad .$$

Here increased capture and emission rates of electrons by the traps has been denoted by $\alpha_n dp_{tg}$ and $\beta_n dn_{te}$ respectively. The increased capture rate of holes has been denoted by $\alpha_p dn_{tg}$ and the emission rate by $\beta_p dp_{te}$. Thus, by applying detailed balance to the square bracketed terms one sees that the analysis goes through with the replacements

$$(n,p,n_2,p_2) \rightarrow (n+\alpha_n/G, p+\alpha_p/H, n_2+\beta_n/G, p_2+\beta_p/H)$$

and the contents of the latter set are defined to be

$$(n^*,\ p^*,\ n_2^*,\ p_2^*) \tag{2.32}$$

Also,

$$(\nu_1,\ \pi_1) \rightarrow (\nu_1+\beta_n t_n/Gt_n',\ \pi_1+\beta_p t_p/Ht_p') \equiv (\nu_1^*,\ \pi_1^*)\ . \tag{2.33}$$

Note that the replacement of n and p by n^* and p^* is not needed in the expressions (2.6) and (2.8) for G and H, and that, with this proviso one just finds again (2.12) for the recombination rate and (2.19) for the steady-state occupation of the traps with $n,\ p,\ n_2,\ p_2$ asterisked. From there one goes to (2.27) and (2.28) with $n,\ p,\ n_o,\ p_o,\ \nu_1$ and π_1 asterisked. For the sake of completeness, the resulting equations are

$$dU^* = \frac{GH(n^*p^*-\nu_1^*\pi_1^*)d(E_{1g})dE_{1g}}{GH(n^*p^*-\nu_1^*\pi_1^*)(t_n+t_p)+H(ap^*+b\pi_1^*)(1+G\nu_1^*t_n')+G(b_n^*+a\nu_1^*)(1+H\pi_1^*t_p')}$$

and

$$\left(\frac{dp_{tg}}{dn_{tg}}\right)^*\left(\frac{dn_{tg}}{dp_{tg}}\right)_o^* = \frac{GH\{n_o^*\pi_1^*t_p'+\nu_1^*\pi_1^*t_n'(p^*/p_o^*)\}+H\pi_1^*(p^*/p_o^*)+Gn_o^*}{GH\{n^*\pi_1^*t_p'+\nu_1^*\pi_1^*t_n'\}+H\pi_1^*+G^*n}$$

$$\left(\frac{dp_{tg}}{dn_{tg}}\right)^*\left(\frac{dn_{tg}}{dp_{tg}}\right)_o^* = \exp(\gamma_o^*-\gamma_t^*)$$

Thus, the equilibrium Fermi level and the trap quasi-Fermi level are also affected by the extra carriers. Turning to equation (2.25), in the presence of extra carriers the fraction of traps filled is $(1+x)^{-1}$ where

$$x = \left(\frac{1+e^{-\delta_p}}{1+e^{-\delta_n}}\right) e^{\eta_t-\gamma_t^*}\ .$$

(b) Discussion of the Recombination Rate

The interpretation of the recombination rate equation (2.27) is simplified if one considers equal numbers of excess electron and holes.

$$n_e = n - n_o = p - p_o \ .$$

N_t traps per unit area will be assumed with energy levels $(E_{og}, E_{1g}, E_{oe}, E_{1e})$. Then

$$np - n_i^2 = (n_o + p_o + n_e)n_e \ .$$

One can define the surface recombination in an analogous way to the lifetime in bulk recombination,

$$\frac{1}{s} \equiv \frac{n_e}{U} \ .$$

Hence, using (2.27)

$$s = \frac{GH(n_o+p_o+n_e)N_t}{GH(n_o+p_o+n_e)n_e(t_n+t_p)+H(ap_o+an_e+b\pi_1)(1+G\nu_1 t_n')+G(bn_o+bn_e+a\nu_1)(1+H\pi_1 t_p')}$$

Rearranging this equation,

$$\frac{1}{s} = \frac{(t_n+t_p)}{N_t}n_e + \left(\frac{ap_o+b\pi_1+an_e}{n_o+p_o+n_e}\right)\left(\frac{1}{GN_t} + \frac{\nu_1 t_n'}{N_t}\right) + \left(\frac{bn_o+bn_e+a\nu_1}{n_o+p_o+n_e}\right)\left(\frac{1}{HN_t} + \frac{\nu_1 t_n'}{N_t}\right) \tag{2.34}$$

and it is possible to define

$$\frac{1}{s_n} \equiv \frac{1}{GN_t} + \frac{\nu_1 t_n'}{N_t} \ , \qquad \frac{1}{s_p} \equiv \frac{1}{HN_t} + \frac{\nu_1 t_p'}{N_t} \tag{2.35, 2.36}$$

Thus, s_n is the surface recombination velocity in a strongly p-type material and s_p is the recombination velocity in a strongly n-type material, where in both cases, the number of excess carriers n_e or the time delays t_n and t_p are sufficiently small as to allow the neglect of the first term of (2.34). For thermal equilibrium, $n_e = 0$, .

$$\frac{1}{s_o} = \left(\frac{ap_o+b\pi_1}{n_o+p_o}\right)\frac{1}{s_n} + \left(\frac{bn_o+a\nu_1}{n_o+p_o}\right)\frac{1}{s_p} \quad . \tag{2.37}$$

Note that s_o is a superposition of two extreme recombination velocities for heavy n-type and heavy p-type doping. By noting $p_o = n_i^2/n_o$, and using the forms of G and H given by (2.6) and (2.8),

$$\frac{1}{s_n} = \frac{1}{N_t[T_1^s+T_1n_o+T_2n_i^2/n_o+(T_1+T_2)n_e]} + \frac{\nu_1 t_n'}{N_t} \quad ,$$

$$\frac{1}{s_p} = \frac{1}{N_t[T_2^s+T_3n_o+T_4n_i^2/n_o+(T_3+T_4)n_e]} + \frac{\pi_1 t_p'}{N_t}$$

One can differentiate these expressions for s_n and s_p with respect to the equilibrium Fermi level (γ_o) through n_o. Note that the definitions of ν_1 and π_1, (2.21) and (2.22) show that ν_1 and π_1 are independent of γ_o. Hence, they will be regarded as independent of n_o in the differentiation, although at first sight this appears not to be the case.

$$\frac{ds_n}{dn_o} = N_t\left\{\frac{1}{[T_1^s+T_1n_o+T_2n_i^2/n_o+(T_1+T_2)n_e]} + \frac{V_1t_n'}{N_t}\right\}^{-2}\left|\frac{T_1-T_2n_i^2/n_o^2}{[T_1^s+T_1n_o+T_2n_i^2/n_o+(T_1+T_2)n_e]^2}\right| ,$$

and for an extremum,

$$T_1 - T_2n_1^2/n_0^2 = 0 \quad ,$$

$$n_0 = \sqrt{\frac{T_2}{T_1}}\, n_i \quad .$$

Differentiating again,

$$\frac{d^2 s_n}{dn_o^2} = N_t\left\{\frac{1}{[T_1^s+T_1 n_o+T_2 n_i^2/n_o+(T_1+T_2)n_e]} + \frac{\nu_1 t_n'}{N_t}\right\}^{-2}\left|\frac{2T_2 n_1^2/n_o^3}{[T_1^s+T_1 n_1+T_2 n_i^2/n_o+ T_1+T_2)n_e]}\right|^2$$

$$-2N_t\left\{\frac{1}{[T_1^s+T_1 n_o+T_2 n_i^2/n_o^2+(T_1+T_2)n_e]} + \frac{\nu_1 t_n'}{N_t}\right\}^{-2}\left|\frac{(T_1-T_2 n_i^2/n_o^2)^2}{[T_1^s+T_1 n_o+T_2 n_i^2/n_o^2+(T_1+T_2)n_e]^3}\right|$$

$$+2N_t\left\{\frac{1}{[T_1^s+T_1 n_o+T_2 n_i^2/n_o^2+(T_1+T_2)n_e]} + \frac{\nu_1 t_n'}{N_t}\right\}^{-3}\left|\frac{T_1-T_2 n_i^2/n_o^2}{[T_1^s+T_1 n_o+T_2 n_i^2/n_o^2+(T_1+T_2)n_e]^2}\right|^2$$

At the extremum,

$$T_1 - T_2 n_i^2/n_o^2 = 0$$

and so

$$\frac{d^2 s_n}{dn_o^2} > 0 \ ,$$

indicating that this is a minimum of s_n. One can find a minimum also for s_p, by symmetry of the two expressions for s_n and s_p, this occurs when

$$T_3 - T_4 n_i^2/n_o^2 = 0 \ .$$

Thus, the minimum values for s_n and s_p are

$$(s_n)_{min} = \frac{N_t}{[T_1^s+(T_1+T_2)n_e+2\sqrt{T_1 T_2}\ n_o]^{-1}+\nu_1 t_n'} \ , \qquad (2.38)$$

$$(s_p)_{min} = \frac{}{[T_2^s+(T_3+T_4)n_e+2\sqrt{T_3 T_4}\ n_o]^{-1}+\pi_1 t_p'} \ . \qquad (2.39)$$

The surface recombination velocities s_n and s_p can be shown to be mainly constant across the band gap and almost equal to their mimimum values, unless the electron or hole concentration is very large. When the equilibrium Fermi level is near one of the bands, or for a very large number of excess electrons and holes (about 10^{17} cm^{-3} in Si), the velocities s_n and s_p rise steeply.

For very large excess carrier concentration, n_e, the surface recombination velocity given by (2.34) tends to the approximate form

$$\frac{1}{s} \doteq \frac{n_e(t_n+t_p)}{N_t} + \frac{a}{s_n} + \frac{b}{s_p}$$

Using the approximate forms of s_n (2.35) and s_p (2.36) at large excess carrier concentrations

$$\frac{1}{s} \doteq \frac{n_e(t_n+t_p)}{N_t} + \frac{a}{N_t[T_1^s+T_1 n_e+T_2 n_e]} + \frac{b}{N_t[T_2^s+T_3 n_e+T_4 n_e]} ,$$

and the first term dominates the expression for large enough n_e. This leads to the maximum steady-state recombination rate,

$$(U)_{max} = (n_e s)_{max} = \frac{N_t}{t_n+t_p} . \qquad (2.40)$$

This reflects the inability of the traps to act infinitely rapidly in recombination because of the finite time required for the trap to relax to the appropriate ground state once an electron or hole is captured.

As noted at the end of Section 2.2, the discussion goes through substantially unchanged for bulk (rather than surface) recombination However, because of the different dimensions of the recombination rate in the bulk, n_e/U is a time (rather than a reciprocal of velocity).

Thus $1/s$ is then to be replaced by a recombination lifetime τ .

2.5 A Simple Trap Spectrum

The position on the energy scale of the level E_{1g} determines the positions of the other three levels (E_{og}, E_{oe}, E_{1e}) through the physics of the centre as explained in Section 2.2. In order to integrate over the trap spectrum, E_{1g} will be varied but it will be assumed that δ_n and δ_p of (2.20) remain constant during this variation. This is unlikely to be correct, but for a small range of integration it may be an acceptable approximation. Also, the density of surface states has to be specified. The simplest approach is to put, using (2.20),

$$D(E_{1g})\,\frac{dE_{1g}}{dE_t}\,dE_t = D_1(E_t)dE_t$$

and

$$D_1(E_t)dE_t = \begin{cases} D_s dE_t, & E_\ell < E_t < E_u \ , \\ 0 \ , \quad \text{otherwise} \ . \end{cases} \tag{2.41}$$

This assumption eliminates the need to know precisely how E_{og} varies as E_{1g} is changed, since D_1 is stipulated and it depends on the difference between them. Equation (2.27) can now be integrated to yield the total recombination rate per unit area, U ,

$$U = \int_{E_\ell}^{E_u} \frac{GH(np-\nu_1\pi_1)D_s dE_t}{GH(np-\nu_1\pi_1)(t_n+t_p)+H(ap+b\pi_1)(1+G\nu_1 t_n)+G(bn+a\nu_1)(1+H\pi t_p')}$$

Writing $\eta_t = E_t/k_BT$ and denoting

$$A = GH(np-\nu_1\pi_1)D_s k_B T \ ,$$

$$B = GH\{(t_n+t_p)np+\nu_1\pi_1(t'_n+t'_p)\} + Hap + Gbn \quad ,$$

$$C = \{GHapt'_n+Ga\}N_c e^{-\eta_c} \quad ,$$

$$D = \{GHbnt'_p+Hb\}N_v e^{\eta_v} \quad ,$$

then,

$$U = \int_{\eta_\ell}^{\eta_u} \frac{Ad\eta_t}{B+C\,e^{\eta_t} + De^{-\eta_t}}$$

Multiplying both the numerator and denominator by e^{η_t} and completing the square,

$$U = \int_{\eta_\ell}^{\eta_u} \frac{Ae^{\eta_t}d\eta_t}{C(e^{\eta_t}+B/2C)^2+D-B^2/4C} \quad .$$

Splitting the integral up by partial fractions,

$$U = \int_{\eta_\ell}^{\eta_u} \frac{Ae^{\eta_t}d\eta_t}{\sqrt{B^2-4CD}} \left(\frac{1}{e^{\eta_t}+B/2C-\sqrt{B^2/4C^2-D/C}} - \frac{1}{e^{\eta_t}+B/2C+\sqrt{B^2/4C^2-D/C}} \right) \quad .$$

Performing the two integrals,

$$U = \frac{A}{\sqrt{B^2-4CD}} \left[\ln\left\{ \frac{Ce^{\eta_t}+\frac{1}{2}(B-\sqrt{B^2-4CD}}{Ce^{\eta_t}+\frac{1}{2}(B+\sqrt{B^2-4CD})} \right\} \right]_{\eta_\ell}^{\eta_u}$$

Hence,

$$U = \frac{k_B T D_s (np-\nu_1\pi_1)}{V} \ln\left\{ \frac{[Y_e^{\eta_u-\gamma_o}+\frac{1}{2}(X-V)][Y_e^{\eta_\ell-\gamma_o}+\frac{1}{2}(X+Y)]}{[Y_e^{\eta_u-\gamma_o}+\frac{1}{2}(X+V)][Y_e^{\eta_\ell-\gamma_o}+\frac{1}{2}(X-Y)]} \right\}, \quad (2.42)$$

where

$$V = \sqrt{X^2-4WY}$$

$$W = p_o b(nt'_p+1/G) \ ,$$

$$Y = n_o a(pt'_n+1/H) \ ,$$

and

$$X = np(t_n+t_p) + bn/H + ap/G+\nu_1\pi_1(t'_n+t'_p) \ .$$

As in Section (2.4b), the interpretation of this result is simplified by assuming equal numbers of excess holes and electrons:

$$n_e = n - n_o = p - p_o \ .$$

The steady-state surface recombination in this case is

$$s = \frac{k_B T(n_o+p_o+n_e)D_s}{V'} \ln\left\{\frac{[Y'e^{\eta_u-\gamma_o+\frac{1}{2}(X'-V')}][Y'e^{\eta_\ell-\gamma_o+\frac{1}{2}(X'+V')}]}{[Y'e^{\eta_u-\gamma_o+\frac{1}{2}(X'+V')}][Y'e^{\eta_\ell-\gamma_o+\frac{1}{2}(X'-V')}]}\right\} \quad (2.43)$$

where

$$W' = p_o b\{(n_o+n_e)t'_p + 1/G\} \ ,$$

$$X' = n_e(n_o+p_o+n_e)(t_n+t_p)+b(n_o+n_e)/H+a(p_o+n_e)/G+\nu_1\pi_1(t_n+t_p+t'_n+t'_p) \ ,$$

$$Y' = n_o a\{(p_o+n_e)t'_n + 1/H\} \ ,$$

$$V' = \sqrt{X'^2-4W'Y'} \ ,$$

and

$$G = T_1^s + T_1 n_o + T_2 p_o + (T_1+T_2)n_e \ ,$$

$$H = T_2^s + T_3 n_o + T_4 p_o + (T_3+T_4)n_e \ .$$

In a similar way to (2.37), one can write in thermal equilibrium

$$s_o = \frac{k_B T D_s(n_o+p_o)}{V_o} \ln\left\{\frac{2Y_o e^{\eta_u-\gamma_o+X_o-V_o}}{2Y_o e^{\eta_u-\gamma_o+X_o+V_o}} \frac{2Y_o e^{\eta_\ell-\gamma_o+X_o+V_o}}{2Y_o e^{\eta_\ell-\gamma_o+X_o-V_o}}\right\} \quad (2.44)$$

where V_o, W_o, X_o, Y_o are the equilibrium values of V, W, X and Y. Expanding the bracketed term and dividing both the numerator and denominator by Y_o,

$$s_o = \frac{k_B T D_s (n_o+p_o)}{V_o} \ln\left\{\frac{Y_o e^{\eta_u+\eta_\ell-2\gamma_o} + \frac{1}{2} e^{-\gamma_o}\{(X_o+V_o)e^{\eta_u}+(X_o-V_o)e^{\eta_\ell}\}+W_o}{Y_o e^{\eta_u+\eta_\ell-2\gamma_o} + \frac{1}{2} e^{-\gamma_o}\{(X_o-V_o)e^{\eta_u}+(X_o+V_o)e^{\eta_\ell}\}+W_o}\right\} .$$

Now,

$$V_o^2 = X_o^2-4W_oY_o = (bn_o/H_o)^2 + (ap_o/G_o)^2 + n_o^2p_o^2(t_n+t_p+t'_n+t'_p)^2 + 2abn_op_o/GH +$$
$$(2an_op_o^2)(t_n+t_p+t'_n+t'_p) + (2bn_o^2p_o/H)(t_n+t_p+t'_n+t'_p)$$
$$- 4abn_o^2p_o^2t'_nt'_p - 4abn_o^2p_ot'_p/H_o - 4qbn_op_o^2t'_n/G_o - 4abn_op_o/G_oH_o .$$

Thus,

$$V_o = bn_o/H_o - ap_o/G_o + n_op_o(t_n+t'_n-t'_p-t_p) ,$$

or alternatively

$$V_o = bn_o(p_ot'_n+1/H_o) - ap_o(n_ot'_p+1/G_o) .$$

One finds

$$X_o-V_o = 2(ap_o/G+an_op_ot'_p) = 2W_oa/b ,$$

$$X_o+V_o = 2(bn_o/H+bn_op_ot'_n) = 2Y_ob/a .$$

Hence,

$$s_o = \frac{k_B T D_s (n_o+p_o)}{V_o} \ln\left\{\frac{Y_o e^{\eta_u+\eta_\ell-2\gamma_o} + Y_o e^{\eta_u-\gamma_o} b/a + W_o e^{\eta_\ell-\gamma_o} a/b + W_o}{Y_o e^{\eta_u+\eta_\ell-2\gamma_o} + Y_o e^{\eta_\ell-\gamma_o} b/a + W_o e^{\eta_u-\gamma_o} a/b + W_o}\right\} ,$$

and so

$$s_o = \frac{k_B T D_s (n_o+p_o)}{b/a\ Y_o - a/b W_o} \ln\left\{\frac{(e^{\eta_\ell-\gamma_o}+b/a)(a/b\ W_o+Y_o e^{\eta_u-\gamma_o})}{(e^{\eta_u-\gamma_o}+b/a)(a/b\ W_o+Y_o e^{\eta_\ell-\gamma_o})}\right\}$$

Finally, from the definitions of W_o and Y_o, the equilibrium recombination velocity is

$$s_o = \frac{G_o H_o (n_o+p_o) k_B T D_s (\eta_u-\eta_\ell)}{G_o n_o b(1+H_o p_o t_n')-H_o p_o a(1+G_o n_o t_p')} \ln\left[\left(\frac{ae^{\eta_\ell-\gamma_o}+b}{ae^{\eta_u-\gamma_o}+b}\right)\left\{\frac{(1+H_o p_o t_n')\ Gn_o+H_o p_o(1+G_o n_o t_p')e^{\gamma_o-\eta_u}}{(1+H_o p_o t_n')Gn_o+H_o p_o(1+G_o n_o t_p')e^{\gamma_o-\eta_\ell}}\right\}\right]$$

For large excess carrier concentrations, (2.43) tends to the following expression,

$$s = \frac{k_B T D_s n_e}{V''} \ln\left[\frac{Y''\ e^{\eta_u+\eta_\ell-2\gamma_o} + \frac{1}{2}\ e^{-\gamma_o}\{(X''+V'')e^{\eta_u} + (X''-V'')e^{\eta_\ell}\} + W_o}{Y''\ e^{n_u+\eta_\ell-2\gamma_o} + \frac{1}{2}\ e^{-\gamma_o}\{(X''-V'')e^{\eta_u} + (X''+V'')e^{\eta_\ell}\}+ W_o}\right]$$

where

$$X'' \doteqdot V'' \doteqdot n_e^2(t_n+t_p)$$

$$W'' \doteqdot p_o b n_e\ t_p' \ , \ Y'' \doteqdot n_o a n_e t_n'$$

and using the binomial expansion of V',

$$X'' - V'' \doteqdot X''\left(1-(1-2W''Y''/X''^2+\ldots)\right) \ ,$$

$$X'' - V'' \doteqdot 2W''Y''/X'' \ .$$

One finds

$$X'' - V'' \doteqdot \frac{2n_o p_o (bt_n'at_p')n_e^2}{n_e^2(t_n+t_p)} << X'' + V'' \ ,$$

hence for large excess carrier densities

$$s \sim \frac{k_B T D_s}{n_e(t_n+t_p)} \ln\left[\frac{(X''+V'')e^{\eta_u-\gamma_o}}{(X''+V'')e^{\eta_\ell-\gamma_o}}\right]$$

and therefore U has an upper limit given by

$$(U)_{max} = (n_e s)_{max} \sim \frac{k_B T D_s (\eta_u - \eta_\ell)}{(t_n + t_p)} \quad .$$

Note that $k_B T D_s (\eta_u - \eta_\ell)$ is the total number of traps in the distribution, and the above result is very similar to (2.40) for a single trap level.

2.6 Discussion of the Figures

Some results using the data of Tables 2.1, 2.2 and 2.3 are presented in Figures 2.3, 2.4 and for Si and 2.6 and 2.7 for CdS The curves are terminated at Fermi levels which lie $3k_B T$ from the band edges because the effects of degeneracy have not been included in this work.

The features of curve (a) of Figures 2.3 and 2.6 can be broadly classified into four ranges of the Fermi level, F_o, using the intrinsic Fermi level, F_i, as follows:

(i) $E_v + 3k_B T < F_o < E_t$

In this case $p_o >> \pi_1 >> n_o, \nu_1$ by (2.21) and (2.22) because the Fermi level F_o is well below the trap level situated at mid-gap. From (2.37), $s_o \sim s_n/a$, since p_o is large. The recombination rate is limited by the rate at which electrons can be captured from the conduction band, since these are the minority carriers. Electron capture provides the surface recombination velocity s_n/a. The traps are largely unoccupied and any which become filled are rapidly emptied because of the large hole density in the valence band. The velocities s_n and s_p, given by (2.35) and (2.36) together with (2.6) and (2.8) rise in virtue of Auger effects as the valence band edge E_v is approached. s_n and s_p remain fairly constant in the intermediate region. Thus, s_n is largely determined by the Auger process T_2 (Fig. 2.3) near the valence band.

(ii) $E_t < F_o < F_i$.

In this case

$$\pi_1 >> p_o >> n_o, \nu_1 \quad \text{and} \quad s_o \sim p_o s_n/\pi_1 b \quad \text{from (2.37)..} \qquad (2.45)$$

By (2.25) with (2.22), a fraction

$$\left\{1 + \left[\frac{1+\exp(-\delta_p)}{1+\exp(-\delta_n)}\right] \frac{p_o}{\pi_1}\right\}^{-1}$$

of the traps are filled, which decreases with falling p_o . Also, the recombination velocity falls further with the increase of F_o , as fewer traps are available to capture electrons. One finds a minimum surface recombination velocity , s_o , when the Fermi level, F_o , is near the intrinsic Fermi level, F_i , associated with the change of minority carriers from electrons to holes. By (2.45), the minimum velocity will depend on the trap level, E_t , through π_1 . Thus, a lower trap level leads to a smaller minimum value of s_o .

(iii) $F_i - E_t < F_o - E_t < 2(F_i - E_t)$.

In this case

$$\pi_1 >> n_o >> p_o, \nu_1 \quad \text{and} \quad s_o \sim s_n n_o/\pi_1 b \ . \qquad (2.46)$$

Because the traps are largely full, hole capture has an appreciable contribution to the recombination velocity (s_p/b). However, there are insufficient electrons to recombine with every trapped hole and electron capture provides the larger contribution to the overall recombination velocity given by (2.46).

(iv) $2F_i - E_t < F_o < E_c - 3k_B T$.

Here,

$$n_o >> \pi_1 >> p_o, \nu_1 \quad \text{and} \quad s_o \sim s_p/b \ . \qquad (2.47)$$

This region is the converse of region (i), with the roles of electrons and holes interchanged. The Auger process T_3 (Fig.1) gives the larger term in H (and hence s_p (2.36)) as the Fermi level approaches the conduction band.

The description of curve (b) follows similar lines. In the order of increasing Fermi level, the four regions are

(i) $E_v + 3k_BT < F_o < E_\ell$,

(ii) $E_\ell < F_o < F_i$,

(iii) $F_i < F_o < E_u$,

(iv) $E_u < F_o < E_c - 3k_BT$

so that $n_o << p_o$ in regions (i) and (ii) and $n_o >> p_o$ in regions (iii) and (iv). The surface recombination velocity is effectively a superposition of recombination velocities, s_o , derived from curve (a) for different trap levels. The lower trap levels produce a greater reduction in the minimum recombination velocity through the central regions (ii) and (iii) as explained by (2.45) for curve (a) and as displayed in Figure 2.4. For trap levels in the upper half of the gap, the argument is simply a mirror of the description for a trap level in the lower half of the energy gap. Figure 2.4 shows that the smaller lying trap levels lead to a lower minimum value of s_o . This is because π_1 is larger for lower trap levels and thus $s_n p_o/\pi_1 b$ is smaller. Also, for Fermi levels higher in the gap, the term $s_n n_o/\pi_1 b$ is then smaller. The contribution (smaller) of the majority carriers to the recombination velocity is shown dotted in each case.

A description of similar processes in bulk (volume) recombination was given by Blakemore (1962), where a recombination lifetime was considered and Auger effects were not examined.

Curve (c) of Figure 2.3 can be explained in the same way as curve (a). However, the recombination velocities, s_n and s_p are constants throughout the band gap if Auger transitions are neglected and curve (c) is otherwise identical to curve (a).

The curves of Figure 2.6 for cadmium sulphide tend to fall to a smaller minimum recombination velocity in the middle of the band-gap because of the wide energy gap in CdS. This leads to a much wider variation in n_o and p_o and hence in s_o through (2.37).

Turning to Figures 2.5 and 2.7, curve (a) in each figure shows a increase of s with excess carrier density as a result of increased Auger transitions. The recombination velocity drops again for larger values of n_e. The reason is that large values of n_e tends to saturate the traps thus reducing the number of traps which are available for recombination traffic. If one has a distribution of traps, about the single level envisaged in curve (a), the spread of traps makes saturation more difficult to achieve. Hence the maximum of s in the resulting curve (b) of Figure 2.5 lies higher and also occurs at a higher excess carrier concentration. One would expect an increase in s if the traps relax more easily to their ground states (smaller t_n and t_p) as this makes it again more difficult to saturate them. The algebraic form of the upper limit of (2.40) of the recombination velocity confirms this expectation. A lower Auger effect reduces the maximum in s, and it is removed altogether if the effect is negligible [curves (c) and (d)].

In Figure 2.7, curve (b) is shown the effect of reducing the relaxation time of the traps, the rise of s owing to Auger effects dominates. The smaller value of t_p makes it more difficult to saturate the traps and so the recombination continues to rise.

Suppose the extra carriers of Section 4(a) qualify to represent part of the excess concentration δn_e of electrons and holes considered in Section 4(b). Figure 2.5 then shows that their effect is to increase s if $n_e + \delta n_e$ lies below the maximum of s. Their effect could be to decrease s if $n_e + \delta n_e$ lies above this maximum.

2.7 Conclusions

It has been shown that the Shockley-Read Hall statistics can be generalised to include Auger effects, trap relaxation, extra carriers and a simple trap spectrum. The surface recombination velocity s tended to dip to a minimum value for near intrinsic material, due to a combination of the occupation of the traps and the lack of electrons to recombine with every trapped hole. Near the band edges s rose owing to Auger effects. A simple trap distribution increased these tendencies.

As a function of excess carrier concentration, it is found that s passes through a maximum which occurs as a result of an increase of s due to Auger effects and a decrease due to a saturation of the traps. A trap distribution again makes this maximum more pronounced. Earlier work of Dhariwal, Kothari and Jain (1981) and Landsberg (1982a) is thus confirmed and extended. Note that if time delays and Auger effects are important, then experimental curves corresponding to Figure 2.5 should enable one to infer valuable

information concerning the magnitude of these effects.

The present work has used an energy level model which is basically that due to Dhariwal, Kothari and Jain (1981) and more complicated than in the Schockley-Read model. The parameters n_1 and p_1 of Shockley-Read statistics, which one is tempted to use here are therefore not quite appropriate. The relation has been clarified by the use of new parameters ν_1 and π_1 [see eg. (2.21) and (2.22).]

TABLE 2.1

DATA USED IN THE GRAPHS FOR SILICON

Parameter	Numerical Value	Dimensions	References and Notes
E_G	1.1	eV	Sreedhar et al., 1969
k_B	8.625×10^{-5}	eVK^{-1}	Boltzmann's constant
T	300	K	Temperature
N_c	2.9×10^{19}	cm^{-3}	Landsberg and Klimpke, 1980
N_v	1.1×10^{19}	cm^{-3}	Landsberg and Klimpke, 1980
T_1^s	1.12×10^{-8}	cm^3s^{-1}	From capture cross-section X thermal velocities (Barrett and and Vapaille, 1976)
T_2^s	1.12×10^{-8}	cm^3s^{-1}	
T_1	3.66×10^{-25}	cm^6s^{-1}	
T_2	3.66×10^{-25}	cm^6s^{-1}	Evans and Landsberg , 1963
T_3	3.66×10^{-25}	cm^6s^{-1}	and Robbins and Landsberg, 1980
T_4	3.66×10^{-25}	cm^6s^{-1}	
t_n	1.0×10^{-10}	s	Dhariwal, Kothari and Jain,
t_p	1.0×10^{-10}	s	1981.
δ_n	8.0		
δ_p	8.0		
N_t	10^{13}	cm^{-2}	
D_s	2×10^{13}	$cm^{-2}eV^{-1}$	Lane, 1968
E_u-E_v	0.8	eV	
$E_\ell-E_v$	0.3	eV	

When N_t traps at a single energy level are used, it is assumed that they are at mid-gap. When a trap spectrum is used it has constant density D_s per unit area per unit energy and extends symmetrically by 0.25eV about the mid-gap position.

TABLE 2.2

NUMBERS DERIVED FROM TABLE 2.1

Parameters	Numerical Value	Dimensions
t'_n	3×10^{-7}	s
t'_p	3×10^{-7}	s
$n_1 = \nu_1$	8.1×10^{9}	cm^{-3}
$p_1 = \pi_1$	3.1×10^{9}	cm^{-3}
n_2	2.4×10^{13}	cm^{-3}
p_2	9.2×10^{12}	cm^{-3}
Z_o/Z_1	3.58×10^{9}	-

TABLE 2.3

DATA USED FOR FIGURES 2.6 AND 2.7 (FOR CdS)

Parameter	Numerical Value	Dimensions	References and Notes
E_G	2.42	eV	
N_c	1.76×10^{18}	cm^{-3}	
N_v	1.17×10^{19}	cm^{-3}	
T_1^s	1.66×10^{-11}	$cm^3 s^{-1}$	Robbins and Landsberg, 1980
T_2^s	1.66×10^{-11}	$cm^3 s^{-1}$	
T_1	2.87×10^{-26}	$cm^6 s^{-1}$	
T_2	1.24×10^{-26}	$cm^6 s^{-1}$	
T_3	2.87×10^{-26}	$cm^6 s^{-1}$	
T_4	1.24×10^{-26}	$cm^6 s^{-1}$	
t_n	1.0×10^{-12}	s	
t_p	1.0×10^{-17}	s	
δ_n	30.4		
δ_p	13.0		
N_t	10^{13}	cm^{-2}	
E_t-E_v	0.34	eV	

ALL OTHER DATA AS TABLES 2.1 AND 2.2

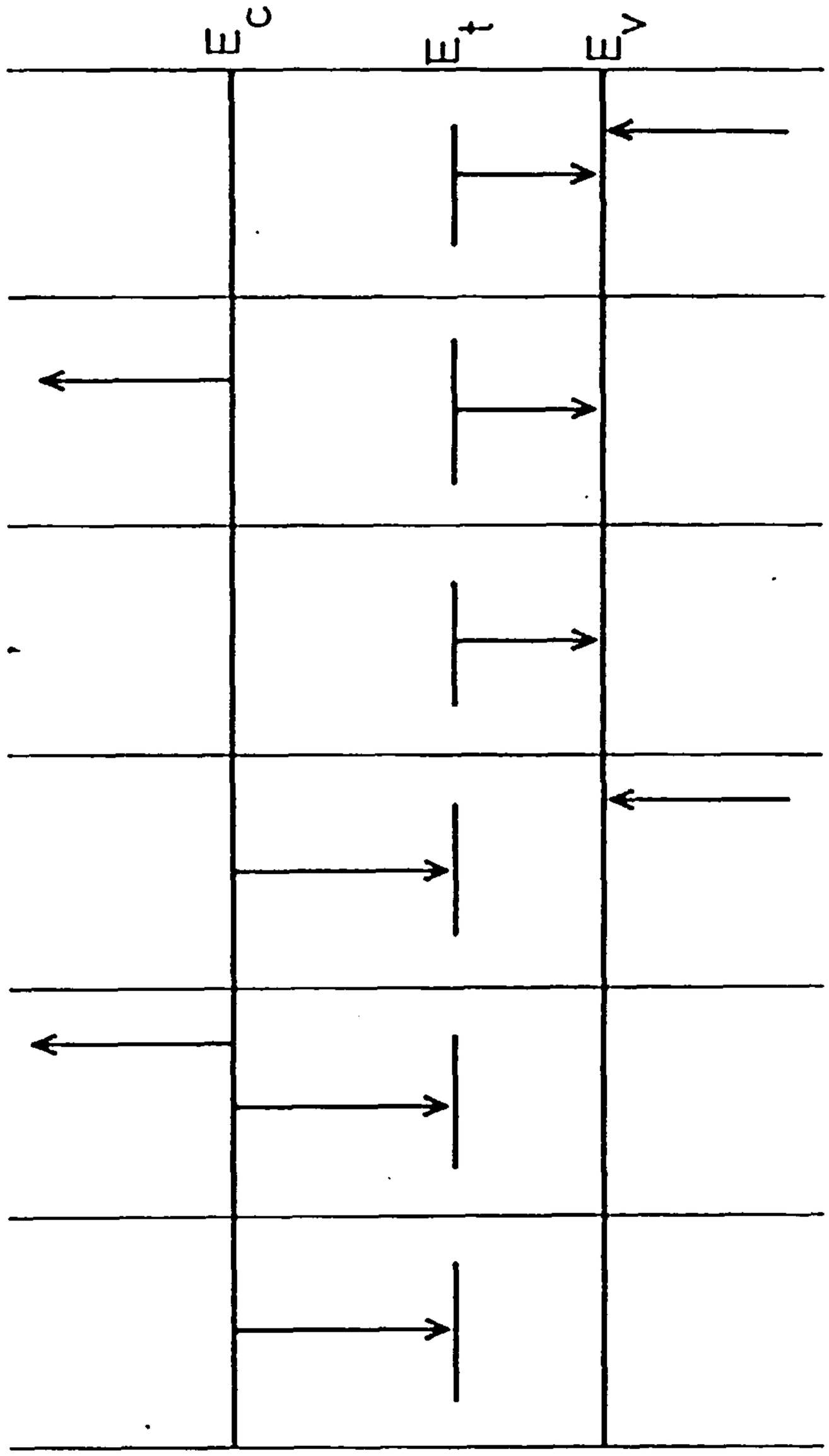

Figure 2.1 Reaction constants for single-electron and Auger processes involving t

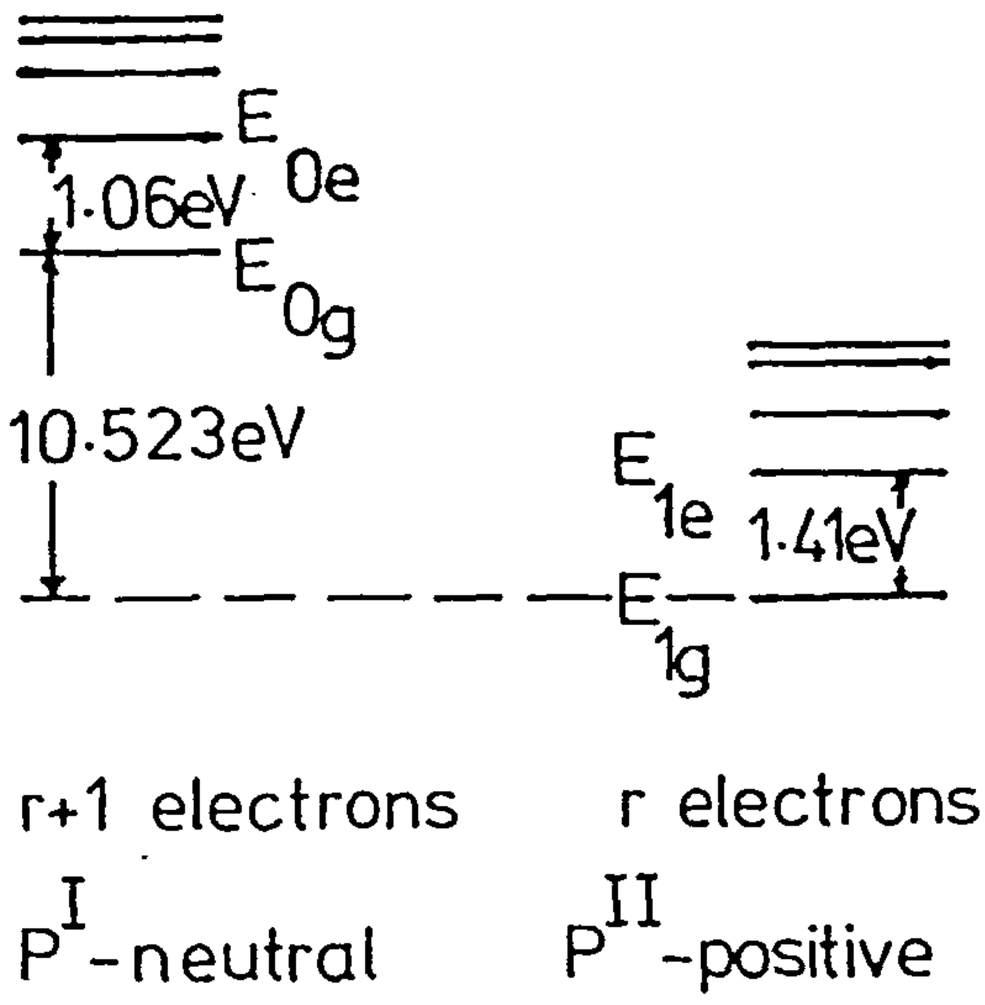

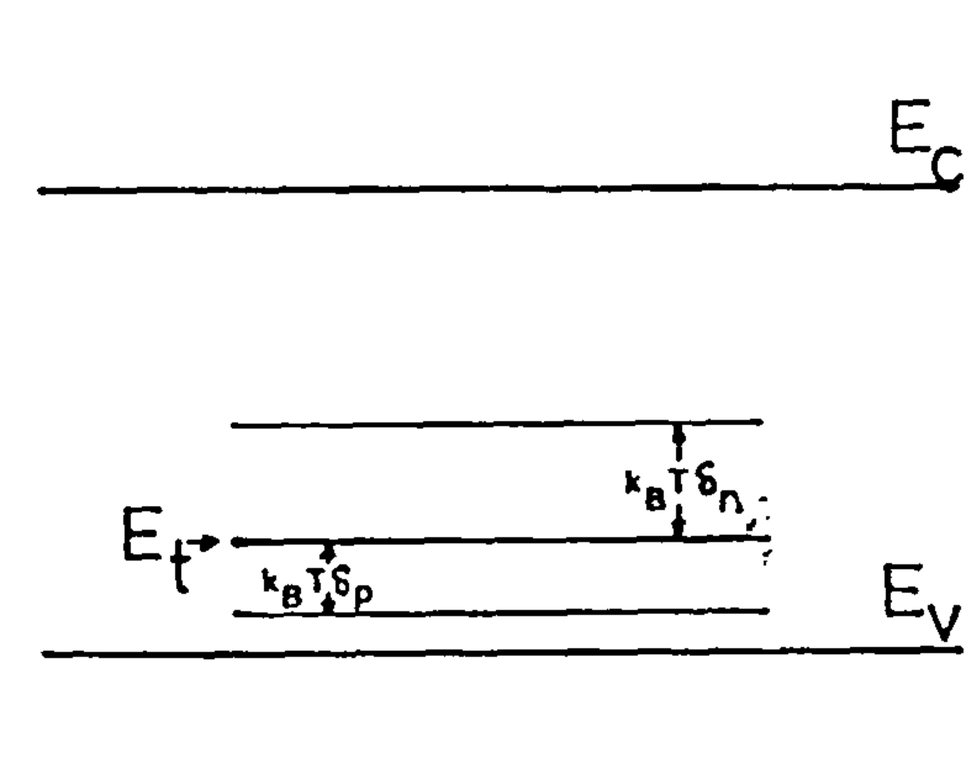

Figure 2.2 Trap r-electron energy levels and single-electron energy representations of these r-electron energy levels.

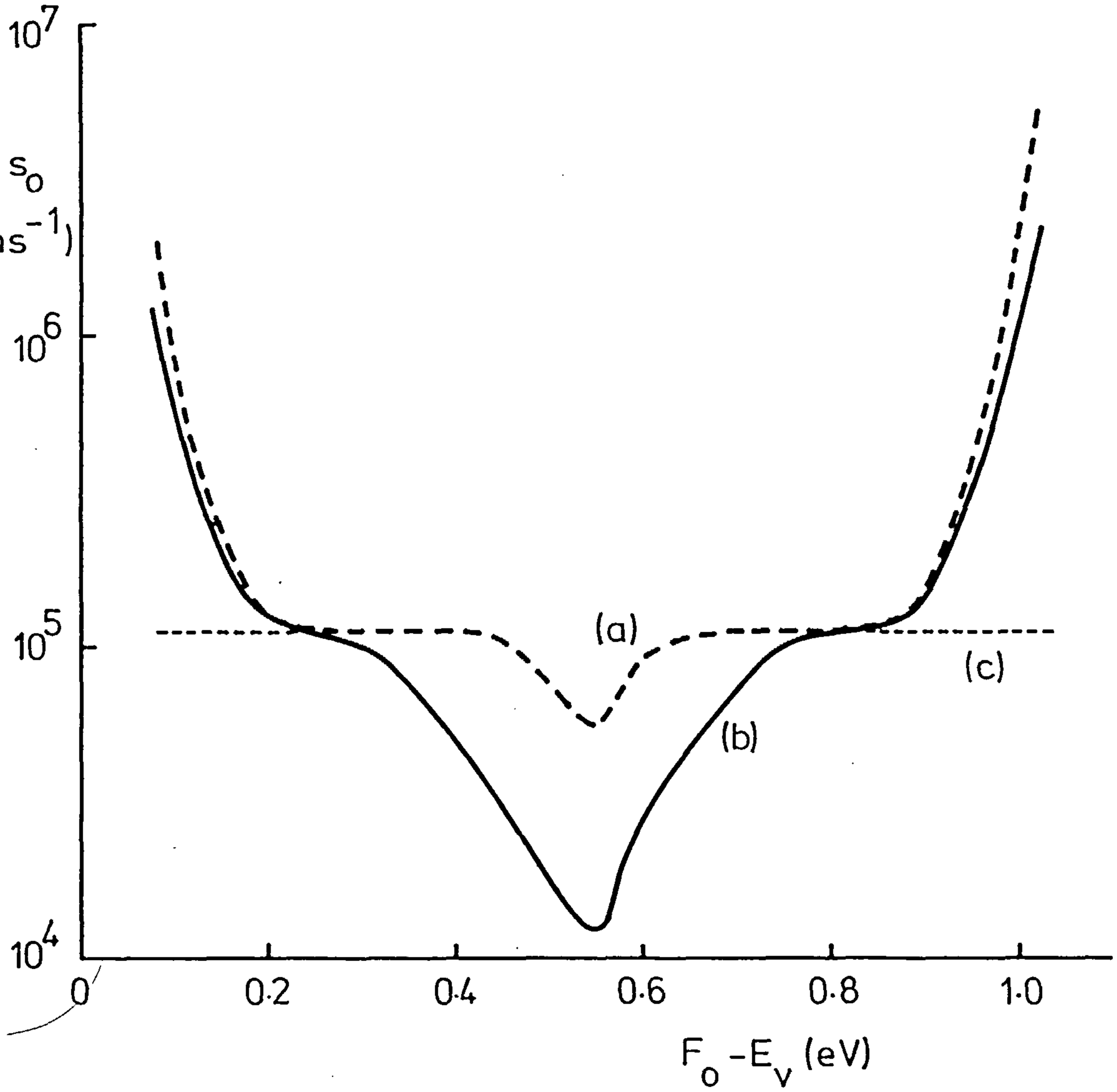

Figure 2.3 Thermal equilibrium surface recombination velocity as a function of Fermi level for the data of Table 2.1. (a) N_t traps at mid-gap, using (4.6). (b) N_t traps uniformly distributed about mid-gap, using (5.4). (c) As (a) without Auger effects.

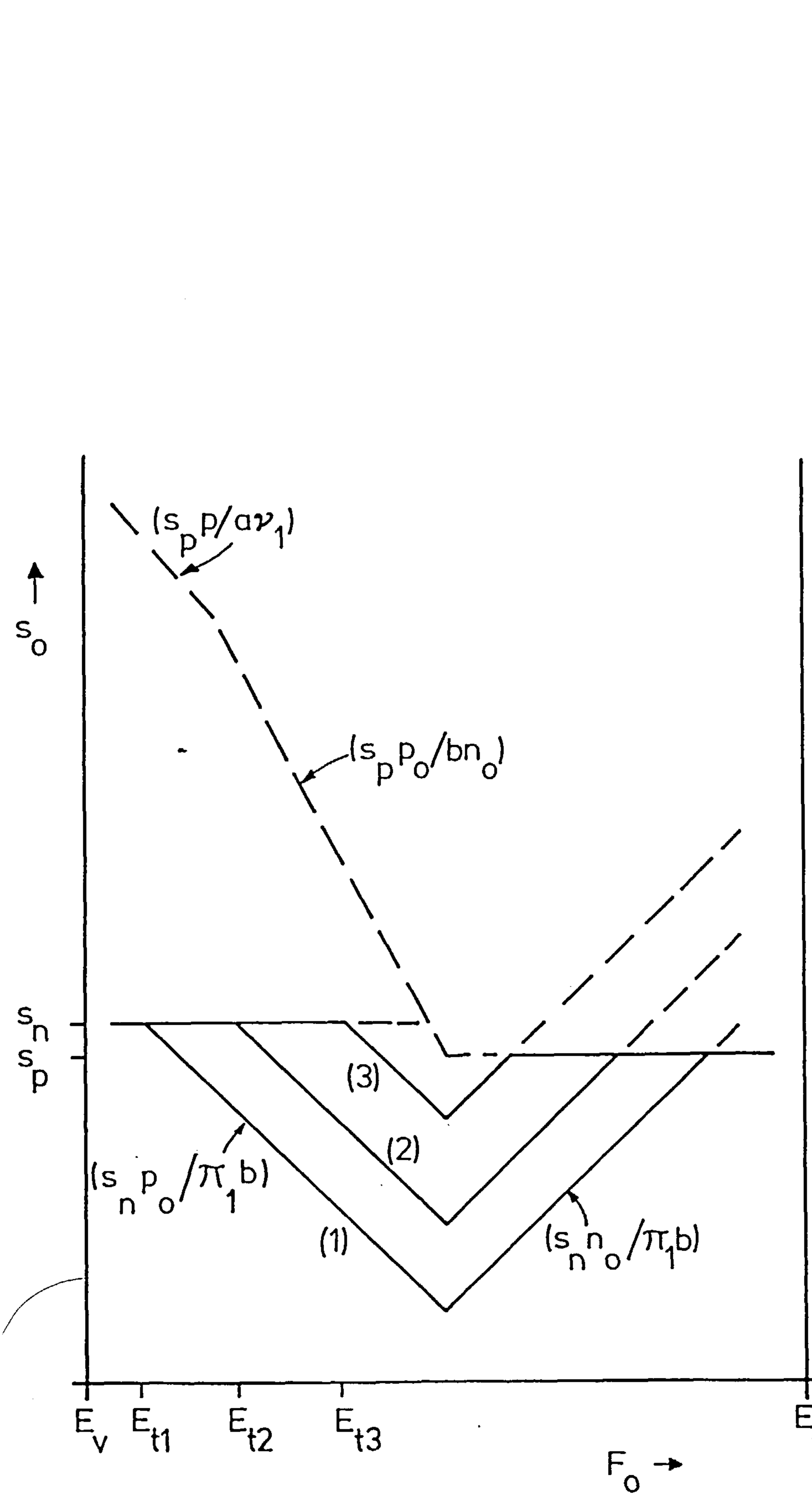

Figure 2.4 Surface recombination velocity for three trap levels as a function of equilibrium Fermi level. Auger effects are neglected.

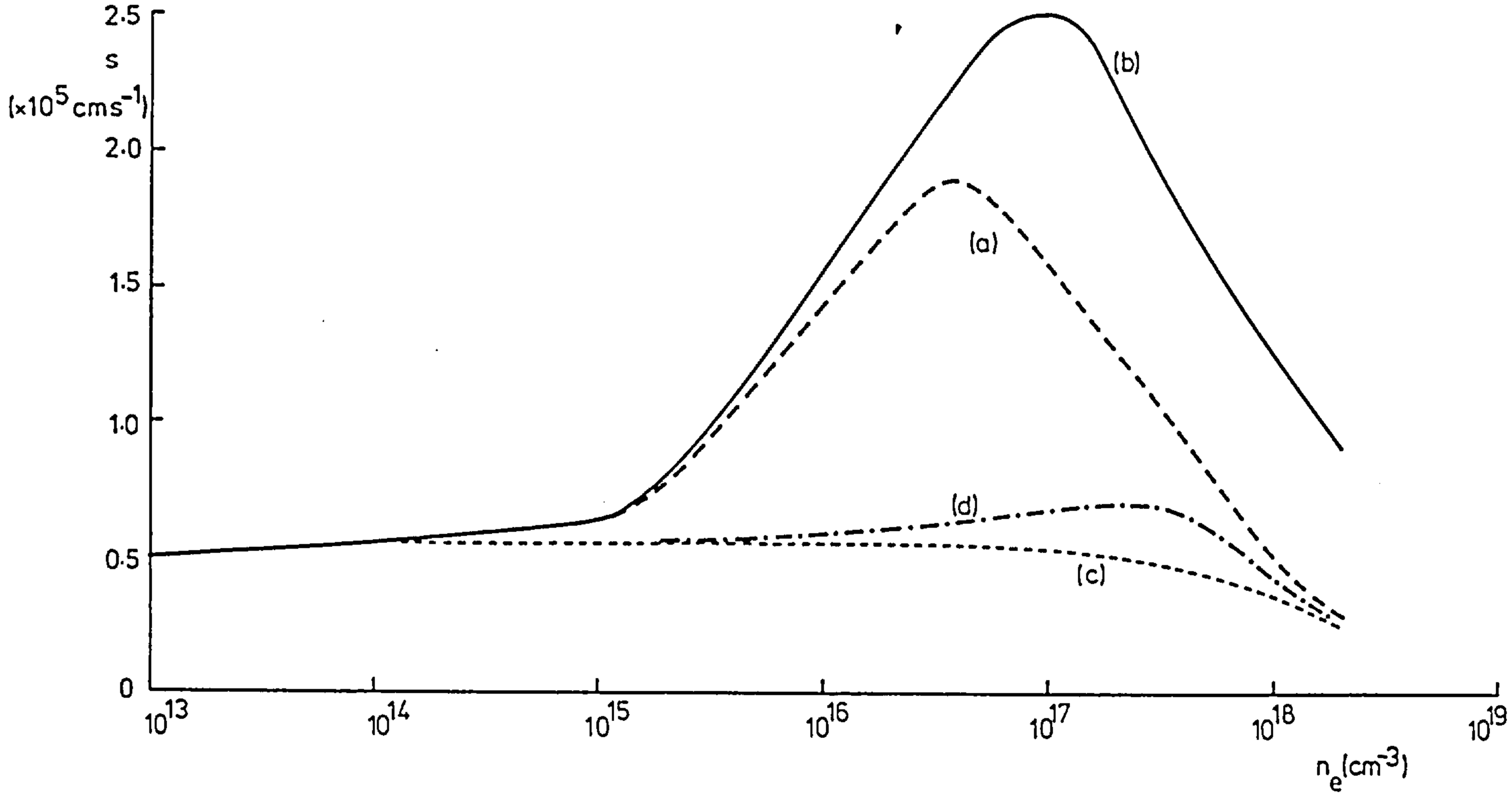

Figure 2.5 Steady-state surface recombination velocity as a function of excess carrier concentration for the data of Table 2.1, and $F_0-E_v=0.55$ eV. (a) N_t traps at mid-gap, using (4.3). (b) N_t traps uniformly distributed about mid-gap, using (5.3). (c) As (a) without Auger effects. (d) As (a) with the smaller Auger reaction constants, $T_1=T_3=2.87\times10^{-26}$ cm^6s^{-1}, $T_2=T_4=1.24\times10^{-26}$ cm^6s^{-1} (Haug, 1981). The lower Auger effect curve corresponding to a trap distribution as for curve (b) lies indistinguishably close to the curve labelled (d).

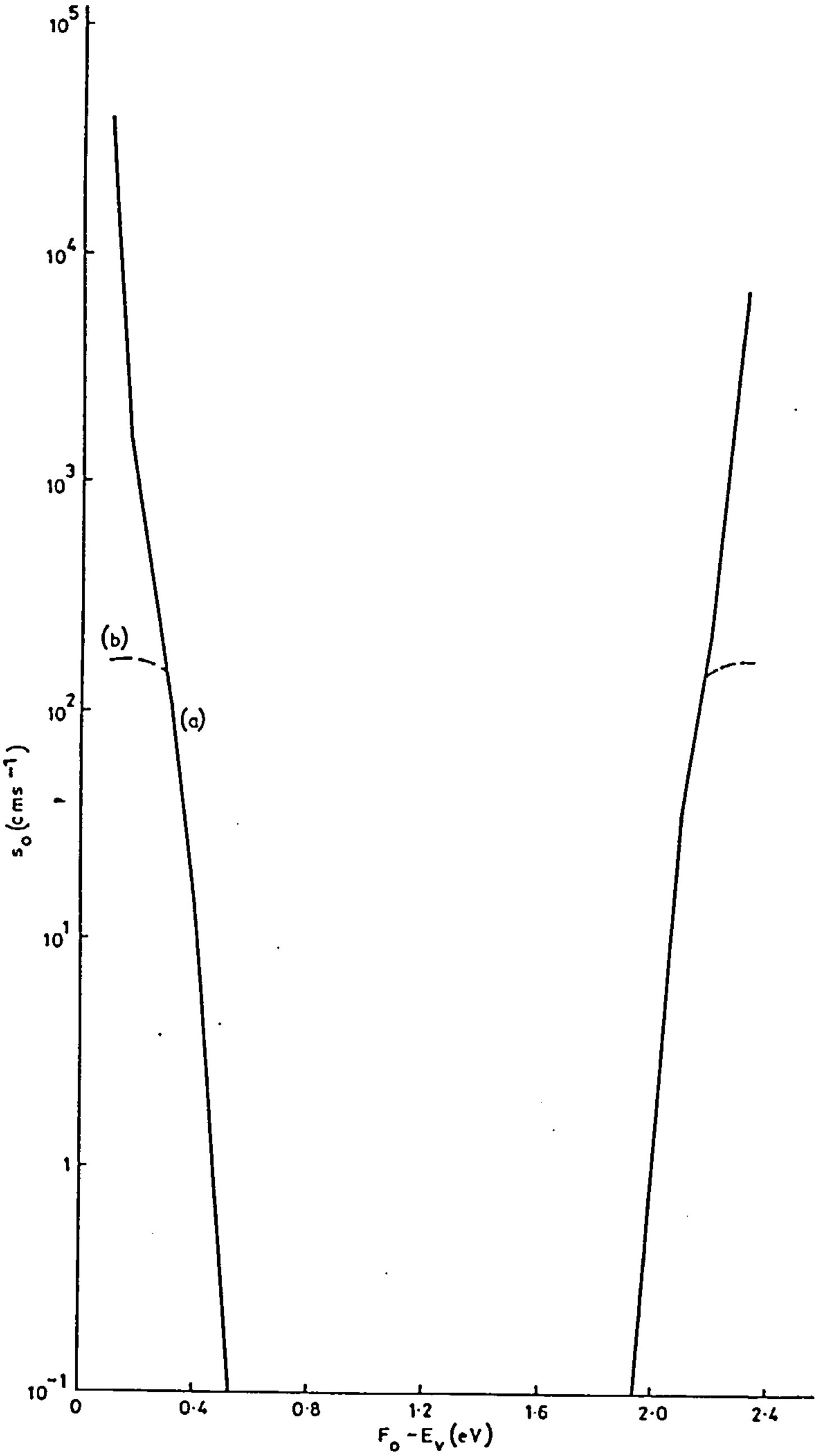

Figure 2.6 Thermal equilibrium surface recombination velocity as a function of Fermi level for the data of Table 2.3 for CdS. (a) N_t traps per unit area at $E_t - E_v = 0.34$ eV, using (4.6). (b) As (a) without Auger effects.

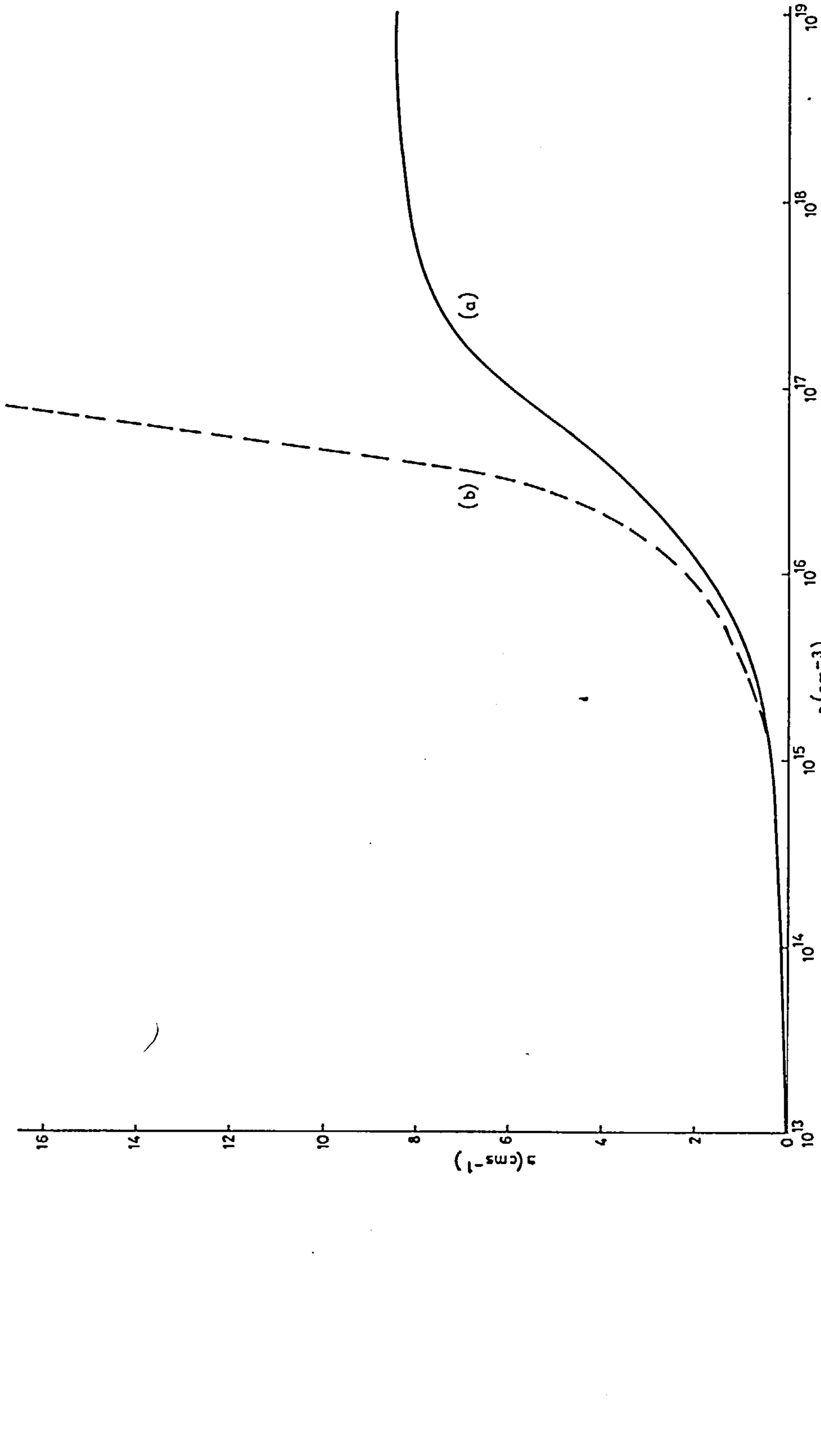

Figure 2.7 Steady-state surface recombination velocity as a function of excess carrier concentration (a) using the data of Table 2.3 and $F_o - E_v = 1.2$ eV. (b) $t_p = 10^{-17}$ secs, other data as curve (a).

CHAPTER 3

EFFECTS OF SURFACE STATES AND OF EXCITATION ON BARRIER HEIGHTS AT A GRAIN BOUNDARY

3.1 Introduction

The recent wide interest in the electrical properties of grain boundaries is largely due to the considerable potential of polycrystalline devices. Examples are polysilicon emitter transistors, thin-film resistors and solar cells. Because of these applications the main interest is in transport properties across grain boundaries. These are strongly affected by the barrier height, ϕ_B ,due to charged interface states and compensating space-charge regions on either side. Such a comparatively crude model of a grain boundary dates back to 1952 (Taylor et al., 1952), has proved relatively successful, and is in fact similar to Schottky-type barriers which form for the same reason between semiconductors or between a metal and a semiconductor. The very crudeness of the model is responsible for the possibility of its wider use.

This model is adopted also in the present work, which is rigorously confined to a theoretical study of how the barrier height is affected by the obvious parameters: Doping density, Fermi-level separation and the number of surface states and their position in the energy gap. This leads to a straight-forward problem in electrostatics whose only complication is due to the non-linearity of the Poisson equation: The electrostatic potential, ϕ , is determined by the carrier concentrations n and p whose values depend themselves on ϕ . This has led to the use or the depletion approximation in which only the fixed space-charge

$q(N_o^+ - N_A^-)$ of donors and acceptors is used in the Poisson equation. The present work jettisons this approximation but does not solve the problem in all generality since an assumption of parallel quasi-Fermi levels is made. The approach used here dates from 1955 (Kingston and Neustadter, 1955) where it was used to model Schottky barrier heights at a surface in equilibrium and later for parallel flat quasi-Fermi levels (Garrett and Brittain, 1955). This model (see Section 3.3), which was first proposed as a solution to the grain boundary problem by Fossum and Lindholm (1980a) and Fossum and Sundaresan (1982). is treated here exactly and analytically (Section 3.4). It thus removes the need for computer solutions and the need to assume the surface level to be at mid-gap. Our approach leads to simple interpretations of the behaviour of ϕ_B (Section 3.5) and enables one to obtain approximate analytical expressions for some cases (Section 3.6).

Although excellent summaries of work up to 1979/80 are given by Kazmerski (1980) and by Orton and Powell (1980), it may be helpful to review briefly work relevant to the present study. The popularity of the depletion approximation is illustrated for example by transport studies in polycrystalline silicon (Baccarani et al., 1978a, 1978b; Seager and Castner, 1978, Seto, 1975). Both single surface levels and a distribution of surface levels were considered. Because of the neglect of $p - n$ in Poisson's equation the variation of the quasi-Fermi levels with distance plays little part in such models. Strictly, one neglects p and n separately, but this was relaxed to the neglect of $p - n$ by Seager (1981) where barrier heights and currents were obtained both experimentally and theoretically in the presence of illumination. Experimental and theoretical studies on illuminated grain boundaries were also carried out partly to elucidate the behaviour of polysilicon

solar cells (Card and Yang, 1977, Panayotatos and Card, 1980). In the work by Panayotatos and Card, (1980) the depletion approximation was used and it was inferred that the minority quasi-Fermi level is not flat. Indeed the behaviour of the quasi-Fermi levels in Schottky barrier solar cells had been studied earlier (Klimpke and Landsberg, 1979 and 1981) and the existence of extrema in both majority and minority quasi-Fermi levels had been emphasized (Pimpale and Landsberg, 1982). The experimental determination of the spectrum of surface surface states in the energy gap at grain boundaries has also been very active (Cheng and Shyu, 1981, Shyu and Cheng, 1982, Srivastava et al., 1982, de Graaf et al., 1982). All of this work has been carried out in polysilicon, with the exception of the work of Taylor et al. (1952), which dealt with Germanium. In Gallium Arsenide, two surface states were found (Spencer et al., 1983) and measurement of the mobility and conductivity in Cadmium Sulphide evaporated thin films has been reported (Wu and Bube, 1974, Ma and Bube, 1977).

Continuing this work, parallel quasi-Fermi levels are considered here since this must be a reasonable approximation if bulk and surface recombination occur at comparable rates. At first, a single level of surface states is taken as one is interested in how the properties of barrriers depend on the energy level of the states. The effect of a distribution of states can in principle be synthesized from this information and this is examined in later sections. The barrier heights, ϕ_B, calculated with this model are utilised in a simple calculation of the mobility and diffusion length in a grain.

3.2 Main Assumptions

The assumptions required to analyze the grain boundary recombination and the dependence of the barrier height on surface state density, doping and recombination are as follows:

A1 The grain boundary is a flat surface with separated identical grains. This makes a one-dimensional treatment appropriate. A p-type grain will be assumed so that the energy bands bend according to Figure 3.1.

A2 The system is non-degenerate and both surface and bulk recombination occur via a generalized form of the Schockley-Read-Hall mechanism.

A4 The bulk trap density makes a negligible contribution to the space charge.

This model leads to analytical, though transcendental, results for the barrier height, surface recombination rate and surface recombination velocity.

It was convenient for our numerical work to add the following assumptions:

B1 The acceptors in the space-charge region are assumed fully ionized. This would automatically be the case for a non-degenerate sample with shallow acceptor levels.

B2 The surface states of the grain boundary are assumed to be N_{DS} donors at a single energy level E_{DS}.

B3 The same values of the capture coefficients G and H which occur in the Shockley-Read-Hall statistics are used throughout (see the last two entries in Table 3.1). i.e. G and H are independent of the position of the energy level of the state E_{DS}.

There is a third group of assumptions which is often made, but is not required here:

C1 Surface recombination dominates the bulk recombination in the space-charge region so that the latter is neglected.

C2 The depletion approximation is not needed to solve Poisson's equation here. However, it will be introduced at various points in the curve descriptions (Section 3.5) to illustrate the underlying physics of some results.

The departure from equilibrium in the theory is imposed by taking various specific separations between the Fermi levels as given. This separation can be established by injection or by optical excitation which has to overcome recombination in the bulk of the grain. In this way of looking at the problem it is therefore not necessary to introduce bulk recombination explicitly.

3.3 Formulation of the Model.

To obtain the barrier height, $e\phi_B$, (Figure 3.1) an integration of Poisson's equation is required, where Poisson's equation takes the form

$$\frac{d^2\phi}{dx^2} = \frac{e}{\varepsilon\varepsilon_o}(p-n-N_A^-) \quad , \quad [\phi(0) \equiv \phi_B, \ \phi(w) \equiv 0] \ . \tag{3.1}$$

Here S.I. units, assumptions A1 and A4 are used, $N_A^-(x)$ is the concentration of charged acceptors, n and p are the electron and hole concentrations and $\varepsilon\varepsilon_o$ is the permittivity of the semiconductor. Also, using A2,

$$N_A^-(x) \doteq N_A\{\exp[\eta_A(x)-\gamma_h]+1\}^{-1} = N_A\{\exp[\eta_A(w)-(e\phi(x)/k_BT)-\gamma_h]+1\}^{-1} \ , \tag{3.2}$$

$$n(x) = N_c \exp[\gamma_e - \eta_c(x)] \equiv n(w)\ \mu(x) \ , \qquad (3.3)$$

$$p(x) = N_v \exp[\eta_v(x) - \gamma_h] \equiv p(w)/\mu(x) \ . \qquad (3.4)$$

A standard notation has been used with $\gamma_e \equiv F_e/k_BT$, $\gamma_h \equiv F_h/k_BT$ and

$$\mu(x) \equiv \exp[e\phi(x)/k_BT] \ . \qquad (3.5)$$

Note, in writing (3.2) it has been assumed that the occupation of the acceptors may be obtained using Fermi-Dirac statistics and that the effect of the minority Fermi level on the acceptor level occupation can be neglected.

By introducing the readily obtained quantities $n(w)$ and $p(w)$ the two variables $n(x)$ and $p(x)$ have been replaced by a single variable $\mu(\tilde{x})$ whose value at $x = 0$ will yield the barrier height , $e\phi_B$, later. Two boundary conditions are needed to integrate Poisson's equation. At the edge of the space-charge region, $x = w$ in Figure 3.1,

$$\left.\frac{d\phi}{dx}\right|_{x=w} = 0 \ . \qquad (3.6)$$

At the grain boundary surface, $x = 0$, Gauss's theorem is used; taking a small "pill box" of unit area which crosses the grain boundary surface as in Figure 3.2,

$$\int_S \underline{E}.\underline{n}\ dS = \sum_i \frac{q_i}{\varepsilon\varepsilon_o} \ .$$

Taking the limit as, ℓ , the length of the pill box tends to zero, the charges q_i contained within it are equal to the charge density of the surface states, Q_s , per unit area. Also, the field , $\underline{E}$, emerges from the end of the pill box, so that one may write,

$$-2\left.\frac{d\phi}{dx}\right|_{x=0} = \frac{Q_s}{\varepsilon\varepsilon_o} , \qquad (3.7)$$

where the charge per unit area on the surface is an integral over the energy levels, E_S, of surface states in the energy gap,

$$Q_s = \int_{E_{vS}}^{E_{cS}} e\left\{N_{DS}(E_S)\left(1-f(E_S,e\phi_B)\right)-N_{AS}(E_S)f(E_S,e\phi_B)\right\}dE_S . \qquad (3.8)$$

Here, N_{DS} and N_{AS} are the numbers per unit area (of the grain boundary surface) per unit energy range of donor and acceptor traps; $f(E_S,e\phi_B)$ is the occupation probability of a surface energy level E_S in the presence of a barrier height $e\phi_B$.

The Shockley-Read-Hall probability $f(E_S,e\phi_B)$ is displayed as a generalisation of the Fermi-Dirac distribution utilizing assumptions A2 and A3. Using standard notation, this probability is given by (see Chapter 2, equation 2.31)),

$$f(E_S,e\phi_B) = \frac{G(o)n(w)\mu(o)+H(o)p_1(E_S)}{G(o)[n(w)\mu(o)+n_1(E_S)]+H(o)[p(w)/\mu(o)+p_1(E_S)]} . \qquad (3.9)$$

Here (O) indicates evaluation of a parameter at the grain boundary surface $x = 0$, and (3.3) and (3.4) have been used. Dividing the right hand side of (3.9) throughout by the numerator, one can write f in the form

$$f = (1+X)^{-1}$$

where

$$X = \frac{G(o)n_1(E_S)+H(o)p(w)/\mu(o)}{G(o)n(w)\mu(o)+H(o)p_1(E_S)} .$$

Using

$$n(w)p(w)\exp(\gamma_h-\gamma_e) = n_1(E_s)p_1(E_s) = n_i^2 , \qquad (3.10)$$

the denominator of X can be rearranged to give

$$X = \left\{\frac{G(o)n_1(E_S)+H(o)p(w)/\mu(o)}{G(o)n_1(E_S)\exp(\gamma_e-\gamma_h)+H(o)p(w)/\mu(o)}\right\}\frac{p(w)/\mu(o)}{p_1} ,$$

where also (3.4) and the definition of p_1 (see equation (2.30)) have been used. A function $g(E_s, e\phi_B)$ is defined by

$$g(E_S,e\phi_B) = \frac{G(o)n_1(E_S)+H(o)p(w)/\mu(o)}{G(o)n_1(E_S)\exp(\gamma_e-\gamma_h)+H(o)p(w)/\mu(o)}$$

and $f(E_S,e\phi_B)$ may therefore be displayed as

$$f(E_S,e\phi_B) = \frac{1}{g(E_S,e\phi_B)\exp(\eta_S-\gamma_h)+1} . \qquad (3.12)$$

It is seen at once that the equilibrium condition leads to the implications

$$\gamma_e = \gamma_h(=\gamma_o) \rightarrow g(E_S,e\phi_B) = 1 . \qquad (3.13)$$

The occurrence of the reduced majority carrier Fermi level in (3.12) is convenient as it will be assumed unchanged by the disturbance (see Panayotatos and Card, 1980). However, the display of the steady-state Shockley-Read type of probability (3.9) as a generalized Fermi-Dirac distribution is always possible, even for bulk recombination. As this may be of wider interest, it is useful to develop a formulation of $f(E_S,e\phi_B)$ which is symmetric in n and p, using the neutral notation f_t, $\eta_t \equiv E_t/k_BT$ instead of $f(E_S,e\phi_B)$ and E_S, for surface and bulk recombination:

$$f_t = \frac{1}{h\exp(\eta_t-\gamma_o)+1} \qquad (3.14)$$

where

$$h = \exp(\gamma_o - \eta_t)\left\{\frac{G(o)n_1(E_S)+H(o)p(w)/\mu(o)}{G(o)n(w)\mu(o)+H(o)p_1(E_S)}\right\} .$$

Rearranging h ,

$$h = \frac{G(o)n_o(w)\mu(o)+H(o)p_1(E_S)\exp[\gamma_o-\gamma_h]}{G(o)n(w)\mu(o) + H(o)p_1(E_S)}$$

or alternatively using (3.3)

$$h(E_t, e\phi_B, \gamma_e, \gamma_h, \gamma_o) = \frac{G(o)n(w)\mu(o)\exp[\gamma_o-\gamma_e]+H(o)p_1(E_S)\exp[\gamma_o-\gamma_h]}{G(o)n(w)\mu(o) +H(o)p_1(E_S)} . \qquad (3.15)$$

This is the simplest form in which to express h , but one can go further to emphasize the symmetry,

$$h = \exp\{\gamma_o-(\gamma_e+\gamma_h)/2\}\left\{\frac{G(o)n(w)\mu(o)\exp[(\gamma_h-\gamma_e)/2]+H(o)p_1(E_S)\exp[\gamma_e-\gamma_h)/2]}{G(o)\ (w)\mu(o)+H(o)p_1(E_S)}\right\}$$

and hence using

$$\cosh\theta = (e^{\theta}+e^{-\theta})/2 ,$$

$$h = \exp\{\gamma_o-(\gamma_e+\gamma_h)/2\}\cosh\left[\alpha+\frac{1}{2}(\gamma_e-\gamma_h)\right]/\cosh\alpha \qquad (3.16)$$

where α is given by

$$\alpha = 1/2\ \ln[H(o)p_1(E_S)/G(o)n(w)\mu(o)] .$$

However,

$$n(w) = n_o(w)\ e^{\gamma_e-\gamma_o}$$

and then

$$h = \exp\{\gamma_o-(\gamma_e+\gamma_h)/2\}\cosh[\alpha_o+1/2(\gamma_o-\gamma_h)]/\cosh[\alpha_o+1/2(\gamma_o-\gamma_e)] \qquad (3.17)$$

where

$$\alpha_o = 1/2 \ln[H(o)p_1(E_S)/G(o)n_o(w)\mu(o)] .$$

Note, in (3.17) the term $\mu(o)$ in α_o is the steady-state value and not the equilibrium value $\mu_o/(o)$.

In Section 3.6, one uses the Shockley-Read recombination rate (Chapter 2, equation (2.27)) via the grain boundary surface states in the non-equilibrium steady-state and this is per unit area

$$dU_S = \frac{G(o)H(o)\{n(w)p(w)-n_i^2\}[N_{DS}(E_S)+N_{AS}(E_S)]dE_S}{G(o)\{n(w)\ (o)+n_1(E_S)\}+H(o)\{p(w)/\mu(o)+p_1(E_S)\}}. \qquad (3.18)$$

It is useful to define a surface recombination velocity $s(o)$ by

$$s(o) \equiv \{1/n_e(o)\} \int_{E_{vS}}^{E_{cS}} dU_S \qquad (3.19)$$

where $n_e(o)$ is the number of excess carriers per unit volume at the surface of the grain,

$$n_e(o) = n(o) - n_o(o)\{ = n(w)\mu(o) - n_o(w)\mu_o(o)\} .$$

Also the recombination current density is defined by

$$J(o) = eU_S/2 \qquad (3.20)$$

The factor of one half arises because of the assumption of identical grains giving two equal current densities on either side of the grain boundary. The factor of a half has to be omitted if a simple surface is discussed.

3.4 The Barrier Height

From the equations of Section 3.3, an analytic, though transcendental equation for the barrier height, ϕ_B, at $x = 0$ in equilibrium and in the steady-state will be developed.

Equations (3.2) to (3.5) are used to write Poisson's equation (3.1) in the following form,

$$-\frac{d^2\phi}{dx^2} = \frac{e}{\varepsilon\varepsilon_o}\left\{p(w)\exp[-e\phi/k_BT]-n(w)\exp[e\phi/k_BT] - \frac{N_A}{\exp[\eta_A(w)-e\phi/k_BT-\gamma_h]+1}\right\} \qquad (3.21)$$

Multiplying both sides of (3.21) by $(d\phi/dx)$ and integrating from $x = 0$ to $x = w$,

$$\frac{1}{2}\left(\frac{d\phi}{dx}\right)^2\Bigg|_{x=w} - \frac{1}{2}\left(\frac{d\phi}{dx}\right)^2\Bigg|_{x=0} =$$

$$-\frac{k_BT}{\varepsilon\varepsilon_o}\Bigg[-p(w)\exp[-e\phi/k_BT]-n(w)\exp[e\phi/k_BT]+N_A\ \ln\{\exp[\eta_A(w)-e\phi/k_BT-\gamma_h]+1\}\Bigg]_{x=0}^{w} .$$

Using the boundary condition (3.6) at $x = w$, one has

$$\frac{d\phi}{dx}\Bigg|_{x=0} = -\left(\frac{2k_BT}{\varepsilon\varepsilon_o}\right)^{\frac{1}{2}}\left[-p(w)\{1-\mu(o)^{-1}\}+n(w)\{\mu(o)-1\}+N_A\ \ln\left\{\frac{\exp[\eta_A(w)-\gamma_h]+1}{\mu(o)^{-1}\exp[\eta_A(w)-\gamma_h]+1}\right\}\right]^{\frac{1}{2}}$$

where the negative root has been chosen in order to give the correct sign of the barrier height. Introducing the boundary conditions (3.7) and (3.8) at $x = 0$, a transcendental equation is obtained for the barrier height, $(k_BT/e)\ \ln\mu(o)$:

$$\left[n(w)\{\mu(o)-1\}+p(w)\{\mu(o)^{-1}-1\}+N_A\left\{\ln\mu(o)-\ln\left(\frac{\exp[\eta_A(w)-\gamma_h]+1}{\mu(o)^{-1}\exp[\eta_A(w)-\gamma_h]+1}\right)\right\}\right]^{\frac{1}{2}}$$

$$= \left(\frac{e^2}{8k_BT\varepsilon\varepsilon_o}\right)^{\frac{1}{2}}\int_{E_{vs}}^{E_{cS}}\left\{\frac{N_{DS}(E_S)}{1+g(E_s,e\phi_B)^{-1}\exp[\gamma_h-\eta_s]} - \frac{N_{AS}(E_S)}{1+g(E_s,e\phi_B)\exp[\eta_s-\gamma_h]}\right\}dE_s \ . \qquad (3.22)$$

The equilibrium barrier height, ϕ_{Bo} , is obtained in the limit (3.13). Writing the Shockley-Read occupation probability in the form (3.12) of the Fermi-Dirac statistics together with utilization of the limit (3.13) has allowed the display of the equilibrium result as a special case of the steady-state equation; separate treatments of the equilibrium and steady-state barrier heights are then avoided. Note, if the depletion approximation was used to solve (3.1) one would arrive at equation (3.22) with effectively

$$n(w) = p(w) = 0$$

in the left hand side. Thus, the depletion approximation yields also a transcendental equation for the barrier height. Physically, equation (3.22) expresses charge balance between the space-charge and the charge on the surface states.

To simplify the numerical calculations, the additional assumptions, B_1, B_2 and B_3 are made. Neutrality in the grain bulk is assumed, locating the positions of the quasi-Fermi levels in the energy gap at $x = w$ via

$$p(w) - n(w) - N_A^- = 0 \ . \qquad (3.23)$$

A quadratic equation for $p(w)$ is formed from equations (3.23) and (3.10),

$$p(w)^2 - n_i^2 \exp[\gamma_e - \gamma_h] - N_A\, p(w) = 0 \ .$$

The solution of this quadratic equation is

$$p(w) = N_A/2 \pm \{N_A^2/4 + n_i^2 \exp[\gamma_e - \gamma_h]\}^{\frac{1}{2}} \ .$$

Using assumptions B1 to B3, where we see that the acceptors in the bulk are all ionized, the surface traps are all donor type at an energy, E_{DS} ,

and that $G(o)$ and $H(o)$ are not functions of E_{DS}, equation (3.22) becomes

$$[n(w)\{\mu(o)-1\}+p(w)\{\mu(o)^{-1}-1\}+N_A \ln\mu(o)]^{\frac{1}{2}} = \frac{eN_{DS}}{(8\varepsilon\varepsilon_o k_B T)^{\frac{1}{2}}}\left[\frac{1}{1+g(E_{DS}, e\phi_B)^{-1}\exp[\gamma_h-\eta_{DS}]}\right]$$

Defining two dimensionless parameters by

$$a \equiv (8\varepsilon\varepsilon_o k_B T N_A)^{\frac{1}{2}}/eN_{DS} \qquad (3.24)$$

and

$$\nu \equiv p(w)/N_A \quad (1-\nu = n(w)/N_A \text{ by } (3.23)) ,$$

then one has

$$a[(1-\nu)\{\mu(o)-1\}+\nu\{\mu(o)^{-1}-1\}+\ln\mu(o)]^{\frac{1}{2}} = \left\{1+g(E_{DS}, e\phi_B)^{-1}\exp[\gamma_h-\eta_{DS}]\right\}^{-1} .$$

Utilizing equation (3.11) for $g(E_{DS}, e\phi_B)$ and noting that

$$p(w)\mu(o)^{-1}/p_1(E_{DS}) = \exp[\eta_{DS}-\gamma_h] ,$$

equation (3.22) yields

$$\frac{\mu(o)p_1(E_{DS})}{p(w)} = \left[\frac{G(o)n_1(E_{DS})+H(o)p(w)\mu(o)^{-1}}{G(o)n_1(E_{DS})\exp[\gamma_e-\gamma_h]+H(o)p(w)\mu(o)^{-1}}\right] \times \left[\frac{1}{a[(1-\nu)\{\mu(o)-1\}+\nu\{\mu(o)^{-1}-1\}+\ln\mu(o)]^{\frac{1}{2}}}\right]^{-1}$$

Finally, dividing the numerator and denominator by N_A and rearranging factors,

$$\mu(o) = \frac{\nu N_A}{ap_1}\left[\frac{G(o)(n_1/N_A)\mu(o)+H(o)\nu}{G(o)(n_1/N_A)\mu(o)\exp[\gamma_e-\gamma_h]+H(o)\nu}\right] \times \left[\frac{1}{[(1-\nu)\{\mu(o)-1\}+\nu\{\mu(o)^{-1}-1\}+\ln\mu(o)]^{\frac{1}{2}}} - a\right] . \qquad (3.25)$$

In equations (3.24) and (3.25), the quantities regarded as given are those of Table 3.1 and also N_A, N_{DS}, $E_{DS} - E_{VS}$ and $F_e - F_h$. The values of n_1 and p_1 may then be deduced. Next, $p(w)$ is obtained by solving the quadratic resulting from (3.23) and (3.10). This gives F_h referred to the standard energy $E_v(w)$. From this F_e is determined since $F_e - F_h$ is regarded as given. Equation (3.25) is then solved iteratively for the barrier height, $e\phi_B$, and solutions are presented in Figures 3.3 to 3.14. The theory can be easily extended to n-type grains and this form of it has been used below in Figures 3.12 and 3.13.

3.5 Explanation of Figures 3.3 to 3.10

Figures 3.3 and 3.4 can be understood physically if one recognizes that the curves of each figure are of similar shape and differ only as regards the donor concentrations N_{DS}. Thus, an intuitive argument for one of the curves will describe the nature of them all. A physical understanding will enable the development of some simplified mathematical formulae for the barrier height in Section 3.6.

For small enough acceptor concentrations ($N_A < 10^{19} cm^{-3}$) the Fermi level at $x = 0$ lies above the surface donor levels, E_{DS}. Their (small) degree of ionization causes some band bending. At the acceptor concentration increases one may think of the band edges and the donor level to move down rigidly in Figure 3.1, pulled by the faster moving Fermi level. This process causes more ionization and $e\phi_{Bo}$ increases as in Figure 3.3. The barrier height reaches a maximum when the Fermi level and E_{DS} are at the same energy.

Note, this is where the model developed here differs from those of Baccarani et al., (1978a, 1978b), Seager (1978), Seager and Castner (1978), Seto (1975) which use the depletion approximation. Using the

depletion approximation, as the number of acceptors (N_A) tends to zero, the space-charge (also N_A) tends to zero; whereas in our model there is a contribution to the space-charge $(p-n-N_A)$ from the electrons and holes. Thus, the depletion approximation incorrectly calculates very large band-bending for small N_A in order to very largely neutralize the charge on the donor surface state. As N_A is increased from zero in the depletion approximation, the barrier height falls in opposition to our result which rises.

In Figures 3.3 and 3.4, once the Fermi level lies below E_{DS}, the donors are almost fully ionized while the ionized acceptor concentration continues to increase as acceptors are added. The balance of (positive) charge on the surface with that in the space-charge region then requires the (negative) charge per unit area

$$q_B = e \int_o^w (p-n-N_A^-)dx \qquad (3.26)$$

to remain almost constant. It follows from (3.26) that $p-n$ increases (w decreases) and hence $\mu(o)$ and ϕ_B increase. Alternatively, using the depletion approximation

$$w = \frac{Q_S}{2eN_A}, \quad \phi_B = \frac{eN_A w^2}{2\epsilon\epsilon_o} \qquad (3.27, 3.28)$$

verifying the decrease in w_1 and showing also that ϕ_B decreases as more acceptors are added.

Consider next the barrier height for fixed N_A but different surface donor concentrations and at two different energy levels (Figures 3.5 and 3.6). For high enough surface donor concentrations $(N_{DS} \gtrsim 10^{16} cm^{-2}$, if $N_A \sim 10^{21} m^{-3})$ in the grain boundary surface, the equilibrium Fermi

level lies above the donor level. Injection of electron-hole pairs raises the quasi-Fermi level for electrons above that for holes as in Figure 3.1. The occupation of the surface donors increases. The decrease in Q_S is expected in (3.27) and (3.28) to lead to a decrease in w and hence in ϕ_B. This explains the general slope of the curves in Figures 3.5 and 3.6. [Strictly speaking, raising F_e increases n, and hence the surface donor occupation by virtue of increased recombination traffic. It is assumed that this is understood in the further comments made below.]

The flat parts of the curves can be understood as follows: The Fermi level lies below the donor level in equilibrium. As the Fermi level for electrons detaches itself from the hole quasi-Fermi level with increasing electron-hole pair injection, the effect on the space-charge region is comparatively slight as the donors remain largely ionized. Further injection raises the electron quasi-Fermi level above the donor surface level E_{DS} and the donors begin to fill with electrons. The barrier height then falls with increasing Fermi level separation as was seen before.

The generally larger barrier heights observed in Figure 3.6 above those in Figure 3.5 are due to the greater value of Q_s for the higher donor level (if other things are equal). Note that the position of F_h is not fixed by the value adopted for N_A by virtue of (3.10) and (3.23) is then assumed largely unaltered by electron-hole pair injection in this discussion. This is satisfactory for $F_e - F_h \lesssim 0.5$ eV when the excess hole concentration reaches 10% of the equilibrium concentration, at which point the hole quasi-Fermi level moves slowly down towards the valence band edge.

The depletion approximation is not involved in the present theory, it is used merely for discussion purposes in the form of equations (3.27) and (3.28). Nonetheless it is of interest to estimate the kind of error which can occur by making this approximation. Quite simply, the depletion approximation is equivalent to setting:

$$n(w) = p(w) = 0 \ ,$$

in the left hand side of equation (3.22). A comparison of the two models is given in Figures 3.7 and 3.8. One sees from Figure 3.7 curves (a) and (b) that the depletion approximation (b) overestimates the barrier height by 6% in equilibrium. Using a flat Fermi level and including the space charge contribution from electrons and holes as the present theory of curve (a) does, the barrier height so calculated is exact in equilibrium.

The error in the barrier height calculated by the depletion approximation is expected to be greater when the barrier is low or for very low doping concentrations. Since the charge density is given by

$$q(x) = p(w)\mu(x)^{-1} - n(w)\mu(x) - N_A^- \ ,$$

the depletion approximation calculation will be in error when the contribution to the total space-charge by $n(w)\mu(x)$ is large (i.e. for very large barriers), or when $p(w)\mu(x)^{-1}$ is large (i.e. for small barriers).

Turning to the non-equilibrium steady-state barrier height, curves (a) and (b), the depletion approximation progressively underestimates the space-charge by a larger amount because it neglects the electron contribution and therefore too large a barrier is calculated. In curves (c) and (d), initially the depletion approximation neglects the hole contribution thus overestimating the space-charge, calculating

too small a barrier. As the quasi-Fermi level separation increases, the electron concentration becomes larger until it exceeds the hole concentration; this leads to an overestimate of the barrier height when the depletion approximation is used.

In Figures 3.9 and 3.10 the barrier height is shown as a function of surface donor energy and they indicate again that higher donor levels have a greater degree of ionization leading to larger barriers. The reference energy is chosen to be $E_v(w)$ since this is unaffected by barrier height. As a result, the hole quasi-Fermi level is a fixed vertical line, and the electron quasi-Fermi levels are displaced from it as shown. The straight sloping lines represent the surface band edges; one sees, for example that $E_{vS} - E_v(w)$ becomes more negative as the barrier height increases. In this representation any horizontal (or vertical) distance from E_{cS} to E_{vS} gives the value of the energy gap.

In equilibrium ($F_e = F_h$ curve of Figure 3.9), one sees that as the donor surface energy is raised from a point low in the energy gap, the barrier height increases. However, the degree of ionization of the donor state has only a slight increase (the donor level moves a little closer to the Fermi level in Figure 3.9). From (3.26) using the depletion approximation in the crudest sense, the total space-charge per unit area remains fixed because N_A is constant. Hence, as the donor surface level is raised in the energy gap, the barrier height increases in such a way as to keep $E_{DS} - F_o$ constant and the balancing space charge is constant. Of course, as the barrier height is increased, electrons flow into the space-charge region, holes flow out of it and the surface donors become a little more ionized to balance the increased space-charge.

Turning to any curve of fixed positive $F_e - F_h$, it is seen to consist of three parts each of which may be specified by the two dominant electronic transitions involving the donor surface level. Passing from left to right:

(i) Donor-valence band interactions dominate, so that

$$H(o)p_1 >> G(o)n(o),\ H(o)p(o) >> G(o)n_1 \quad . \tag{3.29}$$

(ii) The downward electronic transitions (i.e. electron and hole capture) dominate, so that

$$G(o)n(o) >> H(o)p_1\ ,\ H(o)p(o) >> G(o)n_1 \quad . \tag{3.30}$$

(iii) Donor-conduction band interactions dominate, so that

$$G(o)n(o) >> H(o)p_1\ ,\ G(o)n_1 >> H(o)p(o) \quad . \tag{3.31}$$

In part (i), ϕ_B follows the equilibrium curve since the conduction band is hardly involved and F_h is fixed. One can see this result mathematically from (3.25),

$$p(w) \doteqdot N_A\ ,\ n(w) \doteqdot (n_i^2 \exp[\gamma_e - \gamma_h])/N_A\ ,$$

thus

$$\nu \doteqdot 1\ ,\ 1-\nu \doteqdot (n_i^2 \exp[\gamma_e - \gamma_h])/N_A^2 \quad .$$

The Fermi level dependence of the second factor of (3.25) is normally negligible because of the small factor n_i^2/N_A^2, while $G(o)n_1$ in the first factor is negligible by the assumption for part (i). Part (iii) is analogous to part (i) with the roles of the conduction band and the valence band reversed. The flatness of part (ii) of the curve is expected from (3.30) and the first factor of (3.25).

The three parts of the curves discussed above lead one to look for a case in which the upward electronic transitions dominate,

$$G(o)n_1 >> H(o)p(o) \ , \ H(o)p_1 >> G(o)n(o) \ . \qquad (3.32)$$

This is indeed realized if $F_e < F_h$ for part (iv) of the curve shown in Figure 3.9.

Complete ionization can be reached in Figure 3.9 only if the surface donor level and the equilibrium Fermi level enter the conduction band. However, complete ionization is possible for the lower surface donor concentration used in Figure 3.10. The flat part of the curves on the right hand side represent this case.

3.6 Approximations for the Barrier Height

Approximate relations for most parts of the curves of Figures 3.3 to 3.14 will be obtained in this section. Considering first equilibrium conditions, as shown in Figure 3.3, an approximate expression for the barrier height in the region to the right (larger N_A) of the maximum has already been obtained by Seager and Castner (1978). It was shown that the barrier height is proportional to $1/N_A$ in this region because the surface donor traps are all ionized.

To the left of the maximum (smaller N_A) in Figures 3.3 and 3.4, the bracketed factor of (3.25) is equal to unity. Equations (3.23) and (3.10) have the approximate solutions

$$p(w) \doteqdot N_A \ , \ n(w) \doteqdot n_i^2/N_A (<< N_A) \qquad (3.33,3.34)$$

and therefore

$$e\phi_B \doteqdot k_B T \ln(N_A/ap_1) + k_B T \ln\left[\left\{(n_i^2/N_A^2)\{\mu(o)-1\}+\{\mu(o)^{-1}-1\}+1n\mu(o)\right\}^{-\frac{1}{2}}-a\right].$$

Using the data of Table 3.1, (also $N_A < 10^{22}\ m^{-3}$ for $N_{DS} > 10^{15}\ m^{-2}$) and a single trap level at mid-gap, one finds $a << 1$. Also, since $n_i^2/N_A^2 << 1$ and $\mu(o) >> 1$ (from Figures 3.3 and 3.4)

$$e\phi_{Bo} \doteqdot k_B T \ln(N_A/ap_1) - (k_B T/2) \ln\{\ln\mu(o)\} .$$

The last term of the above equation is very small in comparison with the first two terms and hence

$$e\phi_{Bo} \doteqdot k_B T \ln(N_A/aN_v) + E_{DS}-E_{vS} . \qquad (3.35)$$

Equation (3.35) explains the straight line regions of Figures 3.3 and 3.4.

For larger N_A, approaching the maximum barrier height value of N_A^{max}, one can rely on (3.33) and (3.34) which enables (3.25) to be recast in equilibrium as

$$\{p_1\mu(o)/N_A+1\}^2[\mu(o)^{-1}-1+\ln\mu(o)] = a^{-2} . \qquad (3.36)$$

The maximum of ϕ_{Bo} in Figures 3.3 and 3.4 can be estimated by differentiating (3.36) with respect to N_A:

$$[\mu(o)^{-1}-1+\ln\mu(o)]\left\{-\frac{2p_1\mu(o)}{N_A^2}[p_1\mu(o)/N_A+1]+\frac{2p_1}{N_A}\frac{d\mu(o)}{dN_A}[p_1\mu(o)/N_A+1]\right\} +$$

$$\left\{p_1\mu(o)/N_A+1\right\}^2[\mu(o)^{-1}-\mu(o)^{-2}]\frac{d\mu(o)}{dN_A} = -\frac{2}{a^3}\frac{da}{dN_A}$$

At the maximum,

$$\frac{d\mu(o)}{dN_A} = 0$$

and from equation (3.24),

$$\frac{da}{dN_A} = \frac{a}{2N_A} \quad ,$$

which yields

$$2p_1\mu(o)N_A^{-1}\left\{p_1\mu(o)N_A^{-1}+1\right\}[\mu(o)^{-1}-1+\ln\mu(o)] = a^{-2} \quad . \qquad (3.37)$$

Dividing (3.37) by (3.36) leaves

$$\frac{p_1\mu(o)N_A^{-1}+1}{2p_1N_A^{-1}\mu(o)} = 1$$

and therefore at the maximum,

$$[\mu(o)]_{max} = N_A^{max}/p_1 \quad .$$

Now, using (3.4) and (3.33) yields

$$[N_v\exp(\eta_{vS}-\eta_{DS}) =]p_1 = \left\{N_A/\mu(o)\right\}_{max}[= N_v\exp(\eta_{vS}-\gamma_o)] \quad . \qquad (3.38)$$

The expressions in square brackets in (3.38) show that the Fermi level lies approximately at the surface donor level for this condition. To calculate $\mu(o)_{max}$, we first obtain N_A^{max}, the doping density which leads to the maximum barrier height; thus (3.37) is recast into an equation for N_A^{max} using (3.38),

$$4\left\{(N_v\exp[\eta_{vS}-\eta_{DS}]/N_A^{max})-1+\ln(N_A^{max}\exp[\eta_{DS}-\eta_{vS}]/N_v)\right\} = a^{-2} \quad .$$

Neglecting $\ln(N_A^{max}/N_v)$ by virtue of (3.33),

$$\left\{\eta_{DS}-\eta_{vS}+(N_v\exp[\eta_{vS}-\eta_{DS}]/N_A max)-1\right\} = 1/4a^2 \quad ,$$

or alternatively using (3.24),

$$N_A^{max} = \frac{(e^2N_{DS}^2/32\varepsilon\varepsilon_o k_B T) - N_v\exp[\eta_{vS}-\eta_{DS}]}{\eta_{DS} - \eta_{vS} - 1} \quad . \qquad (3.39)$$

Using again equation (3.38), the maximum barrier height is given by

$$(e\phi_{Bo})_{max} = k_B T \ln\left\{\frac{(e^2 N_{DS}^2/32\varepsilon\varepsilon_o k_B T N_v)\exp[\eta_{DS}-\eta_{vS}]-1}{\eta_{DS}-\eta_{vS}-1}\right\} \quad . \qquad (3.40)$$

Equations (3.39) and (3.40) are in reasonable agreement with the maxima of Figures 3.3 and 3.4, the error between (3.40) and $(e\phi_{Bo})_{max}$ taken from Figure 3.3 for $N_{DS} = 10^{16}\ m^{-2}$ is 4.5%.

Turning now to non-equilibrium, Figures 3.5 to 3.10, some additional results can be derived. These relations are obtained in a similar way to (3.35). In addition, equations (3.36) to (3.38) are used to simplify the second factor of (3.24). These results can be used to understand the curves of Figures 3.5 to 3.10.

Considering the steep region (i) of Figures 3.9 and 3.10, we have the inferred condition of (3.29) because E_{DS} is low in the energy gap. These conditions are inapplicable to Figures 3.5 and 3.6. Using (3.29) the second factor of (3.25) is unity. Equation (3.23) has the approximate solutions

$$p(w) \doteqdot N_A \ , \ n(w) = n_i^2 \exp[\gamma_e-\gamma_h]/N_A << N_A \qquad (3.41,\ 3.42)$$

in low injection. Thus, one again finds (3.35) for the barrier height,

$$e\phi_B \doteqdot e\phi_{Bo} \doteqdot k_B T \ln(N_A/aN_v) + E_{DS} - E_{vS} \ .$$

From equation (3.18), using (3.29), (3.23) and (3.10) as above, the recombination rate U_s is given approximately by

$$U_s \doteqdot \frac{G(o)H(o)N_{DS}n_i^2(\exp[\gamma_e-\gamma_h]-1)}{H(o)\{N_A/\mu(o)+p_1\}} \ .$$

Utilizing the form of $\mu(o)$ given by (3.35),

$$U_S \doteqdot G(o)N_{DS}n_1(\exp[\gamma_e-\gamma_h]-1)/(a+1) \ .$$

The surface recombination velocity in this case is given by (3.19) where the number of excess electrons is

$$n_e(o) = (n_i^2/N_A)(\exp[\gamma_e-\gamma_h]-1)\mu(0)$$

Using equation (3.42), but from (3.35)

$$\mu(o) = N_A/ap_1$$

and hence

$$s(o) = G(o)N_{DS}\ a/(a+1) \ . \qquad (3.43)$$

Similarly, the recombination current $J(o)$ was given by (3.20), which in this case is

$$J(o) = eG(o)N_{DS}n_1\{\exp(\gamma_e-\gamma_h)-1\}/2(a+1) \ .$$

Note, the units of U_S are $m^{-2}s^{-1}$, of $s(o)$ are ms^{-1} and $J(o)$ has units Am^{-2} in the S.I. system.

Turning to the flat regions (ii) of Figures 3.9 and 3.10, the conditions of (3.30) are inferred because E_{DS} is near mid-gap. This set of conditions also applies to figure 3.5 for $F_e-F_h > 0.3$ eV when $N_{DS} > 10^{16}m^{-2}$. Taking high enough carrier injection, the second factor of (3.25) (in round brackets) is approximately

$$H(o)N_A/G(o)n_1\mu(o)\exp[\gamma_e-\gamma_h] \ .$$

Thus

$$\mu(o)^2 \doteqdot \frac{H(o)N_A^2}{aG(o)n_i^2\exp[\gamma_e-\gamma_h]}\cdot\left[\frac{1}{\left\{(1-\nu)\{\mu(o)-1\}+\nu\{\mu(o)^{-1}-1\}+\ln\mu(o)\right\}^{\frac{1}{2}}}-a\right] .$$

Again, appealing to

$$a << 1,\ n_i^2\exp[\gamma_e-\gamma_h]/N_A^2 << 1 ,$$

and neglecting the third factor of (3.25) (in square brackets) on taking logarithms because

$$\ln\mu(o) << \mu(o) ,$$

the barrier height for an energy level of donor traps near mid-gap is given approximately by

$$e\phi_B \doteqdot (k_BT/2)\ln\{H(o)N_A^2/aG(o)n_i^2\} - (F_e-F_h)/2 . \qquad (3.44)$$

Equation (3.44) is similar to equation (17) of Fossum and Lindholm (1980a) but has an extra factor of a . This factor provides closer agreement of the approximate result with a detailed solution of (3.25) under the appropriate conditions. Equation (3.44) applies only to the non-equilibrium steady-state. The recombination rate (3.18) using the conditions of (3.30)is approximately

$$U_S \doteqdot \frac{G(o)H(o)n_i^2\{\exp[\gamma_e-\gamma_h]-1\}N_{DS}}{G(o)n(w)\mu(o)+H(o)p(w)\mu(o)^{-1}}$$

and hence using (3.44)

$$U_S \doteqdot \frac{\{G(o)H(o)\}^{\frac{1}{2}}n_i\{\exp[\gamma_e-\gamma_h]-1\}N_{DS}}{\exp\{(\gamma_e-\gamma_h)/2\}/a^{\frac{1}{2}}+a^{\frac{1}{2}}\exp\{(\gamma_e-\gamma_h)/2\}} .$$

Dividing throughout by $a^{-\frac{1}{2}}\exp(\gamma_e-\gamma_h)/2$ yields

$$U_S = 2N_{DS}\{G(o)H(o)\}^{\frac{1}{2}}n_i a^{\frac{1}{2}}\sinh\{(\gamma_e-\gamma_h)/2\}/(a+1) . \qquad (3.45)$$

Assuming the carrier injection creates equal concentrations of excess electrons and holes, i.e.

$$n_e(o) = n(o) - n_o(o) = p(o) - p_o(o) \ , \tag{3.46}$$

thus,

$$n(o)p(o) - n_i^2 = \{n_o(o) + p_o(o) + n_e(o)\}n_e(o) \ .$$

Then the recombination velocity at the grain boundary using equation (3.19) is

$$s(o) = \frac{G(o)H(o)N_{DS}\{n_o(o)+p_o(o)+n_e(o)\}}{G(o)\{n_o(o)+n_e(o)+n_1\}+H(o)\{p_o(o)+n_e(o)+p_1\}} \tag{3.47}$$

Letting the number of excess carriers tend to zero defines, in the limit, an equilibrium surface recombination velocity,

$$s_o(o) = \frac{G(o)H(o)N_{DS}\{n_o(w)\mu_o(o)+p_o(w)\mu_o(o)^{-1}\}}{G(o)\{n_o(w)\mu_o(o)+n_1\}+H(o)\{p_o(w)\mu_o(o)^{-1}+p_1\}} \ . \tag{3.48}$$

Utilizing the conditions of (3.30) for a trap near mid-gap, and (3.35) for the barrier height, the recombination velocity at the grain boundary near equilibrium is

$$s_o(o) = \frac{G(o)H(o)N_{DS}\{n_1 a^{-1}+ap_1\}}{G(o)n_1 a^{-1}+H(o)p_1 a} \ . \tag{3.49}$$

Equation (3.48) is quite general, and may be used for a donor surface level at any energy in the band-gap, providing $\mu_o(o)$ is known. In particular, for a donor level near the valence band edge, the conditions of (3.29) allow one to use equation (3.35) for $\mu_o(o)$ and (3.48) gives again the recombination velocity of equation (3.43).

Away from equilibrium, equation (3.47) is needed for the steady-state recombination velocity. For a donor level near mid-gap, equations (3.44) and (3.35) are used for the barrier heights, (3.46) for the number of excess carriers and (3.10) for $n(w)$, thus

$$n_e(0) = n(w)\mu(0) - n_o(w)\mu_o(0) = \frac{n_i^2}{N_A}\exp[\gamma_e - \gamma_h]\left(\frac{H(0)}{aG(0)}\right)^{\frac{1}{2}}\frac{N_A}{n_i}\exp[(\gamma_h - \gamma_e)/2] - \frac{n_i^2}{N_A}\frac{N_A}{ap_1} ,$$

noting equation (3.44) yields the non-equilibrium steady-state barrier height and equation (3.35) yields the equilibrium barrier height.

A little simplification of the excess carrier density gives

$$n_e(0) = n_i \exp[(\gamma_e - \gamma_h)/2]\{H(0)/aG(0)\}^{\frac{1}{2}} - n_1 a^{-1} .$$

Thus, the recombination velocity (3.47) in the steady-state, utilizing the conditons of (3.30) and $n_e(0)$ above, is

$$s(0) \doteq \frac{G(0)H(0)N_{DS}\{n_i\exp[(\gamma_e - \gamma_h)/2]\{H(0)/aG(0)\}^{\frac{1}{2}} + ap_1\}}{\{G(0)H(0)/a\}^{\frac{1}{2}}n_i\exp[(\gamma_e - \gamma_h)/2] + \{G(0)H(0)a\}^{\frac{1}{2}}n_i\exp[\gamma_e - \gamma_h)/2]}$$

Dividing the denominator and numerator by $n_i\exp[(\gamma_e - \gamma_h)/2]\{G(0)H(0)a^{-1}\}^{\frac{1}{2}}$,

$$s(0) \doteq \{G(0)H(0)a\}^{\frac{1}{2}}N_{DS}\{(H(0)/aG(0))^{\frac{1}{2}} + ap_1 n_i^{-1}\exp[\gamma_h - \gamma_e)/2]\}/(a+1) ,$$

and utilizing equations (3.44) and (3.35), the non-equilibrium steady-state grain boundary recombination velocity is

$$s(0) \doteq N_{DS}\{H(0) + aG(0)\mu(0)\mu_0(0)^{-1}\}/(a+1) , \qquad (3.50)$$

for a donor surface level near mid-gap. The recombination current density from equation (3.20) and (3.45) is

$$J(0) \doteq en_i N_{DS}\{G(0)H(0)a\}^{\frac{1}{2}}\sinh[\gamma_e - \gamma_h)/2]/(a+1) . \qquad (3.51)$$

Considering the steep regions (iii) for Figures 3.9 and 3.10, the conditions of (3.31) are inferred because the donor surface level is high in the energy-gap. These conditions also apply to Figure 3.6 for $N_{DS} > 10^{16} m^{-2}$. For low enough injection, the round bracketed factor of (3.25) is equal to $\exp[\gamma_h - \gamma_e]$ and also,

$$p(w) \doteqdot N_A \ , \ a << 1 \ , \ n(w) = n_i^2 \exp[\gamma_e - \gamma_h]/N_A << N_A \ ,$$

hence,

$$\mu(0) \doteqdot \frac{N_A}{ap_1 \exp[\gamma_e - \gamma_h]} \left[\frac{1}{\{(1-\nu)(\mu(0)-1)+\nu(\mu(0)^{-1}-1)+\ln\mu(0)\}^{\frac{1}{2}}} - a \right] \ .$$

The third factor of (3.25) [in square brackets here] is neglected on taking logarithms because its largest term is $\ln[\ln\mu(0)]/2$ which is much less than $\mu(0)$. Thus,

$$e\phi_B \doteqdot k_B T \ln(N_A/aN_v) + E_{DS} - E_{vs} + F_h - F_e \ , \qquad (3.52)$$

is the approximate barrier height for a donor level near the conduction band edge and in the grain boundary surface. Note that this equation is the same as (3.35) in equilibrium, which confirms the extended region (i) in Figures 3.9 and 3.10 for equilibrium. In the steady-state, the barrier height in region (iii) is identical in shape to region (i), but it is displaced by $F_e - F_h$ as equation (3.52) confirms.

Utilizing (3.31), the recombination rate (3.18) is given by

$$U_s \doteqdot \frac{G(0)H(0)N_{DS}n_i^2\{\exp[\gamma_e - \gamma_h]-1\}}{G(0)\{n(w)\mu(0)+n_1\}} \ .$$

The barrier height expression (3.52) and also (3.42) for $n(w)$ yield

$$U_s \doteqdot H(0)N_{DS}ap_1\{\exp[\gamma_e - \gamma_h]-1\}/(a+1) \ . \qquad (3.53)$$

In a similar way, the surface recombination velocity (3.47) at the grain boundary under the conditions (3.31) is obtained,

$$s(0) \doteqdot \frac{G(0)H(0)N_{DS}\{ap_1+(n_i^2/N_A)\exp[\gamma_e - \gamma_h](N_A/ap_1)\exp[\gamma_h - \gamma_e]\}}{G(0)\{(n_i^2/N_A)\exp[\gamma_e - \gamma_h](N_A/ap_1)\exp[\gamma_h - \gamma_e]+n_1\}} \ ,$$

where (3.42), (3.52) have been used. Dividing throughout the above expression by $G(0)n_1$,

$$s(0) \doteqdot \frac{H(0)N_{DS}\{ap_1/n_1+1/a\}}{\{1/a+1\}} \ . \qquad (3.54)$$

It is interesting to note that for energy levels of donor states low in the energy gap or high in the energy gap the approximate forms, (3.43) and (3.54) respectively, for the grain boundary recombination velocity are independent of the quasi-Fermi level separation in the

steady-state. For a trap level near mid-gap, the grain boundary recombination velocity (3.50) is a weak function of the quasi-Fermi level separation.

The recombination current density (3.20) is given by

$$J(0) \doteqdot eap_1 H(0) N_{DS} \{\exp[\gamma_e - \gamma_h] - 1\}/2(a+1) \qquad (3.55)$$

for a trap level high in the energy gap, where equation (3.54) has been used.

3.7 Comparison with Experiments

The theory of Section 3.4 has been used to fit some recent experimental results. In each case it is necessary to obtain values for the parameters required by equation (3.25). Where this data has not been supplied by the authors of the experimental work, the accepted values for silicon have been used and are given in Table 3.1.

In Figures 3.11 and 3.12 each experimental point corresponds to a differently doped sample, but nonetheless the present theory has been used in Figure 3.12 with a single value of the surface state density and energy position and, in Figure 3.11, with <u>two</u> values of surface state density (at one and the same level). The reason is that there is a greater spread of values in Figure 3.11 so that de Graaff and his co-authors (1982) have also used two theoretical curves to fit the data. They chose one surface state density and two different energy levels.

The satisfactory fit represents an experimental check on the theoretical curves of Figures 3.3 and 3.4. Note that only one type of surface state - donors on a p-type grain or acceptors on an n-type grain has been used. This removes one additional fitting parameter arising from the possibility of both donor and acceptor states being at the same level, as for example in Seager and Castner,(1978). Also, the depletion approximation was not used here.

We turn lastly in this section to non-equilibrium barrier heights as a function of illumination (Figures 3.13, 3.14). The satisfactory fit here represents an experimental check on the theoretical curves of Figures 3.5 and 3.6. The experimental results of Figure 3.13 have been fitted equally well by Seager (1981) using diffusive transport and an

infinite grain boundary recombination velocity. It is interesting that such good fits are possible based on such different premises.

For a general explanation of the curves, see Section 3.5.

The numerical data of Seager (1981) and Card et al., (1982) for the generation rate by illumination was given in the units of suns and Wm^{-2} respectively. It is necessary to convert this data into an equivalent separation of Fermi levels. For the data of Seager (1981), equation (2.3) there was used to find the number of minority carriers (holes in an n-type grain) at the edge of the depletion region, and this equation is

$$p(w) = p_\infty \frac{\sqrt{\pi}}{e} \left(\frac{\varepsilon\varepsilon_o}{eN_D}\right)^{\frac{1}{2}} \frac{(k_B T)^{\frac{1}{2}}}{x_L} . \qquad (3.56)$$

Here p_∞ is the number of holes at infinity,

$$p_\infty = L\tau ,$$

Where L is the uniform generation rate of carriers ($m^{-3}S^{-1}$) and τ is the lifetime(s). Also, N_D is the number of donors in the bulk and x_L is the diffusion length (m). Equation (23) of Seager was obtained by solution of the minority carrier diffusion equation with uniform generation rate in an infinite half plane of a silicon bicrystal. From (3.56) and (3.10) the separation of the Fermi levels is obtained, using also

$$n(w) \doteq N_D \qquad (3.57)$$

The following numerical data from Seager (1981) was adopted: generation rate $L = 10^{26} m^{-3}S^{-1}$ for 1 sun, lifetime $\tau = 10^{-7}$s , diffusion length $x_L = 10^{-6}$m , and number of donors, $N_D = 1.3 \times 10^{22}\ m^{-3}$.

Calculation of the Fermi level separation for Figure 3.14 involves converting the power density

$$p = h\nu N_o$$

where N_o is the number of incident photons and $h\nu$ the energy of a single photon, into an equivalent number of photo-generated carriers using

$$n(w) = \alpha N_o \tau \frac{\sqrt{\pi}}{e}\left[\frac{\varepsilon\varepsilon_o}{eN_A}\right]^{1/2} \frac{(k_B T)^{1/2}}{x_L} .$$

Again, Seager's (1981) equation (23) was used to find $n(w)$ and hence the Fermi level separation by (3.10). In this case, $N_A = 3 \times 10^{21} m^{-3}$ was used. Throughout the work of this section, all other data was taken from Table 3.1.

3.8 A Simple Surface State Spectrum

Some recent experimental work (Sah, 1976, Singh and Srivastava, 1983) has examined the surface-state energy levels at the interface between between the oxide and semiconductor layers of MOS devices. In general, the distribution of states found in U-shaped (Sah, 1976, Herman and Kazowski, 1981, Nicollian, 1977) with more states near the band edges than in the centre of the energy gap. Few authors (Brown and Gray, 1968) have indicated which levels are donor-type and which are acceptor-type in their results. In the absence or any firm results for the distribution of surface states at a grain boundary, one can only postulate that similar results to the above will be found. The nearest approximation to the U-shaped distribution for which the right-hand side of equation (3.22) for the barrier height can be integrated is the constant distribution of energy levels (Chapter 2, Section 2.5).

Introducing constant distributions N_{DS} of donor states and N_{AS} of acceptor states, and the probability of occupation $f(E_S, e\phi_B)$ from equation (3.9), the charge on the grain boundary surface per unit area is by equation (3.8),

$$Q_s = eN_{DS}(E_{cS}-E_{vS}) - \int_{E_{vS}}^{E_{cs}} \frac{e(N_{DS}+N_{AS})[G(O)n(w)\mu(O)+H(O)p_1(E_S)]dE_S}{G(O)[n(w)\mu(O)+n_1(E_S)]+H(O)[p(w)\mu(O)^{-1}+p_1(E_S)]}. \quad (3.58)$$

To integrate equation (3.58), it is useful first to change variables to:

$$z \equiv \exp(\eta_s-\eta_{vS}),\ A \equiv G(O)N_c\exp(-\eta_G),\quad B \equiv G(O)n(w)\mu(O)\ ,$$

$$C \equiv H(O)p(w)\mu(O)^{-1}\ ,\ D \equiv H(O)N_v\ .$$

Then one has

$$Q_S = eN_{DS}E_G - \int_1^{\exp\eta_G} \frac{e(N_{DS}+N_{AS})Bz+D)k_BTdz/z}{Az^2+(B+C)z+D}\ . \quad (3.59)$$

Completing the square in the denominator of (3.59):

$$Q_S = eN_{DS}E_G - \int_1^{\exp\eta_G} \frac{e(N_{DS}+N_{AS})(B+Dz^{-1})k_BTdzA^{-1}}{[z+(B+C)/2A]^2-\beta^2/4A^2} \qquad (3.60)$$

where

$$\beta^2 \equiv (B+C)^2 - 4AD \ .$$

Factorizing the denominator of (3.60),

$$Q_S = eN_{DS}E_G - \int_1^{\exp\eta_G} \frac{ek_BT(N_{DS}+N_{AS})(B+Dz^{-1})dz}{\beta} \left\{\frac{1}{z+(B+C-\beta)/2A} - \frac{1}{z+(B+C+\beta)/2A}\right\} \ .$$

One can then factorize the numerator and integrate the terms containing β in the numerator,

$$Q_S = eN_{DS}E_G - \frac{e(N_{DS}+N_{AS})k_BT}{\beta}\left[\ln\left\{\frac{2Az+B+C-\beta}{2Az+B+C+\beta}\right\}\right]_1^{\exp\eta_G} +$$

$$\frac{e(N_{DS}+N_{AS})k_BT}{\beta} \int_1^{\exp\eta_G} \frac{Ddz}{z} \left\{\frac{1}{z+(B+C-\beta)/2A} - \frac{1}{z+(B+C+\beta)/2A}\right\} \ .$$

Continuing to separate the remaining integral into partial fractions

$$Q_S = eN_{DS}E_G - \frac{e(N_{DS}+N_{AS})k_BTB}{\beta}\left[\ln\left\{\frac{2Az+B+C-\beta}{2Az+B+C+\beta}\right\}\right]_1^{\exp\eta_G} +$$

$$+ \frac{e(N_{DS}+N_{AS})Dk_BT}{\beta} \int_1^{\exp\eta_G} \left\{\left(\frac{1}{z+(B+C-\beta)/2A} - \frac{1}{z}\right)\frac{2A}{(B+C-\beta)} + \left(\frac{1}{z} - \frac{1}{z+(B+C+\beta)/2A}\right)\frac{2A}{(B+C+\beta)}\right\}dz$$

Integrating the latter terms and rearranging,

$$Q_S = eN_{DS}E_G - \frac{e(N_{DS}+N_{AS})k_BT}{2}\left[\frac{(B-C)}{\beta}\ln\left(\frac{2Az+B+C-\beta}{2Az+B+C+\beta}\right) + \ln\left(\frac{Az^2+(B+C)z+D}{Az^2}\right)\right]_1^{\exp\eta_G} \ ,$$

and finally,

$$Q_S = eN_{AS}E_G - \frac{e(N_{DS}+N_{AS})k_BT}{2}\left[\frac{(B-C)}{\beta}\ln\left\{\frac{2A\exp\eta_G+B+C-\beta}{2A\exp\eta_G+B+G+\beta}\,\frac{2A+B+C+\beta}{2A+B+C-\beta}\right\} + \ln\right.$$

$$\left. + \ln\left\{\frac{A\exp 2\eta_G+(B+C)\exp\eta_G+D}{A+B+C+D}\right\}\right] \qquad (3.61)$$

The equation (3.22) for the barrier height, ϕ_B, in the presence of a constant distribution of states becomes

$$n(w)\{\mu(0)-1\}+p(w)\{\mu(0)^{-1}-1\}+N_A\left\{\ln\mu(0)-\ln\left[\frac{\exp[\eta_A(w)-\gamma_h]+1}{\mu(0)^{-1}\exp[\eta_A(w)-\gamma_h]+1}\right]\right\} = \frac{eQ_S^2}{8\epsilon\epsilon_o k_B T}, \quad (3.62)$$

where Q_s is given by equation (3.61). Equations (3.61) and (3.62) when combined, yield a transcendental equation for the barrier height in the case of a constant distribution of levels. The process for solving this equation follows exactly the process for obtaining solutions to equation (3.25) when a single donor level in the surface was considered.

Sample thoeretical curves are shown in Figures 3.15 for equilibrium and 3.16 for the steady-state. In Figure 3.15 donor surface states only are used. One sees the general shape of the curves in equilibrium is similar to Figures 3.3 and 3.4. However, to the right of the maximum barrier height (larger N_A), the barrier height falls less rapidly than it did for a single level of donor states. This is because not all of the higher lying donor states are filled unlike the case when a single level of donors near mid-gap was used (see Section 3.5).

In Figures 3.16, the barrier height falls with increasing Fermi level separation. The reason is broadly that electron injection into the bulk region begins to fill the surface traps with electrons and thus the positive surface charge on the donor traps decreases. This decrease in Q_s in turn leads to a decrease in the space-charge region width and hence in ϕ_B. For a complete description of the nature of Figure 3.16, which is similar to Figures 3.5 and 3.6, see Section 3.5.

As an experimental test of this theory in equilibrium, comparison is made with the results of Seager and Castner (1978) and de Graaff et al., (1982) and is shown in Figures 3.17 and 3.18. In Figure 3.17 donor and acceptor states were used, but in Figure 3.18 donor states only were used. The slower decrease of the barrier height with N_A increasing beyond the maximum barrier, with a distribution of donor states (curve a), than the fall of ϕ_B with a single level of donors (curve b), allows a better fit to the experimental data.

In the steady-state, the procedure of Section 3.7 is followed to convert experimental data (Wu and Bube, 1974) of the barrier height in CdS evaporated thin films as a function of the quasi-Fermi level separation. In Figure 3.19 is shown the barrier height using the data of Table 3.2 for CdS. It is interesting to find good agreement in a different material and further substantiates the use of a distribution of acceptor states in the grain boundary.

3.9 Some Applications for the Barrier Height Calculation

In the present work, the barrier height has been calculated at a grain boundary as a function of the obvious parameters (N_A, E_{DS}, N_{DS}). The barrier height is an important parameter in the study of grain boundary recombination (Fossum and Lindholm, 1980a, Seager, 1981) and of thermionic emission-diffusion currents over the barriers (Seager and Castner, 1978, Baccarani et al., 1978a).

The barrier height at a grain boundary is not an item which can be directly measured by experiment, it is calculated from measurements of resistivity, conductivity and Hall-effect mobility (Orton and Powell, 1980). In MOS devices (Ando et al., 1982) the potential barrier at the interface between the oxide and semiconductor layers is calculated from capacitance or conductance measurements. This section calculates the grain boundary or surface barrier height as a function of (a) mobility and (b) capacitance. This allows comparison of the present work with resistivity measurements in polysilicon (Ghosh et al., 1980, Seto, 1975) and also shows how the mobility and capacitance depend on the basic parameters (N_A,E_{DS},N_{DS}).

(a) Mobility and Resistivity in Polysilicon

The "over-the-barrier" current is calculated using Thermionic emission-diffusion theory for two barriers back-to-back with a recombination plane separating them. This approach is derived from the condition of a thermionic recombination velocity v_R near the interface. The configuration of the potential barriers with an applied voltage V is shown in Figure 3.20 for a p-type semiconductor, the origin of the barriers in equilibrium has been considered in the previous section.

Throughout the barrier regions between $x = 0$ and $x = w_2$, the edge of the barrier region, and between $x = -w_1$ and $x = 0$ as in Figure 3.20, the hole current density is given by

$$J = \upsilon p(x) \frac{dF_h}{dx} \tag{3.63}$$

(see for example, Sze, 1969) where υ is the mobility and $p(x)$ is the hole concentration

$$p(x) = N_v \exp[\eta_v - \gamma_h] \ . \tag{3.64}$$

The current flow is described also by an effective recombination velocity v_R at the potential barrier maximum:

$$J = ev_R(p_m - p_o) \tag{3.65}$$

where p_m is the total hole density at $x = 0$ when the current is flowing, also p_o is the equilibrium hole density at $x = 0$. Thus, for non-degeneracy,

$$p_m = N_v \exp[\eta_v(0) - \gamma_h(0)] \ , \tag{3.66}$$

and p_o is given by

$$p_o = N_v \exp[\eta_v(w_2) - \gamma_h(w_2)] \exp[-e\phi_{Bo}/k_B T]$$

or

$$p_1 = N_v \exp[\eta_v(-w_1) - \gamma_h(-w_1)] \exp[-e\phi_{Bo}/k_B T] \ .$$

Evaluating (3.63) at general x together with (3.64) to eliminate $p(x)$, one has

$$\frac{J \exp[-\eta_v(x)]}{\upsilon N_v k_B T} = \exp[-\gamma_h(x)] \frac{d\gamma_h}{dx} \ .$$

Integrating this equation from $x = -w_1$ to $x = 0$ yields

$$-J/(eN_v v_{D1}) = \exp[\eta_v(0)-\gamma_h(0)]-\exp[\eta_v(0)-\gamma_h(-w_1)]$$

where an effective diffusion velocity is defined by

$$v_{D1}^{-1} \equiv -\int_{-w_1}^{o} (e/\upsilon k_B T)\exp[\eta_v(0)-\eta_v(x)]dx \ .$$

Utilizing equation (3.66), the hole current density is given by

$$-J/(eN_v v_{D1}) = -\exp[\eta_v(-w_1)-\gamma_h(-w_1)]\exp\{-e\phi_{B1}/k_B T\}+p_m/N_v$$

where ϕ_{B1} is the barrier height between $x = -w_1$ and $x = 0$ in the steady-state. Hence, by equation (3.65)

$$\frac{J}{ev_{D1}} = -\frac{J}{ev_R} + n_o\{\exp(e\phi_{Bo}-e\phi_{B1})/k_B T-1\}$$

and finally

$$J = \frac{ep_o v_R}{1+v_R/v_{D1}} \{\exp(e\phi_{Bo}-e\phi_{B1})/k_B T-1\} \ . \qquad (3.67)$$

The corresponding current flow over the barrier region for $0 =< x < x_2$ is

$$J = -\frac{ep_o v_R}{1+v_R/v_{D2}} \left\{\exp(e\phi_{Bo}-e\phi_{B2})/k_B T-1\right\}$$

where ϕ_{B2} is the barrier height and where

$$v_{D2}^{-1} \equiv -\int_{o}^{w_2} \frac{e}{k_B T} \exp\{\eta_v(0)-\eta_v(x)\}dx \ .$$

Near equilibrium, one makes the assumption that

$$v_D \equiv v_{D1} \doteqdot v_{D2} \ ;$$

the net current flow from left to right in Figure 3.20 is

$$J = \frac{ep_o v_R \exp(e\phi_{Bo}/k_B T)\{\exp(-e\phi_{B1}/k_B T) - \exp(-e\phi_{B2}/k_B T)\}}{1+v_R/v_D} \ .$$

Assuming that the applied voltage is equal to the difference of the two steady-state barriers, i.e.

$$V = \phi_{B2} - \phi_{B1}$$

as in Figure 3.20, then near equilibrium $(w = w_1 \doteqdot w_2, \ \phi_{B2} \doteqdot \phi_{B1} \doteqdot \phi_{Bo})$

$$J \doteqdot \frac{ep(w)\exp(-e\phi_{Bo}/k_B T) v_R \{\exp(eV/k_B T) - 1\}}{1+v_R/v_D} \qquad (3.68)$$

where equation (3.4) has been used for p_o .

If the diffusion velocity is very much larger than the recombination velocity, the thermionic emission dominates the current, i.e.

$$J = ep(w) \left(\frac{A^* T^2}{eN_v}\right) \exp(-e\phi_{Bo}/k_B T)\{\exp(eV/k_B T) - 1\} \qquad (3.69)$$

where the recombination velocity is given by

$$v_R \equiv \left(\frac{A^* T^2}{eN_v}\right) \qquad (3.70)$$

and $A^* (\equiv 4\pi e m_v^h k_B^2/h^3)$ is the effective Richardson constant (Sze, 1969). However, if the diffusion velocity, v_D , is much smaller than the recombination velcoty, v_R , then the diffusion of carriers in the barrier limits the current flow. Near equilibrium the diffusion velocity is equal to the drift velocity of holes (see Chapter 5, Section 5.2), i.e.

$$v_D \doteqdot \upsilon|\underline{E}|$$

where $|\underline{E}|$ is the modulus of the electric field in the barrier. Thus the diffusion current over the barrier is

$$J = ep(w)\upsilon|\underline{E}|\exp[-e\phi_{Bo}/k_BT]\{\exp[eV/k_BT - 1\}. \qquad (3.71)$$

In summary, equation (3.68) calculates an excess current density, J , which is a synthesis of a diffusion current and an emission current. It predicts a current in agreement with thermionic emission in equation (3.69) if $v_D/v_R >> 1$ and a current in agreement with diffusion theory in equation (3.71) when $v_D/v_R << 1$. If the grain boundary barrier height is large, there is a large electric field, $\underline{E}$, and the diffusion velocity is large. Under these conditions, thermionic emission currents dominate. Conversely, if the barrier is small, the diffusion current will dominate.

For very small voltages, $V(<< k_BT/e)$, across the grain boundary space-charge region, the exponential on the right hand side of the equation (3.68) may be expanded (Seto, 1975):

$$J \doteqdot \frac{e^2p(w)v_RV\exp[-e\phi_{Bo}/k_BT]}{k_BT(1+v_R/v_D)} \quad . \qquad (3.72)$$

This leads to an Ohmic current voltage relationship for very small voltages and a barrier resistance may be defined by

$$J = V/R_B \quad .$$

The resistivity of the barrier region near equilibrium is therefore

$$\rho_B = R_B/2w$$

and thus

$$\rho_B = k_B T(1+v_R/v_D)\exp(e\phi_{Bo}/k_B T)\{e^2 p(w) v_R 2w\}^{-1} \quad . \tag{3.73}$$

The total crystal resistivity, ρ , of the polycrystalline semiconductor is the sum of the barrier resistivity, ρ_B , and the bulk resistivity, ρ_c , and is given by

$$\rho = 2\rho_B w/\ell + \rho_c(1-2w/\ell) \tag{3.74}$$

where ℓ is the grain size.

Experimental measurements of the resistivity of p-type polysilicon have been performed by Seto (1975), these results are repeated here as crosses in Figure 3.21. These results were explained by Seto (1975) with a model of the barrier height using the depletion aprpoximation (curve b of Figure 3.21). The barrier heights inferred by Seto from his resistivity measurements are large enough that the diffusion velocity, V_D $(= \upsilon\phi_{Bo}/w)$, is greater than the effective recombination velocity and hence thermionic emission currents dominate diffusion. The largest contribution to the resistivity, ρ, is made by the barrier resistivity because the grain size, ℓ , is very small. Thus, the resistivity is given by

$$\rho \doteqdot Nk_B\exp(e\phi_{Bo}/k_B T)\{eN_A A^* T\ell\}^{-1} \tag{3.75}$$

where equations (3.70), (3.73) and (3.74) have been used and also equation (3.33) is used to obtain the majority carrier density at the edge of the barrier. Equation (3.75) together with equation (3.25) for the barrier height with a single donor level are used to calculate the resistivity as a function of N_A in Figure 3.21 curve a. In addition to the parameters of Table 3.1, the following data was needed: $T = 300K$, $m_v^h = 0.52m_o$, $\ell = 200\ \mathring{A}$, $E_{DS} - E_{vS} = 0.44eV$, and $N_{DS} = 2.40 \times 10^{16} m^{-2}$, where m_o is the electron rest mass. Again,

the present theory yields reasonable agreement with the experimental results. One would expect closer agreement of the present theory with experiment than when the depletion approximation is used to calculate the barrier height because the approximation of a flat Fermi level used here is exact in equilibrium.

The barrier region conductivity, σ_B , and mobility , υ_B , are given in terms of the resistivity by

$$\sigma_B = 1/\rho_B \tag{3.76}$$

and

$$\upsilon_B = \sigma_B/ep(w) \ . \tag{3.77}$$

The effective mobility, υ , is determined by the barrier, υ_B , and bulk, υ_c , mobilities by

$$\upsilon = 1/(\upsilon_B^{-1}+\upsilon_c^{-1}) \ .$$

One can write the diffusion coefficient, D , in terms of the mobility using the Einstein relation

$$D = \upsilon k_B T/e$$

and the diffusion length is given by

$$L \equiv (D\tau)^{\frac{1}{2}} = (\upsilon k_B T\tau/e)^{\frac{1}{2}}$$

Hence, the effective diffusion length in polycrystalline seminconductors is

$$L = \left\{\frac{\tau\upsilon_c\upsilon_B k_B T}{e(\upsilon_c+\upsilon_B)}\right\}^{\frac{1}{2}} \tag{3.78}$$

The mobility in the barrier region is given by equations (3.75), (3.76) and (3.77):

$$\nu_B = (A^*T^2\ell/ N_c)\exp(-e\phi_{Bo}/k_BT)$$

The diffusion length L is then by equation (3.78):

$$L = \left\{\frac{(\tau\nu_c A^*T^2\ell/eN_c)\exp(-e\phi_{Bo}/k_BT)}{\nu_c+(A^*T^2\ell/N_c)\exp(-e\phi_{Bo}/k_BT)}\right\}^{\frac{1}{2}} \quad . \qquad (3.79)$$

In Figure 3.22, curve I shows the diffusion length calculated from equation (3.79) using the data of Table 3.1 together with the following parameters: τ = 1.0 μs, ν_c = 1300 $cm^2V^{-1}s^{-1}$, m_v^h = 0.52 m_o, T = 300K, $e\phi_{Bo}$ = 0.18 eV , where m_o is the electron rest mass. The diffusion length as a function of grain size, ℓ , has been measured by Ghosh et al., (1980) and the experimental results (circles and triangles) are shown in Figure 3.22. Also shown is the existing theory, curve II is calculated using an effective barrier mobility and curve III is calculated using an effective lifetime and effective mobility. The effective lifetime (Ghosh et al., 1980) is calculated by assuming that the grain boundary recombination centres can be smeared throughout the bulk and then the single crystal theory is utilised.

(b) Capacitance at a Grain Boundary

Taylor, Odell and Fan (1952) were the first to study the capacitanc3 of a grain boundary. In their work, the effects of temperature and applied voltage on the capacitacne were used to measure the barrier height. In the study of surface states in MOS devices, deep level transient spectroscopy (Singh and Srivastava, 1983) and capacitance (Ando et al., 1982) have been used to obtain information about the number and energy distribution of traps. These techniques were used recently

to examine the surface states at a grain boundary (Shyu and Cheng, 1982; Spencer et al., 1983; Werner et al., 1982).

The capacitance per unit area of a grain boundary has contributions from the two space-charge regions on either side of the boundary, and is given by

$$\frac{1}{C} = \frac{1}{C_1} + \frac{1}{C_2} \ . \tag{3.80}$$

Here, C_1 and C_2 are the differential capacitances defined by

$$C_1 \equiv \frac{\partial q_1}{\partial \phi_{B1}} \ , \ C_2 \equiv \frac{\partial q_2}{\partial \phi_{B2}} \tag{3.81}$$

where $q_1, -q_2$ are the space-charges per unit area of the grain boundary in each of the barriers and ϕ_{B1}, ϕ_{B2} are the barrier potentials.

In equilibrium or under steady-state illumination the barrier heights are the same, i.e.

$$\phi_{B1} = \phi_{B2} = \phi_B \ .$$

and the barriers contain the same space-charge density

$$q_1 = q_2 = q_B \ .$$

Thus, the grain boundary capacitance is

$$C = \frac{1}{2} \frac{\partial q_B}{\partial \phi_B} \tag{3.82}$$

where the grain boundary space-charge is obtained by Gauss's law (3.7) using also equation (3.22),

$$q_B = \varepsilon\varepsilon_o \left.\frac{d\phi}{dx}\right|_{x=0} = (2\varepsilon\varepsilon_o k_B T)^{\frac{1}{2}}[n(w)\{\mu(0)-1\}+p(w)\{\mu(0)^{-1}-1\}+N_A \ln\mu(0)]^{\frac{1}{2}}, \quad (3.83)$$

where the bulk acceptors N_A are assumed fully ionized. Differentiating (3.83) with respect to ϕ_B, and using the notation of (3.5),

$$C = \left(\frac{e^2\varepsilon\varepsilon_o}{8k_B T}\right)^{\frac{1}{2}} \frac{n(w)\mu(0)-p(w)\mu(0)^{-1}+N_A}{\sqrt{[n(w)\{\mu(0)-1\}+p(w)\{\mu(0)^{-1}-1\}+N_A \ln\mu(0)]}} \quad (3.84)$$

For the data of Table 3.1, including N_{DS} donors at a single energy level E_{DS} equal to 0.91 eV above the valence band at the surface, the capacitance per unit area in equilibrium is shown in Figure 3.23.

The increase of capacitance for larger N_A can be understood as follows: the barrier height ϕ_B is very small, i.e.

$$\ln\mu(0) = e\phi_B/k_B T << 1 ,$$

so one may write

$$\mu(0) = 1 + \Delta\mu$$

Using also (3.23), (3.84) can be rewritten as

$$C = \left(\frac{e^2\varepsilon\varepsilon_o}{8k_B T}\right)^{\frac{1}{2}} \frac{n(w)\{\mu(0)-1\}+p(w)\{1-\mu(0)^{-1}\}}{\sqrt{[\mu(w)\{\mu(0)-1n\mu(0)-1\}+p(w)\{\mu(0)^{-1}+1n\mu(0)-1\}}},$$

and so using the expansion for small $\Delta\mu$,

$$C = \left(\frac{e^2\varepsilon\varepsilon_o}{8k_B T}\right)^{\frac{1}{2}} \frac{n(w)\Delta\mu+p(w)\{\Delta\mu-\Delta\mu^2+...\}}{\sqrt{[n(w)\{\Delta\mu^2/2+\Delta\mu^3/3+...\}+p(w)\{\Delta\mu^2/2-2\Delta\mu^3/3+...\}]}}$$

To first order in $\Delta\mu$, one obtains the "flat-band" capacitance (Ando et al., 1982)

$$C_{fb} = \left\{ \frac{e^2 \varepsilon \varepsilon_o \{n(w)+p(w)\}}{4k_B T} \right\}^{\frac{1}{2}} \quad . \tag{3.85}$$

By (3.23) and (3.10), in p-type material for large N_A

$$p(w) \doteq N_A \ , \qquad n(w) << p(w) \ ,$$

thus C is proportional to $N_A^{\frac{1}{2}}$ and is rapidly increasing.

For smaller N_A, the capacitance is largely independent of N_A but depends strongly on N_{DS}. The larger is N_{DS}, the greater is the charge stored at the grain boundary and so the capacitance is expected to be larger.

3.10 Conclusions and Discussion

A model of the grain boundary surface recombination and barrier height has been developed in which Poisson's equation was solved by assuming flat, parallel quasi-Fermi levels, and dropping the depletion approximation. The solution is a transcendental equation for the barrier height.

In the course of the mathematical treatment, the Shockley-Read-Hall statistics was displayed as a generalization of the Fermi-Dirac statistics. This enabled a single treatment of the equilibrium and non-equilibrium steady-state conditons to be given.

The work of Fossum and Lindholm (1980a) and Fossum and Sundaresam (1982) has been confimed and extended by considering surface states at levels other than at mid-gap. Also, Auger effects have been included . In fact, for the data of Table 3.1 their effect on the

barrier height is negligible, the carrier concentrations being too low.

Curves have been given for the barrier height under various equilibrium and steady-state conditions and their shape has been explained physically in Section 3.5, approximate relations for most of the curves have been derived in Section 3.6, and agreement with experiment was shown to be satisfactory in Sections 3.7 and 3.8.

The equilibrium barrier height displays a maximum with respect to doping in the bulk, a feature noted by some authors (Fossum and Lindholm, 1980a, Seto, 1975, Baccarani et al., 1978b, Card and Yang, 1977 for example) but not all (Seager and Castner, 1978). It was found in Section 3.6 that this occurs when the Fermi level lies approximately at the surface state level. The maximum occurs because of the two opposing effects discussed in Section 3.5. This feature appears to be of importance also in the steady-state case: The effect of the Fermi level separation is a marked drop in the barrier height if the doping concentration is less than that for the maximum, while the barrier height remains constant (prior to a drop) with Fermi level separation for doping concentrations above those for the maximum.

The drop in barrier height with, for example, increasing illumination is due to the rapid surface recombination which keeps most of the surface states neutral and so reduces the width of the space-charge region. This is therefore not to be interpreted as an approach to single crystal behaviour.

The potential barrier height calculated with a constant distribution of surface levels is an amalgam of the barrier heights

calculated using single surface levels. The surface states of donor type lying higher in the energy gap of p-type material contribute more to the barrier height because of their greater degree of ionization.

Table 3.1: Data Used for Si

ε	ε_o	E_G	N_c	N_v	n_i	$k_B T$
11.8	8.854×10^{-12}	1.1	2.8×10^{25}	1.0×10^{25}	4.67×10^{15}	0.026
-	Fm^{-1}	eV	m^{-3}	m^{3}	m^{3}	eV

G(o)	H(o)	α	τ	$h\nu$
10^{-13}	10^{-15}	6×10^{5}	1×10^{-6}	1.1
$m^3 s^{-1}$	$m^3 s^{-1}$	m^{-1}	s	eV

Table 3.2: Data Used for CdS

ε	ε_o	E_G	N_c	N_v	$k_B T$	G(o)	H(o)
10	8.854×10^{-12}	2.42	2×10^{24}	10^{25}	0.026	2.5×10^{-14}	2.5×10^{-14}
-	Fm^{-1}	eV	m^{-3}	m^{-3}	eV	$m^3 s^{-1}$	$m^3 s^{-1}$

N_D	τ	α	$h\nu$	N_{AS}
1.1×10^{23}	10^{-7}	6×10^{5}	2.42	8.5×10^{15}
m^{-3}	s	m^{-1}	eV	$m^{-2}eV^{-1}$

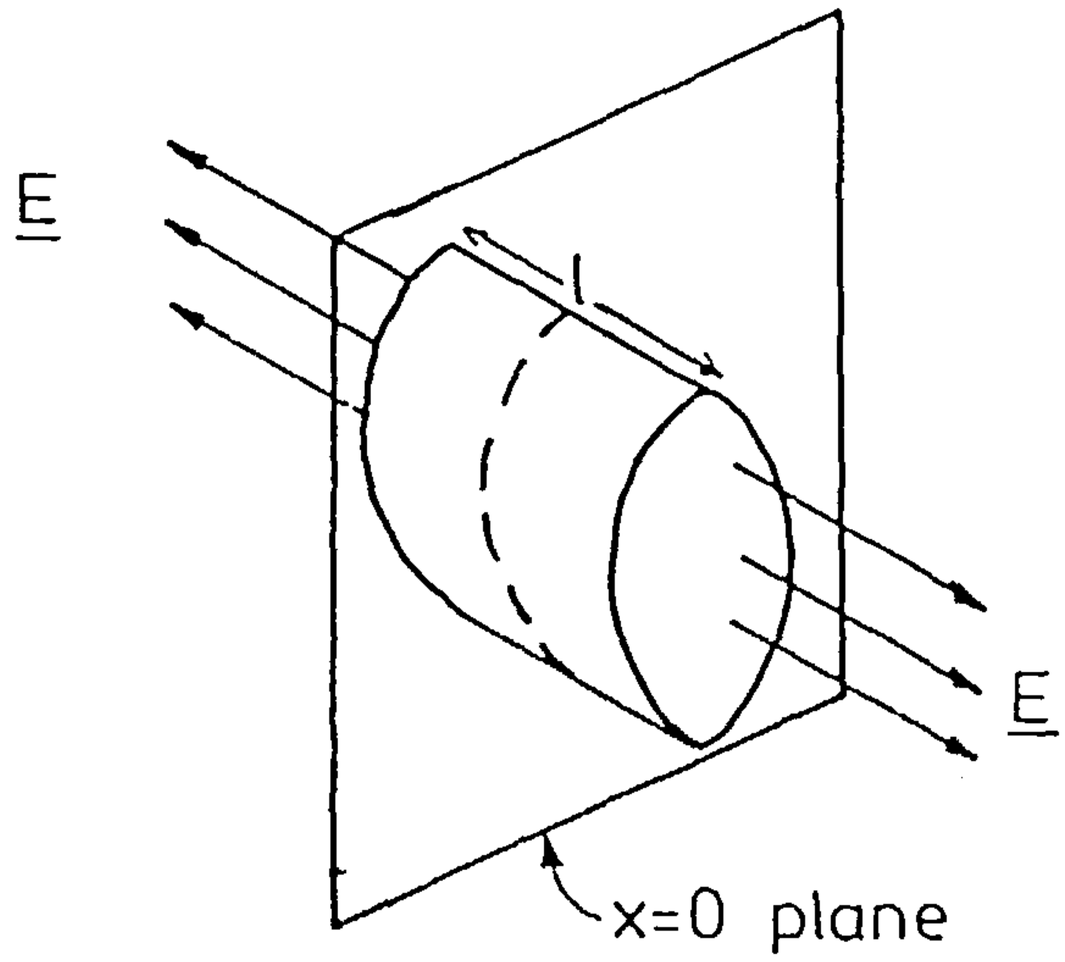

Figure 3.1 The Gaussian pill-box with its axis cutting through the plane x=0 of the grain boundary.

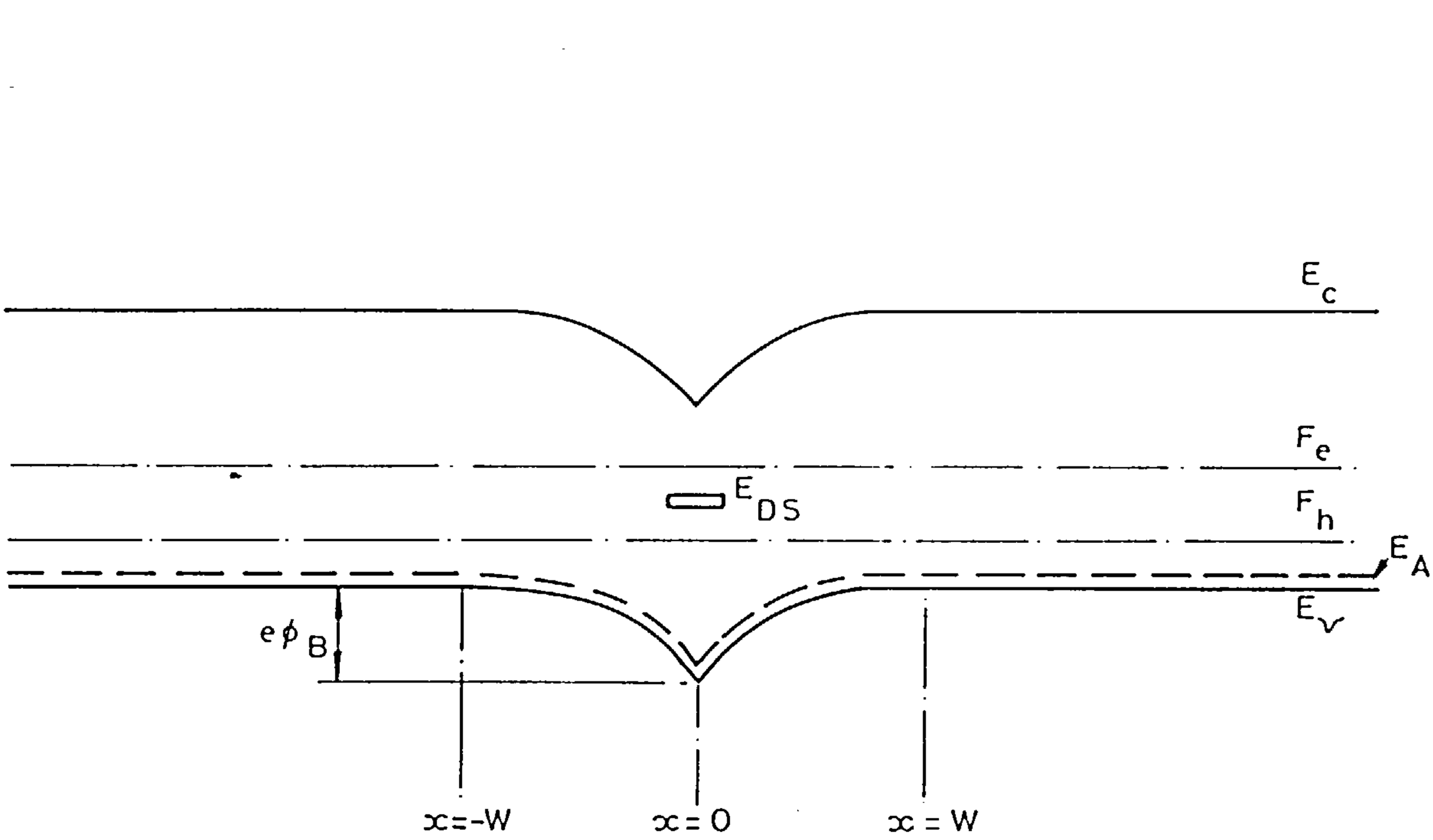

Figure 3.2 The steady-state energy band diagram for a single donor energy level, E_{DS}.

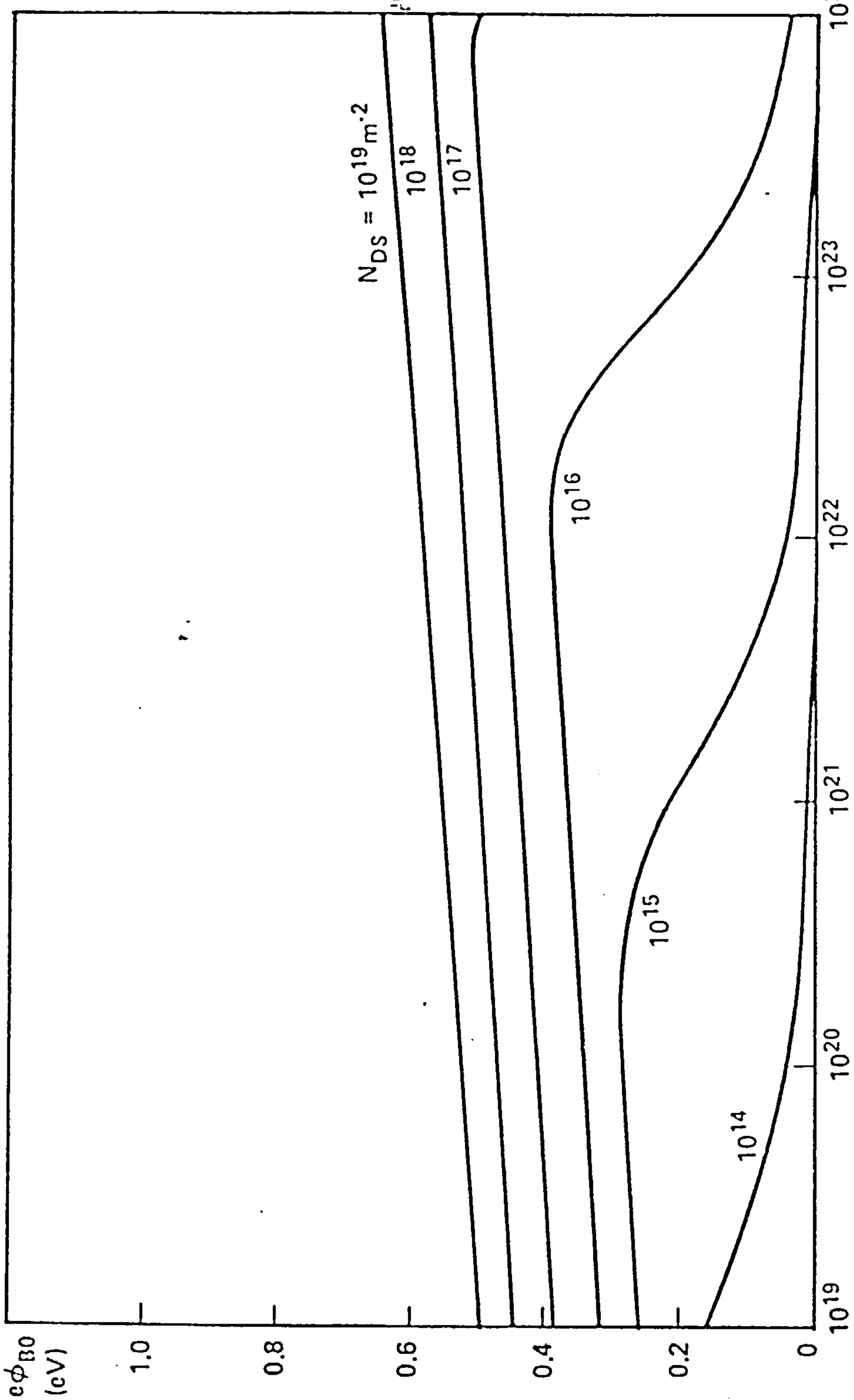

Figure 3.3 The equilibrium barrier height as a function of the doping density in the bulk, using equation (3.25) with the data of Table 3.1, a single mid-gap surface energy level and various surface donor densities.

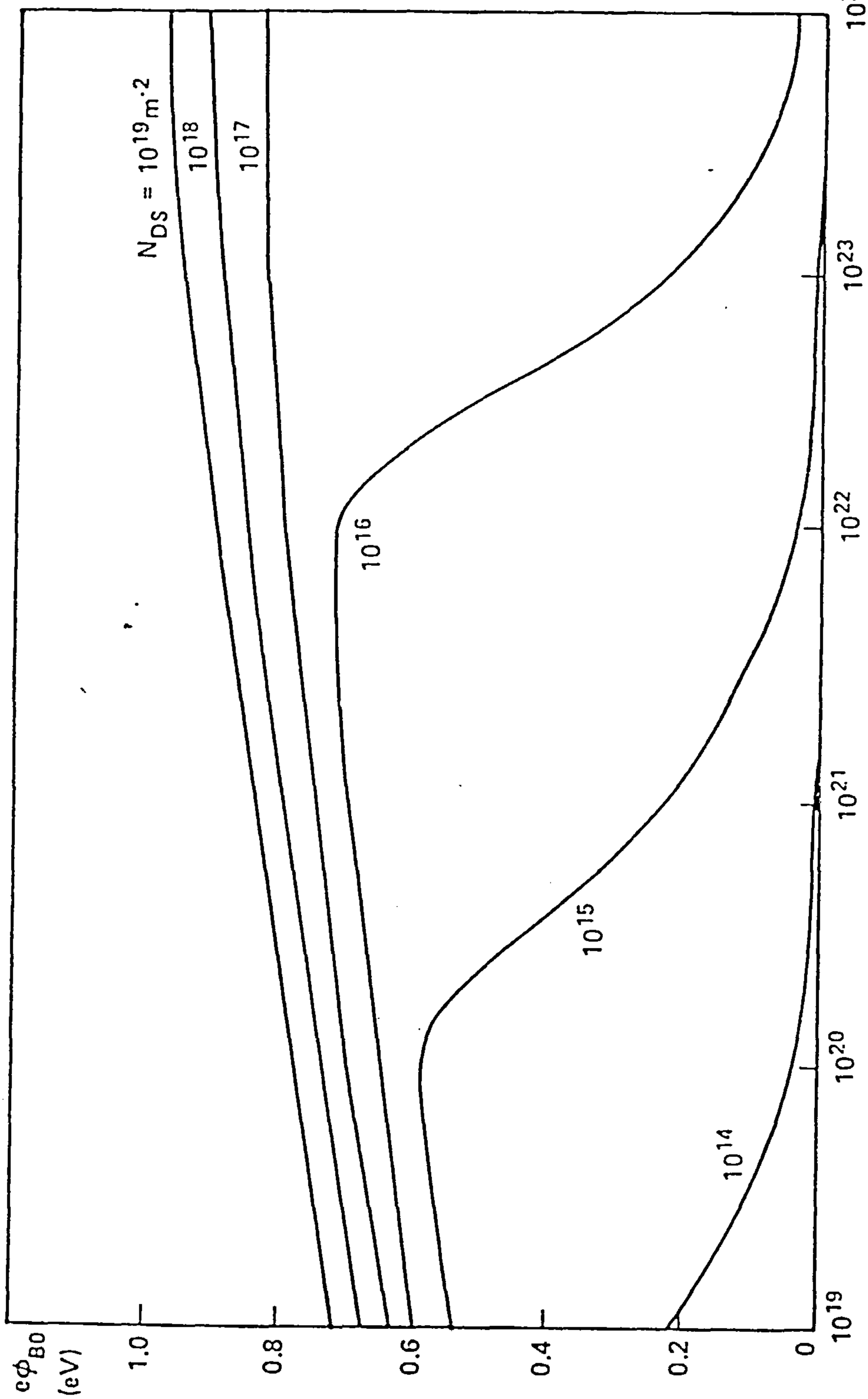

Figure 3.4 The equilibrium barrier height as a function of doping density and surface donor concentration as Figure 3.3, but for a single energy level 0.91 eV above the valence band edge.

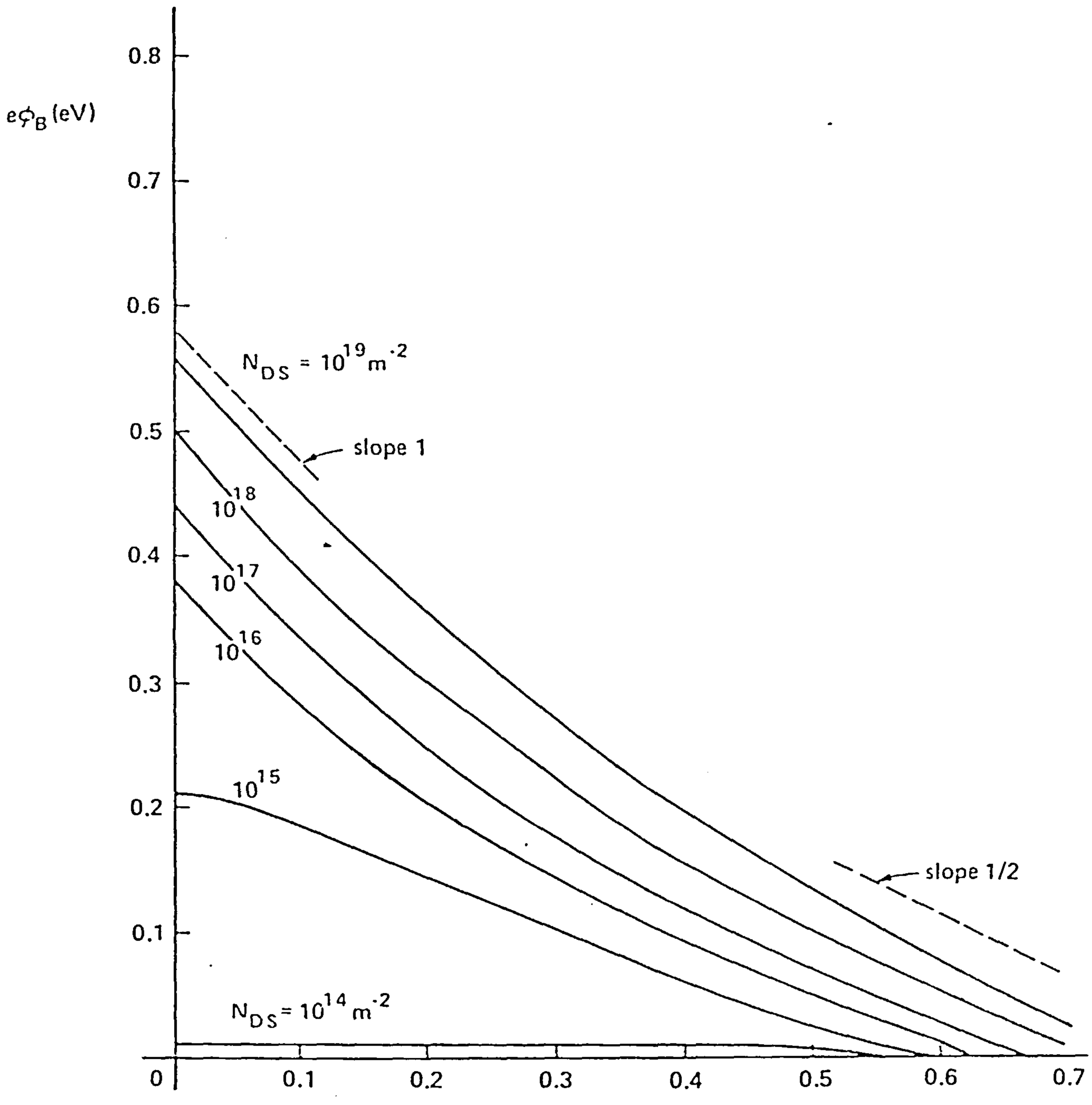

Figure 3.5 The steady-state barrier height using the data of Table 3.1 and equation (3.25), as a function of quasi-Fermi level separation. Various donor densities in the surface at a single mid-gap energy level and a doping density, $N_A = 10^{21} m^{-3}$, in the grain are considered.

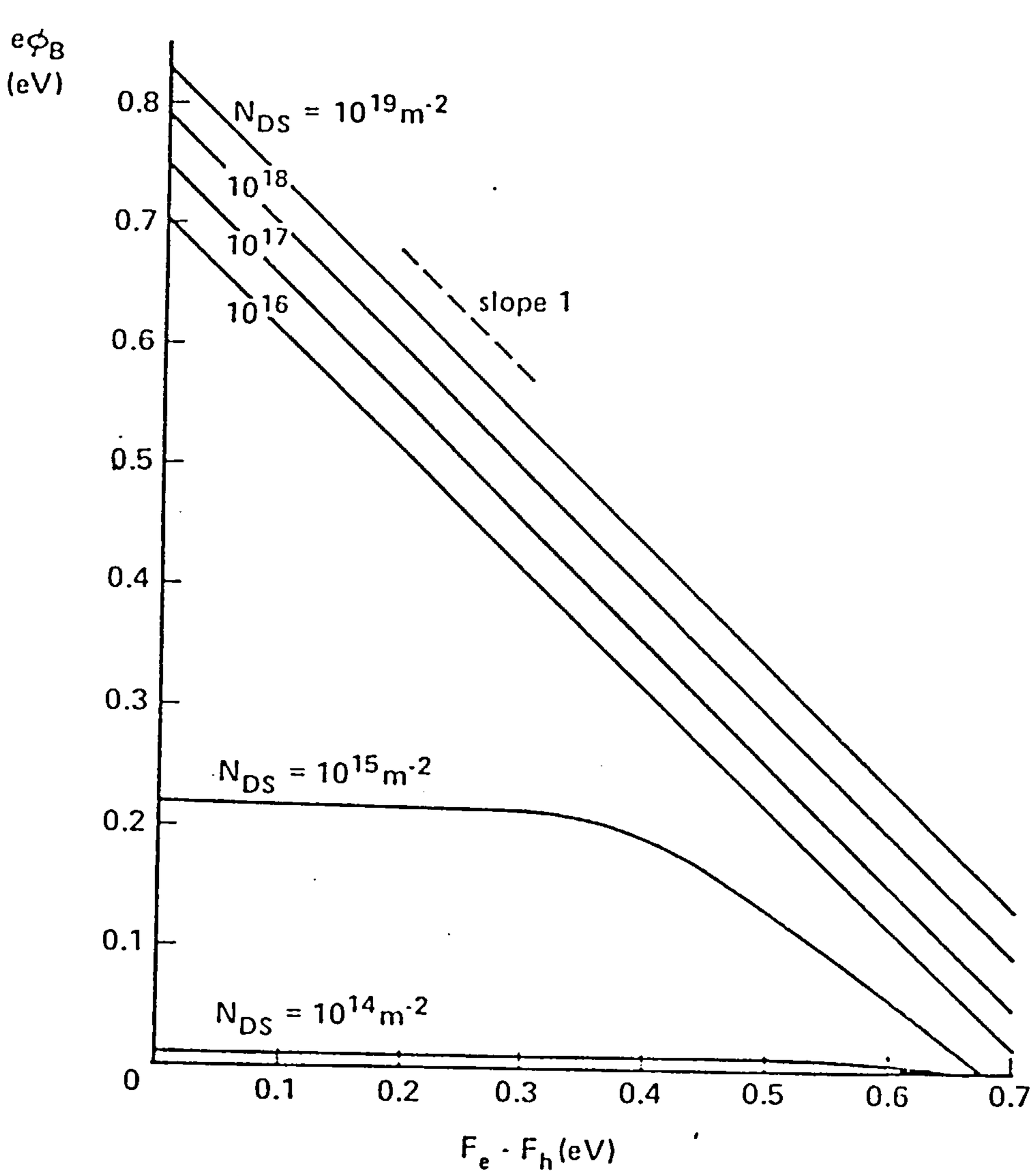

Figure 3.6 As Figure 3.5, but for a single energy level 0.91 eV above the valence band edge.

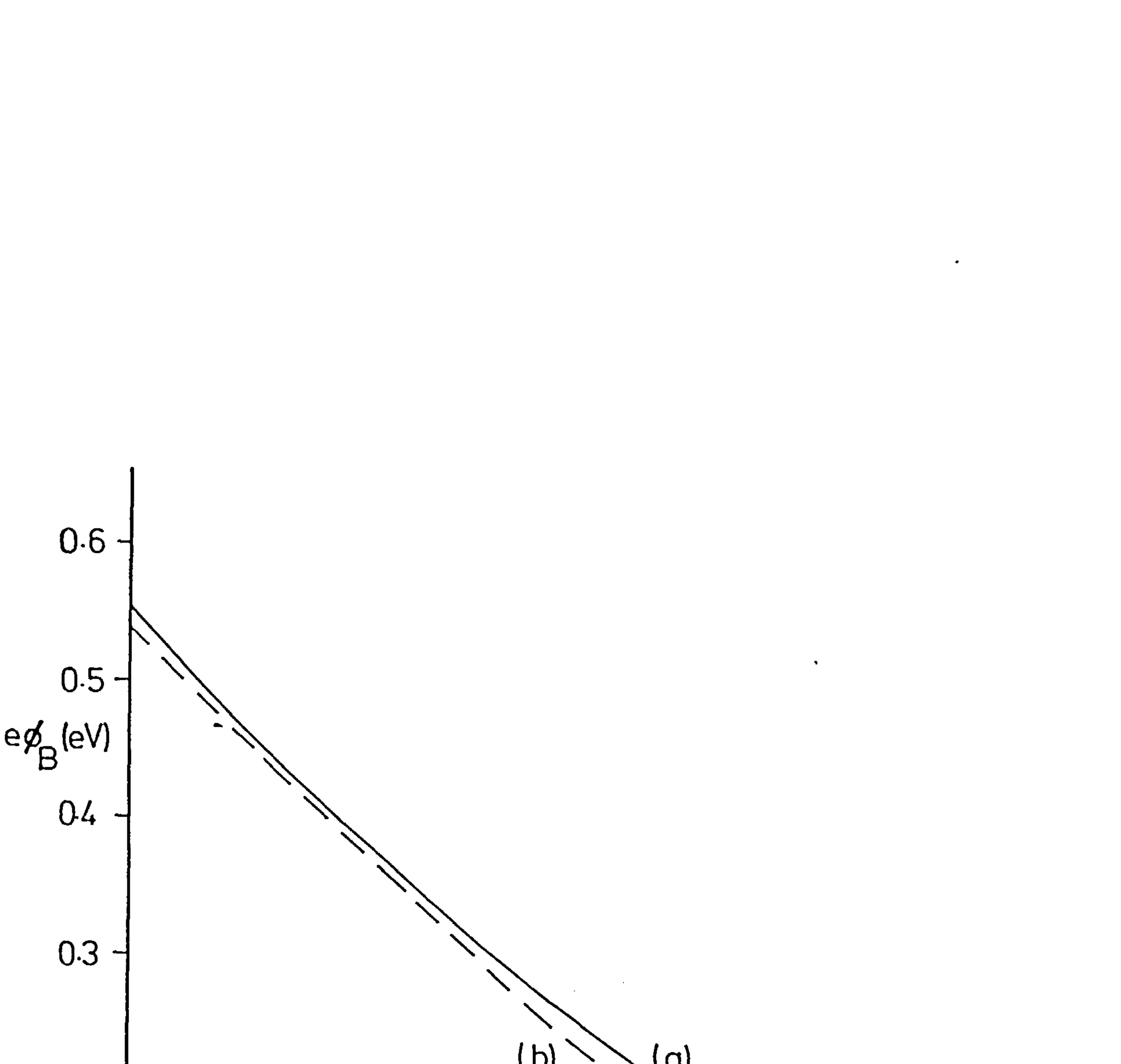

Figure 3.7 As Figure 3.5, curves (a), $N_{DS}=10^{19}m^{-2}$, and (c), $N_{DS}=10^{15}m^{-2}$, use the present theory, whereas curves (b), $N_{DS}=10^{19}m^{-2}$, and (d), $N_{DS}=10^{15}m^{-2}$, use the depletion approximation.

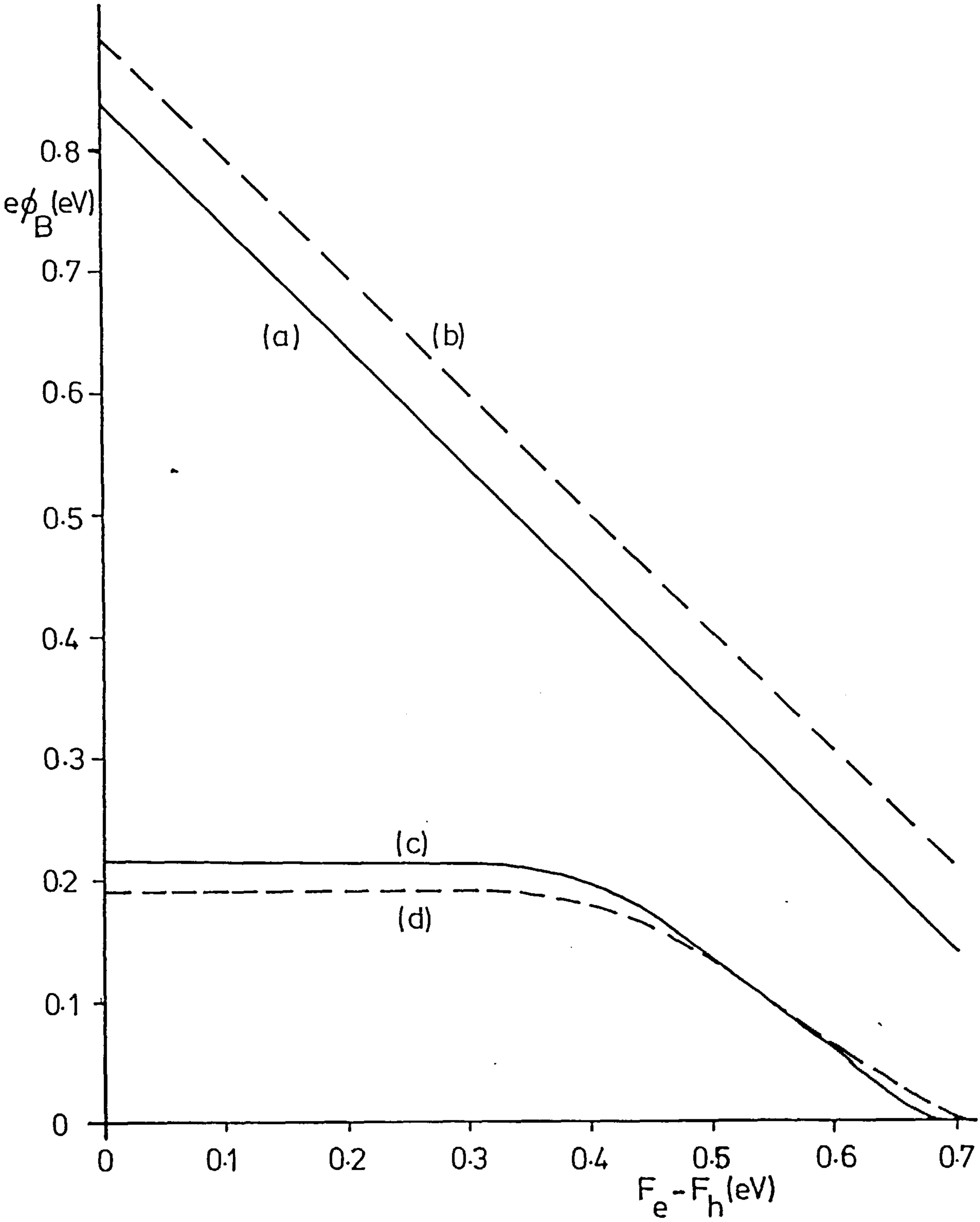

Figure 3.8 As Figure 3.6, curves (a), $N_{DS}=10^{19}m^{-2}$, and (c), $N_{DS}=10^{15}m^{-2}$, use the present theory, whereas curves (b), $N_{DS}=10^{19}m^{-2}$, and (d), $N_{DS}=10^{19}m^{-2}$, use the depletion approximation.

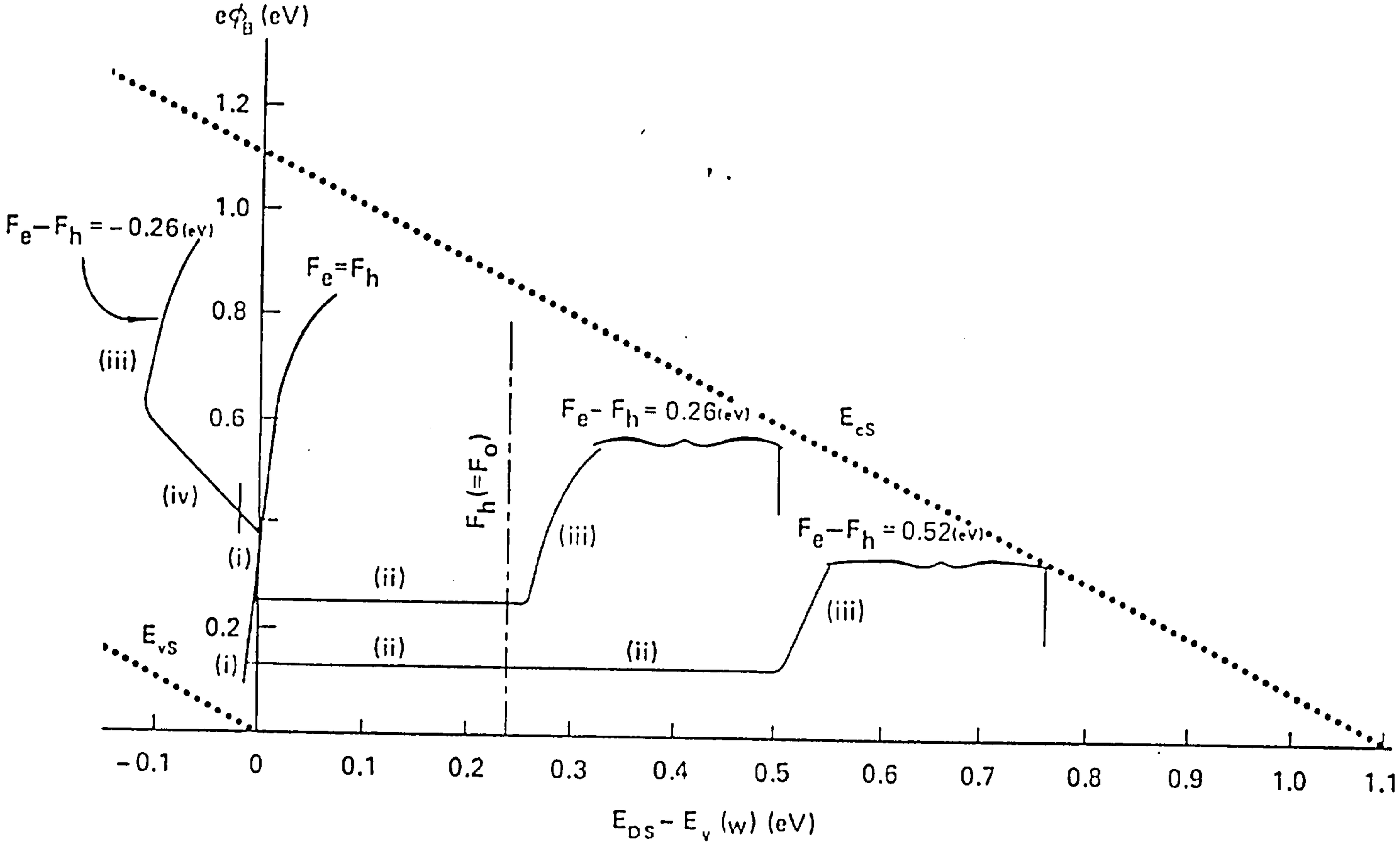

Figure 3.9 Equilibrium and steady-state barrier height as a function of the energy difference between the surface donor level and the valence band edge at the end of the space charge region, x=w. Various quasi-Fermi level separations are considered using equation (3.25), the data of Table 3.1, $N_{DS} = 10^{19} m^{-2}$, $N_A = 10^{21} m^{-3}$. The positions of the quasi-Fermi levels are indicated by vertical lines.

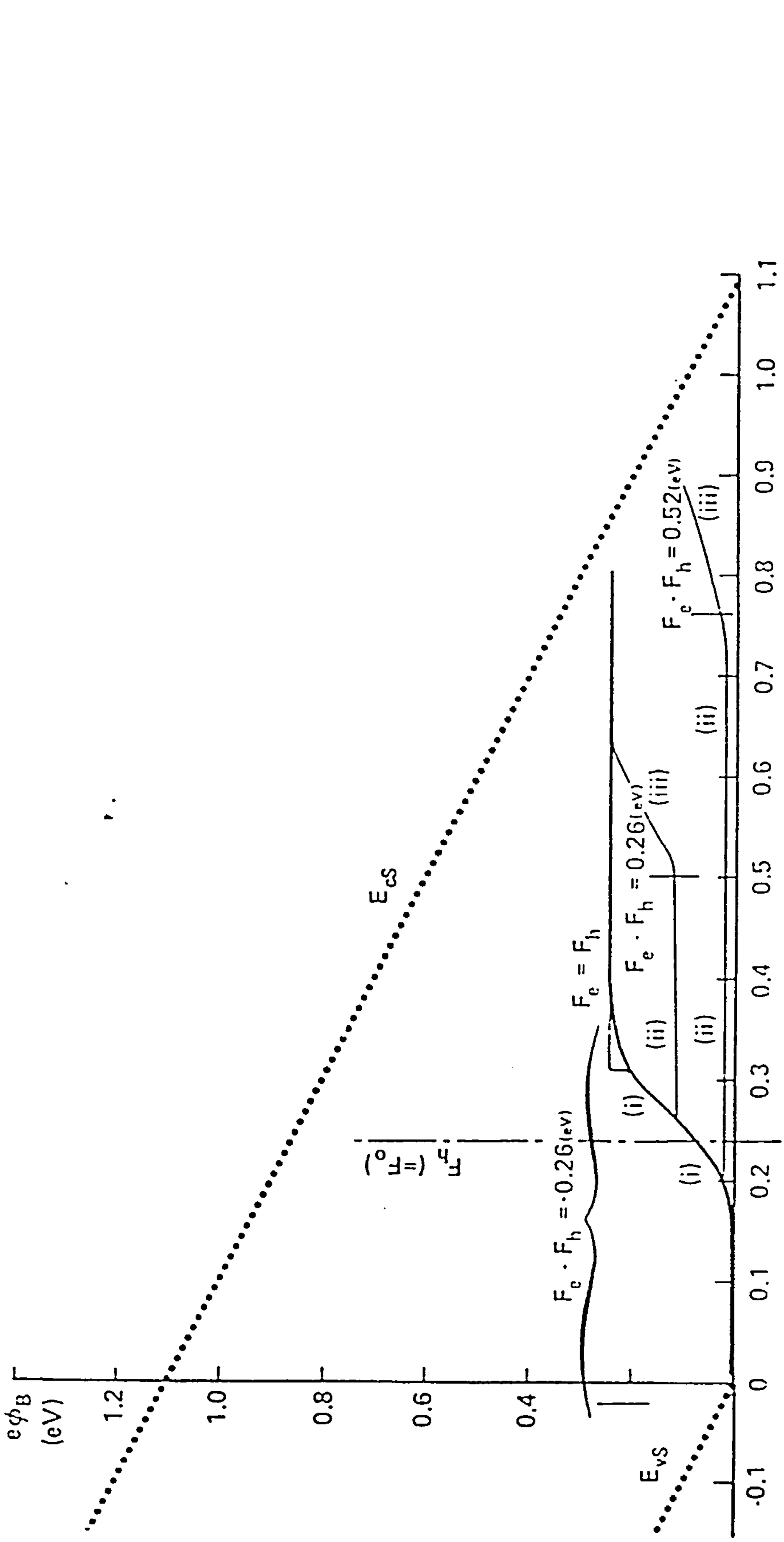

Figure 3.10 As Figure 3.9, but for $N_{DS} = 10^{15}\,m^{-2}$.

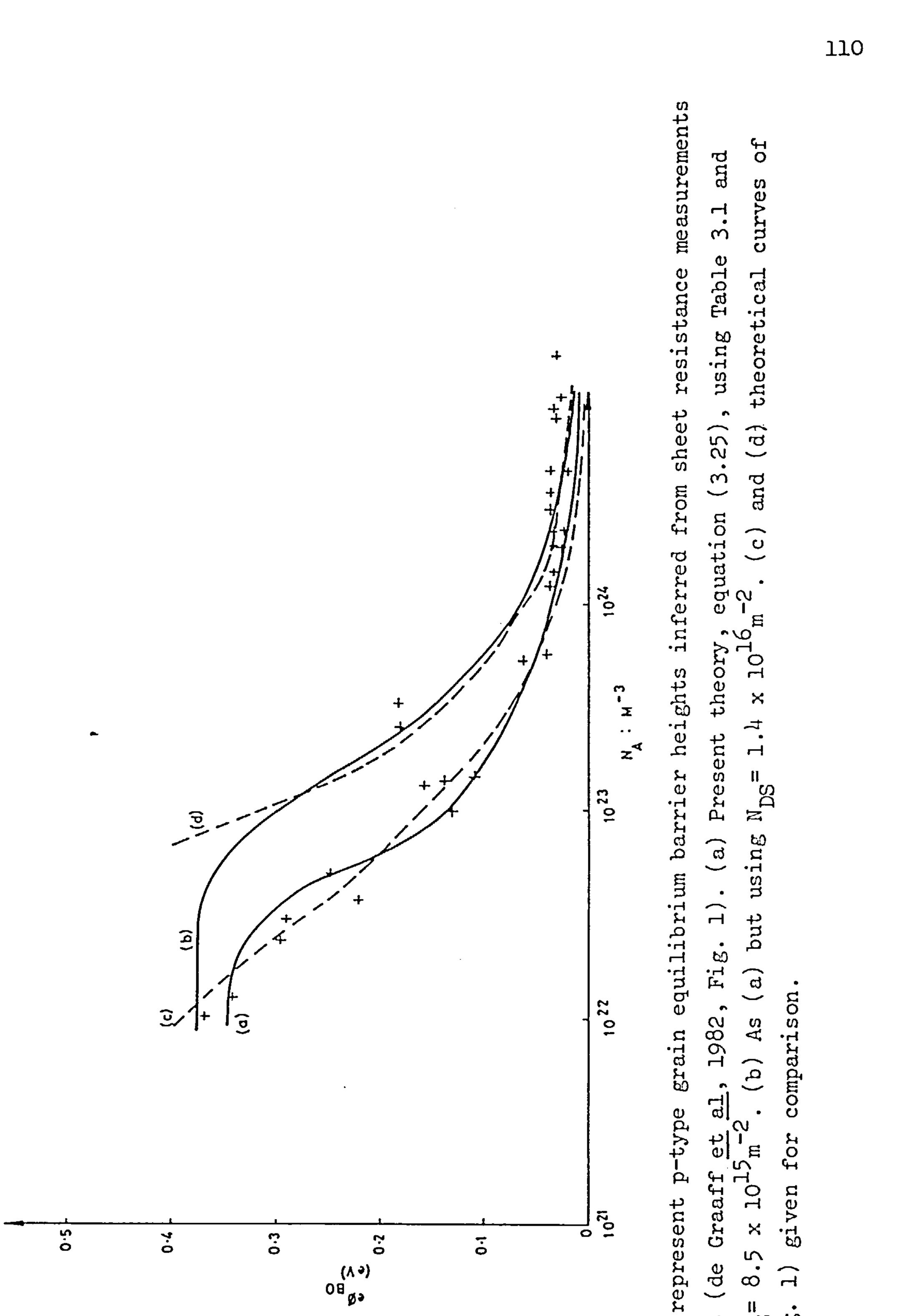

Figure 3.11 Crosses represent p-type grain equilibrium barrier heights inferred from sheet resistance measurements in polysilicon diodes (de Graaff et al, 1982, Fig. 1). (a) Present theory, equation (3.25), using Table 3.1 and $E_{DS}-E_{vS}$= 0.53 eV, N_{DS}= 8.5 x 10^{15} m^{-2}. (b) As (a) but using N_{DS}= 1.4 x 10^{16} m^{-2}. (c) and (d) theoretical curves of de Graaff (1982, Fig. 1) given for comparison.

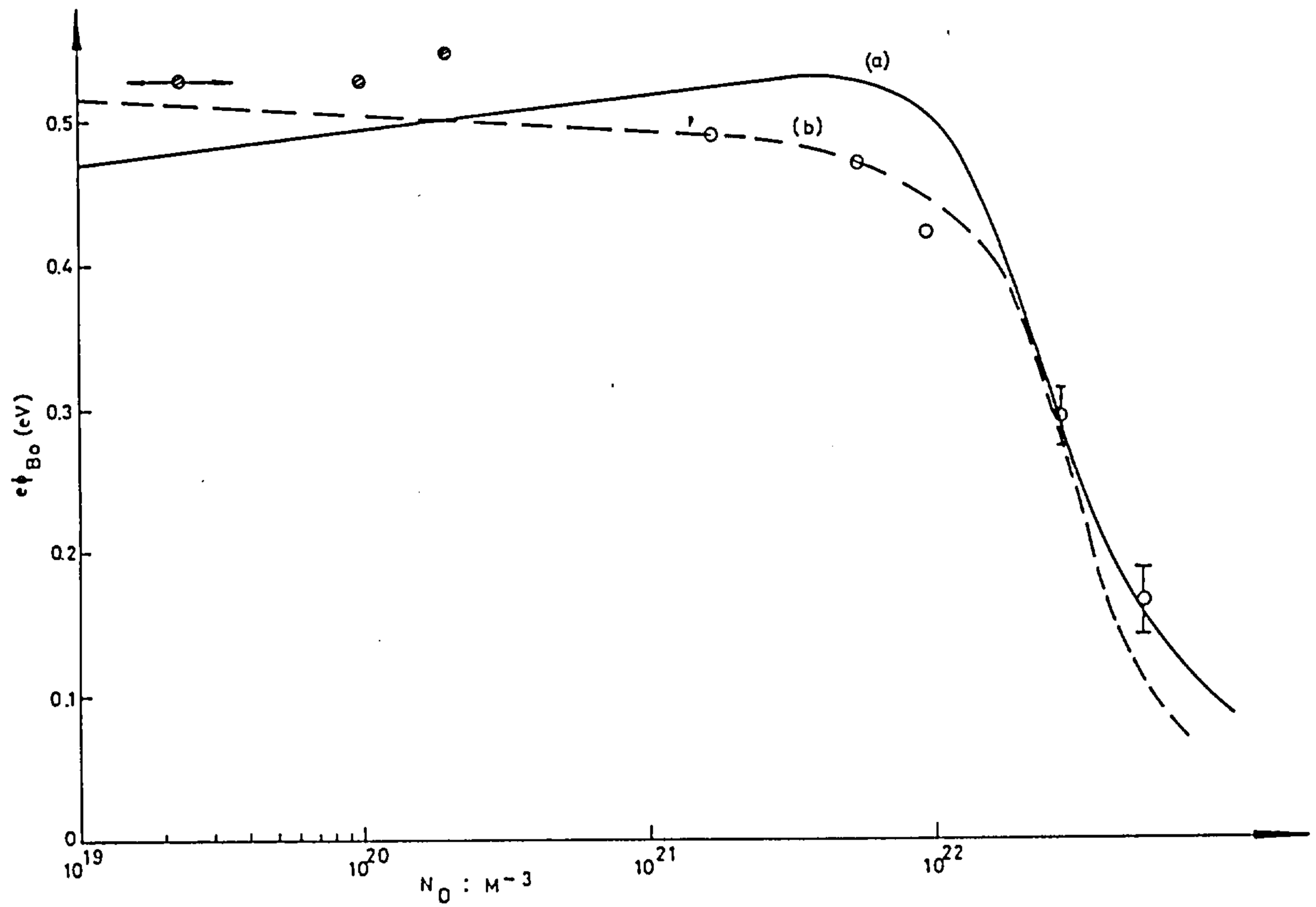

Figure 3.12 Circles represent n-type grain equilibrium barrier heights in polysilicon from 270 K resistivity data (●) and from potential rpofile experiments(O) of Seager and Castner (1978). (a) Present theory, equation (3.25) using Table 3.1 data but with T=270 K, $E_{AS}-E_{vS}$= 0.34 eV and N_{AS}= 6.0 x $10^{15} m^{-2}$. (b) Theoretical curve (Seager and Castner, 1978) given for comparison with a net surface acceptor concentration, 5.4 x $10^{15} m^{-2}$, at an energy position $E_{AS}-E_{vS}$= 0.626 eV.

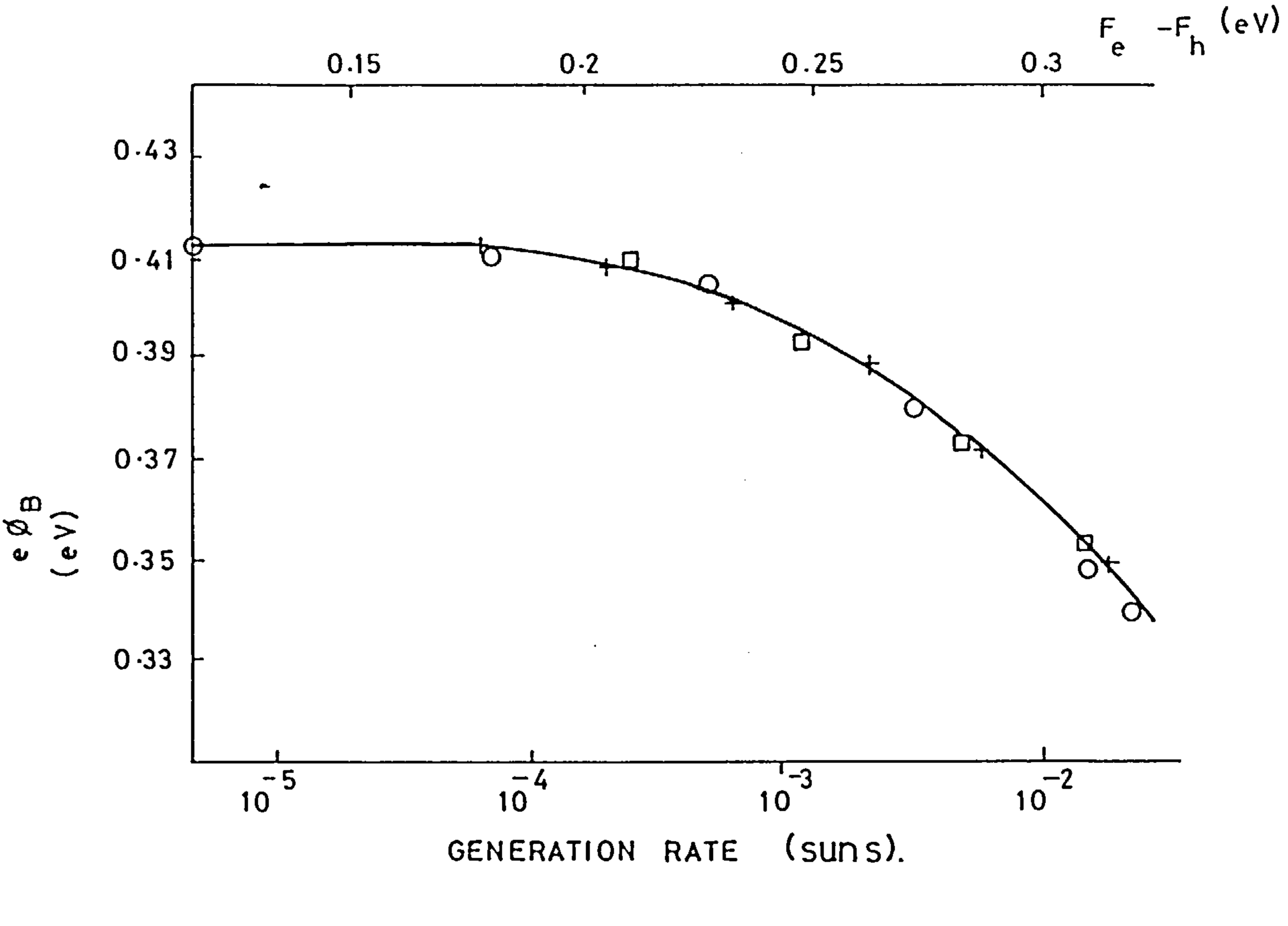

Figure 3.13 Barrier heights for an illuminated n-type silicon bicrystal obtained from capacitance and conductance measurements (Seager, 1981). The curve is for the present theory, equation (3.25) using $N_{AS} = 5.0 \times 10^{15} m^{-2}$, $N_D = 1.3 \times 10^{22} m^{-3}$, T= 278 K and $E_{AS} - E_{vS} =$ 0.77eV. For other parameters see text.

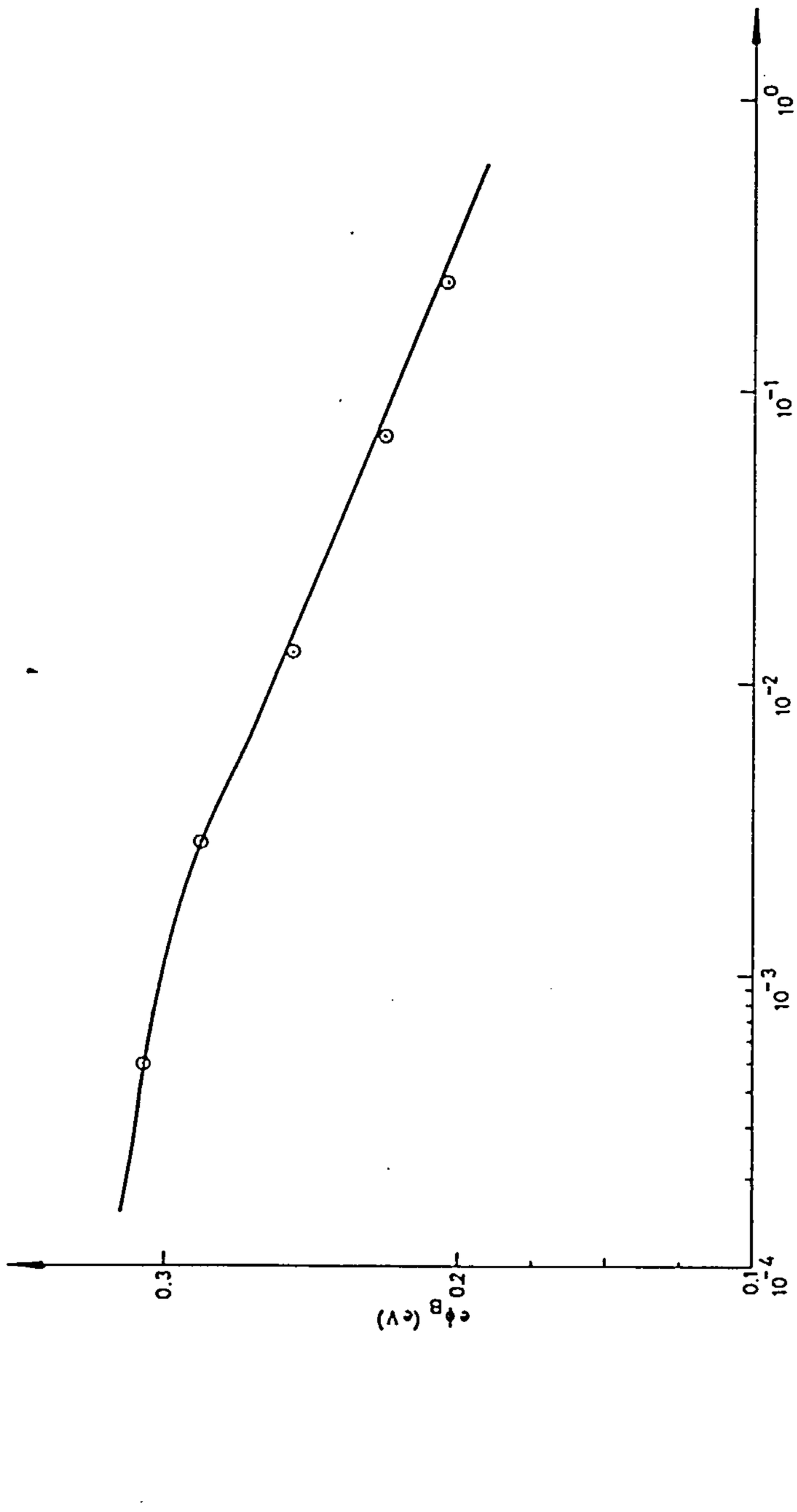

Figure 3.14 Barrier height as a function of illumination intensity for an illuminated isolated grain boundary in p-type silicon (Carnegie sample B-12). The curve is for the present theory with N_{DS}= 2.75 x $10^{15}m^{-2}$, N_A= 3 x $10^{21}m^{-3}$, T= 293 K and $E_{DS}-E_{VS}$= 0.77 eV and using data given in the text.

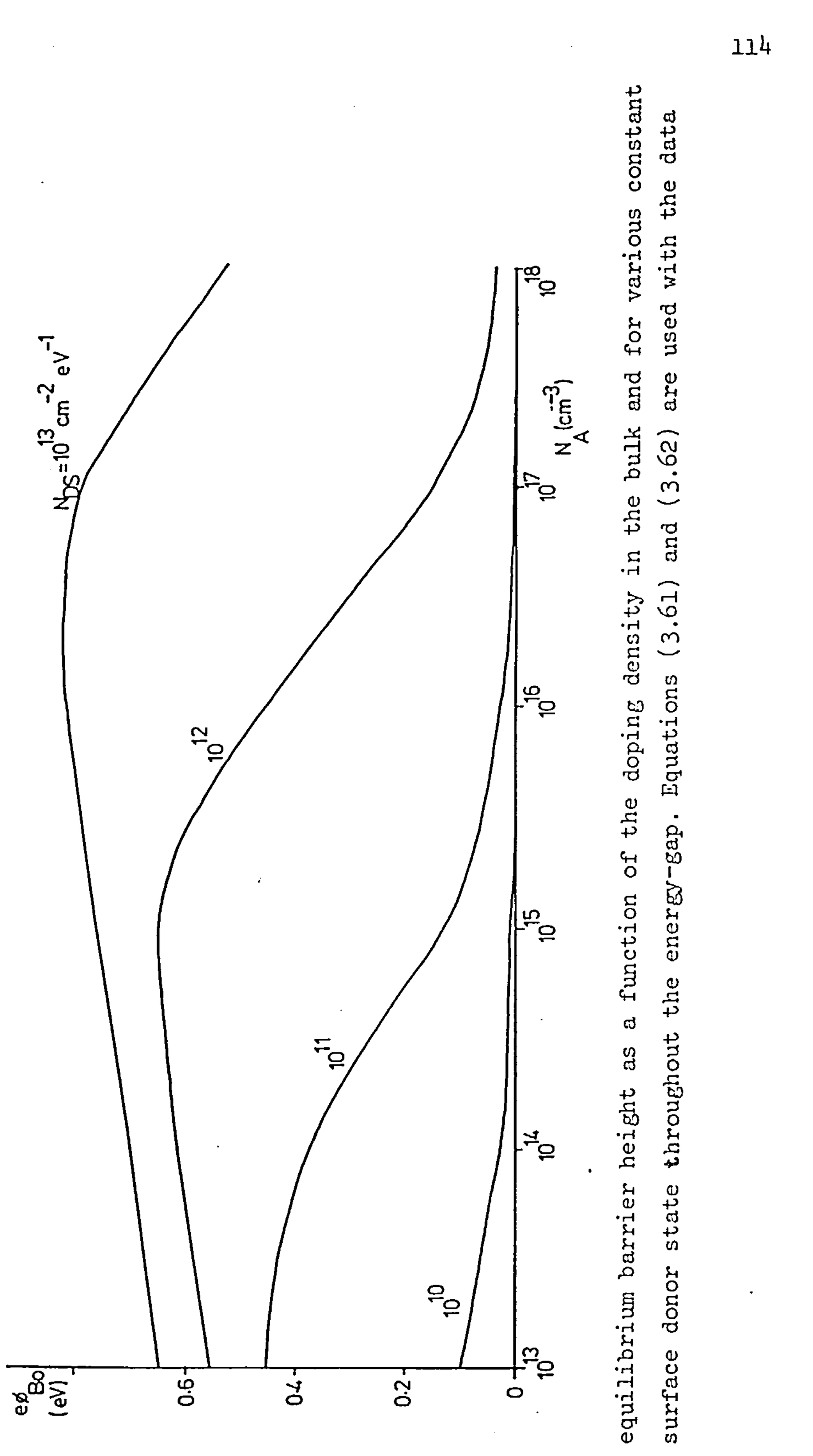

Figure 3.15 The equilibrium barrier height as a function of the doping density in the bulk and for various constant distributions of surface donor state throughout the energy-gap. Equations (3.61) and (3.62) are used with the data of Table 3.1.

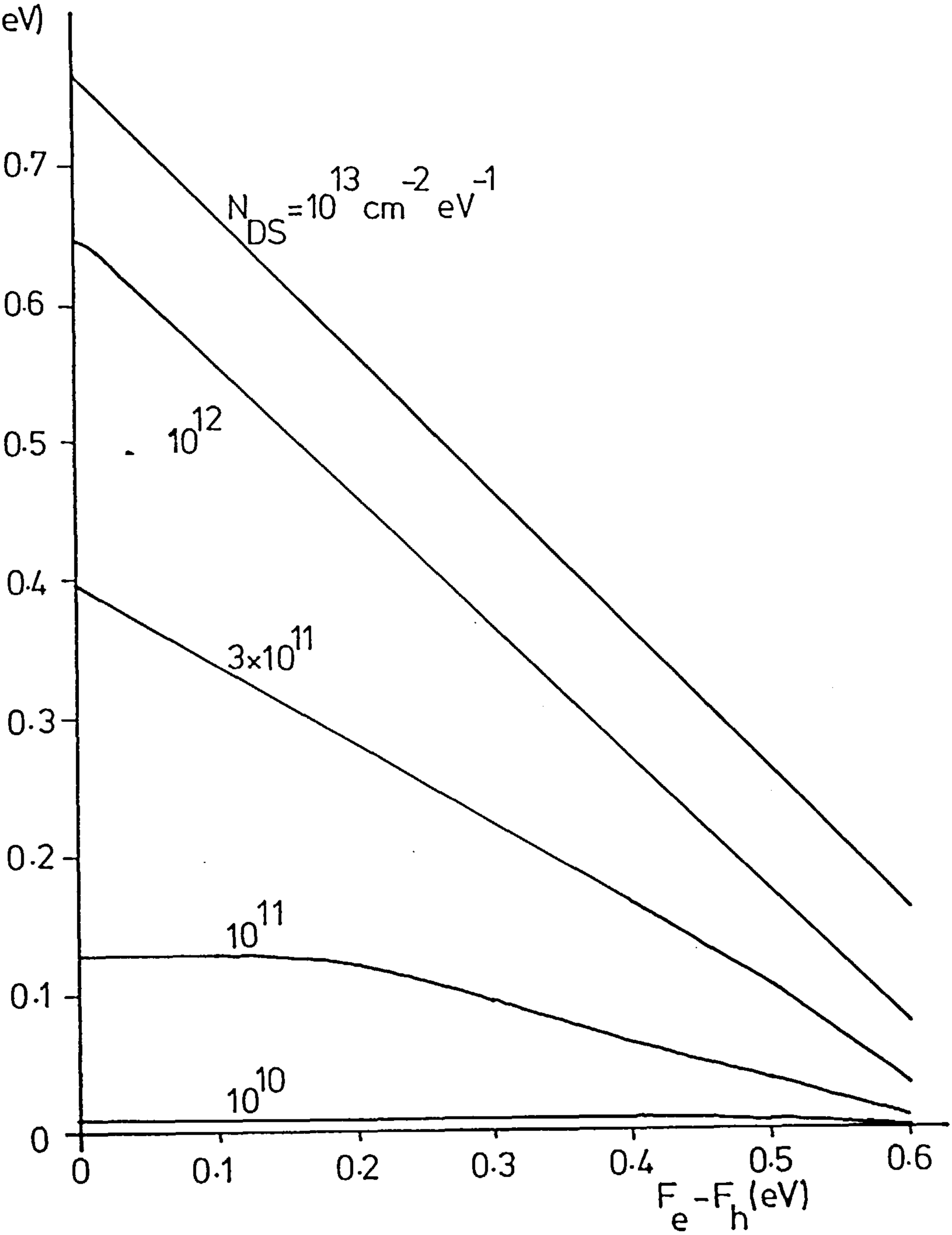

Figure 3.16 The steady-state barrier height as a function of the quasi-Fermi level separation using equations (3.61) and (3.62) with the data of Table 3.1 for various surface donor densities in a constant distribution throughout the energy-gap and a doping density of $10^{21}\,m^{-3}$ in the bulk.

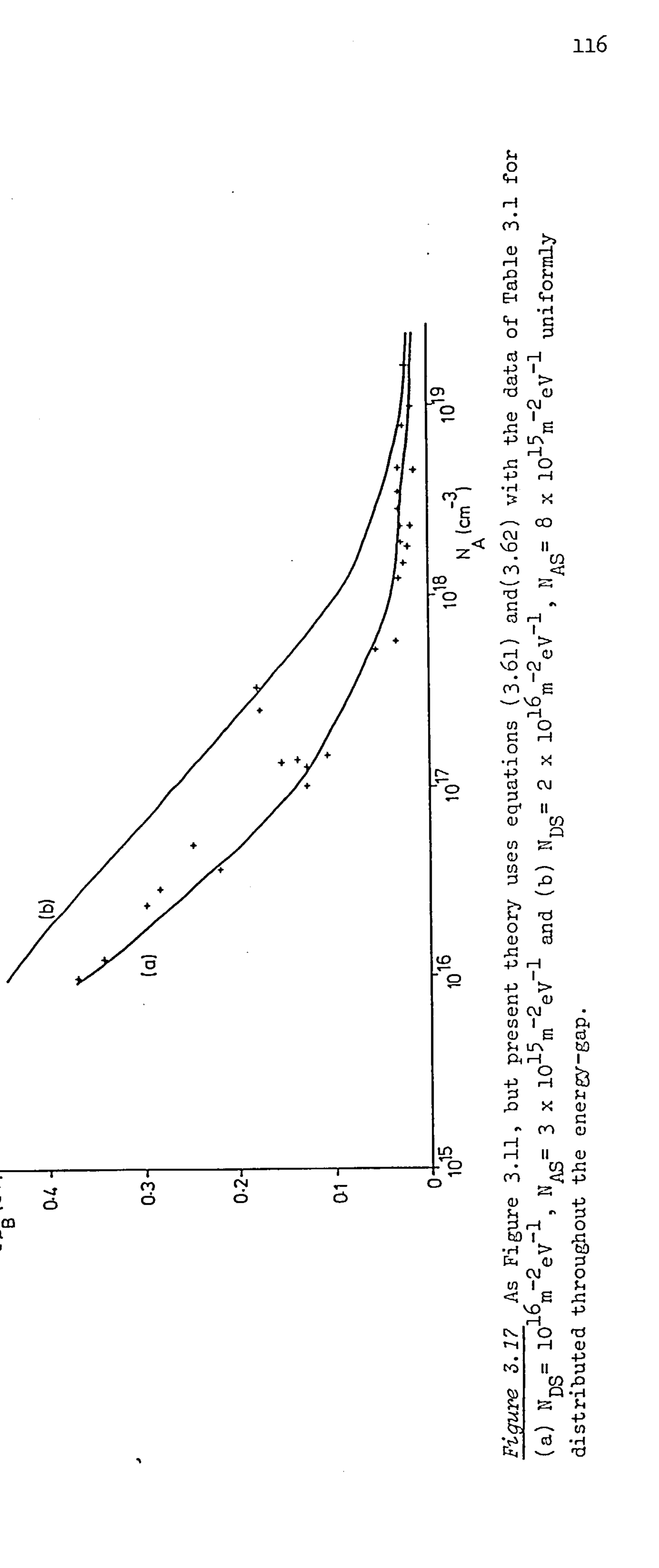

Figure 3.17 As Figure 3.11, but present theory uses equations (3.61) and(3.62) with the data of Table 3.1 for (a) $N_{DS} = 10^{16} m^{-2} eV^{-1}$, $N_{AS} = 3 \times 10^{15} m^{-2} eV^{-1}$ and (b) $N_{DS} = 2 \times 10^{16} m^{-2} eV^{-1}$, $N_{AS} = 8 \times 10^{15} m^{-2} eV^{-1}$ distributed throughout the energy-gap.

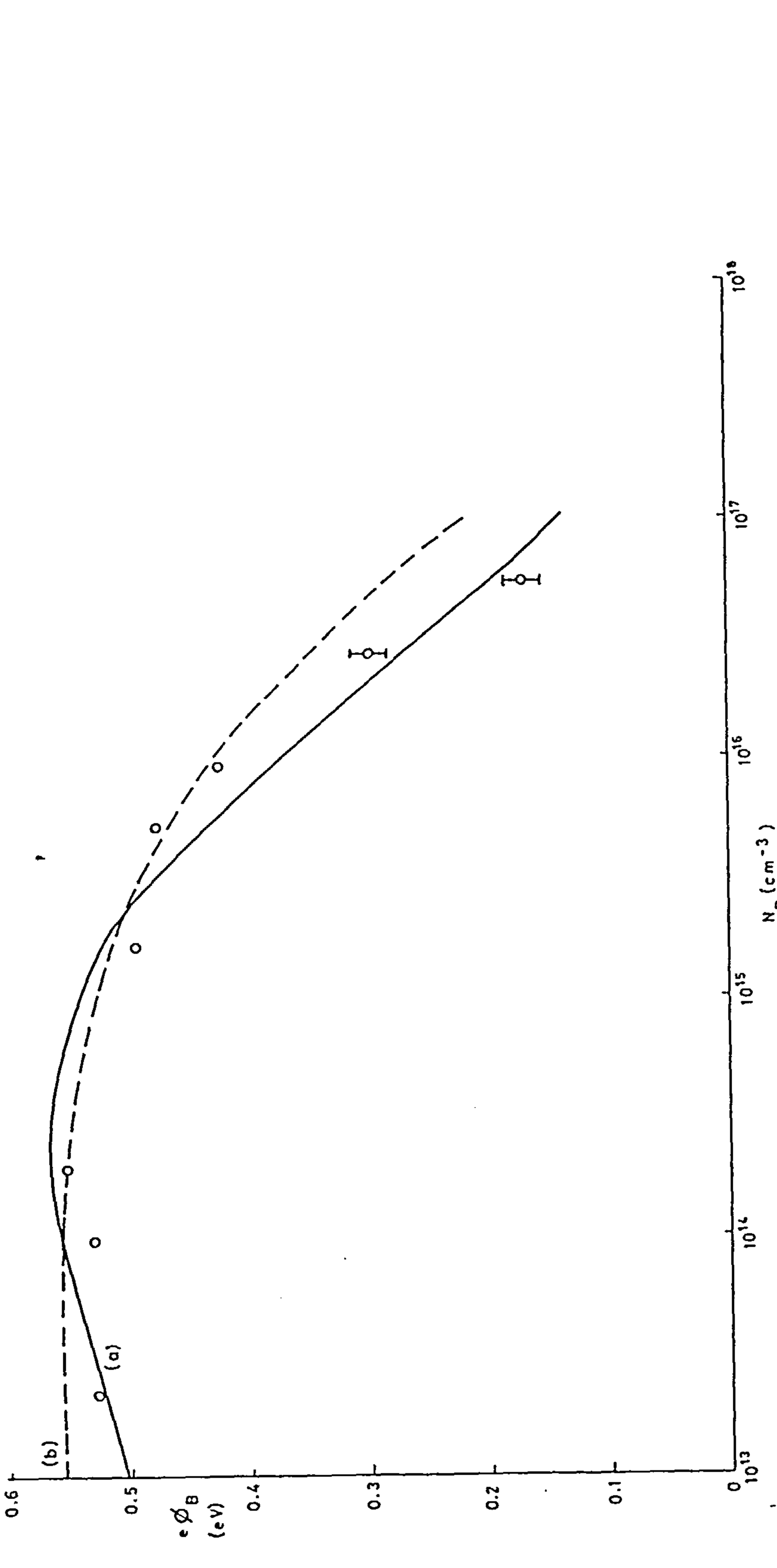

Figure 3.18 Circles represent n-type grain equilibrium barrier heights (Seager and Castner, 1978). (a) Present theory as Figure 3.12 but with equations(3.61) and(3.62) for a constant donor state distribution, $N_{DS} = 5.45 \times 10^{15}$ $m^{-2}eV^{-1}$, (b) theoretical curve (Seager and Castner, 1978) using a constant distribution of donor and acceptor states.

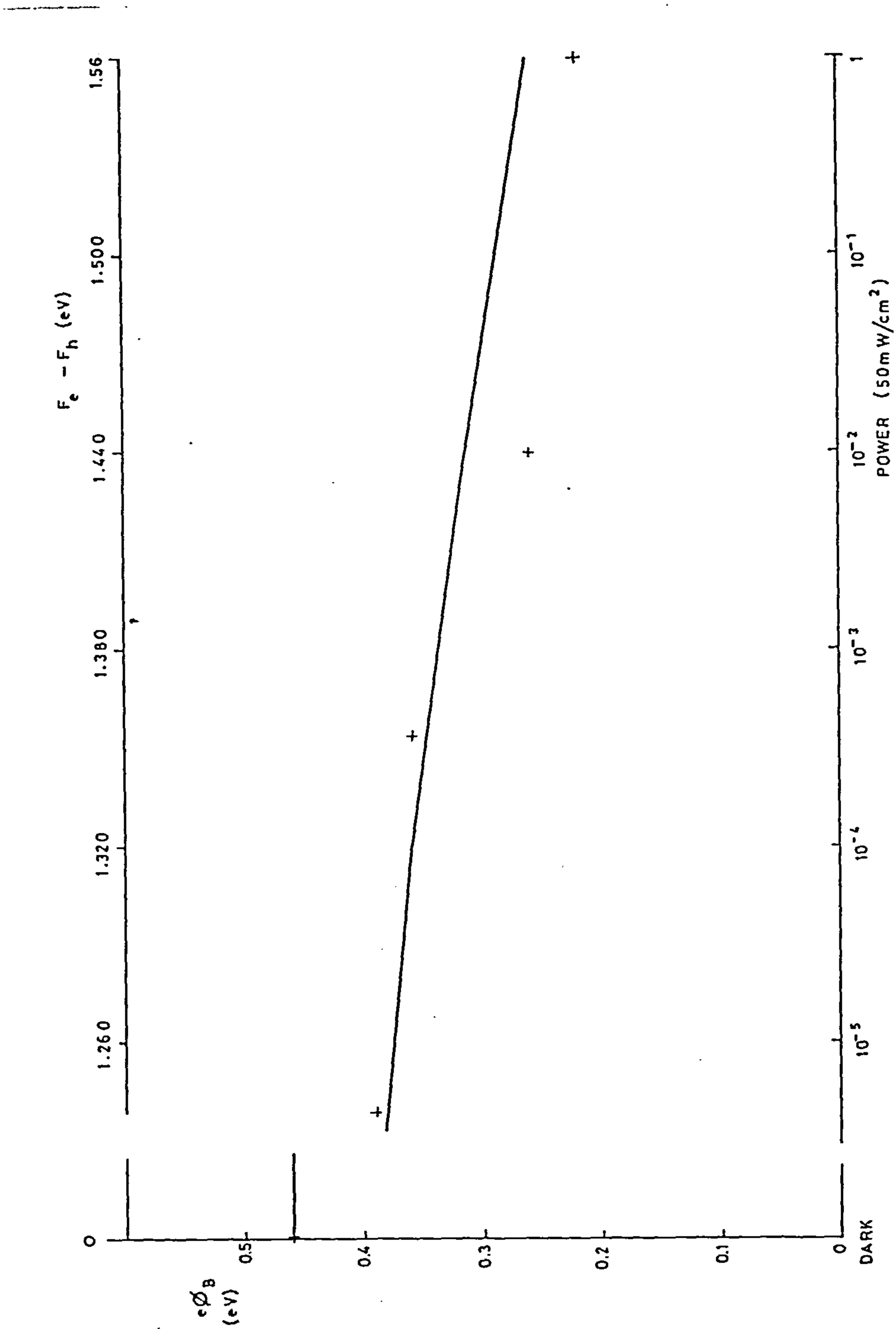

Figure 3.19 The steady-state barrier height in CdS (n-type) as a function of illumination. Crosses are experimental points (Wu and Bube, 1974) and the curve is the present theory of equations (3.61) and (3.62) with the data of Table 3.2.

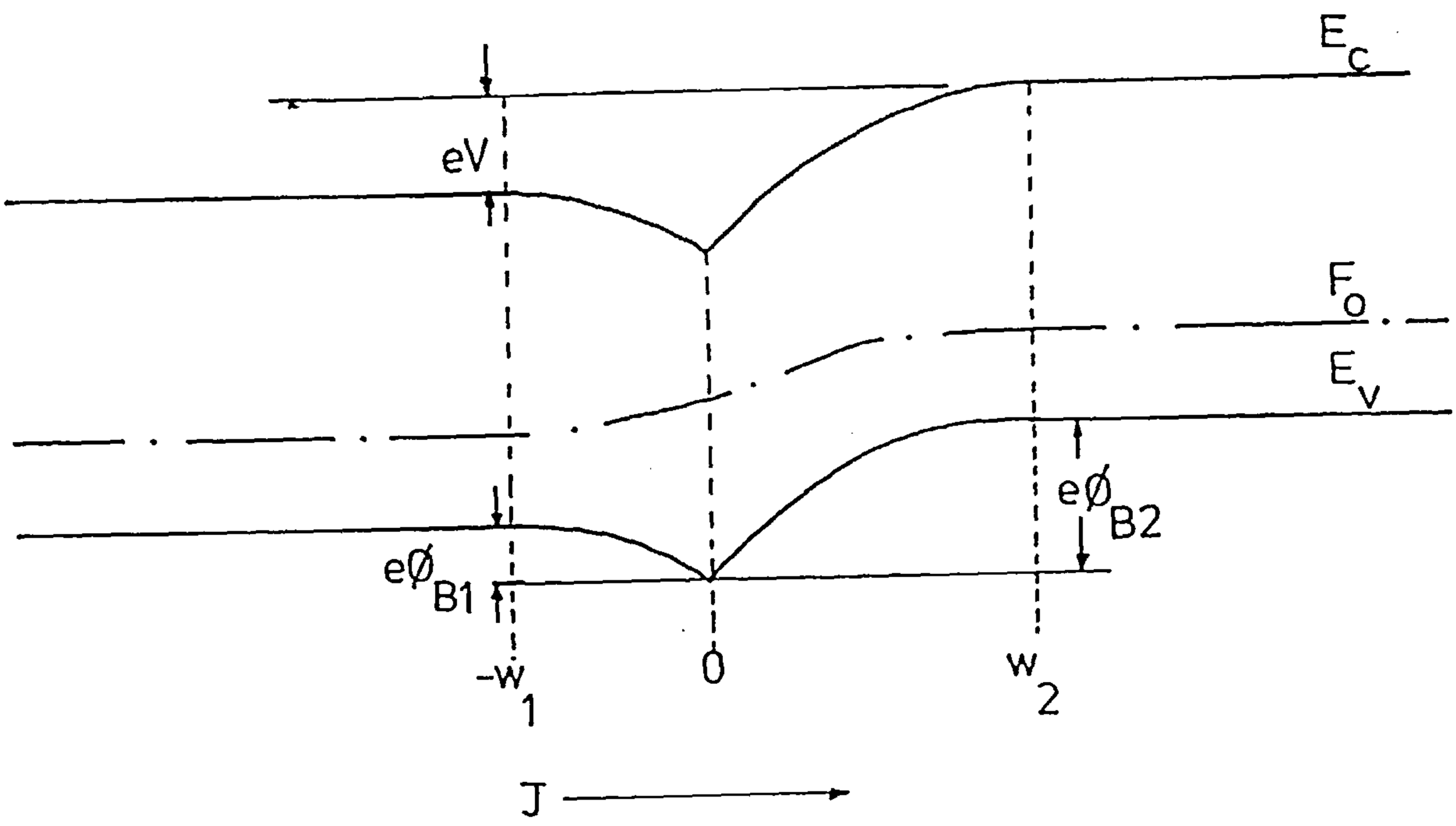

Figure 3.20 The energy bands with a voltage, V, applied across the grain boundary.

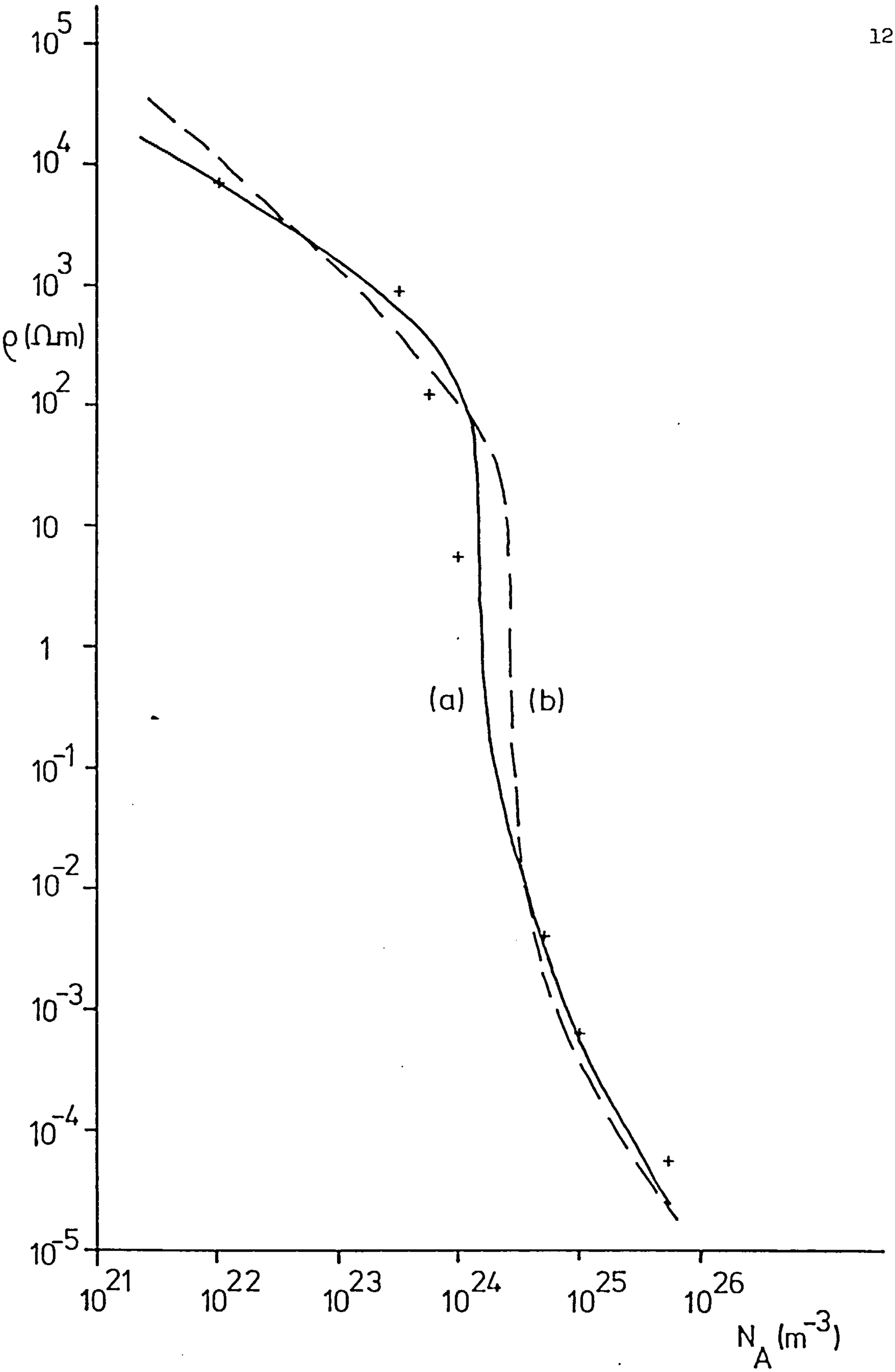

Figure 3.21 The resistivity in equilibrium in polysilicon as a function of doping density. Crosses are experimental points (Seto, 1975). (a) Present theory using equations (3.75) and (3.25) with the data of Table 3.1 and further parameters given in the text. (b) Theoretical curve (Seto, 1975) using thermionic emission and a depletion approximation model of the barrier height.

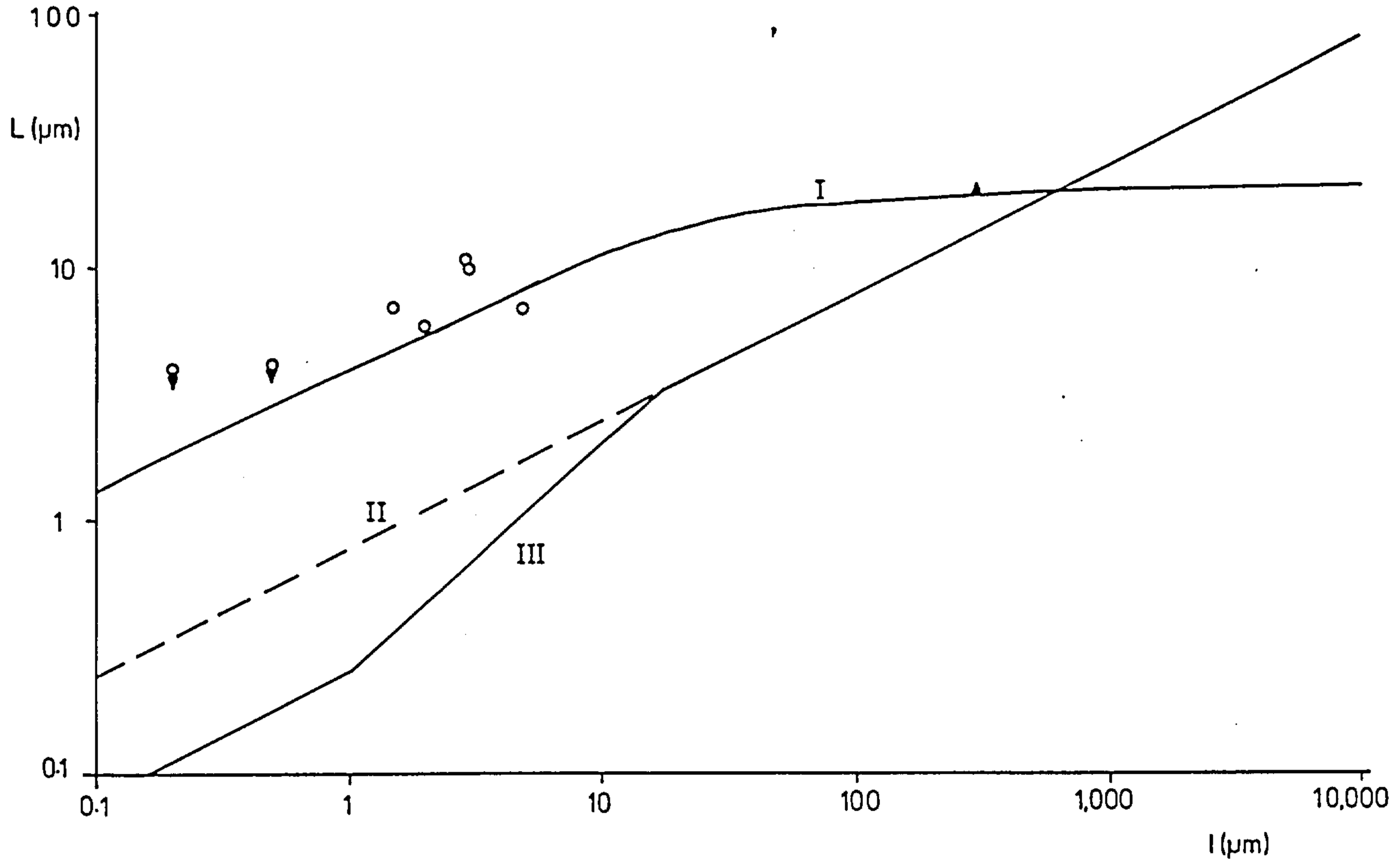

Figure 3.22 The diffusion length in polysilicon as a function of grain size. Circles and triangles are experimental points (Ghosh et al, 1980). Curve I shows the present theory of equation (3.79) and data given in the text. Curves II and III are theoretical curves (Ghosh et al, 1980) and are explained in the text.

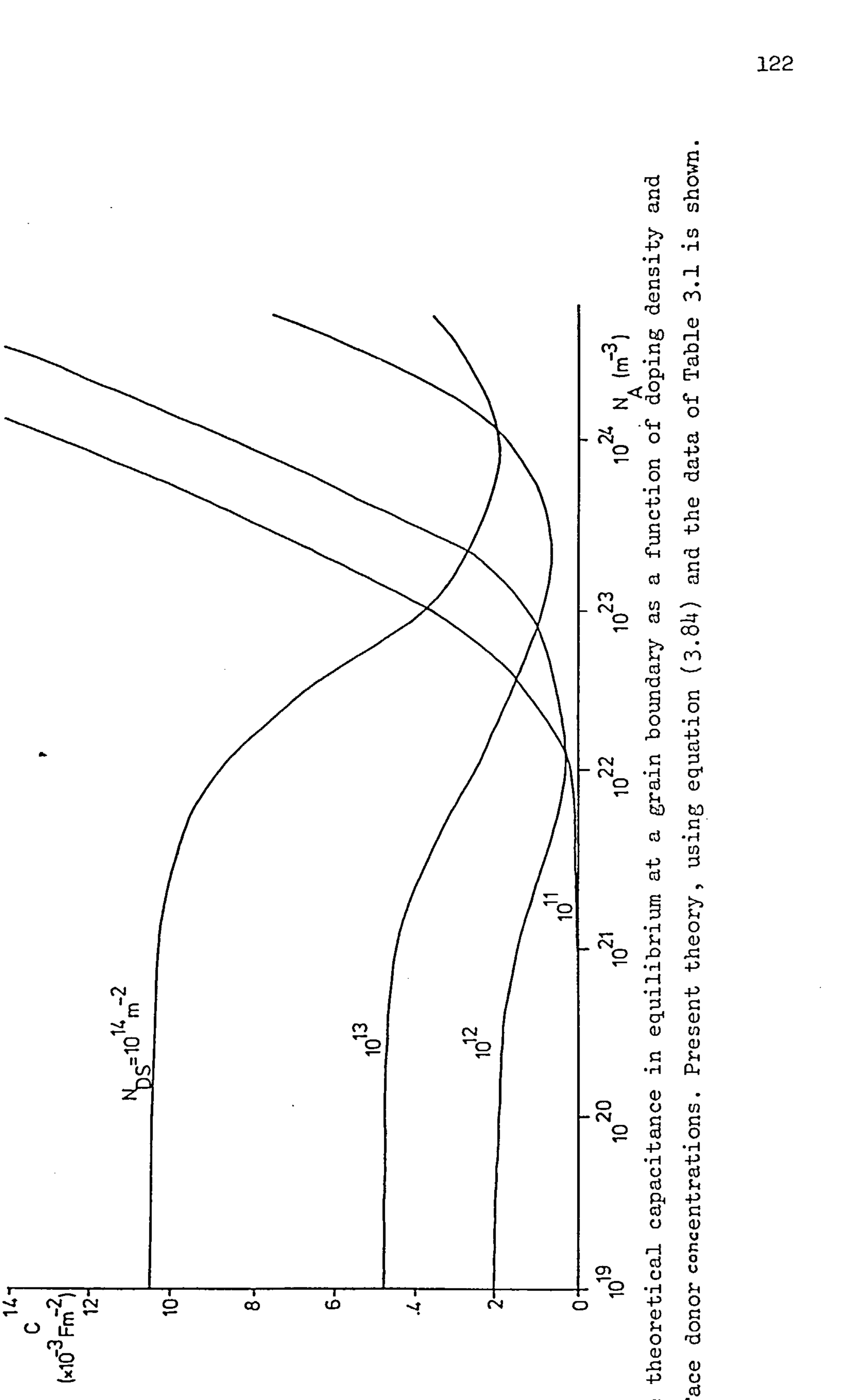

Figure 3.23 The theoretical capacitance in equilibrium at a grain boundary as a function of donor concentrations. Present theory, using equation (3.84) and the data of Table 3.1 is shown for various surface doping density and

CHAPTER 4

EVIDENCE OF NO k-SELECTION IN THE RADIATIVE RECOMBINATION SPECTRA OF AlGaAs QUANTUM WELL LASER DIODES

4.1 Introduction

GaAs semiconductor injection lasers (Casey and Panish, 1978) have been the centre of considerable research activity since their discovery more than twenty years ago (Hall et al., 1962). The gain curves of a GaAs laser can be calculated as a function of wavelength or energy by evaluating the theoretical stimulated emission rate ($r_{stim}(E)$ of Lasher and Stern, 1964). This radiative emission rate per unit energy per unit volume at an energy, E , is stimulated in a laser by photo-pumping an active layer with photons or by passing a large electrical current through the laser diode. In this work mainly the latter type of stimulating action has been considered.

Normally one takes the radiative emission to be an average over the two directions of polarization and over the photon wavevector $\underset{\sim}{k}$. For a review with special reference to the averaging process and the question of $\underset{\sim}{k}$-selection versus no $\underset{\sim}{k}$-selection rule, see Adams and Landsberg (1969). Marinelli (1965) and Unger (1967) have given approximate results to the integral for stimulated emission (Lasher and Stern, 1964). Russer (1980) used complex variable analysis to obtain an analytic solution for $r_{stim}(E)$ in the case of parabolic energy bands. A new result for $r_{stim}(E)$ in the case of constant density of states in each band is given here.

Recent work by Dutta (1982) and Dutta et al., (1983) has examined the so-called "quantum-size effects" which are seen when the active layer of a GaAs - $Al_x Ga_{1-x}As$ 'double heterostructure is made very

narrow (50 ∿ 200 Å). The energy of electrons in one dimension is restricted to quantum well levels in all bands, but the energy bands retain their usual parabolic form in the other two directions. The conduction and valence bands are split into a series of parabolic sub-bands, each has a constant, two-dimensional like density of states function. A good review of quantum-well lasers was given by Holonyak et al., (1980), where radiative emission was treated experimentally and theoretically.

As in the three-dimensional case, the argument for adopting $\underset{\sim}{k}$-selection or no $\underset{\sim}{k}$-selection rules in the transitions from band to band arises. It is suggested here, contrary to present views, that the processes which give rise to radiation in lightly doped or even undoped quantum-wells are not subject to strict $\underset{\sim}{k}$-selection rules. The reason is contained in the good fit of experimental TE polarization gain spectra of Dutta et al., (1983) and Kobayashi et al., (1983) which are obtained on the basis of no $\underset{\sim}{k}$-selection rules. In real systems one would expect partial $\underset{\sim}{k}$-selection, which follows from a finite relaxation time and allows a range of wavevectors to be involved in the transition. The two extreme cases of this are: (i) strict $\underset{\sim}{k}$-selection in which the relaxation time is very long, and (ii) no $\underset{\sim}{k}$-selection in which the relaxation time is very short.

4.2 Energy Bands in a Quantum-Well Structure

In a two-dimensional system (Ando et al., 1982), the energy bands are modified from their familiar form in the bulk material. Because there is one allowed state per volume $(2\pi/L)^2$ in a box of side L in $\underset{\sim}{k}$-space of two dimensions, the total number of states with wavevector less than k is given by $(L/2\pi)^2$ multiplied by the area of a circle of radius k,

$$N(k) = 2(L/2\pi)^2 \pi k^2$$

where a factor 2 is included for spin degeneracy. If the electron energy can be written in the form

$$E = E_o + \frac{\hbar^2 k^2}{2m}$$

where $\hbar$ is the reduced Planck's constant and m is the effective mass, then

$$dE = \frac{\hbar^2 k dk}{m}$$

The density of states in two dimensions per unit <u>volume</u> and per unit energy is

$$D(E) = \frac{dN(k)}{dK}\left(\frac{dk}{dE}\right)\frac{1}{V} = \frac{mL^2}{\pi\hbar^2 V} \quad (E > E_o\ ,\ 0 \quad \text{otherwise}).$$

In this case, the volume V extends to L in the x and y directions, but only to L_z in the z-direction since it is confined by the quantum well, therefore

$$D(E) = \frac{m}{\pi\hbar^2 L_z} \quad (E > E_o\ ,\ 0 \quad \text{otherwise}). \qquad (4.1)$$

Note that the density of states per unit volume and per unit energy depends on the thickness of the quantum well in the third dimension, but it is independent of the depth of the well in energy.

Dingle (1975) has given the depths of the quantum-wells in the conduction (ΔE_c) and valence bands (ΔE_v) as

$$\Delta E_c = (0.85 \pm 0.03)\Delta E_G \tag{4.2}$$

and

$$\Delta E_v = (0.15 \pm 0.03)\Delta E_G \tag{4.3}$$

where ΔE_G is the difference of the energy band gaps of the GaAs active layer and the $Ga_{1-x}Al_xAs$ barrier layers, see Casey and Panish (1978) where

$$\Delta E_G \equiv E_G(Al_xGa_{1-x}As) - E_G(GaAs) = 1.2470x \quad (\text{for } x < 0.45) \ . \tag{4.4}$$

The energy levels of a single quantum-well structure are determined by the energy eigenvalues to Schrödinger's equation, see Schiff (1955)

$$-\frac{\hbar^2}{2m}\frac{d^2}{dz^2} + (V_o - E)\psi = 0 \ .$$

Inside the quantum well ($-a \lesssim z \lesssim a$ where $a = L_z/2$), the wavefunction is

$$\psi_3 = A_3 \sin\beta_3 z + B_3 \cos\beta_3 z \quad [\beta_3 \equiv (2m_3E/\hbar^2)^{\frac{1}{2}}] \ , \tag{4.5}$$

where β_3 is the allowed wavenumber. Outside the quantum well ($z < -a$, $z < a$) the wavefunction is exponentially decaying,

$$\psi_1 = A_1 \exp(\beta_1 z) \quad (\text{for } z<-a) \ ,$$

$$\psi_2 = B_2 \exp(-\beta_2 z) \quad (\text{for } z>a), \ [\beta_1 = \beta_2 = \{2m_1(V_o - E)/\hbar^2\}^{\frac{1}{2}}] \ . \tag{4.6}$$

The solutions are matched on the boundaries ($z = \pm a$) by requiring ψ and $\frac{1}{m}\left(\frac{d\psi}{dz}\right)$ to be continuous. The latter boundary condition arises because the steady-state current of electrons across the boundary is continuous, e.g.

$$[J = ep/m=]e(i\hbar\nabla\psi_1)/m_1 = e(-i\hbar\nabla\psi_3)/m_3$$

at $z = -a$. This boundary condition takes into account the change of effective mass in passing from one region into the next and leads to the following set of equations:

$$A_1\exp[-\beta_1 a] = -A_3\sin\beta_3 a+B_3\cos\beta_3 a \ , \qquad [\psi(-a)]$$

$$m_3\beta_1 A_1\exp[-\beta_1 a]= m_1\{\beta_3 A_3\cos\beta_3 a+\beta_3 B_3\sin\beta_3 a\} \ , \qquad [m^{-1}\psi'(-a)]$$

$$B_2\exp[-\beta_2 a] = A_3\sin\beta_3 a+B_3\cos\beta_3 a \ , \qquad [\psi(a)]$$

$$m_3\beta_2 B_2\exp[-\beta_2 a] = m_2\{-\beta_3 A_3\cos\beta_3 a+\beta_3 B_3\cos\beta_3 a\} \ . \qquad [m^{-1}\psi'(a)]$$

By subtracting various of these equations and noting that $m_1 = m_2$, $\beta_1 = \beta_2$, the following sets are obtained:

$$(A_1-B_2)\exp[-\beta_1 a] = -2A_3\sin\beta_3 a \ , \qquad (4.7)$$

$$(A_1+B_2)\exp[-\beta_1 a] = 2B_3\cos\beta_3 a \ , \qquad (4.8)$$

$$\beta_1 m_3(A_1-B_2)\exp[-\beta_1 a] = 2\ {}_3m_1 A_3\cos\beta_3 a \ , \qquad (4.9)$$

$$\beta_1 m_3(A_1+B_2)\exp[-\beta_1 a] = 2\ {}_3m_1 B_3\sin\beta_3 a \ . \qquad (4.10)$$

Unless $A_3 = 0$ and $A_1 = B_2$, from (4.7) and (4.9) one has

$$(m_3/m_1)\beta_1 = -\beta_3\cot\beta_3 a \ , \qquad (4.11)$$

similarly unless $B_3 = 0$ and $A_1 + B_2 = 0$, it is found from (4.8) and (4.10) that

$$(m_3/m_1)\beta_1 = \beta_3\tan\beta_3 a \ . \qquad (4.12)$$

Also, combining β_1 and β_3 from equations (4.5) and (4.6)

$$(\beta_1^2/m_1) + (\beta_3^2/m_3) = 2V_o/\hbar^2 \quad . \tag{4.13}$$

Equations (4.11) or (4.12) together with (4.13) are solved numerically for the wavenumbers β_1 and β_3 ; a graphical estimate of the wavenumbers can be obtained from Figures such as 4.1 (see also Schiff, 1955) where the curves are given by equations (4.11) to (4.13) and they cross at permitted wavenumbers. The energy eigenvalues are given by

$$E = \hbar^2\beta_3^2/2m_3 \quad . \tag{4.14}$$

When the barrier potential, V_o , is very large, one can use the approximation of an infinite barrier height. The wavefunctions in the barriers $\{\Delta E_c/e, \ \Delta E_v/e\}$ are zero and the boundary conditions for Schrodinger's equation are $\psi(\pm a) = 0$. The wavefunction in the well is given by equation (4.5) with

$$\beta_3 = n\pi/2a, \ A_3 = 0$$

where n is the principle quantum number and an integer. The energy levels associated with the quantum wells in the conduction and valence bands are

$$E_{n\alpha}^{\ell,h} = \frac{\hbar^2}{2m_\alpha^{\ell,h}} \left(\frac{n\pi}{L_z}\right)^2 \qquad [\alpha = C, \ v; \ n = 1,2,3,\ldots]$$

and all levels with the same value of n have the same value of $k_z(= \beta_3)$ in the wavevector. The superscripts ℓ, h here and in Tables 4.1 and 4.2 refer to light and heavy-hole quantities respectively. In real structures (Dutta et al., 1983; Kobayashi et al., 1983) the energy levels obtained numerically from equations (4.11) to (4.14) differ from the infinite well approximation given above and the latter calculation is inadequate to give good agreement with experiment.

Further complications are found in the multi-quantum well structure (Kobayashi et al., 1983) shown in Figure 4.2, the barriers are no longer infinitely wide and the energy levels of neighbouring wells are coupled by resonant tunneling (Kittel, 1976). Here, an approximate result for the energy states of the multi-quantum well structure is obtained. The six inner wells of Figure 4.2 are symmetric, but the two outer or end wells are asymmetric with different barrier heights because of the different composition of the barrier and cladding layers. In this work, the barrier thicknesses are assumed to be large enough that the effect of tunneling between neighbouring wells on the energy levels of the quantum wells may be neglected

For the quantum wells in the centre of the structure, the procedure of equations (4.11) to (4.14) is used to calculate the energy levels. The two end quantum wells are of finite depth with different barrier heights, V_1 and V_2, see Figure 4.3. Their energy levels are calculated with the assumption of no tunneling into neighbouring wells as follows: in the barrier regions, the wavefunctions of Schrodinger's equation are given by

$$\psi_i = A_i \exp(\beta_i z) + B_i \exp(-\beta_i z) \quad , \quad [i = 1,2; \ \beta_i = \{2m_i(V_i - E)/\hbar^2\}^{\frac{1}{2}}] \quad ,$$

and in the quantum well, the wavefunction is given by equation (4.5). One uses again the boundary conditions ψ_i and $\frac{1}{m_i}\left(\frac{d\psi_i}{dz}\right)$ are continuous at the walls, $z = \pm a$, and requires $\psi(\pm z)$ to tend to zero for large z in the barriers. These conditions lead to the following set of equations:

$$B_2\exp(-\beta_2 a) = A_3\sin\beta_3 a + B_3\cos\beta_3 a \quad , \qquad [\psi(a)]$$

$$m_3\beta_2 B_2\exp(-\beta_2 a) = m_2\beta_3(-A_3\cos\beta_3 a + B_3\sin\beta_3 a) \quad , \qquad [m^{-1}\psi'(a)]$$

together with

$$(\beta_1^2/m_1) + (\beta_3^2/m_3) = 2V_1/\hbar^2 \quad , \tag{4.15}$$

$$(\beta_2^2/m_2) + (\beta_3^2/m_3) = 2V_2/\hbar^2 \quad . \tag{4.16}$$

The first four equations can be transformed ito a matrix equation

$$\begin{pmatrix} Q & 0 & 0 & -\beta_3 \\ R & 0 & -\beta_3 & 0 \\ 0 & S & 0 & -\beta_3 \\ 0 & T & -\beta_3 & 0 \end{pmatrix} \begin{pmatrix} A_1 \\ B_2 \\ A_3 \\ B_3 \end{pmatrix} = 0$$

where

$$Q = \exp(-\beta_1 a)\{(\beta_1/m_1)\sin\beta_3 a + (\beta_3/m_3)\cos\beta_3 a\} \quad ,$$

$$R = \exp(-\beta_1 a)\{(\beta_1/m_1)\cos\beta_3 a - (\beta_3/m_3)\sin\beta_3 a\} \quad ,$$

$$S = \exp(-\beta_2 a)\{(\beta_3/m_3)\cos\beta_3 a + (\beta_2/m_2)\sin\beta_3 a\} \quad ,$$

and

$$T = \exp(-\beta_2 a)\{(\beta_3/m_3)\sin\beta_3 a - (\beta_2/m_2)\cos\beta_3 a\} \quad .$$

Using the Gauss elimination method on the matrix, one obtains

$$\begin{pmatrix} Q & -S & 0 & 0 \\ R & -T & 0 & 0 \\ 0 & S & 0 & -\beta_3 \\ 0 & T & -\beta_3 & 0 \end{pmatrix} \begin{pmatrix} A_1 \\ B_2 \\ A_3 \\ B_3 \end{pmatrix} = 0 \ ,$$

which has a non-trivial solution if the determinant of the matrix is zero (Lennox and Chadwick, 1970), i.e.

$$\beta_3^2 \begin{vmatrix} Q & -S \\ R & -T \end{vmatrix} = 0 \ .$$

Thus, a solution of

$$QT - SR = 0$$

is sought. Using the expressions given above for Q, R, S and T, the following transcendental equation is found:

$$(\beta_3/m_3)\{(\beta_1/m_1)+(\beta_2/m_2)\}\cos\beta_3 L_z+\{(\beta_1/m_1)(\beta_2/m_2)-(\beta_3/m_3)^2\}\sin\beta_3 L_z = 0 \ .$$

This equation is solved numerically together with equations (4.15) and (4.16) for the allowed wavenumbers β_3 of the asymmetric quantum well and the energy levels are obtained from equation (4.14).

The minimum energy of transition, E_G^*, from the conduction band to the heavy-hole valence band is slightly larger than the energy gap, E_G, of bulk GaAs because of the addition to E_G of the quantum well ground state energies in each gand. Superimposed on this effect is the probable reduction of E_G by band-gap shrinkage (see for example In kson, 1976) since the carrier concentrations in a laser are high. This is assumed here to be of a similar magnitude in GaAs quantum well structures as it is in bulk GaAs material.

The result of the quantization of the z-component of the wavevector is that the energy bands are split into a series of sub-bands as shown in Figure 4.4. The energy in the conduction band is divided up between the various wavevector components by

$$E = E_c + \frac{\hbar^2}{2m_c}\left\{k_x^2 + k_y^2 + k_z^2\right\}$$

or in the valence bands by

$$E = E_v - \frac{\hbar^2}{2m_v}\left\{k_x^2 + k_y^2 + k_z^2\right\}$$

where k_x and k_y vary continuously and k_z $(= \beta_3)$ is determined by the appropriate quantum well model. Each of the sub-bands has the same density of states (4.1) depending on the effective mass of the quantum well. This leads to a step-like function for the total density of states in each band and is shown in Figure 4.5.

The electron and hole concentrations in this band structure are governed by the Fermi-Dirac statistics for the occupation probability and by the density of states (4.1) of each sub-band. The electron concentration, N, per unit volume is given by

$$N = \sum_{r=1}^{r_t}\left(\frac{m_c}{\pi\hbar^2 L_z}\int_{E_{rc}}^{\infty}\frac{dE}{\exp\{\eta-\gamma_e\}+1}\right),$$

where η is the energy state, E, divided by k_BT, $k_B(= 8.6171 \times 10^{-5} eVK^{-1})$ is Boltzmann's constant T is the temperature and γ_e is the electron quasi-Fermi level, F_e, divided by k_BT. The hole concentration, P, is that given by the sum of the light and heavy-hole densities,

$$P = \sum_{i=\ell,h} \left\{ \sum_{s^i=1}^{s_t^i} \left[\frac{m_v^i}{\pi h^2 L_z} \int_{-\infty}^{E_{sv}^i} \frac{dE}{\exp(\gamma_h - \eta)+1} \right] \right\} \quad ,$$

where γ_h is the hole quasi-Fermi level, F_h, divided by $k_B T$. The calculation of the electron and hole concentrations is simplified in a finite depth quantum well because the total number of levels $\{r_t, s_v^\ell, s_v^h\}$ in each of the bands is usually small.

In the present work, the energetic positions of the electron and hole quasi-Fermi levels are calculated by assuming that the separation of the Fermi levels is known, for example it can be found from the gain spectrum, and that there is charge neutrality in the quantum well. Hence,

$$P - N - N_A^- + N_D^+ = 0$$

where N_A^- is the number of charged acceptors per unit volume and N_D^+ is the number of charged donors per unit volume. In lightly doped or undoped quantum wells (Dutta et al., 1983, Kobayashi et al., 1983), one solves the simple equation,

$$(N=P=) \sum_{r=1}^{r_t} \frac{m_c k_B T}{\pi \hbar^2 L_z} \left\{ - \ln\left[\frac{1}{1+\exp[\gamma_e - \eta_{rc}]} \right] \right\} = \sum_{i=\ell,h} \sum_{s^i=1}^{s_t^i} \frac{m_v^i k_B T}{\pi \hbar^2 L_z} \left\{ -\ln\left[\frac{1}{1+\exp[\eta_{sv}^i - \gamma_h]} \right] \right\}$$

where N and P are the electron and hole concentrations obtained from the integrals given above. Therefore, the following equation is solved iteratively for γ_h, where $\gamma_e - \gamma_h$ is known:

$$\sum_{r=1}^{r_t} \ln\left\{ 1+\exp[\gamma_e - \gamma_h + \gamma_h - \eta_{rc}] \right\} = \sum_{i=\ell,h} \left[\sum_{s^i=1}^{s_t^i} \ln\left\{ 1+\exp[\eta_{sv}^i - \gamma_h] \right\} \right] .$$

Once γ_e is also obtained, the electron and hole concentrations can be calculated from the expression above.

4.3 The Stimulated Emission Rate

In a quantum well laser the electron and hole populations in the well region described above are made very large by carrier injection. This gives rise to stimulated photon emission as the electrons and holes recombine in the active layer. The theory of optical absorption and emission permits radiative transitions which conserve the wavevectors of the electron, the hole and the photon. Since the momentum of the photon is very small in relation to the scale of the Brillouin zone, radiative transitions are allowed between energy states with effectively the same wavevector. When dopant impurities, for example, are added to the semiconductor the wavefunctions are modified and $\underset{\sim}{k}$-selection rules no longer apply. It was commonly presumed until now that $\underset{\sim}{k}$-selection rules could be relaxed only in heavily-doped quantum well structures, but recent arguments put forward by Sugimura (1983) suggest that even under heavy-doping conditions the $\underset{\sim}{k}$-selection rules should be obeyed.

(a) Electron Transitions with $\underset{\sim}{k}$-selection rules

The permitted transitions for stimulated photon emission shown in Figure 4.4 are either vertically up or down in energy to conserve the wavevector of the electron. Of course, the radiative transitions conserve k_z as well as k_x and k_y and so transitions are allowed between sub-bands in the quantum well which have the same quantum number.

If an infinite depth to the wells in both bands is assumed, the energy levels in each band with the same quantum number have identical

k_z components of the wavevector. When a more detailed calculation of the energy levels is made assuming a finite depth to each quantum well, the k_z components corresponding to energy levels with the same quantum number in the conduction and valence bands are slightly different. Thus, if k-selection is to be applied to radiative transitions from one band to another, some other process is needed to take up the slight change of electronic momentum. In support of this, Holonyak et al., (1980) have observed (1-LO) phonon assisted laser operation in quantum well structures and expect phonon participation to play a more important part in radiative transitions in quantum well structures than in bulk transitions in III-V semiconductors.

The net rate of transition from an energy level A in the lowest conduction band to the energy level b in the highest heavy-hole valence band, see Figure 4.4, is

$$r_{stim}(E) = C(E)\rho_c(A)\rho_v(B)[f_c(A)(1-f_v(B))-f_v(B)(1-f_c(A))] \qquad (4.17)$$

where C(E) incorporates the matrix element for transitions from A to B and ρ_c , ρ_v are the density of states in the bands. Here, f_c and f_v are the Fermi-Dirac probabilities of finding an electron each each of the bands,

$$f_c(A) = \frac{1}{\exp[\theta_c/k_BT]+1} , \quad f_v(B) = \frac{1}{\exp[\theta_v/k_BT]+1} \qquad (4.18,4.19)$$

where also

$$\theta_c \equiv E_c + E_{1c} + \varepsilon_c - F_e , \quad \theta_v \equiv E_v - E^h_{1v} - \varepsilon_v - F_h , \qquad (4.20,4.21)$$

E_c and E_v are the band edge energies, E_{1c} and E^h_{1v} are the

first quantum-well energy levels, η_c and η_v are the energies associated with the k_x and k_y wavevectors for each band F_e and F_h are the electron and hole quasi-Fermi levels. Thus, the energy of level A is

$$E_c + E_{1c} + \epsilon_c = E_c + \frac{\hbar^2}{2m_c}\left\{k_x^2 + k_y^2 + k_z^2\right\} . \qquad (4.22)$$

A similar expression (Ando, Fowler and Stern, 1982) for holes in the heavy-hole valence band at energy level B is

$$E_v - E_{1v}^h - \epsilon_v = E_v - \frac{\hbar^2}{2m_v^h}\left\{k_x^2 + k_y^2 + k_z^2\right\} . \qquad (4.23)$$

In the adopted notation, the energy of transition from A to B is

$$E = E_G + E_{1c} + \epsilon_c + E_{1v}^h + \epsilon_v = E_G + \frac{\hbar^2}{2}\left\{\frac{1}{m_c} + \frac{1}{m_v^h}\right\}\left[k_x^2+k_y^2+k_z^2\right] . \qquad (4.24)$$

Eliminating the wavevector dependence of (4.20) and (4.21) using (4.22), (4.23) and (4.24), one has

$$\theta_c = E_c - F_e + \frac{m_v^h}{m_c+m_v^h}(E-E_G) , \qquad (4.25)$$

$$\theta_v = E_v - F_h - \frac{m_c}{m_c+m_v^h}(E-E_G) . \qquad (4.26)$$

Using equation (4.1), the density of states in the lowest conduction sub-band and in the highest valence (heavy-hole) sub-band are

$$\rho c = \frac{m_c}{\pi\hbar^2 L_z} \quad , \quad \rho_v^h = \frac{m_v^h}{\pi\hbar^2 L_z} \quad .$$

Thus, one may write the stimulated emission rate with $\underset{\sim}{k}$-selection as

$$r_{stim}(E) = C(E)\,\frac{m_c m_v^h}{\pi^2\hbar^4 L_z^2}\left[\frac{1}{\exp[\theta_c/k_BT]+1} - \frac{1}{\exp[\theta_v/k_BT]+1}\right] \qquad (4.27)$$

where θ_c (4.25) and θ_v (4.26) are given above. Equation (4.27) applies when the lowest sub-bands are the only bands involved in the transitions, i.e. for

$$E_G \lesssim E < F_e - F_h < E_{2c} + E_{2v}^h + E_G \quad .$$

When higher-sub-bands are involved, the stimulated emission rate is

$$r_{stim}(E) = \sum_{n=1}^{\nu} \frac{C(E) m_c m_v^h}{\pi^2\hbar^4 L_z^2} \frac{\sinh\tfrac{1}{2}(\gamma_e-\gamma_h-\eta)}{\cosh\tfrac{1}{2}(\gamma_e-\gamma_h-\eta)+\cosh\tfrac{1}{2}(\eta_v-\gamma_h+\eta_c-\gamma_e+\delta(\eta-\eta_G))} \qquad (4.28)$$

where $\delta = (m_v^h-m_c)/(m_v^h+m_c)$, η denotes energies divided by k_BT and γ's are Fermi levels divided by k_BT. Here, the Fermi-Dirac probability functions have been rearranged over a common denominator to give hyperbolic functions. The limit ν of the sum is given by

$$E_{\nu c} + E_{\nu v}^h < F_e - F_h - E_G < E_{\nu+1 c} + E_{\nu+1 v}^h \; ; \qquad (4.29)$$

for energy sub-bands separated by more than F_e-F_h , absorption is found, but there is no stimulated emission (Pilkuhn, 1968). It will be assumed here (Lasher and Stern, 1964) that the probability of transition $C(E)$ is independent of energy. The shape of $r_{stim}(E)$ is given by the difference of the two probability functions and is

shown in Figure 4.6. It can be seen at once from equations (4.25) and (4.26) that $f_c(A)$ decreases and $f_v(B)$ increases with the energy of transition E ; $r_{stim}(E)$ has a negative slope in all cases. This is in agreement with the simple theory of Burt (1983), but weakly bowed curves replace the downward sloping straight lines given in Figure 1 there. Kasemset et al., (1983) performed a more detailed theory of k-selection in radiative emission which also gave monotonically decreasing gain curves as a function of energy, E .

In three dimensions, the density of states functions ρ_c and ρ_v are proportional to energy E in such a way as to pull r_{stim} down to zero at $E = E_G$. Hence, $r_{stim}(E)$ has a maximum at an energy greater than E_G. The rise in the shape of r_{stim} is due to the density of states and the drop at larger energies is due to the density probability term. In two dimensions and in the simple case involving the lowest levels in the wells, the density of states functions are independent of the energy of transition, E . Since the probability term is largest at $E = E_G$, r_{stim} has its maximum at that energy.

(b) Electron Transitions Without k-selection Rules

If k-selection rules are relaxed because the process involved in the transition can take up significant parts of the electronic momentum, for example when many impurities are present, one finds the stimulated emission rate is given by (Lasher and Stern, 1964)

$$r_{stim}(E) = \int_0^{E-E_G} C\, \rho_c(E')\rho_v(E'-E)[f_c(E')-f_v(E'-E)]dE' \quad . \qquad (4.30)$$

Here, E' is the energy measured up from the edge of the conduction band.

For k-selection to be relaxed, any transition of an electron from the conduction band quantum well to the valence band quantum well needs some process, for example Coulomb interaction, to take up the change in the electron wavevector. It is plausible that this may be possible for the k_x and k_y components because these components of the wavevector are continuous and then k-selection is relaxed in the way that it is in bulk transitions. However, the z-component of the wavevector is dictated by the discrete energy levels of the conduction band or valence band quantum wells. The probability of a process occurring by which the z-component of the electron wavevector changes by exactly the right amount for the electron to enter a sub-band of the hole quantum well with a different quantum number than the sub-band it left is negligibly small. For this reason, only the transistions which preserve the quantum number, n , of the well are permitted when k-selection is relaxed.

Each of the sub-bands has a constant density of states for all energies above its quantum well level and the combined density of states of all the sub-bands has the step-like form shown in Figure 4.5. Thus, the stimulated emission rate is given by

$$r_{stim}(E) = \sum_{i=\ell,h} \sum_{n=1}^{\nu_i} \frac{Cm_c m_v^i}{\pi^2 \hbar^4 L_z^2} \int_0^{E-E_G-E_{nc}-E_{nv}^i} [f_c(E')-f_v(E'-E)]dE' \qquad (4.31)$$

where the upper limit of the sub-bands ν^i is given by (4.29), the index i denotes light and heavy-hole bands.

In the simplest case, only the lowest (n=1) conduction band and highest (n=1) heavy-hole band quantum well levels are involved, and the stimulated emission rate is

$$r_{stim}(E) = \frac{Cm_c m_v^h k_B T}{\pi^2 \hbar^4 L_z^2} \int_0^{-\eta_G-\eta_{1c}-\eta_{1v}^h} \left\{ \frac{1}{\exp(\eta'+\eta_c+\eta_{1c}-\gamma_e)+1} - \frac{1}{\exp(\eta'+\eta_c+\eta_{1c}-\eta-\gamma_h)+1} \right\}$$

This integral may be performed exactly and the result is (Hess et al., 1980)

$$r_{stim}(E) = \frac{Cm_c m_v^h k_B T}{\pi^2 \hbar^4 L_z^2} \ln\left[\frac{1+\exp[\gamma_e-\eta_c-\eta_{1c}])(1+\exp[\gamma_h-\eta_v-\eta_{1v}^h])}{(1+\exp[\gamma_e-\eta_v-\eta_{1v}^h-\eta])(1+\exp[\gamma_h+\eta-\eta_c-\eta_{1c}])} \right], \qquad (4.32)$$

for $E > E_G + E_{1c} + E_{1v}^h$. The logarithm term of (4.32) has zeros at $E = E_G + E_{1c} + E_{1v}^h$ and $E = F_e - F_h$, this is the same as in the three-dimensional emission (Pilkuhn, 1968). However, the shapes of the gain curves are different, in three-dimensional regions the gain curves are asymmetric with a maximum (Marinelli, 1965) at

$$E \doteq \{E_G+2(F_e-F_h)\}/3$$

provided $F_e - F_h < E_G + 2k_BT$. In two-dimensional regions, the maximum of the stimulated emission is found as follows: differentiating equation (4.32) with respect to E,

$$\frac{1}{\exp[\eta+\eta_v+\eta_{1v}^h-\gamma_e]+1} - \frac{1}{\exp[\eta_c+\eta_{1c}-\eta-\gamma_h]+1} = 0$$

at the maximum. Thus,

$$\eta + \eta_v + \eta_{1v}^h - \gamma_e = \eta_c + \eta_{1c} - \eta - \gamma_h$$

and the maximum lies at

$$E = [E_G + E_{1c} + E_{1v}^h + (F_e-F_h)]/2 \; . \qquad (4.33)$$

One finds a symmetric stimulated emission rate as a function of energy with a maximum situated in the centre of the energy range of emission.

If transitions between the higher quantum wells of the conduction band and heavy- and light-hole bands occur because of larger energies of emission, E, equation (4.31) has the result

$$r_{stim}(E) = \sum_{i=\ell,h} \sum_{n=1}^{\nu} \frac{C m_c m_v^i k_B T}{\pi^2 \hbar^4 L_z^2} \ln\left[\frac{(1+\exp[\gamma_e-\eta_c-\eta_{nc}])(1+\exp[\gamma_h-\eta_v-\eta_{nv}^i])}{[(1+\exp[\gamma_e-\eta_v-\eta_{nv}^i-\eta])(1+\exp[\gamma_h+\eta-\eta_c-\eta_{nc}])}\right] . \tag{4.34}$$

Here, the index i refers to light and heavy-hole quantities and C is taken to be the same constant for all transitions. The stimulated emission rate again has zeroes at

$$E = E_G + E_{1c} + E_{1v}^h$$

and

$$E = F_e - F_h .$$

However, it is now asymmetric with a maximum at an energy greater than half-way up the energy range of emission.

4.4 Gain Spectra

The shape of the emission spectrum of a laser is altered by internal and external losses. For unpolarized gain spectra, the net gain per unit length (Hakki and Paoli, 1975) is given by

$$G = \Gamma g - \Gamma\alpha_{int} - (1-\Gamma)\alpha_{ext} - (1/L)\ln(1/R) . \tag{4.35}$$

Here, Γ is the optical confinement factor, g in the optical gain, α_{int} is the internal loss, α_{ext} is the external loss, L is the length of the laser cavity and R is the reflectivity of the end

mirrors. The optical gain g is the same as the stimulated emission rate r_{stim} given by (4.28) or (4.34). The internal loss, α_{int}, is

$$\alpha_{int} = \sigma_n N + \sigma_p P$$

where $\sigma_n = 3.0 \times 10^{-18} cm^{-2}$ and $\sigma_p = 7.0 \times 10^{-18} cm^2$ (Casey and Panish, 1978) are the photon capture cross-sections in GaAs. One therefore expects the internal loss to depend on the separation of the quasi-Fermi levels through the carrier concentrations N and P.

It is convenient in the numerical work to recast (4.35) in the form

$$G(E)/\Gamma = A^{\ell} I^{\ell}(E) + A^{h} I^{h}(E) - B' = A^{\ell} I^{\ell} + A^{h} I^{h} - B - [(1-\Gamma)\alpha_{ext} + (1/L)\ln(1/R)]/\Gamma \ . \tag{4.36}$$

Here B' is the total of internal and external losses and B is the internal loss term only. The constants A^{ℓ} and A^{h} contain the matrix element for the transitions to light hole and heavy-holes levels and also the appropriate density of states functions given by equation (4.1). In comparing theory with experimental results, A^{h} and B', or B, are regarded as fitting parameters and A^{ℓ} is fixed by the ratio (see for example, Dutta, 1982),

$$A^{\ell}/A^{h} = m_v^{\ell}/m_v^{h} \ ,$$

taken from the density of states in each valence band. $I^{\ell}(E)$, $I^{h}(E)$ are the difference of Fermi-Dirac probability functions when k-selection rules are used and $I^{\ell}(E)$, $I^{h}(E)$ are integrals of the Fermi-Dirac probability functions as given in equation (4.31) when k-conservation is fully relaxed.

Using this background information we have inspected recently determined gain spectra from quantum-well structures. The symmetry of the three gain curves measured by Dutta et al., (1983, Fig.1)

using a single-quantum well laser diode persuaded us that the results should be representable by (4.36) using no k-selection rules (i.e. equation (4.34) for r_{stim}) and emission from a two-dimensional region. As shown in Figure 4.7 the agreement is excellent using the parameters given in Table 4.1, the GaAs masses $m_c = 0.067\ m_o$ $m_v = 0.082\ m_o$, $m_v^h = 0.45\ m_o$ (Casey and Panish, 1978) and the AlAs effective masses $m_c = 0.15\ m_o$, $m_v^h = 0.85\ m_o$, $m_v^\ell = 0.18\ m_o$ (Hess et al., 1973) where m_o is the free electron mass. Note that the effective masses for $Al_xGa_{1-x}As$ are a linear interpolation of the GaAs and AlAs effective masses using

$$m_i(Ga_{1-x}Al_xAs) = xm_i(AlAs) + (1-x)m_i(GaAs) .$$

The effective masses for GaAs have a range of values in the literature (see Blakemore, 1982) of which the set used here is a commonly utilised set of values.

The nearly straight line in Figure 4.7 is the net optical gain spectrum calculated assuming strict k-selection rules. It is clear from this curve that the assumption of k-selection is not compatible with this set of experimental curves. For completeness, the full spectrum assuming k-selection rules is shown in Figure 4.8. The labels H_i indicate the peaks due to an electron transition from the ith conduction sub-band to the ith heavy hole quantum-well sub-band. The labels L_i indicate the equivalent transition to light hole levels. The curve indicates that the highest peak is due to the third heavy-hole level and occurs at the same wavelength as the peak of the experimental curves of Dutta (1983 and Figure 4.7). However, the width of the k-selection spectrum is far greater than the width (in wavelength) of the curves of Dutta et al., (1983).

Due to a larger density of states in the two-dimensional case, the separation of quasi-Fermi levels $F_e - F_h$ corresponding to a given electron concentration is smaller than in three dimensions. Since also the minimum energy of transition in a quantum well structure, E_G^* , is larger than the bulk energy gap, E_G , of GaAs, the width of the gain spectrum should be narrower in quantum well structures than in the standard double heterostructure lasers. Consequently, as theoretically shown by Burt (1983) and confirmed experimentally by Tsang (1984), quantum well lasers are more likely to operate in a single longitudinal mode than conventional lasers. This is expected irrespective of whether k-selection rules are obeyed or not.

Anther pair of gain curves (TE polarization) at lower emission energies but also at room temperature was given by Kobayashi et al., (1983, Figure 1). The no k-selection rule fit is again good as shown by curves (a) and (b) in Figure 4.9 using the data of Table 4.2. The first energy levels in Table 4.2 correspond to the six quantum wells in the centre of the multi-quantum well structure and the second energy levels correspond to the two asymmetric quantum wells at the end of the structure. The values given correspond to finite depth quantum wells as described in Section 4.2.

The two curves for TM polarization given by Kobayashi et al., (1983) exhibit a lack of symmetry which might at first suggest that the two-dimensional no k-selection theory cannot explain them. However, the fit (curves (c) and (d) in Figure 4.9) using this theory shows that the measured TM gain spectra agree reasonably well with it. A polarization dependent selection rule is used (Kobayashi et al., 1983; Iwamura et al., 1983). Only transitions between the conduction and light-hole bands contribute to the emission of TM-polarized

light from two-dimensional structures, whereas transitions to both valence bands contribute to the TE polarization. Also, the matrix element for the TM polarization is expected to be about 2 times larger than for the TE polarization (Burt, 1984). Since the constants A^{ℓ} and A^{h} are proportional to the matrix element squareds, $A^{\ell}(TM)$ is about four times as large as $A^{\ell}(TE)$. The theoretical curves of Figure 4.9 (curves (c) and (d)) confirm that this model can account for the shift of the TM gain peak relative to the TE gain peak and for the asymmetry of the TM gain spectra in multi-quantum well structure.

In the above analysis of a multi-quantum well laser, the splitting of the levels caused by an interaction of bound states from adjacent wells separated by a thin barrier (Dingle, 1975) has been neglected. Also, the difference in the composition of the cladding and barrier layers has an effect on the energy levels in a multi-quantum well and this has been considered in an approximate way (see Section 4.2). Neither was any allowance made for well size fluctuations that may occur in practice when islands of different thickness are formed during crystal growth (Holonyak et al., 1981, Goldstein et al., 1983). An increase of the well thickness by one atomic layer ($\sim$ 3Å) would pull down the first energy level in the inner well by 1.1 meV for electrons, 0.2 meV for heavy holes and 0.4 meV for light holes. All of these effects should manifest themselves in some broadening of the gain spectrum, hence one can expect even better agreement of the no k-selection theory with the measured spectra of Figure 4.9 if a more detailed examination was undertaken.

4.5 Conclusions

Current ideas that the processes leading to radiative emission involve k-selection strict rules are probably not always right in quantum well structures. Even in cases where the doping is low or when there is no doping of the active layer, gain spectra (Dutta et al., 1983, Kobayashi et al., 1983) have been measured which conform to the no k-selection theory. It was presumed until now that k-selection rules could be relaxed only in heavily doped quantum well structures (see for example Kasemset et al, 1983, Dutta, 1982) and it has been argued that even under heavy doping conditions the k-selection rule should be obeyed (Sugimura, 1983). A possible explanation of the no k-selection observation may be due to the strong carrier - carrier interaction, enhanced compared to conventional lasers by the higher carrier concentrations required at threshold in quantum well lasers (cf. Tables 4.1c and 4.2c). This interpretation seems to be supported by the fact that the emission spectra of lasers used by Dutta et al., (1983), and Kobayashi et al., (1983) are shifted towards longer wavelengths than those calculated with no bandgap shrinkage.

The involvement of strict no k-selection rules in stimulated emission of radiation from undoped or lightly doped quantum wells may not be as common as has been suggested previously, and special steps may have to be taken to obtain gain curves which represent such processes. While a partial k-selection theory using intraband relaxation processes (see for example Yamada, 1983) would be expected to yield good agreement with experiment, its extreme limit of no k-selection already does this and has the merit of greater simplicity.

Table 4.1 Parameters Used for the fit of the Gain Spectra of Dutta et al., (1983)

A. Energy levels in meV			
n	E_{nc}	E_{nv}^{ℓ}	E_{nv}^{h}
1	9.79	1.51	6.21
2	39.15	6.02	24.61
3	87.96	13.52	53.28

b. Current-independent parameters				
	$A^{h}(cm^{-1})$	$A^{\ell}(cm^{-1})$	$B'(cm^{-1})$	T(K)
no k-selection theory	23.0×10^{3}	4.1×10^{3}	0.79×10^{3}	295
k-selection theory	5.0×10^{3}	0.9×10^{3}	0.14×10^{3}	295

c. Current-dependent parameters				
	I(mA)	E_G(eV)	$F_e - F_h$(eV)	$N(cm^{-3})$
no k-selection theory	67	1.4190	1.5757	4.26×10^{18}
	63	1.4196	1.5749	4.23×10^{18}
	60	1.4197	1.5742	4.19×10^{18}
k-selection theory	67	1.4215	1.5757	4.24×10^{18}

d. Quantum-well parameters		
	L_z(A)	x (of $Al_x Ga_{1-x}As$ barriers)
both k-selection and no k-selection theories	210	0.36

Table 4.2 Parameters Used for the fit of the Gain Spectra of Kobayashi et al., (1983)

a. Energy levels in meV						
n	E_{nc}	E^{ℓ}_{nv}	E^{h}_{nv}	E_{nc}	E_{nv}	E^{h}_{nv}
1	27.2	4.3	12.5	28.4	4.5	13.6
2	104.5	16.6	-	110.4	17.5	-
3	-	31.7	-	-	-	-

b. Current-independent parameters				
Polarization	$A^{h}(cm^{-1})$	$A^{\ell}(cm^{-1})$	$B'(cm^{-1})$	T(K
TE no k-selection theory	103.0×10^{3}	20×10^{3}	10	293
k-selection theory	50×10^{3}	9.1×10^{3}	10	293
TM no k-selection theory	0	73×10^{3}	10	293

c. Current-dependent parameters				
	I(mA)	E_G(eV)	F_e-F_h(eV)	$N(cm^{-3})$
no k-selection theory	101	1.3890	1.4645	2.42×10^{18}
	91	1.3903	1.4579	2.22×10^{18}
k-selection theory	101	1.3963	1.4645	2.41×10^{18}

d. Quantum-well parameters			
	L_z(A)	x (barrier layer)	x (cladding layer)
both k-selection and no k-selection theories	104	0.17	0.26

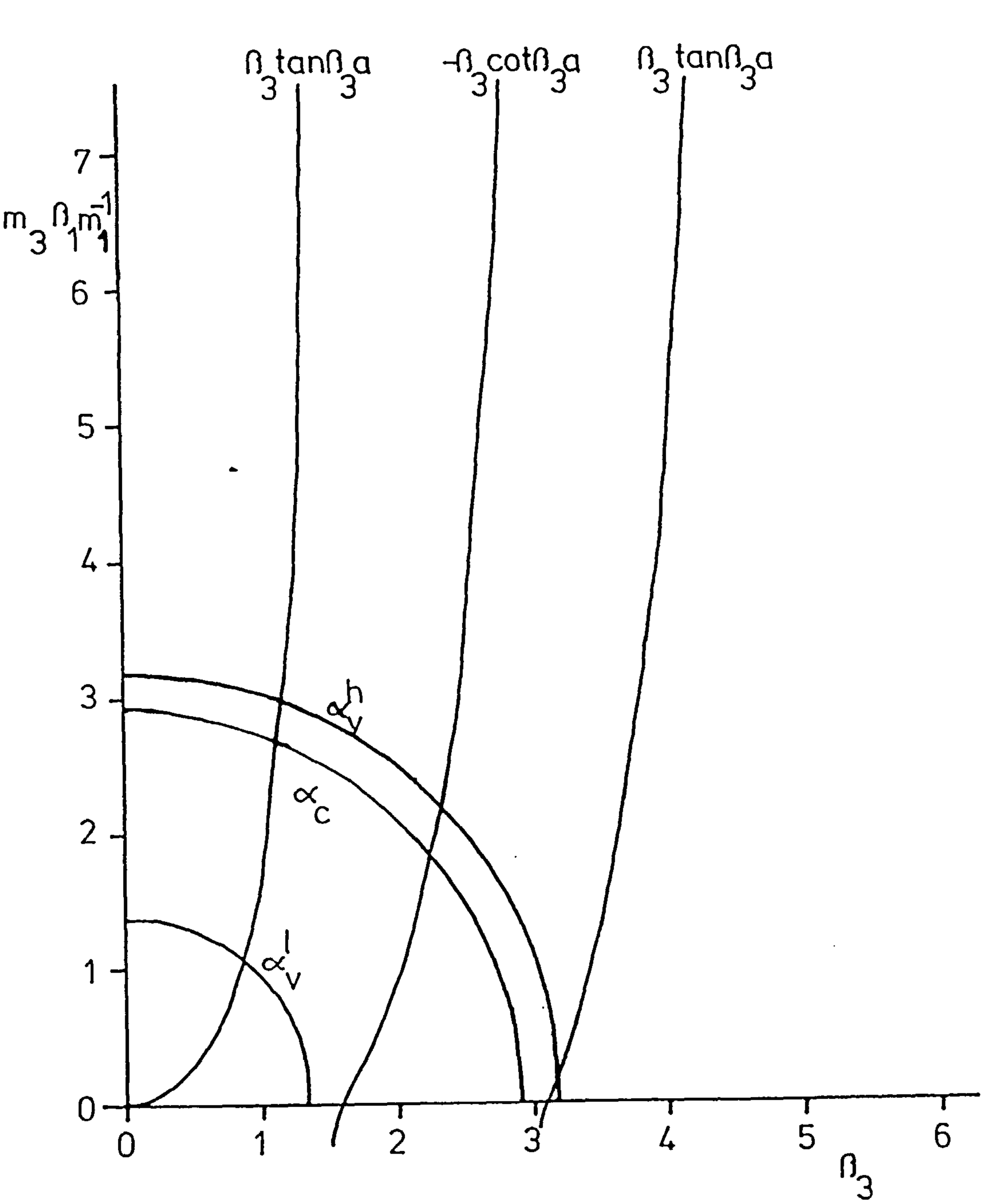

Figure 4.1 Simultaneous solutions of equations (4.11) and (4.12) with (4.13) for the quantum-well levels in a GaAs single quantum-well structure.

Figure 4.2 Conduction band energy levels for a multi-quantum well heterostructure.

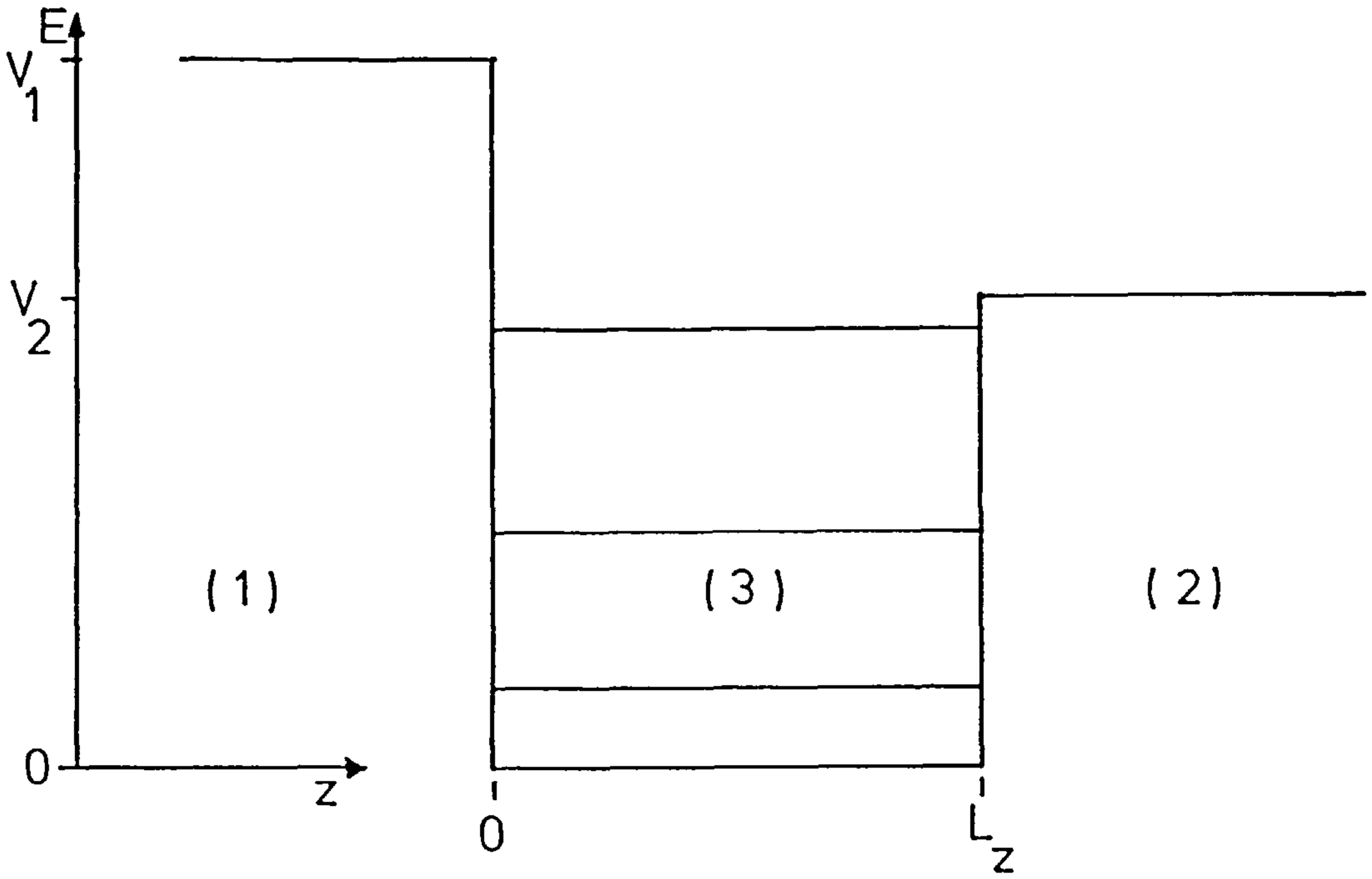

Figure 4.3 An asymmetric quantum-well.

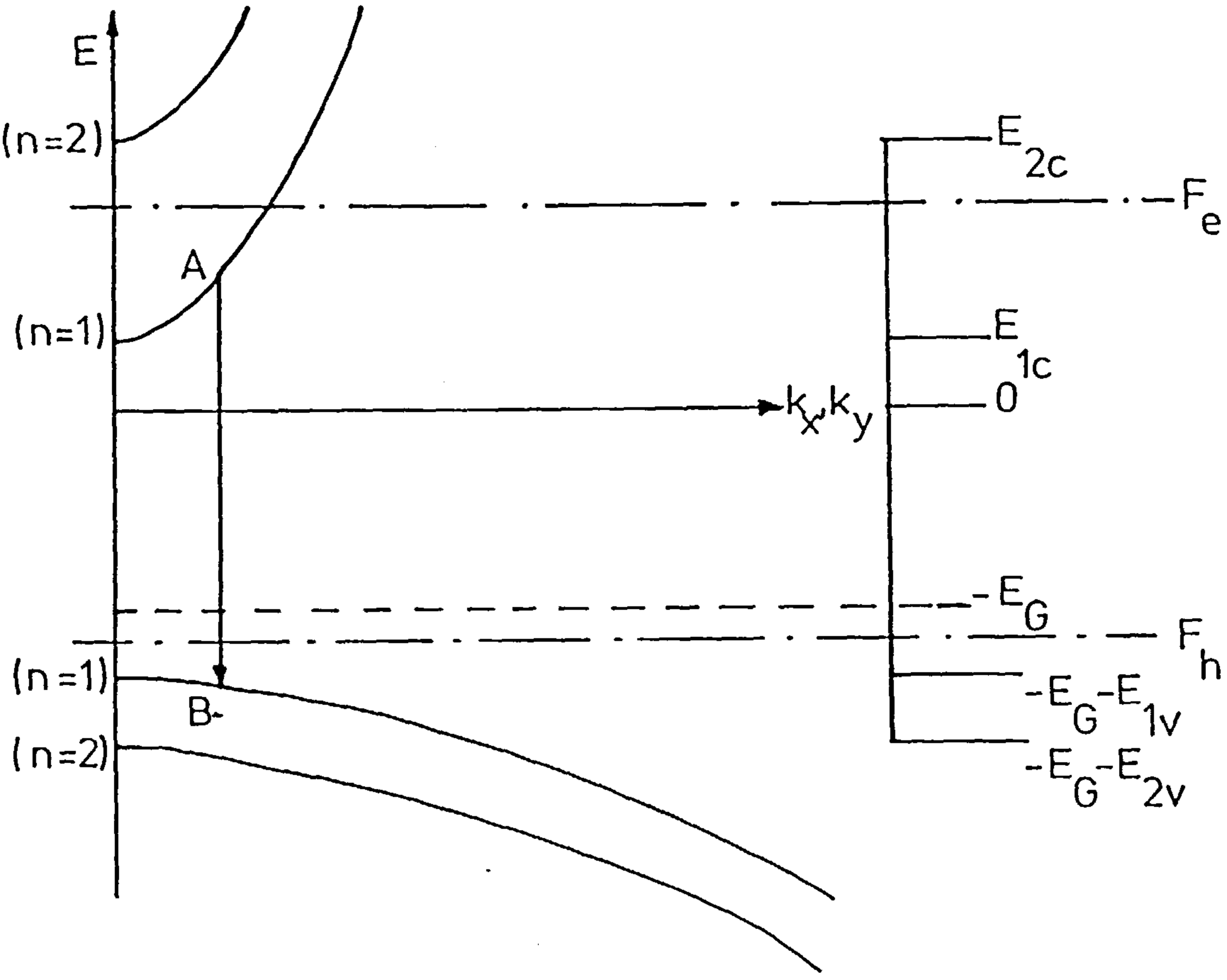

Figure 4.4 Simplified electron energy bands as functions in k-space showing the higher sub-bands formed by the quantum-well levels for the conduction band and the heavy-hole band only.

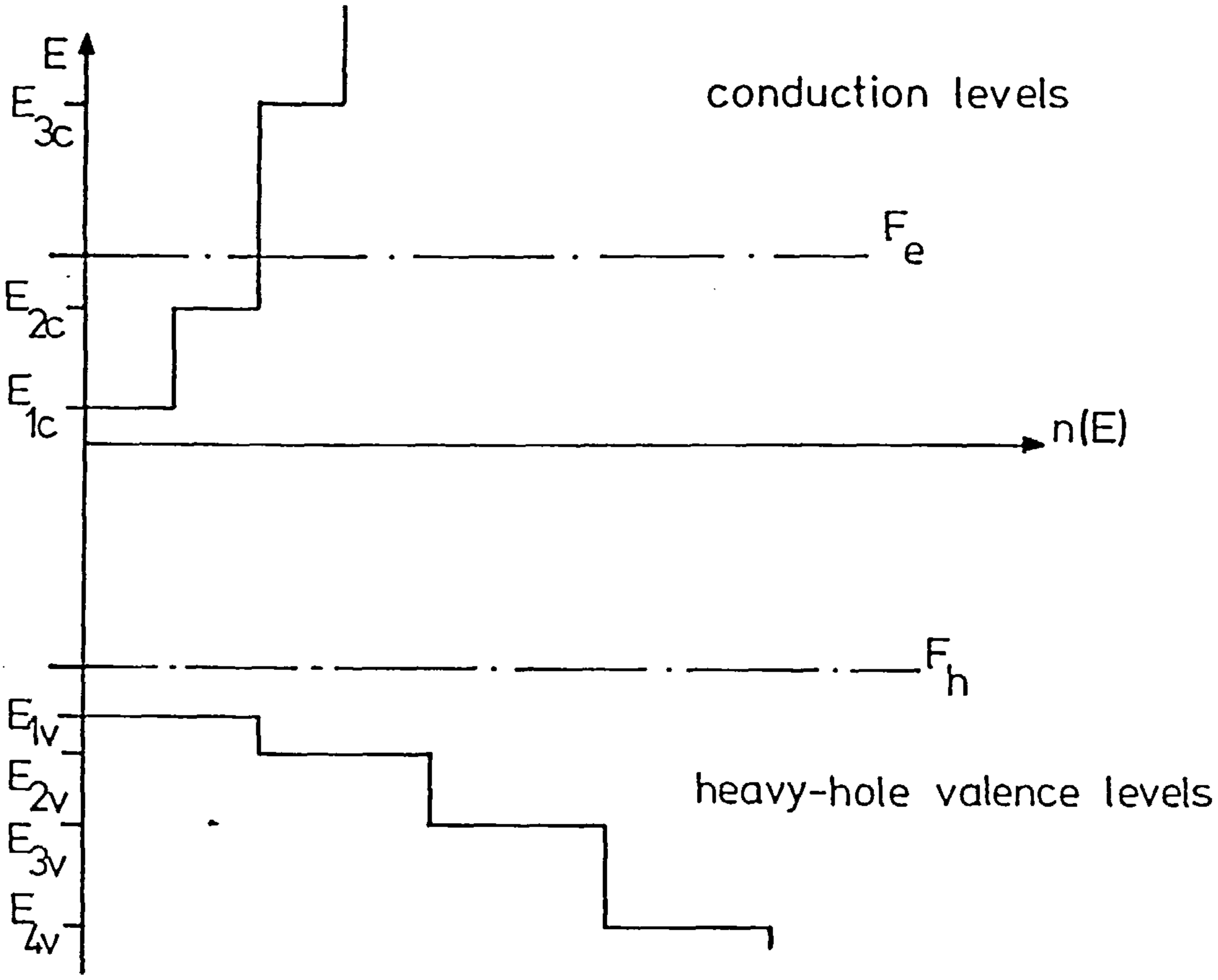

Figure 4.5 The two-dimensional step function density of states as a function of energy for the conduction band and heavy-hole band in a single quantum-well.

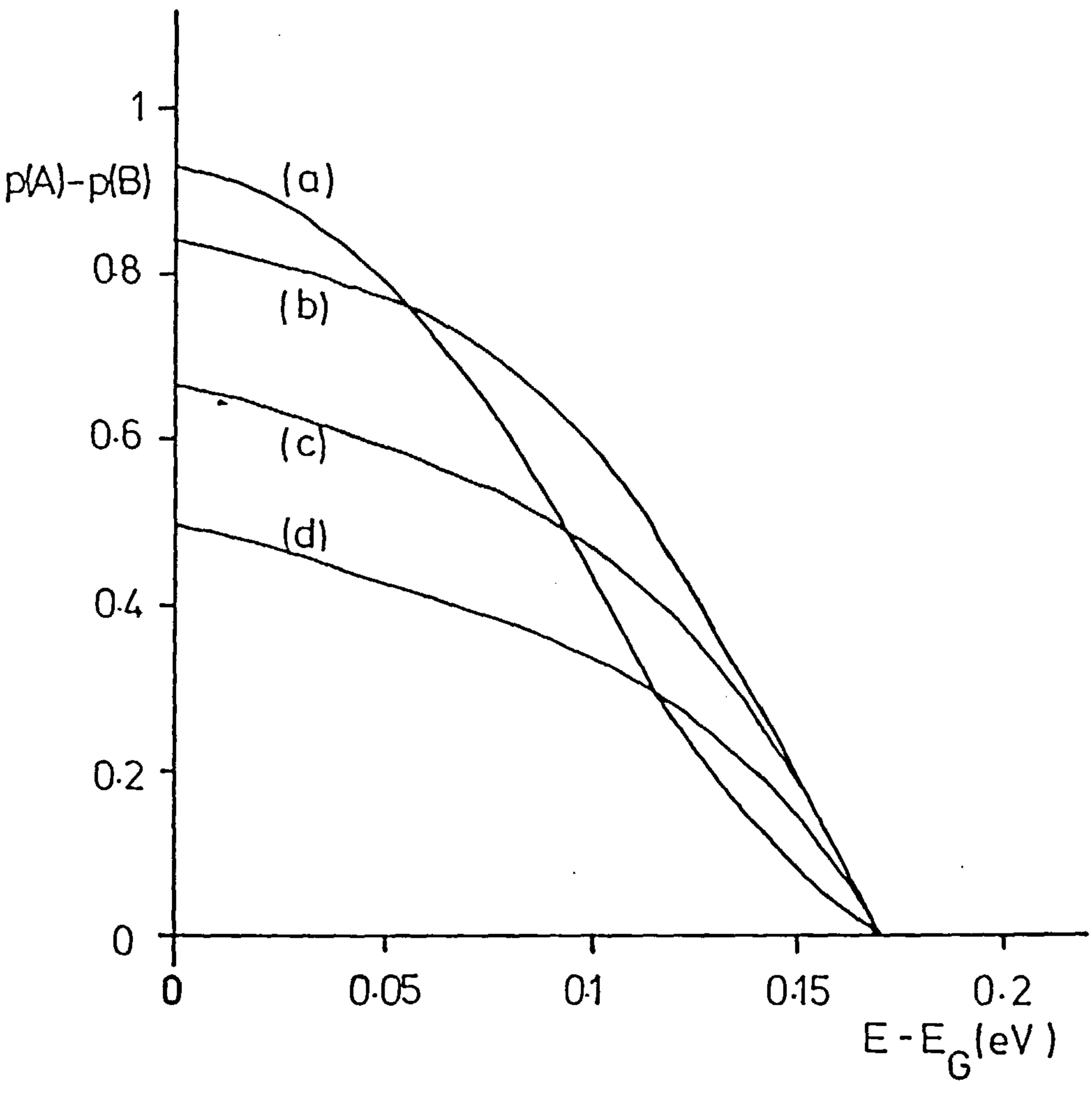

Figure 4.6 The difference of the Fermi-Dirac probability functions as a function of energy for energy levels A and B. This forms the shape of spectrum for the transition of electrons from A to B with k-selection rules in the structure shown in Figure 4.4. (a) $F_e - E_c = 0.17(eV)$, $E_v = F_h$, (b) $F_e - E_c = 0.13(eV)$, $E_v - F_h = 0.04(eV)$, (c) $F_e - E_c = E_v - F_h = 0.085(eV)$, (d) $F_e - E_c = 0.04\,eV$, $E_v - F_h = 0.13(eV)$.

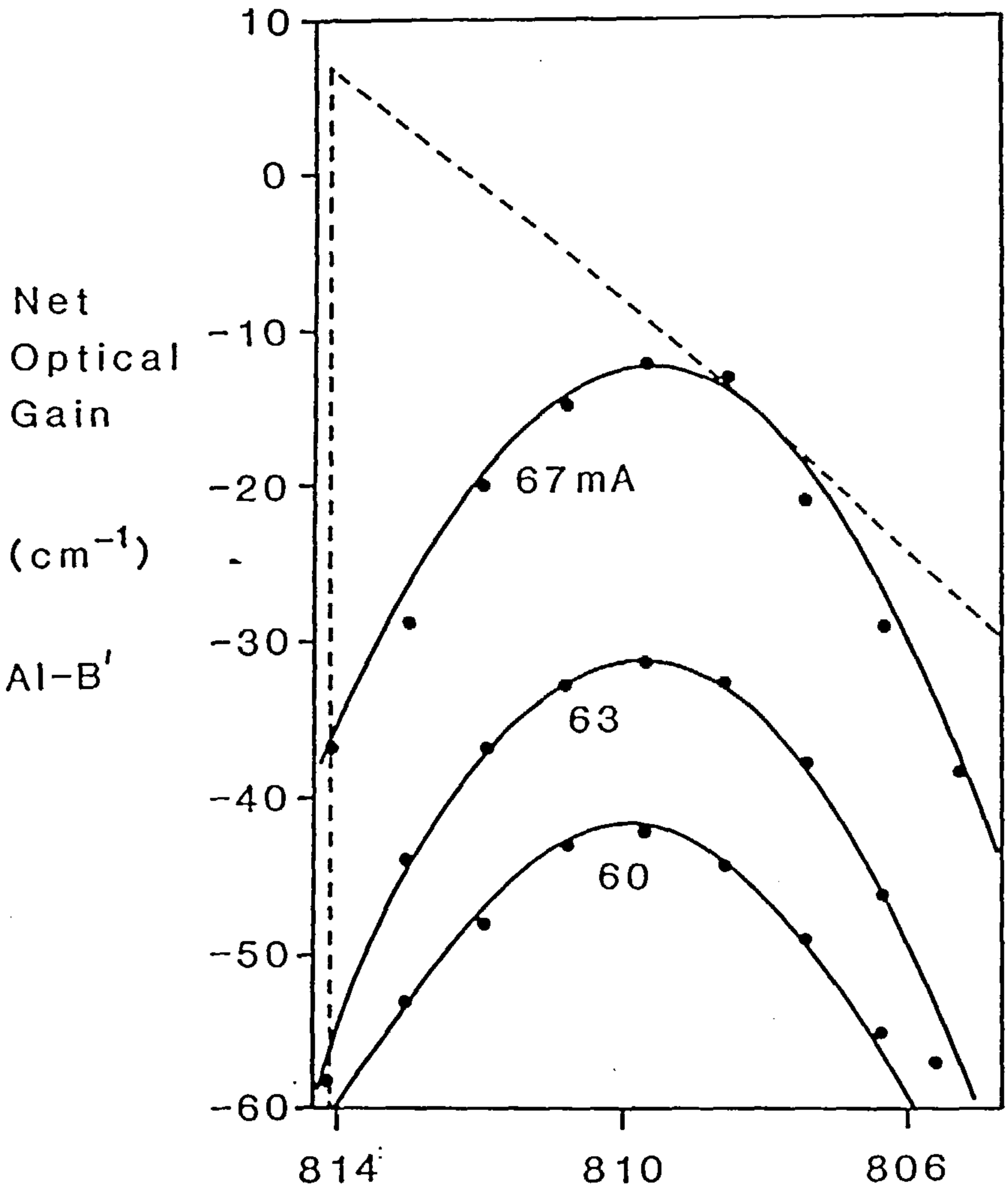

Figure 4.7 Net optical gain for no k-selection rule model, as defined by equation (4.34) with the data of Table 4.1, at three currents; circles are experimental points (Dutta et al, 1983). Also shown (dotted line) is the gain spectrum with the k-selection rule as defined by equation (4.28).

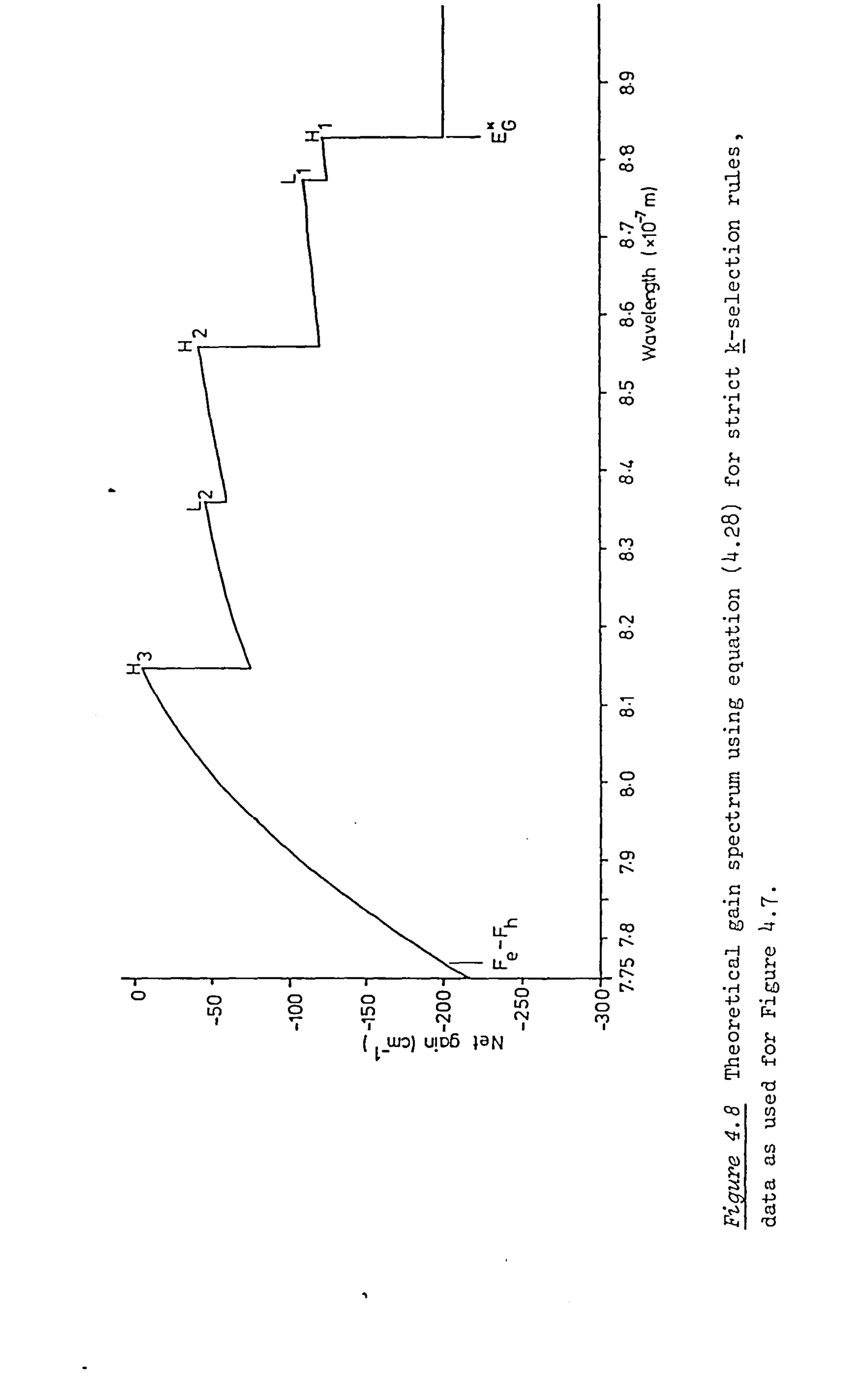

Figure 4.8 Theoretical gain spectrum using equation (4.28) for strict k-selection rules, data as used for Figure 4.7.

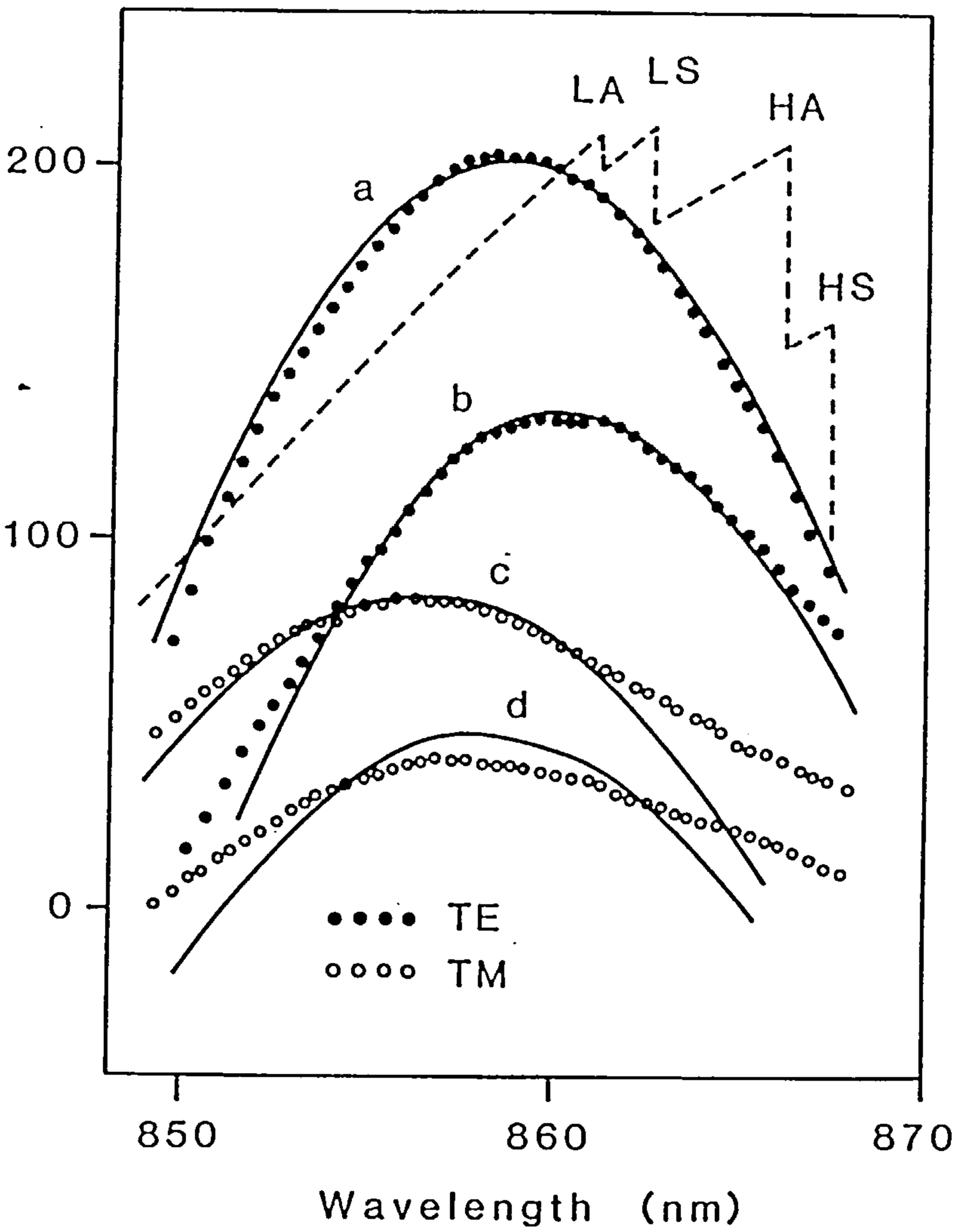

Figure 4.9 Net material gain for no k-selection rule as defined by equation (4.34) with the data of Table 4.2, at two currents and for TE and TM polarizations; circles are experimental points (Kobayashi et al, 1983). Also shown is the gain spectrum using the k-selection rule as defined by equation (4.28) and represented by the dotted curve.

PART B

THE EFFECT OF SURFACE RECOMBINATION ON LIFETIMES IN SOLAR CELLS

CHAPTER 5

THE SOLAR CELL EQUATIONS AND THEIR STEADY-STATE SOLUTIONS

5.1 Introduction

The energy band diagram of an illuminated n-p junction solar cell is shown in Figure 5.1. There is a small concentration gradient in the p-type base with a lower acceptor concentration at the junction than at the back of the solar cell leading to a small constant electric field. The top region which faces towards the illumination is a diffused n-type layer. The diffusion process of n-type donors leads to a concentration gradient in this, the emitter region, and hence leads also to an electric field.

When the physical junction between the n and p regions is formed, electrons flow out of the n-type region, attracted by the holes with which they recombine. This causes a negative space-charge region just inside the p-region and repels further electrons from moving into the p-region. Analogously holes flow from the p-region into the n-type emitter recombining with electrons and leaving a net positive charge in the n-region. In this way, further holes are repelled from moving across into the n-region. Equilibrium is established with a large potential barrier between the n and p regions.

If a photon with energy greater than the band-gap penetrates the solar cell, it has a high probability of being absorbed and will give up its energy to promote an electron into the conduction band leaving a hole in the valence band. The majority carrier, an electron if the photon is absorbed in the n-layer, diffuses to the contact at the end of the solar cell and escapes to give rise to photocurrent into a load. The minority carrier, which is a hole if the photon is absorbed in the n-layer, is trapped unless it can diffuse to the junction before

recombining. Then the minority carrier is swept across the junction to become a majority carrier by the large electric field in the junction and it can escape from the solar cell as a majority carrier.

Some photogeneration takes place in the depletion region as well. The electrons and holes created by the light absorption are swept by the electric field into the n-emitter and p-base respectively because of their opposite charges. The width of the depletion region is narrow enough and the electric field there is large enough that although few photons are absorbed there, the photogenerated carriers almost all leave the depletion region before recombination can occur.

Thus, the current-voltage characteristic of the solar cell is determined by the number of minority carriers which move across the junction without recombining together with a small contribution from carriers generated within the junction depletion region. For this reason, the solar cell is known as a minority carrier device.

Light absorption by the solar cell depends on the absorption coefficient of the semiconductor, the reflectivity of the top surface, and the thickness of the device. The photogenerated carriers are not all collected however because of bulk and surface recombination of electrons with holes. Bulk recombination occurs either by direct band to band recombination or by indirect recombination involving centres in the energy gap known as traps. Surface recombination is dominated by recombination through surface states in the energy gap which arise from electron orbitals that are not taken up by the lattice and from chemical residues, oxides and metal precipitates deposited at the surface. The statistics of surface recombination was discussed in chapter 2. The Shockley-Read model of bulk recombination including Auger transitions is in fact similar to the work of chapter 2, but has been discussed elsewhere (see for example Blakemore, 1962; Landsberg, 1982b). In part B of this work, the effect of recombination at the surfaces of a solar cell

on the carrier densities within the solar cell is examined. Some simple results for the recombination at the back surface and at grain boundaries were obtained in part A, chapters 2 and 3, and will be used in this part of the work.

In previous studies of carrier transport in solar cells, different solutions have been obtained for when there is no current flow (open-circuit conditions, see for example Sharma and Tewary, 1982) or no voltage (short-circuit conditions, see for example Dhariwal et al, 1977). Here an abstract generalisation of the conditions at the surfaces of the solar cell is made so that it is possible to give a solution to the carrier transport equation which encompasses many of the operating conditions in the steady-state. Through the use of Green's function in the steady-state solution in chapter 5, a representation of the photo-generation rate of carriers by a new function is then possible in chapter 6. The abstract generalisation of the conditions at the physical boundaries is also possible for the treatment of transients when one uses a Sturm-Liouville transform in the carrier transport model as in chapter 7. This method can be used to treat lifetime measurements by several experimental techniques using photovoltage decay. Carrier transport in polycrystalline silicon is examined in chapter 8 using a Sturm-Liouville transform and yields theoretical insight into the effects of grain size and grain boundary surface recombination on lifetimes and currents.

5.2 *The carrier transport equations*

In this section, the equations governing the electron and hole distributions are developed.

There are two components to the electrical current density, J, in a semiconductor, the first is provided by the movement of electrons in the conduction band and the second is provided by the valence band holes. The current density due to electrons, J_n, is the sum of the drift current

density and the diffusion current density. The drift current density for electrons is given by

$$\underline{j}_{drift} = -en\underline{v}_d \qquad (5.1)$$

where $\underline{v}_d$ is the drift velocity of electrons in a steady-state electric field, $\underline{E}$,

$$\underline{v}_d = -\upsilon_n \underline{E} \ .$$

Here, υ_n is the mobility of electrons. Also in equation (5.1), n is the concentration of electrons and e is the modulus of the electronic charge. There is a diffusion current density in a semiconductor when there is a concentration gradient of electrons. The net flux of electrons through the solid is related to the gradient of the electron concentration by a phenomenological relation called Fick's law:

$$\underline{j}_{diff} = (-e)(-D_n \underline{\nabla} n) \qquad (5.2)$$

where D_n is the diffusion coefficient for electrons. The total electron current density is given by the sum of the currents in equations (5.1) and (5.2), i.e.

$$\underline{J}_n = e(\upsilon_n n\underline{E} + D_n \underline{\nabla} n). \qquad (5.3)$$

The current density due to holes has also a drift and a diffusion component, but holes are positively charged instead of negatively charged as are electrons and consequently holes drift in the opposite direction to electrons. Thus, the drift current density for holes is

$$\underline{j}'_{drift} = ep\underline{v}'_d \qquad (5.4)$$

where $\underline{v}'_d$ is the hole drift velocity given by

$$\underline{v}'_d = \upsilon_p \underline{E}$$

and is in the opposite direction to the electron drift velocity. The diffusion component of the hole current density is

$$\underline{j}'_{diff} = e(-D_p \underline{\nabla p}) \qquad (5.5)$$

where p is the hole concentration and D_p is the hole diffusion coefficient. Thus the total hole current density is the sum of the drift component (5.4) and the diffusion component (5.5),

$$\underline{J}_p = e(p\upsilon_p \underline{E} - D_p \underline{\nabla p}). \qquad (5.6)$$

Equations (5.3) and (5.6) show the electron and hole current densities in a semiconductor. The total current density is their sum:

$$\underline{J} = \underline{J}_n + \underline{J}_p . \qquad (5.7)$$

The two equations governing the continuity of electrons and holes are in fact very similar, therefore only the electron continuity equation will be developed here. Small changes necessary to obtain the hole continuity equation will be indicated in the text. An arbitrary volume, V, of a semiconductor device is shown in Figure 5.2. Inside the volume, the total number of electrons is

$$\iiint_V n(\underline{r},t)dV.$$

The rate of change of the number of electrons is equal to the number of electrons photogenerated, g_n, inside V per unit time less the number of electrons, U_n, which recombine with holes in V per unit time minus the number of electrons which leave V across the surface S because of drift and diffusion:

$$\frac{\partial}{\partial t}\iiint_V n(\underline{r},t)dV = \iiint_V (g_n - U_n)dV - \iint_S \{-(1/e)\underline{J}_n\}.\underline{\hat{n}}dS \ . \qquad (5.8)$$

Here -e is the electronic charge and $\underline{\hat{n}}$ is the unit normal to the surface

S. The equation of continuity for holes is very similar, except that the flux of holes across the surface involves a factor $(+1/e)J_p$ instead of $(-1/e)J_n$. Of course, in the term on the left hand side of equation (5.8), the hole concentration $p(\underline{r},t)$ replaces the electron density $n(\underline{r},t)$.

Returning to the electron equation of continuity (5.8), the divergence theorem is used and the volume V is made constant in time so that one may write,

$$\iiint_V \left\{ \frac{\partial n(\underline{r},t)}{\partial t} - g_n + U_n - (1/e)\underline{\nabla}.\underline{J}_n \right\} dV = 0. \qquad (5.9)$$

The integral relation (5.9) holds for all choices of the material volume, V, which is only correct if

$$\frac{\partial n(\underline{r},t)}{\partial t} = g_n - U_n + (1/e)\underline{\nabla}.\underline{J}_n \ . \qquad (5.10)$$

This is the electron continuity equation. The hole continuity equation differs because the sign of the electron charge is negative and the sign of the hole charge is positive, and the hole equation is

$$\frac{\partial p(\underline{r},t)}{\partial t} = g_p - U_p - (1/e)\underline{\nabla}.\underline{J}_p. \qquad (5.11)$$

An equation for $n(\underline{r},t)$ is obtained by utilising the electron current density equation (5.3) in the continuity equation (5.10),

$$\frac{\partial n}{\partial t} = g_n - U_n + \upsilon_n(\underline{\nabla}n.\underline{E}) + \upsilon_n n\underline{\nabla}.\underline{E} + D_n\nabla^2 n. \qquad (5.12)$$

A similar equation for holes is obtained from equations (5.6) and (5.11),

$$\frac{\partial p}{\partial t} = g_p - U_p - \upsilon_p(\underline{\nabla}p.\underline{E}) - \upsilon_p p\underline{\nabla}.\underline{E} + D_p\nabla^2 p. \qquad (5.13)$$

The electric field, $\underline{E}$, is related to the electron and hole concentrations by Poisson's equation:

$$\underline{\nabla}.(\varepsilon_s\varepsilon_0\underline{E}) = e(p - n - N_A^- + N_D^+), \qquad (5.14)$$

where ε_s is the relative dielectric constant of the semiconductor, ε_0 is the permittivity of the vacuum, N_A^- is the dopant acceptor charge per unit volume and N_D^+ is the dopant donor charge per unit volume.

Equations (5.12), (5.13) and (5.14) yield a complete solution for the electron and hole concentrations as well as the electric field, but in practice their combined solution is difficult and some simplifying assumptions are made. These assumptions for the bulk n and p regions are:

(i) There is negligible space-charge in the region of interest, i.e. in equilibrium

$$p_0 - n_0 - N_A^- + N_D^+ = 0.$$

The effect of this is to make equation (5.14) into

$$\underline{\nabla}.\underline{E} = 0$$

and therefore the electric field is a constant field.

(ii) Assumption (i) applies away from equilibrium in the steady-state because equal numbers of excess electrons and holes are generated by the incident light,

$$g_n = g_p = g, \quad n - n_0 \doteqdot p - p_0.$$

(iii) The semiconductor has only one dopant of either acceptor or donor type and all of the dopant is ionised. If these are acceptors,

$$p_0 \doteqdot N_A^- \doteqdot N_A, \quad n_0 << p_0, \; N_D = 0.$$

If these are donor dopants,

$$n_O \doteqdot N_D^+ \doteqdot N_D, \quad n_O >> p_O, \quad N_A = O.$$

(iv) Low injection conditions are assumed, then the total number of minority carriers is less than the number of majority carriers in equilibrium: i.e. in p-type regions

$$n_0 << n << p_0 < p,$$

and in n-type regions

$$p_0 << p << n_0 < n.$$

The combined effect of assumptions (ii), (iii) and (iv) is to make fluctuations in the majority carrier density (e.g. holes in p-type emitters) so small that one can regard the majority carrier density as effectively constant. In this way, it is necessary to solve only the electron minority carrier equations.

(v) Consistent with assumption (iv) is the assumption of the recombination rate for electrons and holes being written in terms of constant lifetimes, τ_n and τ_p,

$$U_n = (n - n_0)/\tau_n, \quad U_p = (p - p_0)/\tau_p.$$

Assumptions (i) to (v) will be used here to reduce equations (5.12), (5.13) and (5.14) to a single equation known as the the minority carrier diffusion equation. In a p-type semiconductor, for example the base of the solar cell shown in Figure 5.1, this equation is the electron diffusion equation,

$$D_n \nabla^2 n + 2D_n(\underline{\nabla} n.\underline{f}) + g - \frac{n - n_O}{\tau_p} = \frac{\partial n}{\partial t}. \qquad (5.15)$$

For an n-type region, for example the emitter of the solar cell shown in Figure 5.1, the minority carrier diffusion equation is for holes,

$$D_p \nabla^2 p - 2D_p(\nabla p.\underline{f}) + g - \frac{p - p_0}{\tau_p} = \frac{\partial p}{\partial t} . \qquad (5.16)$$

Here the Einstein mobility relations (Landsberg, 1978, equation (17.23), p.327) have been used

$$eD_n = \upsilon_n k_B T, \qquad (5.17)$$

where k_B is Boltzmann's constant (k_B=1.38$\frac{1}{4}$6x10^{-23}JK^{-1}), T is the temperature and

$$eD_p = \upsilon_p k_B T. \qquad (5.18)$$

Also a vector field, $\underline{f}$, is defined by

$$\underline{f} = e\underline{E}/2k_B T. \qquad (5.19)$$

In the junction depletion region of the solar cell in Figure 5.1, the assumptions (i) to (iii) do not apply. In this region one assumes:

(vi) that the free electrons and holes are completely depleted because of the electric field, i.e.

$$p = n = 0.$$

(vii) the separation of the Fermi levels is given by

$$F_e - F_h = eV,$$

where V is the applied voltage, F_e and F_h are the electron and hole quasi-Fermi levels. The quasi-Fermi levels are assumed to be flat in this region because the electron and hole currents are small and constant here. The result of these assumptions is to reduce equations (5.12) to (5.14) to Poisson's equation,

$$\nabla.(\varepsilon_s \varepsilon_0 \underline{E}) = e(N_D - N_A). \qquad (5.20)$$

Equation (5.20) is solved for the potential distribution in the depletion region. This work has been detailed extensively in the literature (see for example Sze, 1969) and so will not be repeated here. The width of the junction region is usually very small in a diode or solar cell in comparison with the width of the base region. Thus the total generation and recombination rates in the junction are negligible in comparison with those effects in the base and the junction region adds little to the current of the solar cell.

Equation (5.15) will be solved here for the minority electron density in the base of a solar cell under a variety of conditions in the following sections and later chapters. The solution of equations (5.16) for holes in the emitter of the solar cell is in fact similar to the solution of equation (5.15), but with a change of sign of the electric field, $\underline{E}$. Thus it will not be given fully in this work.

In the following case, the minority carrier density in the emitter contributes negligibly to the current output of the solar cell and one need not examine the minority carrier density of holes in the emitter via equation (5.16). When a solar cell is constructed with a narrow, highly doped emitter, relatively few photons are absorbed in this region. The lifetime is one or two orders of magnitude smaller in this region than in the base and many of the carriers generated by the absorption of photons are reabsorbed in the emitter before they can diffuse across the junction. Thus, the contribution of the emitter in this case to the current of the solar cell may be neglected. This case has been named the "neglect of p-n coupling" by Sharma and Tewary (1982).

The diffusion equation for minority carriers (5.15) is treated in a region extending in one dimension from the junction region edge at x=0 to the back surface at x=d of the base of the solar cell as in Figure 5.1. This theory allows for surface recombination at either surface; at x=d the surface recombination velocity is interpreted as taking the place of

the p^+-region which would be present when a back surface field is built in to the solar cell. For an Ohmic contact at the back surface, the surface recombination rate is infinite. A simple geometry is adopted by assuming light is incident normally to the front surface and a single dimension, x, parallel to the incident light direction is used. However a second dimension will be introduced in chapter 7 because of time-dependence and in chapter 8 because of a radial coordinate dependence of the electron density introduced by grain boundary surface recombination. The photo-generation rate per unit volume and per unit wavelength range is denoted by g(x,t) where the dependence on wavelength, λ, will not be given explicitly.

A complete solution to equation (5.15) requires boundary conditions at the surfaces which define the edges of the bulk region of the solar cell base. A sample of possible boundary conditions which were used by previous authors is shown in Table 5.1. Basically, these conditions are of two types, in cases 1 and 2 at x=0, the minority carrier density is calculated in terms of the applied voltage, V. In all of the other cases, the minority carrier density is given in terms of a current flow across the surface.

The electron density at the edge of the junction space-charge region is obtained as a function of the applied voltage as follows: Boltzmann statistics are assumed because the semiconductor is non-degenerate, then

$$n = N_c \exp(\gamma_e - \eta_c)$$

and

$$p = N_v \exp(\eta_v - \gamma_h),$$

where N_c and N_v are the effective densities of states for the conduction and valence bands. Here γ_e and γ_h are the quasi-Fermi levels for electrons and holes divided by $k_B T$, and η_c ahd η_v are the conduction and valence

band edge energies divided by $k_B T$. Thus, the product of n and p is

$$np = n_i^2 \exp(\gamma_e - \gamma_h)$$

where n_i^2 is defined by

$$n_i^2 = N_c N_v \exp(\eta_v - \eta_c)$$

Utilising assumptions (iii) and (vii)

$$n = n_0 \exp(eV/k_B T)$$

where

$$n_0 = n_i^2/p_0 \doteq n_i^2/N_A.$$

The boundary conditions of Table 5.1, case 2 at x=0 arises when V=0.

In one dimension x, using equation (5.17), the electron current density equation (5.3) is

$$J_n = eD_n\left(2fn + \frac{\partial n}{\partial x}\right),$$

where f is the modulus of the field $\underline{f}$ acting along the x-axis. At x=0 in cases 3 and 4 the electron current at the junction is zero. This condition is representative of open-circuit conditions. At x=0 in case 5, a more general condition is used, whereby the electron current density at the junction is J(t).

At the back surface of the solar cell, x=d, in cases 1 to 5 of Table 5.1, the electron current flow is determined by the recombination current:

$$J_n = -eU.$$

For low injection conditions the recombination rate, U, at the back surface is defined (chapter 2) in terms of a constant surface recombination velocity, s, by

$$U = s(n - n_0).$$

An Ohmic back contact causes an infinite back surface recombination velocity in case 3.

In case 6, general linear boundary conditions are given. These are used to develop a solution to the minority carrier diffusion equation that encompasses all of the other cases of Table 5.1.

Because of the presence of an electric field acting along the x-axis of the solar cell the equilibrium electron and hole concentrations, n_0 and p_0, are not constants. In equilibrium the electron and hole currents are zero, thus integrating equations (5.3) and (5.6) with the Einstein relations (5.17) and (5.18),

$$n_0(x) = n_0(0)\exp(-2fx)$$

and

$$p_0(x) = p_0(0)\exp(2fx).$$

With these forms for the equilibrium concentrations, $n_0(x)$ and $p_0(x)$, one can eliminate the equilibrium concentrations from equations (5.15) and (5.16) . Therefore, the excess electron concentration, $n-n_0$, and the excess hole concentration, $p-p_0$, are calculated in practice from (5.15) and (5.16).

5.3 Solution of the diffusion equation by a change of variable

In the steady-state, the minority carrier diffusion equation (5.15) for electrons in the base of the solar cell in Figure 5.1 is time-independent and is given by

$$D\frac{d^2n}{dx^2} + 2fD\frac{dn}{dx} + g(x) - \frac{n(x)}{\tau} = 0. \qquad (5.21)$$

Here n is the excess minority carrier density (i.e. $n-n_0$ of the previous section), f is the magnitude of the vector field along the x-axis defined by equation (5.19), and the subscripts n have been removed from the diffusion coefficient, D, and the lifetime, τ, for convenience.

Two methods of solving the diffusion equation (5.21) will be employed in this work, the first is a change of variable and the second uses Green's function (Courant and Hilbert, 1955). The first method is useful when the photogeneration rate has the form (Dunbar and Hauser, 1976) of an exponential decay,

$$g(x,\lambda) = \alpha(\lambda)N_0(\lambda)\exp\{-\alpha(\lambda)x\} \qquad (5.22)$$

where $\alpha(\lambda)$ is the absorption coefficient $|m^{-1}|$ and $N_0(\lambda)$ is the incident photon flux at x=0 $|m^{-2}s^{-1}|$. In section 5.4, Green's function is used to obtain a general solution to equation (5.21) with the boundary conditions of case 6 of Table 5.1, but it is a rather complicated method of solving the inhomogeneous diffusion equation (5.21) with the simple photogeneration rate of equation (5.22).

An easy method of solving the diffusion equation with equation (5.22) is to use the following change of variable to m(x) where

$$m(x) = \exp(fx)\{n(x) + \theta\alpha N_0\exp(-\alpha x)\}, \qquad (5.23)$$

and θ is an arbitrary parameter. The diffusion equation (5.21) is transformed by this change of variable into the following equation:

$$D\frac{d^2m}{dx^2}e^{-fx} - (f^2D + 1/\tau)me^{-fx} + \alpha N_0e^{-\alpha x}[1 - \theta\{D\alpha(2f-\alpha) + 1/\tau\}]=0.$$

If an appropriate value for θ is chosen, for example

$$\theta = 1/|D\alpha(\alpha-2f) - 1/\tau|, \qquad (5.24)$$

then the diffusion equation above is simplified to

$$\frac{d^2m}{dx^2} - \mu^2 m = 0, \qquad (5.25)$$

where

$$\mu = \{f^2 + 1/L^2\}^{\frac{1}{2}}, \qquad (5.26)$$

and L ($=\sqrt{D\tau}$) is the diffusion length. Equation (5.25) has the solution

$$m(x) = m(0)\cosh\mu x + \{m'(0)/\mu\}\sinh\mu x \qquad (5.27)$$

where m'(0) indicates the first differential of m(x) at x=0. However, this way of writing the solution to equation (5.25) is not unique and the solution could equally well have been written as

$$m(x) = m(d)\cosh\mu(d-x) - \{m'(d)/\mu\}\sinh\mu(d-x). \qquad (5.28)$$

This is why some form of boundary condition, like those of Table 5.1, is necessary. Using equations (5.23) and (5.27), the electron concentration is given by

$$n(x) = e^{-fx}\left[\{n(0)+N_1\}\cosh\mu x + (\{n'(0)+fn(0)+N_1(f-\alpha)\}/\mu)\sinh\mu x - N_1 e^{-\alpha x}\right], \qquad (5.29)$$

or using equation (5.28),

$$n(x)=e^{f(d-x)}\left[\{n(d)+N_1e^{-\alpha d}\}\cosh\mu(d-x)-(\{n'(d)+fn(d)+N_1e^{-\alpha d}(f-\alpha)\}/\mu)\right.$$
$$\left.\times\ \sinh\mu(d-x)\right] - N_1e^{-\alpha x} \qquad (5.30)$$

where a concentration N_1 is given by

$$N_1 = \alpha N_0/[D\alpha(\alpha-2f) - 1/\tau]. \qquad (5.31)$$

As a simple example showing how the boundary conditions are used, when the electric field is zero (f=0), and the boundary conditions of cases 2

and 5 of Table 5.1 are adopted at x=0, equation (5.29) yields

$$n(x) = N_1 \cosh\mu x + [(J_L/eD - \alpha N_1)/\mu]\sinh\mu x - N_1 e^{-\alpha x}.$$

where J_L is the light generated current. Utilising the boundary condition of case 2 of Table 5.1 in the steady-state at x=d, one has

$$DN_1\left(\mu\sinh\mu d - \alpha\cosh\mu d + \alpha e^{-\alpha d}\right) + (J_L/e)\cosh\mu d$$

$$= -sN_1\left(\cosh\mu d - (\alpha/\mu)\sinh\mu d - e^{-\alpha d}\right) - (sJ_L/eD\mu)\sinh\mu d. \quad (5.32)$$

Rearranging equation (5.32), the short-circuit current is determined by α, N_1, L, d and s, the back surface recombination velocity and the short-circuit photocurrent is, since μ is equal to 1/L,

$$J_L = -\frac{eN_1 D\left[\{1/L-(\alpha sL/D)\}\sinh d/L+(s/D-\alpha)\{\cosh d/L-e^{-\alpha d}\}\right]}{(sL/D)\sinh d/L + \cosh d/L}. \quad (5.33)$$

Note there were two conditions at the junction, x=0, one condition involved n(0) and the other involved n'(0) and this is why it is useful to write the solution in a form containing n(0) and n'(0). However, the light generated current, J_L, was unknown until the boundary condition at the back surface was imposed.

To use the general boundary conditions of Table 5.1, case 6, they must be transformed into equations utilising m(x). The inverse transform of equation (5.23) is

$$n(x) = m(x)e^{-fx} - N_1 e^{-\alpha x}$$

and thus

$$n(0) = m(0) - N_1, \quad n'(0) = m'(0) - fm(0) + \alpha N_1.$$

Hence the boundary condition at x=0 given by case 6 of Table 5.1 yields a new equation:

$$a_1\left[m(0) - N_1\right] + a_2\left[m'(0) - fm(0) + \alpha N_1\right] = a_3. \qquad (5.34)$$

At x=d, the boundary condition similarly becomes

$$b_1\left[m(d)e^{-fd} - N_1 e^{-\alpha d}\right] + b_2\left[m'(d)e^{-fd} - fm(d)e^{-fd} + \alpha N_1 e^{-\alpha d}\right] = b_3. \quad (5.35)$$

In the steady-state, the time-dependent functions $a_3(t)$ and $b_3(t)$ are constants, labelled by a_3 and b_3 here. Rearranging equation (5.34) yields

$$(a_1 - a_2 f)m(0) + a_2 m'(0) = a_3 + (a_1 - a_2\alpha)N_1 \qquad (5.36)$$

and a second simultaneous equation for m(0) and m'(0) is found when equation (5.27) is substituted into (5.35), i.e.

$$b_3 + (b_1 - b_2\alpha)N_1 e^{-\alpha d} =$$

$$(b_1 - b_2 f)e^{-fd}\{m(0)\cosh\mu d + m'(0)\mu^{-1}\sinh\mu d\} + b_2 e^{-fd}\{\mu m(0)\sinh\mu d + m'(0)\cosh\mu d\}.$$

Rearranging the right hand side of this equation,

$$b_3 + (b_1 - b_2\alpha)N_1 e^{-\alpha d}\, e^{fd} =$$

$$\{(b_1 - b_2 f)\cosh\mu d + b_2\mu\sinh\mu d\}m(0) + \{(b_1 - b_2 f)\mu^{-1}\sinh\mu d + b_2\cosh\mu d\}m'(0). \quad (5.37)$$

Substituting m'(0) from (5.36) into (5.37) an equation for m(0) is obtained,

$$m(0) = -\left\{a_2 e^{fd}\, b_4 - a_4\{(b_1 - b_2 f)\mu^{-1}\sinh\mu d + b_2\cosh\mu d\}\right\}\chi\mu \qquad (5.38)$$

where

$$a_4 = a_3 + (a_1 - a_2\alpha)N_1, \quad b_4 = b_3 + (b_1 - b_2\alpha)N_1 e^{-\alpha d},$$

$$\chi \equiv -1/\left[\mu a_2\{(b_1 - b_2 f)\cosh\mu d + b_2\mu\sinh\mu d\} - (a_1 - a_2 f)\{(b_1 - b_2 f)\sinh\mu d + b_2\mu\cosh\mu d\}\right].$$

Hence an expression for m'(0) is derived from (5.38)and (5.36),

$$m'(0)=-\chi\left\{a_4\{(b_1-b_2f)\cosh\mu d+b_2\mu\sinh\mu d\}-(a_1-a_2f)e^{fd}b_4\right\}\mu. \quad (5.39)$$

Putting m(0) from (5.38) and m'(0) from (5.39) into (5.27), the transformed solution is

$$m(x)=b_4e^{fd}\left\{a_2\cosh\mu x-(a_1-a_2f)\mu^{-1}\sinh\mu x\right\}(-\chi\mu)-\chi\mu a_4 \times$$

$$\left\{\{(b_1-b_2f)\mu^{-1}\sinh\mu d+b_2\cosh\mu d\}\cosh\mu x-\{(b_1-b_2f)\mu^{-1}\cosh\mu d+b_2\sinh\mu d\}\sinh\mu x\right\}.$$

Rearranging the second factor in terms of $\cosh\mu(d-x)$ and $\sinh\mu(d-x)$,

$$m(x) = \{b_3+(b_1-b_2\alpha)N_1e^{-\alpha d}\}e^{fd}\chi\left[(a_1-a_2f)\sinh\mu x-a_2\mu\cosh\mu x\right] +$$

$$\{a_3+(a_1-a_2\alpha)N_1\}\chi\left[(b_1-b_2f)\sinh\mu(d-x)+b_2\mu\cosh\mu(d-x)\right],$$

where

$$\chi=1/\left\{\{a_1b_1-(a_1b_2+a_2b_1)f-a_2b_2/L^2\}\sinh\mu d+(a_1b_2-a_2b_1)\mu\cosh\mu d\right\}. \quad (5.40)$$

Finally, the excess carrier density, n(x), is given by the inverse transform of m(x),

$$n(x) = m(x)e^{-fx} - N_1e^{-\alpha x},$$

thus

$$n(x) = \{a_3+(a_1-a_2\alpha)N_1\}\chi\left[(b_1-b_2f)\sinh\mu(d-x)+b_2\mu\cosh\mu(d-x)\right]e^{-fx}+$$

$$\{b_3+(b_1-b_2\alpha)N_1e^{-\alpha d}\}\chi\left[(a_1-a_2f)\sinh\mu x-a_2\mu\cosh\mu x\right]e^{f(d-x)}-N_1e^{-\alpha x}. \quad (5.41)$$

This is the most general form of the steady-state carrier concentration to be obtained in this section.

The current density at any point, x, is obtained from equation (5.3) which in one dimension for electrons is

$$J_n(x) = eD\left\{\frac{dn(x)}{dx} + 2fn(x)\right\}$$

Differentiating equation (5.41) one obtains the electron current density,

$$J_n(x)=eD\chi e^{-fx}\Big\{a_4[\{b_1f-b_2(\mu^2+f^2)\}\sinh\mu(d-x)+\mu(2b_2f-b_1)\cosh\mu(d-x)]+$$

$$b_4e^{fd}[\{a_1f-a_2(\mu^2+f^2)\}\sinh\mu x+\mu(a_1-2a_2f)\cosh\mu x]\Big\}+eDN_1(\alpha-2f)e^{-\alpha x}.$$

In an abrupt junction solar cell, the depletion region is negligibly thin and its contribution to the current output of the solar cell is neglected and so the current is the sum of the base electron current, $J_n(0)$, passing across the junction and the hole current, $J_p(0)$, passing across the junction from the emitter side. The electron current is separated into the current of carriers injected at the boundaries, J_{inj}, and the current generated by the incident light within the bulk, J_L, i.e.

$$J_n(0) = J_{inj} - J_L$$

(see for example Hovel, 1975, p.51) where

$$J_{inj} = eD\chi[a_3\{(b_1f-b_2(\mu^2+f^2))\sinh\mu d+\mu(2b_2f-b_1)\cosh\mu d\}+b_3e^{fd}\mu(a_1-2a_2f)]$$

and

$$J_L = eD\chi N_1\Big\{(a_1-a_2\alpha)[\{b_2(\mu^2+f^2)-b_1f\}\sinh\mu d+\mu(b_1-2b_2f)\cosh\mu d]$$
$$+(2f-\alpha)\chi^{-1}+(b_1-b_2\alpha)e^{(f-\alpha)d}\mu(2a_2f-a_1)\Big\}.$$

The hole concentration, $p(x)$, is obtained by solving (5.16) in the steady-state, but this process will not be repeated here. Quite simply, one need change the sign of the electric field for holes in equation (5.41) and the hole concentration in the emitter is therefore

$$p(x) = a_{4p}\chi_p\Big\{b'_2\mu_p\cosh\mu_px-(b'_1+b'_2f_p)\sinh\mu_px\Big\}e^{f_p(x+w)}-N_{1p}e^{-\alpha(x+w)}$$

$$+ b_{4p}\chi_p\Big\{(a'_1+a'_2f_p)\sinh\mu_p(x+w)-a'_2\mu_p\cosh\mu_p(x+w)\Big\}e^{f_px}.$$

Here the boundary condition at the front surface is

$$a'_1 p(-w)+a'_2\left\{\frac{dp}{dx}\right\}\Big|_{x=-w} = a'_3$$

and the boundary condition at the junction, x=0, is

$$b'_1 p(0)+b'_2\left\{\frac{dp}{dx}\right\}\Big|_{x=0} = b'_3.$$

Note that the thickness of the emitter is w, f_p is the modulus of the electric field in the emitter divided by $2k_BT$ and

$$\mu_p = (f_p^2+1/L_p^2)^{\frac{1}{2}},$$

$$N_{lp} = \alpha N_0 e^{\alpha w}/[D_p\alpha(\alpha+2f_p)-1/L_p^2],$$

remembering N_0 is the incident photon flux measured at x=0 and

$$\chi_p^{-1}=\left(a'_1b'_1+(a'_1b'_2+a'_2b'_1)f_p-a'_2b'_2/L_p^2\right)\sinh\mu_p w+(a'_1b'_2-a'_2b'_1)\mu_p\cosh\mu_p w,$$

where L_p is the diffusion length for holes. The hole current, $J_p(0)$, across the junction is given by

$$J_p(0) = J'_{inj} - J'_L$$

where using equation (5.6) and the expression above for p(x),

$$J'_{inj}=eD_p\chi_p\Big(a'_3\mu_p e^{f_p w}(b'_1+2b'_2f_p)+b'_3\{[a'_1f_p+a'_2(\mu_p^2+f_p^2)]\sinh\mu_p w - (a'_1+2a'_2f_p)\mu_p\cosh\mu_p w\}\Big)$$

and

$$J'_L = eD_p\chi_p N_{lp}\Big\{(\alpha+2f_p)e^{-\alpha w}\chi_p^{-1}-(a'_1-a'_2\alpha)e^{f_p w}(b'_1+2f_pb'_2)\mu_p$$

$$-(b'_1-b'_2)e^{-\alpha w}[\{a'_1f_p+a'_2(\mu_p^2+f_p^2)\}\sinh\mu_p w-(a'_1+2a'_2f_p)\mu_p\cosh\mu_p w]\Big\}.$$

The usual form of the solar cell equation

$$J = J_0\{\exp(eV/k_BT)-1\} - J_L$$

can be recovered by adopting the boundary condition of case 1 of Table 5.1 at the junction end of the base and similarly at the junction end of the emitter one adopts

$$p(0) = p_0\{\exp(eV/k_BT)-1\}$$

in place of b_1', b_2', and b_3'.

For a general photogeneration rate $g(x)$ one might expect the following transformation of variables to be useful:

$$m(x) = \{n(x) + \theta g(x)\}e^{fx}.$$

However, this transforms the diffusion equation (5.21) into

$$m''(x) - \mu^2 m(x) + \frac{g(x)}{D}\left(1+\frac{\theta}{\tau}\right) - \theta(g''(x)+2fg'(x))e^{fx} = 0.$$

For any given $g(x)$ one would choose θ so that

$$\frac{g(x)}{D}\left(1+\frac{\theta}{\tau}\right) - \theta(g''(x)+2fg'(x)) = 0$$

to obtain the simple diffusion equation (5.25) for the carrier density. One can see that this operation is useful only when $g(x)$ satisfies

$$g'' + 2fg' - g\left(\frac{1}{D\theta} + \frac{1}{L^2}\right) = 0,$$

which restricts the choice of $g(x)$ to functions of the form

$$g = e^{-fx}\{Ae^{\beta x} + Be^{-\beta x}\},$$

where

$$\beta \equiv \{1/D\theta + \mu^2\}^{\frac{1}{2}}.$$

Since θ is a constant and A and B are also constants, the function g(x) has to be a simple exponential to satisfy the transformation above. Thus, the method of a change of variable is seen to be of use only in cases where the generation rate decays exponentially from the front surface.

Using the boundary conditions of case 4 of Table 5.1 on the carrier density (5.41) is equivalent to making the substitutions

$$a_1=2f,\ a_2=1,\ b_1=2f+s/D,\ b_2=1,\ a_3=b_3=0,$$

The result for these boundary conditions is

$$n(x)+N_1e^{-\alpha x} = DN_1e^{-fx}{}_x \qquad (5.42)$$

$$\left\{\frac{(2f-\alpha)\{(f+s/D)\sinh\mu(d-x)+\mu\cosh\mu(d-x)\}+e^{fd-\alpha d}\{2f-\alpha+s/D\}(f\sinh\mu x-\mu\cosh\mu x)}{(sf-1/\tau)\sinh\mu d\ -s\mu\cosh\mu d}\right\}$$

Using the data of Table 5.2 for silicon, some sample excess carrier concentration profiles are shown in Figure 5.3. The relation between curves (a), (c) and (f) may be understood as follows: The surface recombination processes near the back surface act as a sink for the minority carriers, so reducing the excess carrier concentration towards the higher values of surface recombination velocity.

The positive doping induced field present in curves (a), (c) and (f) aids carrier collection at the junction by drawing electrons away from the back surface and increases their density in the region of the junction, x=0. This makes plausible the relation between curves (a) and (b), (c) and (d) and (e) and (f). It is also apparent that in drawing electrons away from the back surface, the electric field raises the total number of electrons in the steady-state. This is because fewer electrons are in the region of the back surface and so the recombination rate is smaller there. This effect is particularly noticeable for the highest value of surface recombination velbcity used in curves (c) and (d).

5.4 Solution of the diffusion equation using Green's function

A solution of the minority carrier diffusion equation of the steady-state (5.21) for a non-exponential photogeneration rate is obtained as a linear superposition of a particular integral, n_{PI}, and a complimentary function, n_{CF}, in this section. The particular integral is a solution of the full equation (5.21) but with homogeneous boundary conditions,

$$a_1 n(0) + a_2 n'(0) = 0 \qquad (5.43)$$

and

$$b_1 n(d) + b_2 n'(d) = 0, \qquad (5.44)$$

imposed and Green's function is utilised to find the particular integral. The complimentary function is a solution of the homogeneous diffusion equation, i.e. equation (5.21) where g(x) is set equal to zero, and the complimentary function satifies the inhomogeneous boundary conditions of case 6 of Table 5.1. The homogeneous diffusion equation is

$$D\frac{d^2n}{dx^2} + 2fD\frac{dn}{dx} - \frac{n}{\tau} = 0 \qquad (5.45)$$

which has the general solution

$$n = (Ae^{\mu x} + Be^{-\mu x})e^{-fx} \qquad (5.46)$$

where μ was given by equation (5.26). To obtain the complimentary function one requires that the general solution satisfies the boundary conditions of case 6 of Table 5.1. This determines the constants A and B through, at x=0,

$$a_1(A+B)+a_2\{A(\mu-f)-B(\mu+f)\} = a_3 \qquad (5.47)$$

and at x=d,

$$b_1(Ae^{\mu d}+Be^{-\mu d})+b_2\{A(\mu-f)e^{\mu d}-B(\mu+f)e^{-\mu d}\}e^{-fd} = b_3 \qquad (5.48)$$

Equations (5.47) and (5.48) may be rearranged into two simultaneous equations for A and B:

$$\{a_1+a_2(\mu-f)\}A+\{a_1-(\mu+f)\}B = a_3$$

and

$$\{b_1+b_2(\mu-f)\}Ae^{\mu d}+\{b_1-b_2(\mu+f)\}Be^{-\mu d} = b_3e^{fd}.$$

Solving the two simultaneous equations by eliminating B, which involves multiplying the first equation by

$$\{b_1-b_2(\mu+f)\}e^{-\mu d}$$

and the second by

$$\{a_1-a_2(\mu+f)\}$$

and subtracting the resulting equations, one has

$$A = -\tfrac{1}{2}\chi\mu\left[a_3\{b_1-b_2(\mu+f)\}e^{-\mu d}-\{a_1-a_2(\mu+f)\}b_3e^{fd}\right]$$

where again

$$\chi=-2/\mu\left[\{a_1+a_2(\mu-f)\}\{b_1-b_2(\mu+f)\}e^{-\mu d}-\{a_1-a_2(\mu+f)\}\{b_1+b_2(\mu-f)\}e^{\mu d}\right].$$

If A is substituted back into one of the simultaneous equations above, an expression for B is obtained,

$$B = \tfrac{1}{2}\chi\mu\left[b_3e^{fd}\{a_1+a_2(\mu-f)\}-a_3\{b_1+b_2(\mu-f)\}e^{\mu d}\right].$$

The complimentary function, $n_{CF}(x)$, which is a solution to the homogeneous equation (5.45) with inhomogeneous boundary conditions is therefore from equation (5.46)

$$n_{CF}(x) = \left\{a_3\left(\{b_1-b_2(\mu+f)\}e^{\mu(x-d)}-\{b_1+b_2(\mu-f)\}e^{\mu(d-x)}\right)-\right.$$
$$\left.b_3e^{fd}\left(\{a_1-a_2(\mu+f)\}e^{\mu x}-\{a_1+a_2(\mu-f)\}e^{-\mu x}\right)\right\}\chi\mu.$$

This expression can be recast in terms of hyperbolic functions

$$n_{CF}(x) = \chi \times$$

$$\{a_3[(b_1-b_2f)\sinh\mu(d-x)+b_2\mu\cosh\mu(d-x)]+b_3e^{fd}[(a_1-a_2f)\sinh\mu x-a_2\mu\cosh\mu x]\} \tag{5.49}$$

where χ is given by equation (5.40). Note that the above equation (5.49) for the complimentary function is independent of the light generation of carriers and that in the following work the light dependence is contained within the particular integral, $n_{PI}(x)$.

To obtain the particular integral of equation (5.21), it is necessary to find Green's function, $u(x;y)$, associated with the operator $\underline{L}$,

$$\underline{L}|u| = \left\{D\frac{d}{dx}\left\{e^{2fx}\frac{d}{dx}\right\} - \frac{e^{2fx}}{\tau}\right\}u \tag{5.50}$$

Green's function is a solution of

$$\underline{L}|u| = \delta(x - y) \tag{5.51}$$

which also satisfies the conditions of equations (5.43) and (5.44). Full details of Green's method of solving differential equations can be found in (Courant and Hilbert, 1955). Green's function is constructed from solutions of (5.51) on either side of $x=y$, where the delta function is zero in the regions $0\leq x<y$ and $y<x\leq d$. The two solutions, $c_0u_0(x)$ and $c_1u_1(x)$, in the separate regions contain arbitrary constants c_0 and c_1 and must be continuous at $x=y$, thus

$$c_0u_0(y) - c_1u_1(y) = 0, \tag{5.52}$$

and Green's function is given by

$$u(x;y) = \begin{cases} c_0u_0(x) & \text{for } 0\leq x\leq y, \\ c_1u_1(x) & \text{for } y\leq x\leq d. \end{cases}$$

Also, the first derivative of Green's function at x=y has a jump discontinuity given by

$$\lim_{\varepsilon\to 0} \frac{du}{dx}\Big|_{x=y-\varepsilon}^{x=y+\varepsilon} = \frac{e^{2fx}}{D} \tag{5.53}$$

where ε is a small length. This may be understood by integrating (5.51) using (5.50) from x=y-ε to x=y+ε:

$$\lim_{\varepsilon\to 0}\left(\int_{x=y-\varepsilon}^{x=y+\varepsilon}\left\{\frac{d}{dx}\left(e^{2fx}\,\frac{du(x;y)}{dx}\right) - \frac{e^{2fx}u(x;y)}{D\tau}\right\}dx = \int_{x=y-\varepsilon}^{x=y+\varepsilon}\frac{\delta(x-y)dx}{D}\right).$$

After an integration of the first factor, one has

$$\lim_{\varepsilon\to 0}\left(\left[e^{2fx}\frac{du}{dx}\right]_{y-\varepsilon}^{y+\varepsilon} - \int_{y-\varepsilon}^{y+\varepsilon}\frac{e^{2fx}}{D}u\,dx = \frac{1}{D}\right),$$

and this expression simplifies to equation (5.53) because u(x;y) is continuous at x=y. Hence, equation (5.53) is obtained and it yields

$$c_1u_1'(y) - c_0u_0'(y) = e^{-2fy}/D.$$

This equation together with (5.52) are solved for c_0 and c_1. One requires for a solution that the determinant or Wronskian of the coefficients of c_0 and c_1 is non-zero, i.e.

$$K \equiv D[u_0(y)u_1'(y) - u_1(y)u_0'(y)]e^{2fy} \neq 0, \tag{5.54}$$

where K is the Wronskian of u_0 and u_1 for the self-adjoint operator, $\underline{L}$ (Courant and Hibert, 1955). The solutions for c_0 and c_1 are

$$c_0=u_1(y)K^{-1}, \quad c_1=u_0(y)K^{-1},$$

and therefore Green's function is

$$u(x;y) = \begin{cases} u_0(x)u_1(y)K^{-1} & \text{for } 0\leq x<y, \\ u_1(x)u_0(y)K^{-1} & \text{for } y\leq x<d. \end{cases} \tag{5.55}$$

The functions $u_0(x)$ and $u_1(x)$ are solutions of the homogeneous diffusion equation (5.45), $u_0(x)$ satisfies the boundary condition (5.43) at x=0 and $u_1(x)$ satisfies the boundary condition (5.44) at x=d. Hence, one uses the general solution (5.46) to it and obtains $u_0(x)$:

$$u_0(x) = (A_0e^{\mu x} + B_0e^{-\mu x})e^{-fx} \tag{5.56}$$

where (5.43) yields

$$a_1(A_0+B_0) + a_2\{(\mu-f)A_0-(\mu+f)B_0\} = 0$$

therefore, equation (5.56) yields

$$u_0 = 2A_0e^{-fx}\{(a_1-a_2f)\sinh\mu x-a_2\mu\cosh\mu x\}.$$

Similarly,

$$u_1 = (A_1e^{\mu x} + B_1e^{-\mu x})e^{-fx} \tag{5.57}$$

and this satisfies (5.44), which yields

$$b_1(A_1e^{\mu d}+B_1e^{-\mu d})+b_2\{A_1(\mu-f)e^{\mu d}-B_1(\mu+f)e^{-\mu d}\} = 0$$

Hence $u_1(x)$ may be rewritten using (5.57),

$$u_1(x) = 2A_1e^{-fx}\{(b_1-b_2f)\sinh\mu(d-x)+b_2\mu\cosh\mu(d-x)\}.$$

The factors A_0 and A_1 remain arbitrary, but one sees from (5.54) and (5.55) that these factors will cancel out of the Green's function. The Wronskian of u_0 and u_1 is obtained by substituting the above expressions for u_0 and u_1 into equation (5.54), and one obtains

$$K/(4A_0A_1D) =$$

$$\{(a_1-a_2f)\sinh\mu y-a_2\mu\cosh\mu y\}[\{b_2(f^2-\mu^2)-b_1\}\sinh\mu(d-y)-b_1\mu\cosh\mu(d-y)]$$

$$+\{(b_1-b_2f)\sinh\mu(d-y)+b_2\mu\cosh\mu(d-y)\}[\{a_1f-a_2(f^2-\mu^2)\}\sinh y-a_1\mu\cosh\mu y].$$

Hence, multiplying together the sinh and cosh terms, one finds

$$\frac{K}{4A_1A_0D} = -\mu[(a_1b_2-a_2b_1)\mu\cosh\mu d+\{a_1b_1-(a_1b_2+a_2b_1)f-a_2b_2/L^2\}\sinh\mu d]=\frac{-\mu}{\chi}.$$

Note that the Wronskian, K, is a constant (Courant and Hilbert, 1955) because the operator $\underline{L}$ is self-adjoint. Thus, Green's function (5.55) is given by

$$u(x;y)=\begin{cases}-e^{-f(x+y)}\{(b_1-b_2f)\sinh\mu(d-y)+b_2\mu\cosh\mu(d-y)\} \\ \qquad \times\chi\{(a_1-a_2f)\sinh\mu x-a_2\mu\cosh\mu x\}/D\mu \quad \text{for } 0\leq x<y, \\ -e^{-f(x+y)}\{(b_1-b_2f)\sinh\mu(d-x)+b_2\mu\cosh\mu(d-x)\} \\ \qquad \times\chi\{(a_1-a_2f)\sinh\mu y-a_2\mu\cosh\mu y\}/D\mu \quad \text{for } y<x\leq d. \end{cases} \tag{5.58}$$

The minority carrier diffusion equation (5.21) with the operator $\underline{L}$ in self-adjoint form is

$$\underline{L}|u| = -g(x)e^{-2fx}$$

and therefore the particular integral is given by (Courant and Hilbert, 1955)

$$n_{PI}(x) = -\int_0^d g(y)e^{2fy}u(x;y)dy$$

Hence, using equation (5.58) the particular integral is

$$n_{PI}(x) = I_1\chi e^{-fx}\{(b_1-b_2f)\sinh\mu(d-x)+b_2\mu\cosh\mu(d-x)\} +$$

$$I_2\chi e^{-fx}\{(a_1-a_2f)\sinh\mu x-a_2\mu\cosh\mu x\}, \tag{5.59}$$

where the integrals I_1 and I_2 have been constructed as follows:

In the addition of the particular integral to the complimentary function (5.49), it is convenient to define two parameters I_1 and I_2 by

$$I_1 \equiv \int_0^d \{(a_1-a_2f)\sinh\mu y-a_2\mu\cosh\mu y\}g(y)e^{fy}dy/D\mu. \qquad (5.60)$$

and

$$I_2 \equiv \int_0^d \{(b_1-b_2f)\sinh\mu(d-y)+b_2\mu\cosh\mu(d-y)\}g(y)e^{fy}dy/D\mu. \qquad (5.61)$$

The complete solution to the steady-state minority carrier diffusion equation is the sum of the particular integral (5.59) and the complimentary function (5.49). Thus, the steady-state excess electron density is

$$n(x) = \chi e^{-fx}\Big[(a_3+I_1)\{(b_1-b_2f)\sinh\mu(d-x)+b_2\mu\cosh\mu(d-x)\} +$$

$$(b_3e^{fd}+I_2)\{(a_1-a_2f)\sinh\mu x-a_2\mu\cosh\mu x\}\Big] \qquad (5.62)$$

using the expression for χ given in equation (5.40) and the integrals I_1 and I_2 given in equations (5.60) and (5.61). These integrals incorporate a general photogeneration rate. If the photogeneration rate has the usual form of an exponential decay as in (5.22), the integrals I_1 and I_2 may be evaluated readily. The result is identical to equation (5.41) where the excess minority carrier density was calculated using the change of variable and so will not be repeated here. In the following chapter, equations (5.60), (5.61) and (5.62) will be used with a special photo-generation rate (Hsieh et al., 1980) which more accurately approximates the absorption of the Sun's spectrum by a silicon solar cell.

5.5 Conclusions

It has been shown here that even in cases where a general photo-generation rate is used as well as the general linear boundary conditions one can obtain a solution to the minority carrier diffusion equation.

This result is displayed in the form of hyperbolic functions. The use of abstract general linear boundary conditions leads to the most general solution which may be obtained from the diffusion equation as given by equation (5.21). Substitution of physical parameters in place of the abstract quantities (a_i, b_i, i= 1, 2, 3) enables a solution given here in equation (5.62) to be representative of all of the different steady-state operating conditions of a silicon solar cell in low injection (Hovel, 1975). The inclusion of an electric field in the base, which can be realised through an exponential doping profile, is preferential to carrier collection at the junction. The steady-state model given here in section 5.3 indicates that there are two benefits. The drift of electrons towards the junction aids the diffusion process and therefore increases the number of minority carriers collected. Also, the drift field keeps electrons away from the back surface where there is often a high surface recombination velocity and the drift field aids carrier collection by preventing recombination.

By developing a solution with a general photogeneration rate the examination of different types of illumination spectra is possible. For example, a new spectral representation of the absorption of sunlight by a silicon solar cell is given in chapter 6.

Table 5.1 Boundary conditions for the diffusion equation in a solar cell

Case	At x=0	At x=d	References
1	$n=n_0\exp(eV/k_BT)$ (Voltage V across j'n)	$D_n\frac{dn}{dx}+2fD_n n=-s(n-n_0)$ $n = n(d)$	Mallinson and Landsberg, 1977.
2	$n=n_0$ (Short-circuit)	$D_n\frac{\partial n}{\partial x} = -s(n-n_0)$ $n = n(d,t)$	Dhariwal et al., 1977; de Vos and Pauwels, 1977.
3	$\frac{\partial n(0,t)}{\partial x} = 0$ (Open-circuit)	$n(d,t)=0$, $s=\infty$, (Ohmic back contact) or $\frac{\partial n(d,t)}{\partial x}=0$, $s=0$. (BSF solar cell)	Von Roos, 1981
4	$D_n\frac{\partial n}{\partial x} + 2fD_n n = 0$ (Open-circuit)	$D_n\frac{\partial n}{\partial x} + 2fD_n n=-s(n-n_0)$ $n = n(d,t)$	Sharma and Tewary, 1982.
5	$eD_n\frac{\partial n}{\partial x} = J(t)$ (Current J across j'n)	$D_n\frac{\partial n}{\partial x} = -s(n-n_0)$ $n = n(d,t)$	Dhariwal and Vasu, 1981
6	$a_1 n + a_2\frac{\partial n}{\partial x} = a_3(t)$ $n = n(0,t)$	$b_1 n + b_2\frac{\partial n}{\partial x} = b_3(t)$ $n = n(d,t)$	General linear boundary cond'ns see text.

Table 5.2 Parameters used for the curves

α	$6000\ cm^{-1}$	$\lvert\underline{E}\rvert$	$2.2 \times 10^{4}\ Vcm^{-1}$
N_O	$3.8 \times 10^{17}\ cm^{-2}s^{-1}$	f	$44.0\ cm^{-1}$
τ	$4.0 \times 10^{-6}\ s$	t_1	$1.0 \times 10^{-8}\ s$
D	$35.0\ cm^{2}s^{-1}$	T	300 K
d	100 μm	N_A	$1.0 \times 10^{16}\ cm^{-3}$
s	$6.0 \times 10^{3}\ cms^{-1}$	k_B	$1.3806 \times 10^{-23} JK^{-1}$

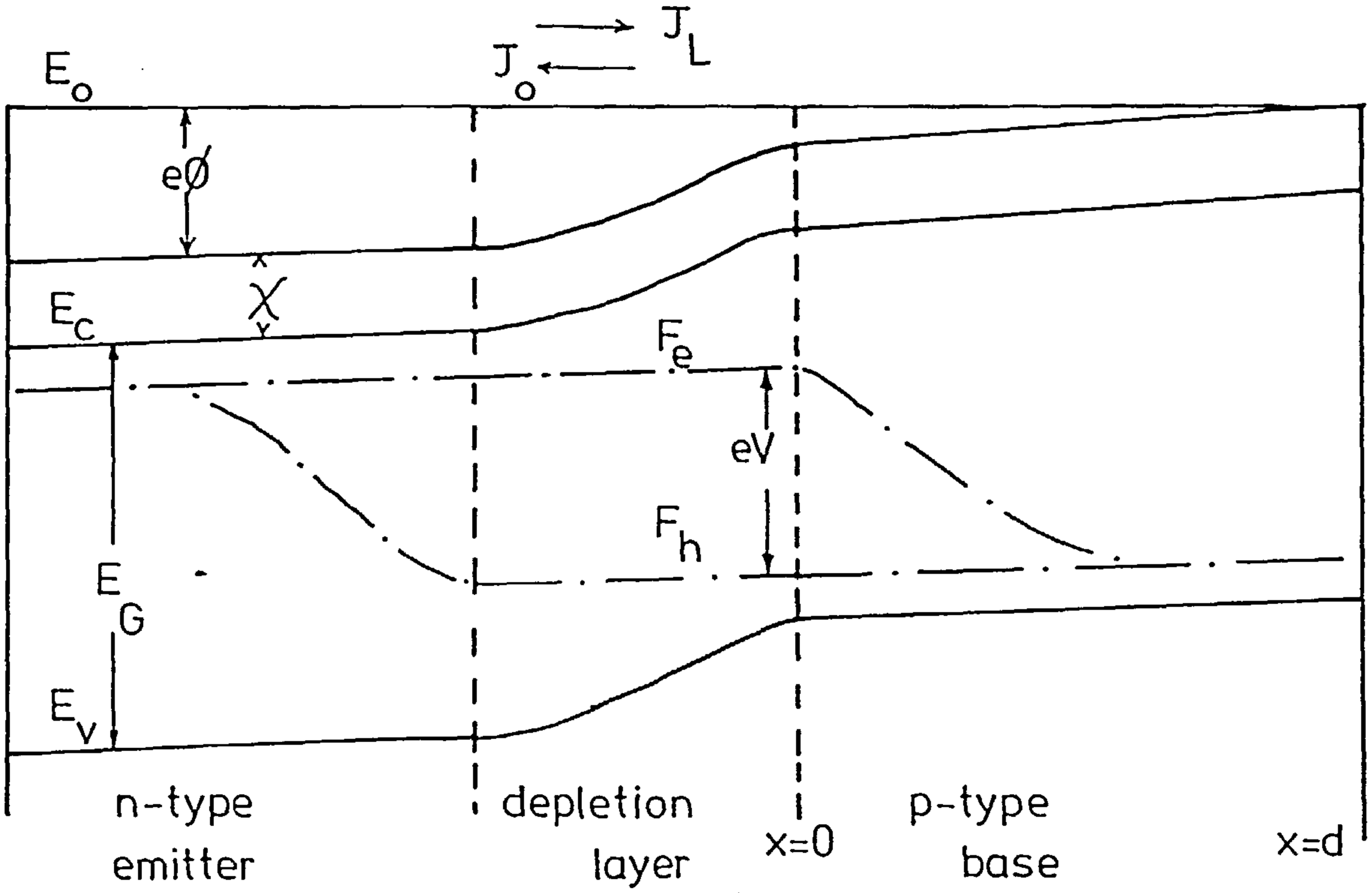

Figure 5.1 The energy bands in an n-p solar cell with constant electric fields in the emitter and in the base.

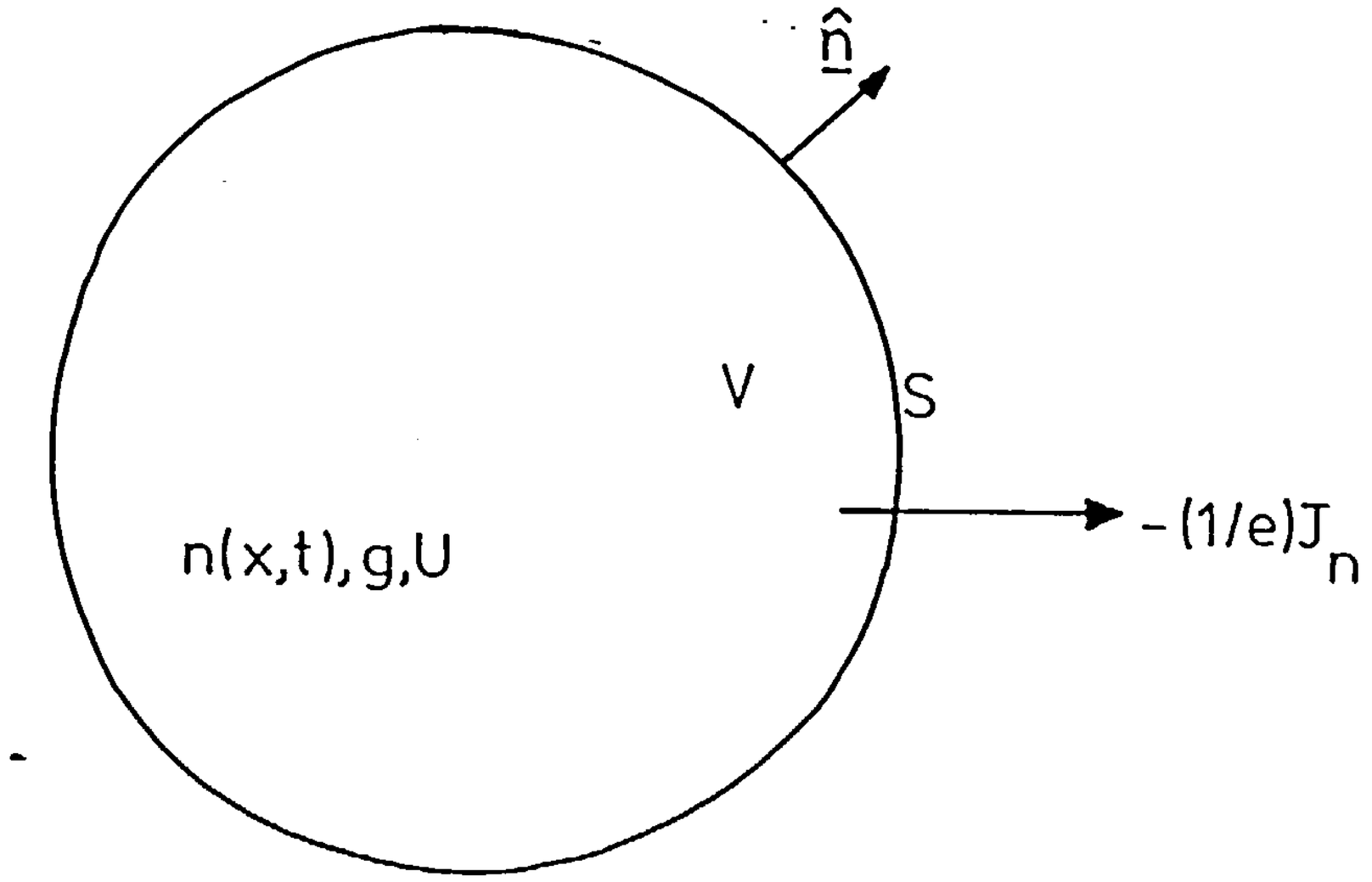

Figure 5.2 The volume element, V, in a region of bulk semiconductor with a concentration n of electrons inside V, recombination rate U, and generation rate, g, and an electron current, J_n, out of V through the surface, S.

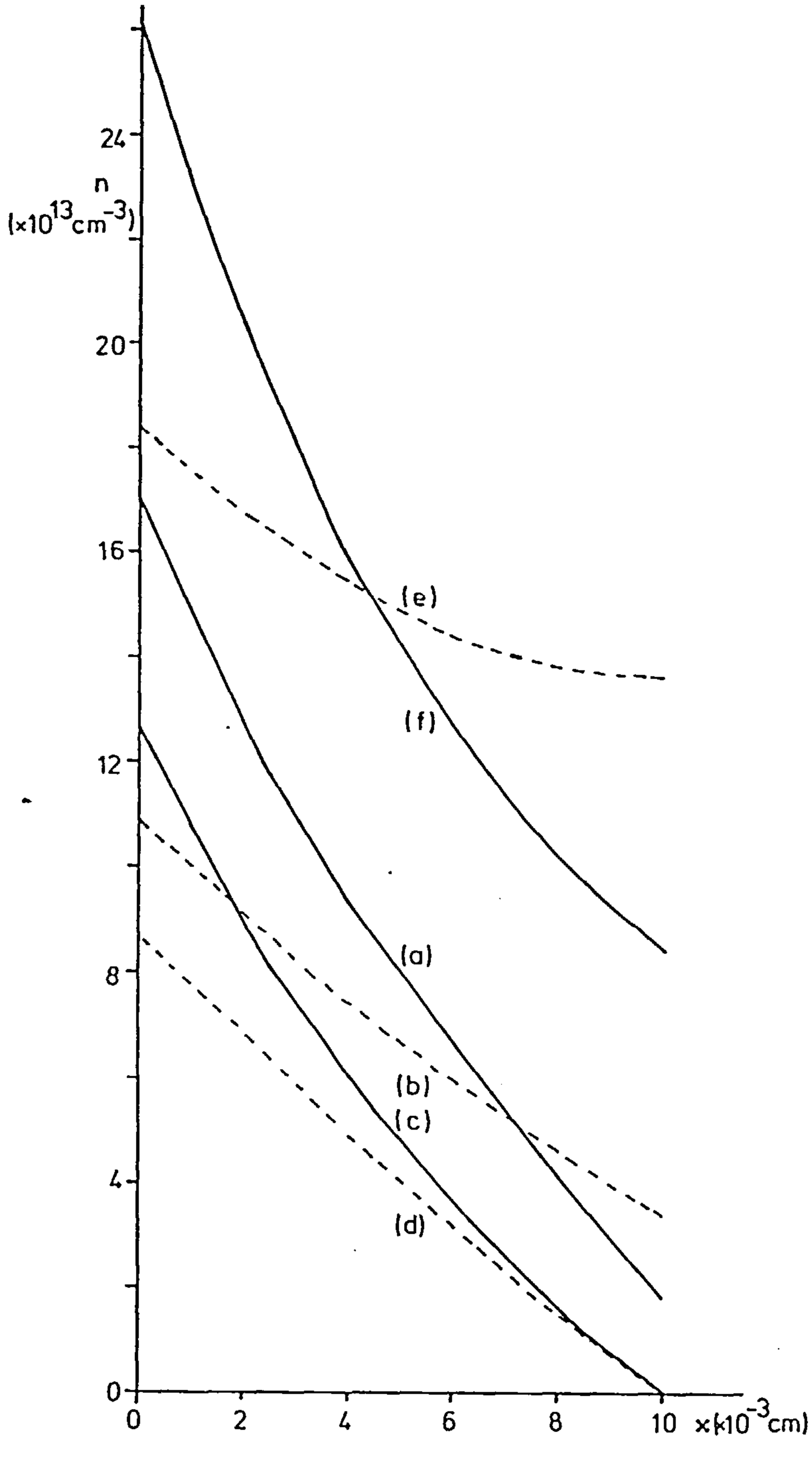

Figure 5.3 Excess carrier density profiles for steady-state illumination using equation (5.42) and the data of Table 5.2 (curve (a)). In the following curves: (b) $\underline{E}=0$, (c) $s=\infty$, (d) $s=\infty$, $\underline{E}=0$, (e) $s=0$, $\underline{E}=0$, (f) $s=0$.

CHAPTER 6

GREEN'S FUNCTION AND THE ANALYSIS OF SOLAR CELL PHOTOCURRENT

6.1 Introduction

The efficiency of conversion of solar energy into electrical energy by a photovoltaic cell depends on (i) the nature of the incident radiation, (ii) the energy and (iii) position dependence of the absorption of the incoming light. In addition, there are (iv) the effects of the material parameters, i.e. the thickness of the device, its junction depth and doping concentrations. For a brief review of effects (i), (ii) and (iv) see Mallinson and Landsberg (1977). Attention will be focussed in this chapter on the effect (iii) of the position dependence of the light absorption, but it will be useful to briefly review the other effects.

(i) Measurements of the solar spectrum have been taken at many locations on the Earth's surface (see for example Dixon, 1978; Condit and Grum,1964; Henderson and Hodgkiss,1964) and for different meteorological conditions. The air mass zero (AM0) spectrum (NASA, 1971) is the estimated Sun's spectrum outside the Earth's atmosphere. Air mass one (AM1) (Dunbar and Hauser, 1976) is the solar spectrum under a clear sky with the Sun vertically overhead, at a position on the Earth's surface. The AM2 spectrum (Fossum,1976) represents average weather conditions with the Sun 60^{o} from vertically overhead. Higher air mass spectra have been calculated for progressively more diffuse and weaker intensity sunlight.

(ii) Germanium and Gallium Arsenide (a direct band-gap semi-conductor) have relatively good and constant absorption coefficients for all energies of incident light greater than their energy gaps (Hovel, 1975). A negligible amount of incident light with energy less than the band-gap is absorbed. Silicon however is not a direct gap semconductor and has a poor absorption coefficient for energies just above its band-gap (Dunbar and Hauser, 1976). For higher

energies, Silicon is a good absorber of sunlight (Hovel, 1975).

(iii) When the absorption coefficient of a material is high, light is absorbed, generating electrons and holes close to the front surface of the solar cell. Reducing the surface recombination at the front of the device is then important, as is the case in Germanium and Gallium Arsenide solar cells. If the absorption coefficient is weaker, more of the light is absorbed in the base region and the properties of recombination in the base are of emphasised importance. This is the case in Silicon solar cells (Hovel, 1975).

(iv) If one chooses to make the thickness of the cell large, the solar cell absorbs more of the light falling on it, but the device loses more of the extra carriers generated un the increased size because of larger bulk recombination. Bigger doping concentrations on either side of the junction can lead to poorer lifetimes of the photogenerated electrons because of extra Auger transitions (see for example Schmid and Reiner, 1982). For a good review of the material effects on solar cell efficiency see Hovel (1975).

Returning to the effect (iii) of the position dependence of light absorption, it is usual to write the generation function, $g(x,\lambda)$ of electron-hole pairs in a solar cell as a function of position, x, and for a given wavelength range, λ to $\lambda+d\lambda$, by

$$g(x,\lambda)d\lambda = \alpha(\lambda)N_0(\lambda)d\lambda\exp\{-\alpha(\lambda)x\}$$

where $N_0(\lambda)$ is the incident flux of photons in the wavelength range and $\alpha(\lambda)$ is the absorption coefficient (see for example Cummerow, 1954 for this equation). One integrates over all wavelengths to obtain the total generation rate inside the solar cell. A new form for the total rate of carrier generation inside the solar cell was recently given (Hsieh et al, 1980) for the AM1 and AM2 spectra and this is

$$g(x) = \sum_{i=1}^{n} g_i/(x+c_i). \qquad (6.1)$$

Note that there is no dependence on wavelength, λ, and that good agreement with experiment is obtained for n equal to 1,2 or 4. This new form of g(x) lends itself to analysis of the steady-state diffusion equation when Green's method is utilised. It has the advantage over the usual exponential generation rate of possessing only a few terms and an integration over the range of incident wavelengths is not required in a full solution.

6.2 The diffusion equation solution.

The minority carrier diffusion equation for electrons in the p-type base of a solar cell where the electric field, $\underline{E}$, is negligibly small is

$$\frac{d^2n}{dx^2} - \frac{n}{L^2} + \frac{g(x)}{D} = 0, \qquad (6.2)$$

where L is the diffusion length, D is the diffusion coefficient and n(x) is the excess electron density. Note that the drift field, $\underline{E}$, has been set equal to zero, this is not necessary to solve equation(6.2), but it does simplify the equations which follow and this is why it has been done. Using the general linear boundary conditions of case 6 of Table 5.1, the general solution to equation (6.2) was obtained in chapter 5, equation (5.41) and it is

$$n(x)=\frac{(a_3+I_1)\{b_1\sinh(d-x)/L+b_2/L\cosh(d-x)/L\}+(b_3+I_2)\{a_1\sinh x/L-a_2/L\cosh x/L\}}{\{a_1b_1-a_2b_2/L^2\}\sinh d/L+\{(a_1b_2-a_2b_1)/L\}\cosh d/L} \qquad (6.3)$$

where f is zero and the parameter μ is the reciprocal of the diffusion length, L. Here the integrals I_1 and I_2 have new forms because of the function g(x) given in (6.1) and these are

$$I_1 = \int_0^x \sum_{i=1}^{n} \left(\frac{g_i L}{D}\right)\left(\frac{a_1\sinh y/L-a_2/L\cosh y/L}{y+c_i}\right)dy \qquad (6.4)$$

and

$$I_2 = \int_x^d \sum_{i=1}^{n} \left(\frac{g_i L}{D}\right) \left(\frac{b_1 \sinh(d-y)/L + b_2/L \cosh(d-y)/L}{y+c_i}\right) dy. \quad (6.5)$$

Although the integrals I_1 and I_2 cannot be performed explicitly one can recast equations (6.4) and (6.5) in terms of the exponential integral (Gradshteyn and Ryzhik, 1980),

$$Ei(x) = \begin{cases} -\int_{-x}^{\infty} (e^{-t}/t)dt & \text{for } x<0, \\ -\lim_{\varepsilon \to 0} \int_{-x}^{-\varepsilon} (e^{-t}/t)dt + \int_{\varepsilon}^{\infty} (e^{-t}/t)dt & \text{for } x>0. \end{cases} \quad (6.6)$$

The exponential integrals are evaluated from tables (Abramowitz and Stegun, 1970) or by the infinite series (Gradshteyn and Ryzhik, 1980)

$$Ei(x) = \gamma + \ln|x| + \sum_{k=1}^{\infty} x^k/(k.k!) \quad (6.7)$$

where γ (=0.57722) is Euler's constant. Expanding the hyperbolic functions of I_1 and I_2 in terms of exponentials and utilising the exponential integral,

$$I_1 = \sum_{i=1}^{n} \left(\frac{g_i L}{2D}\right) \times$$

$$\left[\left(a_1 - \frac{a_2}{L}\right) e^{-c_i/L} \left\{Ei\left(\frac{x+c_i}{L}\right) - Ei\left(\frac{c_i}{L}\right)\right\} + \left(a_1 + \frac{a_2}{L}\right) e^{c_i/L} \left\{Ei\left(\frac{-c_i}{L}\right) - Ei\left(\frac{-x+c_i}{L}\right)\right\}\right], \quad (6.8)$$

$$I_2 = \sum_{i=1}^{n} \left(\frac{g_i L}{2D}\right) \times \quad (6.9)$$

$$\left[\left(b_1 + \frac{b_2}{L}\right) e^{(c_i+d)/L} \left\{Ei\left(\frac{-x+c_i}{L}\right) + Ei\left(\frac{-d+c_i}{L}\right)\right\} + \left(b_1 + \frac{b_2}{L}\right) e^{-(c_i+d)/L} \left\{Ei\left(\frac{x+c_i}{L}\right) - Ei\left(\frac{d+c_i}{L}\right)\right\}\right].$$

It is useful to define functions $K(y)$ and $H(y)$ by

$$K(y) \equiv Ei(y)e^{-y} - Ei(-y)e^{y} \qquad (6.10)$$

and

$$H(y) \equiv \frac{dK(y)}{dy} = -Ei(y)e^{-y} - Ei(-y)e^{y}. \qquad (6.11)$$

Utilising equations (6.8) to (6.11), the integrals I_1 and I_2 are

$$I_1 = \sum_{i=1}^{n}\left(\frac{g_i L}{2D}\right)\left[-a_1 K\left(\frac{c_i}{L}\right) - \frac{a_2}{L}H\left(\frac{c_i}{L}\right) + \left(a_1 - \frac{a_2}{L}\right)e^{-c_i/L}Ei\left(\frac{x+c_i}{L}\right) - \left(a_1 + \frac{a_2}{L}\right)e^{c_i/L}Ei\left(\frac{-x+c_i}{L}\right)\right],$$

$$I_2 = \sum_{i=1}^{n}\left(\frac{g_i L}{2D}\right) \times$$

$$\left[-b_1 K\left(\frac{d+c_i}{L}\right) - \frac{b_2}{L}H\left(\frac{d+c_i}{L}\right) + \left(b_1 + \frac{b_2}{L}\right)e^{(c_i+d)/L}Ei\left(\frac{-x+c_i}{L}\right) + \left(b_1 - \frac{b_2}{L}\right)e^{-(c_i+d)/L}Ei\left(\frac{x+c_i}{L}\right)\right].$$

As a consequence of the above expressions, the minority carrier density, $n(x)$, from equation (6.3) can be written in the following form

$$n(x) = \sum_{i=1}^{n}\left(\frac{g_i L}{2D}\right)\left[K\{(x+c_i)/L\} + A_i\left\{b_1 \sinh\left(\frac{d-x}{L}\right) + \frac{b_2}{L}\cosh\left\{\frac{d-x}{L}\right\}\right\} + B_i\left\{a_1 \sinh\frac{x}{L} - \frac{a_2}{L}\cosh\frac{x}{L}\right\}\right], \qquad (6.12)$$

where

$$A_i = \frac{a_3 2D/(g_i L) - a_1 K(c_i/L) - (a_2/L)H(c_i/L)}{(a_1 b_1 - a_2 b_2/L^2)\sinh d/L + (a_1 b_2 - a_2 b_1)/L \cosh d/L} \qquad (6.13)$$

and

$$B_i = \frac{b_3 2D/(g_i L) - b_1 K\{(d+c_i)/L\} - (b_2/L)H\{(d+c_i)/L\}}{(a_1 b_1 - a_2 b_2/L^2)\sinh d/L + (a_1 b_2 - a_2 b_1)/L \cosh d/L} \qquad (6.14)$$

Note that it has been assumed that the electric field is zero. If it is not zero, one can include its effect in the diffusion equation (6.1) as was shown in chapter 5 or as in the literature (Ellis and Moss, 1970).

One must however regard the electric field as constant in such work.

In equation (6.12) the excess minority carrier concentration of electrons in the p-type material has been calculated, and the total electron concentration is

$$n_T(x) = n(x) + n_0; \tag{6.15}$$

similarly the hole concentration is

$$p_T(x) = p(x) + p_0. \tag{6.16}$$

The material is assumed to be uncharged, i.e. in equilibrium

$$p_0 - n_0 - N_A^- = 0 \tag{6.17}$$

and in the steady-state

$$p_T(x) - n_T(x) - N_A^- = 0 \tag{6.18}$$

where N_A^- is the concentration of charged acceptors. Hence subtracting the two equations (6.17) and (6.18), using also (6.15), (6.16)

$$p(x) - n(x) = 0.$$

One finds in equilibrium, a large concentration of holes, such that

$$p_0 \doteqdot N_A^- >> n_0. \tag{6.19}$$

Away from equilibrium, providing the excess electron concentration is not too large, (6.19) still applies and one may also write

$$p_T(x)n_T(x) = n_i^2 \exp(\gamma_e - \gamma_h) \tag{6.20}$$

where $n_i^2 = n_0 p_0$ and γ_e and γ_h are the electron and hole quasi-Fermi levels divided by $k_B T$ where k_B ($=8.6171 \times 10^{-5}$ eVK^{-1}) is Boltzmann's constant. Thus utilising (6.20) and (6.15),

$$n(x) = (n_i^2/N_A)\{\exp(\gamma_e - \gamma_h) - 1\}$$

where it has been assumed that all of the acceptors are charged. Finally, (6.19) allows one to assume F_h is flat,

$$F_e(x) = F_h + k_B T \ln\{(n(x)N_A/n_i^2) + 1\}; \qquad (6.21)$$

here n(x) is calculated using (6.12). Equation (6.21) has been used to show $F_e - F_h$ as a function of x in the quasi-neutral base region of a solar cell in Figure 6.1 using the parameters of Table 6.1 for Si. The data for the solar spectra AM1 and AM2 was taken from Hsieh et al., (1980, Table 1). The upper curves show open-circuit conditions where the boundary conditions are

$$eD \left.\frac{dn}{dx}\right|_{x=0} = J(0) = 0 \qquad (6.22)$$

and

$$J(d) = eD \left.\frac{dn}{dx}\right|_{x=0} = -esn(d) \qquad (6.23)$$

The lower curves are for short-circuit conditions where the boundary conditions are given by

$$n(0) = 0$$

together with (6.23) for x=d. Under open-circuit conditions, using (6.12), (6.22) and (6.23)

$$n(x) = \sum_{i=1}^{n} \left[K\left(\frac{x+c_i}{L}\right) + A_i\left\{ s \sinh\left(\frac{d-x}{L}\right) + \frac{D}{L}\cosh\left(\frac{d-x}{L}\right)\right\} + B_i\left\{\frac{-D}{L}\cosh\frac{x}{L}\right\}\right]\frac{g_i L}{2D}$$

where

$$A_i = \frac{(D/L)H(c_i/L)}{(D/L)^2 \sinh d/L + (sD/L)\cosh d/L},$$

using (6.12) and also, using (6.14),

$$B_i = \frac{sK\{(d+c_i)/L\} + (D/L)H\{(d+c_i)/L\}}{(D/L)^2 \sinh d/L + (sD/L)\cosh d/L}.$$

Under short-circuit conditions, utilising (6.23) and no excess carrier density at the junction, (6.12) becomes

$$n(x) = \sum_{i=1}^{n} \frac{g_i L}{2D}\left[K\left(\frac{x+c_i}{L}\right) + A_i\left\{s \sinh\left(\frac{d-x}{L}\right) + \frac{D}{L}\cosh\left(\frac{d-x}{L}\right)\right\} + B_i \sinh\frac{x}{L}\right] \qquad (6.24)$$

where (6.13) gives

$$A_i = \frac{-K(c_i/L)}{s \sinh d/L + D/L \cosh d/L}$$

and (6.14) gives

$$B_i = \frac{-\left[sK\{(d+c_i)/L\} + (D/L)H\{(d+c_i)/L\}\right]}{s \sinh d/L + D/L \cosh d/L}.$$

The general slope of the curves in Figure 6.1 for open-circuit conditions is caused by the position dependence of the carrier generation. The absorption rate of photons is high towards the junction end of the of the base region, x=0, and is low in the back surface region of the base as fewer photons are available to be absorbed. This gives rise to a larger separation of the quasi-Fermi levels near the junction and a smaller separation of the quasi-Fermi levels near the back of the device. The high back surface recombination rate influences the carrier concentration and hence the separation of Fermi-levels in the neighbouring region is small. When a large surface recombination velocity exists at the back surface, for example because of an Ohmic metal contact to the semi-

conductor , there is a large carrier current towards the back surface. Consequently, the gradient of the carrier concentration or of the Fermi level separation is large near the back surface.

Under short-circuit conditions, as in the lower curves of Figure 6.1, there is a large carrier current out of the base into the junction region. This current sweeps a large proportion of the excess electron density out of the region of the base adjacent to the junction, so reducing the separation of the Fermi levels at small x values.

In both short-circuit and open-circuit cases the curves for the AM1 spectrum lie above those for the AM2 spectrum. The reason for this lies in the AM1 spectrum having a higher concentration of photons. At a distance of 0.1 μm from the front surface, there are 50% more photons in the AM1 spectrum (Hsieh et al., 1980, Figures 1 and 2) than in the AM2 spectrum. At 1 μm from the front surface however, the difference is reduced to 20%; thus, the difference in the curves is reduced towards the back of the cell. Physically, this change in the relative intensity of the two spectra with increasing diatance from the front surface can be understood as follows: Silicon is a poor absorber of photons with energies just above its energy-gap, but it is a good absorber of higher energy photons. The extra photons that the AM1 spectrum has over the AM2 spectrum tend to have higher energy (in the ultraviolet region). Hence, these photons are easily absorbed by silicon near the front surface, the remaining photons being of smaller energy are absorbed towards the back of the diode. Note that the other main difference in the AM1 and AM2 spectra is that the latter has a larger diffuse component of radiation. Thus, more of the AM2 spectrum is reflected by the front surface of the solar cell and does not penetrate into the device. This effect is not considered here because the data given by Hsieh et al., (1980, Table 1) refers only to measurements made of the spectrum inside the solar cell.

6.3 The current-voltage characteristic

The total current density flowing across the junction of a solar cell has two contributions, one contribution from the minority carriers in the base and a second contribution from the minority carriers in the emitter region. In this case, the base is p-type and the first contribution is by electrons. The second contribution is from holes flowing out of the n-type emitter into the base, but here it will be assumed to be negligibly small (Dhariwal and Vasu, 1981) because the emitter is usually thin and more strongly doped than the base, giving a smaller carrier lifetime.

The electron current from the base at the junction, x=0, is given by

$$J(0) = eD\left|\frac{dn}{dx}\right._{x=0} ,$$

where n(x) was written in equation (6.12). Thus, using (6.11)

$$J(0) = \tfrac{1}{2}e\sum_{i=1}^{n} g_i\left[H\left(\frac{c_i}{L}\right) - A_i\left\{b_1\cosh\left(\frac{d}{L}\right) + \frac{c_2}{L}\sinh\left(\frac{d}{L}\right)\right\} + B_i a_1\right] \quad (6.25)$$

where A_i and B_i were given in equations (6.13) and (6.14). Utilising the boundary conditions of case 1 of Table 5.1, one has

$$J(0) = \frac{e}{2}\sum_{i=1}^{n} g_i\left[K\left(\frac{c_i}{L}\right)\frac{\{sL/D\cosh d/L+\sinh d/L\}}{\{sL/D\sinh d/L+\cosh d/L\}} - \frac{sL/DK\{(d+c_i)/L\}+H\{(d+c_i)/L\}}{\{sL/D\sinh d/L+\cosh d/L\}}\right.$$

$$\left. + H\left(\frac{c_i}{L}\right)\right] - \frac{eDn_0}{L}\left(\frac{sL/D\cosh d/L+\sinh d/L}{sL/D\sinh d/L+\cosh d/L}\right)\{\exp(eV/k_BT)-1\}. \quad (6.26)$$

Note that the current flow is towards negative x and that is why the sign of the dark current is negative. This occurs here because of the choice of an n-p junction diode. In the simplest solar cell, the back surface recombination velocity, s, is infinite because of an Ohmic back contact and also the thickness of the cell, d, is many times larger than

the diffusion length, L. Thus, the current density is

$$J(0) = \tfrac{1}{2}e\sum_{i=1}^{n} g_i\left[H(c_i/L)+K(c_i/L)\right] - \frac{eDn_0}{L}\left\{\exp(eV/k_BT)-1\right\},$$

using also (6.10) and (6.11)

$$J(0) = \tfrac{1}{2}e\sum_{i=1}^{n} g_i Ei(-c_i/L)e^{c_i/L} - (eDn_0/L)\{\exp(eV/k_BT)-1\}. \qquad (6.27)$$

Using the series expansion (6.7) for $Ei(c_i/L)$, the data for the coefficients c_i from Hsieh *et al.*, (1980, Table 1) together with the data of Table 6.1 and the conventional forward current direction, the current density (6.27) as a function of applied voltage and of illumination spectrum is shown in Figure 6.2. The difference between the two curves for AM1 and AM2 spectra is because the weaker intensity AM2 spectrum gives a smaller light generated current, J_L. Note equation (6.27) can be written in the form

$$J(0) = J_L - J_0\{\exp(eV/k_BT)-1\},$$

where one identifies J_L as the first term on the right hand side of (6.27), J_0 is the so-called dark current and first factor of the final term of (6.27). The open-circuit voltage, V_{oc}, is given by

$$V_{oc} = (k_BT/e)\ln(1+J_L/J_0),$$

one notices that the change in J_L has little effect on V_{oc} because the ratio of light current to dark current is very much larger than unity. The dashed lines indicate the current as a function of voltage when the doping is reduced by a factor of five ($N_A=10^{15}$ cm^{-3}, $\tau=15\mu s$, $D=36$ cm^2s^{-1}), here the dark current is larger and there is a smaller open-circuit voltage for both AM1 and AM2 spectra.

de Vos and Pauwels (1977) define the collection efficiency of a solar cell by

$$Q \equiv J_L/eG$$

where

$$G = \sum_{i=1}^{n} \int_0^d \frac{g_i}{x+c_i} dx.$$

Hence, by equation (6.26) when the back surface recombination velocity is infinite, because of an Ohmic contact for example

$$Q = \frac{\sum_{i=1}^{n} \frac{1}{2} g_i \left[H(c_i/L)+K(c_i/L)\text{coth}d/L-K\{(d+c_i)/L\}\text{cosech}d/L\right]}{\sum_{i=1}^{n} g_i \ln(1+d/c_i)} . \qquad (6.28)$$

Using the data of Table 6.1, equations (6.10) and (6.11) for K and H, (6.7) for Ei and the spectral data of Hsieh *et al.*, (1980, Table 1) results for the collection efficiency are given in Table 6.2. Care with the choice of d must be taken because of the nature of the integrated generation rate, G. If

$$\sum_{i=1}^{n} (g_i/c_i)$$

incident photons fall on the cell, when d is made too large, the total of electron-hole pairs generated

$$\sum_{i=1}^{n} g_i \ln(1 + d/c_i)$$

exceeds the number of incident photons and that is impossible. Hence, one must set an upper limit on d.

One finds from Table 6.2 a higher collection efficiency for the AM1 spectrum than for the AM2 spectrum. This is largely due to the light current produced by the AM1 spectrum being larger.

6.4 Conclusions

Solution of the minority carrier diffusion equation using Green's

function provides the benefit of a general solution with general linear boundary conditions. This solution allows one to examine more complicated generating functions (Hsieh et al., 1980) as well as the regular exponential generating function (Mallinson and Landsberg, 1977). In the example shown here there is no wavelength dependence of the generation function (Hsieh et al., 1980) used to represent the Air Mass one (AM1) and Air Mass two (AM2) spectra. This is a disadvantage over existing models (Mallinson and Landsberg, 1977) of atmospheric illumination because one cannot attribute features of the excited carrier population to the various regions of the wavelentgh range of sunlight. However the treatment of the position dependence and size of carrier generation by sunlight explains the magnitude of the short-circuit current under different weather conditions. Also the new representation (Hsieh et al., 1980) of the solar spectrum has so far been published only for the AM1 and AM2 spectra and would be of wider interest if it was available for other solar spectra, particularly for the commonly used AM0 and AM1.5 spectra.

Another feature of the general solution is the adoption of general linear boundary conditions. This has enabled the examination of a whole class of possible boundary conditions with a single solution. It has been found from Figure 6.1 that the choice of boundary condition at the junction has a large effect on the carrier concentration and hence on the Fermi level separation near the junction. The slope of the Fermi level for electrons is a measure of the current flow (shown in Figure 6.2) and is strongly affected by changes in the physical processes at the boundaries which are represented here by the boundary conditions.

Table 6.1 Parameters used for the curves of Figures 6.1 and 6.2.

N_c	2.8×10^{19} cm^{-3}	D	35 cm^{2}s^{-1}
N_v	1.0×10^{19} cm^{-3}	L	1.18×10^{-2} cm
E_G	1.12 eV	d	0.1 cm
k_BT	0.026 eV	n_i	1.6×10^{10} cm^{-3}
s	10^4 cm s^{-1}	N_A	5×10^{15} cm^{-3}
τ	4.0 μs	n_0	5.12×10^4 cm^{-3}

Table 6.2 Collection efficiency, Q, as a function of the illumination spectrum and solar cell thickness, d.

Q	d = 1.0 mm	d = 1.0 cm
AM1	0.86	0.80
AM2	0.83	0.72

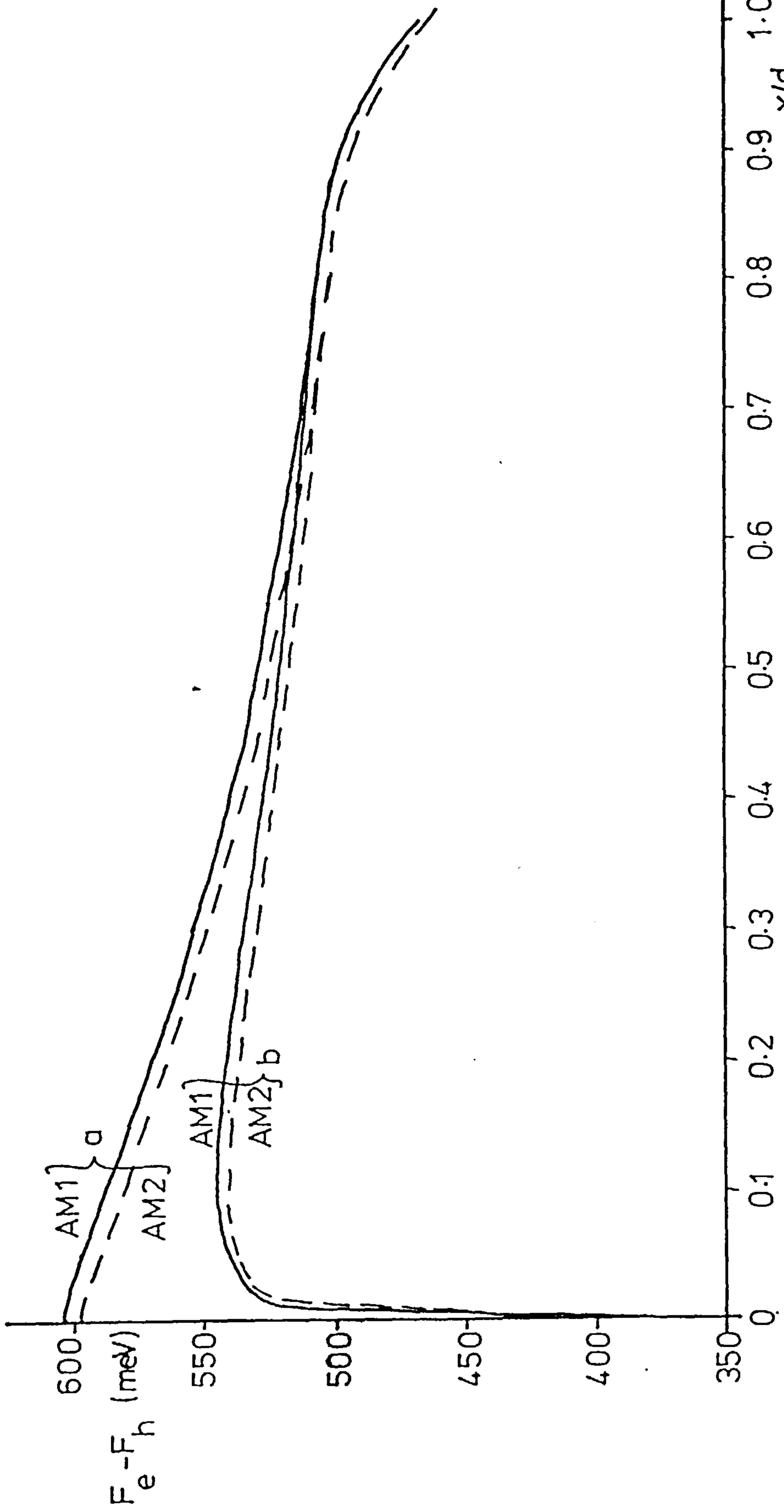

Figure 6.1 The quasi-Fermi level separation as a function of position in the solar cell base using AM1 and AM2 (dotted curves) illumination for (a) open circuit and (b) short circuit conditions. The data of Table 6.1 and equation (6.21) are used.

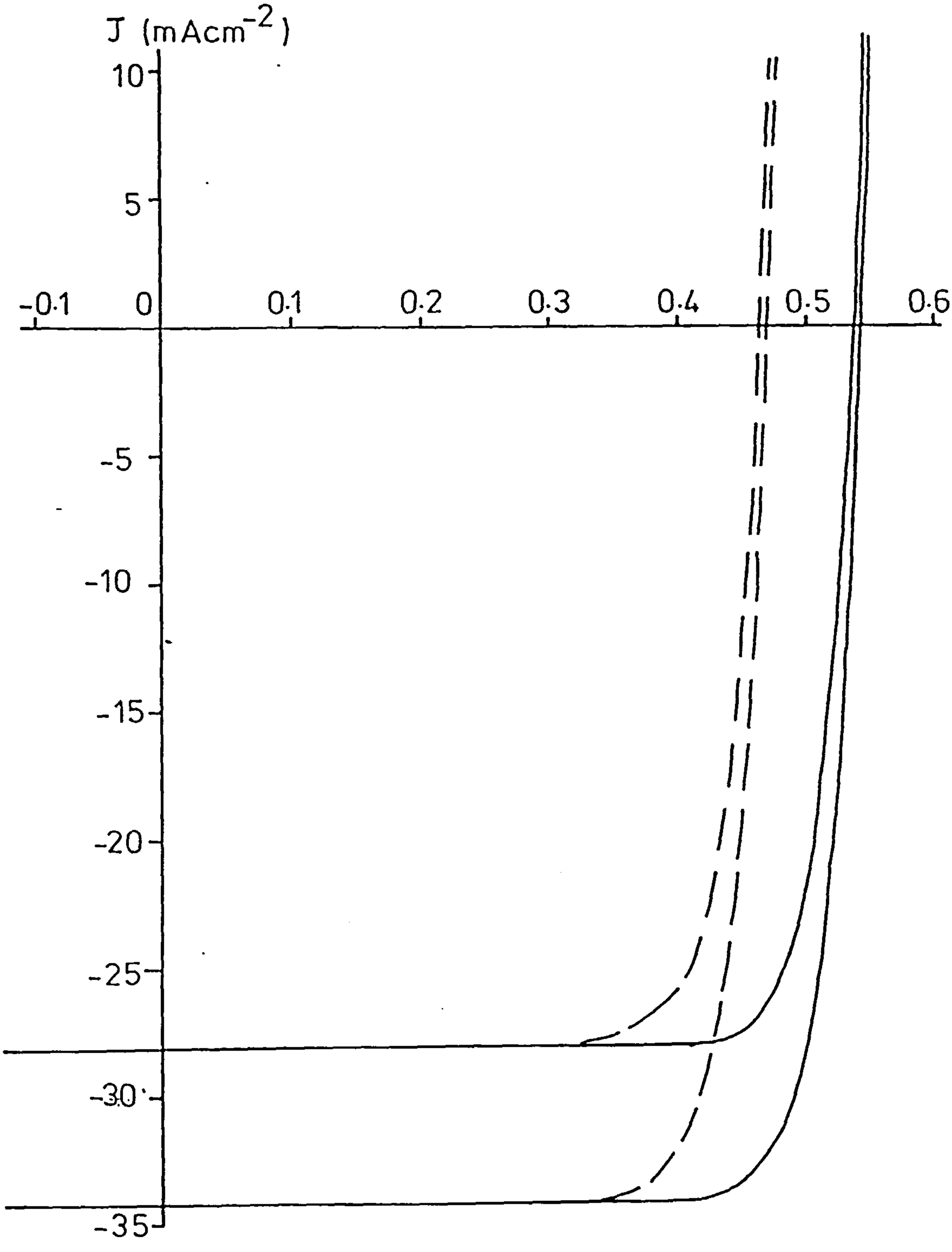

Figure 6.2 The solar-cell current-voltage characteristic, using equation (6.27) and the data of Table 6.1, as a function of the illumination spectra. The dotted curves show the effect of reducing the doping concentration, N_A, to 10^{15} cm^{-3}.

CHAPTER 7

THE TRANSIENT MINORITY CARRIER DIFFUSION EQUATION FOR A SOLAR CELL

7.1 Introduction

The recent development of the photovoltage decay method (Dhariwal et al, 1977) and the current induced voltage decay method (Dhariwal and Vasu, 1981; Von Roos, 1981) for measuring lifetimes in semiconductor solar cells and diodes has led to renewed interest in the time-dependent minority carrier diffusion equation (Sharma and Tewary, 1982). Interest centred initially on the steady-state (see for example Mallinson and Landsberg, 1977). The theory of short-circuit current decay followed, firstly for time-independent boundary conditions (Dhariwal et al, 1977) and secondly for time-dependent boundary conditions (Dhariwal and Vasu, 1981). Fourier (Dhariwal et al, 1977; Dhariwal and Vasu, 1981), Laplace (Von Roos, 1981) and Sturm-Liouville transforms (Sharma and Tewary, 1982) have been utilised in solutions of the diffusion equation in a solar cell. This work shows that one can advance further in this direction to display the hyperbolic functions in the solution for the minority carrier density, $n(x,t)$, for a whole class of boundary conditions. One can with a single treatment of the diffusion equation then find a solution which fulfils all of the operating conditions of a solar cell.

The present work is indebted particularly to the theory of Sharma and Tewary (1982) and incidentally a simplification of their expressions (A20) to (A32) for photovoltage decay from the steady-state has been obtained. An analogous expression has been developed here for the decay of photovoltage following a short pulse of light which confirms and extends their work on lifetimes. Also, a new problem relating to the effect of grain boundary recombination on lifetime in polysilicon (Bohm et al, 1982) is examined with the help of Sturm-Liouville transforms.

7.2 Solution of the transient diffusion equation with a Sturm-Liouville transform.

The diffusion equation for minority carriers is examined in a region extending from the junction at x=0 to the back surface at x=d of the solar cell or n-p junction diode. This theory allows for surface recombination at either boundary; at x=d, surface recombination is interpreted as taking the place of a p^+-region when a back surface field is used. A simple geometry is adopted by assuming light is incident normally to the front surface and a single dimension, x, normal to the front surface is considered. The photogeneration rate of carriers per unit volume per unit wavelength range is denoted by g(x,t) where the dependence on wavelength λ will not be given explicitly.

A generalised diffusion equation for the p-type base of the solar cell in Figure 5.1 is given by equation (5.15) with one positional dimension, x, and time-dependence,

$$D\frac{\partial^2 n}{\partial x^2} + 2fD\frac{\partial n}{\partial x} + g(x,t) - \frac{n(x,t)}{\tau} = \frac{\partial n}{\partial t} \qquad (7.1)$$

where D is the diffusion coefficient, τ is the lifetime and f is a measure of the electric field, $\underline{E}$ ($f=e|\underline{E}|/2k_BT$). Equation (7.1) is transformed with finite Sturm-Liouville transforms (Sneddon,1972 and Appendix A). The boundary conditions of Table 5.1, case 6 are used where the parameters a_3 and b_3 are time-dependent (see Appendix B). The finite Sturm-Liouville transform, $\overline{n_r}(t)$, of the function n(x,t) is given by the inner product of n(x,t) with the r-th eigenfunction $\phi_r(x)$ of the Sturm-Liouville problem. The eigenfunctions $\phi_r(x)$ are solutions of the following equations:

$$\underline{L}\phi_r - \xi_r\phi_r = 0,\ a_1\phi_r(0)+a_2\phi_r'(0)=0,\ b_1\phi_r(d)+b_2\phi_r'(d)=0, \qquad (7.2)$$

where

$$\underline{L} = \left\{\frac{D}{e^{2fx}}\right\}\left\{\frac{d}{dx}\left[e^{2fx}\frac{d}{dx}\right]\right\} - \frac{1}{\tau}, \tag{7.3}$$

ξ_r is the eigenvalue and dashes on ϕ_r indicate differentiation with respect to x. The prefactor of $\underline{L}$ (De^{-2fx}) is used as a weight function in the inner product. Thus, the Sturm-Liouville (SL) transform of a function n(x,t) is given by

$$\bar{n}_r(t) \equiv \int_0^d \frac{e^{2fx}}{D}\phi_r(x)n(x,t)dx. \tag{7.4}$$

There are infinitely many SL transforms of n(x,t), each one being labelled by a subscript r because of the infinite number of eigenfunctions ϕ_r of the SL problem.

Equation (7.2) is an equation for the eigenvalues and eigenfunctions of the SL problem and it is in fact very similar to the homogeneous steady-state diffusion equation (5.45), (ξ_r+1/τ) replaces $1/\tau$ there, i.e.

$$D\frac{d^2\phi_r}{dx^2} + 2fD\frac{d\phi_r}{dx} - \left(\xi_r + \frac{1}{\tau}\right)\phi_r = 0. \tag{7.5}$$

Using the result (5.46) of the homogeneous steady-state equation, the eigenfunctions of (7.5) are given by

$$\phi_r = e^{-fx}\{A_r\exp(\mu_r x) + B_r\exp(-\mu_r x)\} \tag{7.6}$$

where the parameters μ_r involve the eigenvalues ξ_r through

$$\mu_r = \{f^2 + (1/D)[\xi_r + 1/\tau]\}^{\frac{1}{2}}. \tag{7.7}$$

Putting equation (7.6) into the boundary conditions of equation (7.2), one finds at x=0,

$$a_1(A_r+B_r) + a_2\{(\mu_r-f)A_r-(\mu_r+f)B_r\} = 0$$

or alternatively

$$\{a_1+a_2(\mu_r-f)\}A_r + B_r\{a_1-a_2(\mu_r+f)\} = 0. \qquad (7.8)$$

At x=d, the boundary condition requires

$$b_1\left(A_r e^{\mu_r d} + B_r e^{-\mu_r d}\right) + b_2\left(A_r e^{\mu_r d}(\mu_r-f) - B_r e^{-\mu_r d}(\mu_r+f)\right) = 0,$$

or alternatively

$$\{b_1+b_2(\mu_r-f)\}A_r\exp(\mu_r d) + \{b_1-b_2(\mu_r+f)\}B_r\exp(-\mu_r d) = 0. \qquad (7.9)$$

From elementary matrix theory (Lennox and Chadwick, 1970) equations (7.8) and (7.9) have a solution if the determinant of the matrix formed from the coefficients of A_r and B_r is zero, i.e. if

$$\{a_1-a_2(\mu_r+f)\}\{b_1+b_2(\mu_r-f)\}e^{\mu_r d} - \{b_1-b_2(\mu_r+f)\}\{a_1+a_2(\mu_r-f)\}e^{-\mu_r d} = 0$$

which can be rearranged into a transcendental equation for the eigenvalues ξ_r through the parameters μ_r,

$$\{a_1b_1-(a_1b_2+a_2b_1)f-a_2b_2(\mu_r^2-f^2)\}\sinh\mu_r d+(a_1b_2-a_2b_1)\mu_r\cosh\mu_r d = 0, \quad (7.10)$$

Equation (7.10) has μ_r equals zero as one of its many real and imaginary roots. Putting zero for μ_r into equations (7.8) and (7.9) requires that

$$A_r + B_r = 0,$$

thus the corresponding eigenfunction (7.6) is zero. The existence of real solutions to (7.10) and special roots leading to the excluded zero eigenfunction are discussed in Appendix C.

Each root μ_r of (7.10) is used in equation (7.8) to express B_r in terms of A_r,

$$B_r = \frac{-\{a_1+a_2(\mu_r-f)\}}{\{a_1-a_2(\mu_r+f)\}} A_r.$$

Substituting B_r into (7.6) and rewriting (7.6) with hyperbolic functions yields

$$\phi_r = \frac{2A_r e^{-fx}\{a_2\mu_r \cosh\mu_r x+(a_2 f-a_1)\sinh\mu_r x\}}{\{a_1-a_2(\mu_r+f)\}}. \qquad (7.11)$$

The constants A_r are obtained by normalising the eigenfunctions ϕ_r using the weighted inner product,

$$\int_0^d (e^{2fx}/D)\phi_r(x)\phi_s(x)dx = \delta_{rs} \qquad (7.12)$$

where δ_{rs} is the Kronecker delta

$$\delta_{rs} = \begin{cases} 1 & \text{if } r=s, \\ 0 & \text{if } r\neq s. \end{cases}$$

Using equation (7.12) on equation (7.11) defines A_r by

$$\frac{4A_r^2/D}{\{a_2(\mu_r+f)-a_1\}^2}\int_0^d \{a_2^2\mu_r^2\cosh^2\mu_r x+(a_2f-a_1)a_2\mu_r\sinh 2\mu_r x+(a_2f-a_1)^2\sinh^2\mu_r x\}dx=1.$$

Performing the integral,

$$A_r = \qquad (7.13)$$

$$\frac{\{a_2(\mu_r+f)-a_1\}\sqrt{D/2}}{\left(a_2\mu_r\{\mu_r d+\tfrac{1}{2}\sinh 2\mu_r d\}+a_2(a_2f-a_1)(\cosh 2\mu_r d-1)+(a_2f-a_1)^2\{\sinh(2\mu_r d)/2\mu_r-d\}\right)^{\frac{1}{2}}}$$

and hence the eigenfunction is

$$\phi_r = \qquad (7.14)$$

$$\frac{2De^{-fx}\{(a_2f-a_1)\sinh\mu_r x+a_2\mu_r\cosh\mu_r x\}}{\left(a_2\mu_r\{\mu_r d+\tfrac{1}{2}\sinh 2\mu_r d\}+a_2(a_2f-a_1)(\cosh 2\mu_r d-1)+(a_2f-a_1)^2\{\sinh(2\mu_r d)/2\mu_r-d\}\right)^{\frac{1}{2}}}$$

The SL transform has the property that the transform of the self-adjoint operator, $\underline{L}$, acting on n becomes (Appendix A)

$$\overline{(\underline{Ln})}_r=\xi_r\bar{n}_r+\alpha_r\{a_1n(0,t)+a_2n'(0,t)\}+\beta_r\{b_1n(d,t)+b_2n'(d,t)\}, \tag{7.15}$$

where (Sneddon, 1972)

$$\alpha_r = \begin{cases} -a_2^{-1}\phi_r(0) , \\ a_1^{-1}\phi_r'(0) \quad (a_2=0), \end{cases} \tag{7.16}$$

and

$$\beta_r = \begin{cases} b_2^{-1}\phi_r(d)e^{2fd}, \\ -b_1^{-1}\phi_r'(d)e^{2fd} \quad (b_2=0). \end{cases} \tag{7.17}$$

Using (7.14) and (7.16),

$$\alpha_r = \begin{cases} \dfrac{-2A_r\mu_r}{\{a_2(\mu_r+f)-a_1\}} , \\ \\ 2A_r\mu_r/a_1 \quad (a_2=0), \end{cases} \tag{7.18}$$

and by (7.14) and (7.17),

$$\beta_r = \begin{cases} \dfrac{2A_re^{fd}\{a_2\mu_r\cosh\mu_rd+(a_2f-a_1)\sinh\mu_rd\}}{b_2\{a_2(\mu_r+f)-a_1\}}, \\ \\ \dfrac{2A_re^{fd}\{a_1\mu_r\cosh\mu_rd-[a_2(\mu_r^2-f^2)+a_1f]\sinh\mu_rd\}}{b_1\{a_2(\mu_r+f)-a_1\}} \quad (b_2=0), \end{cases} \tag{7.19}$$

where A_r was given above. Thus, when the diffusion equation (7.1) is transformed using (7.4), the boundary conditions of case 6 of Table 5.1 and the result (7.15), one finds for $a_2\neq0$ and $b_2\neq0$ (see Appendix B),

$$\xi_r\bar{n}_r(t) + \alpha_ra_3(t) + \beta_rb_3(t) = \frac{d\bar{n}_r(t)}{dt} - \bar{g}_r(t),$$

since

$$\overline{\left(\frac{\partial n}{\partial t}\right)}_r = \frac{d}{dt}(\bar{n}_r),$$

and also $\overline{g_r}(t)$ is the transform of the photogeneration rate. A simple time-dependent equation is obtained by transforming the diffusion equation

$$\exp(\xi_r t)\frac{d}{dt}\{\exp(-\xi_r t)\overline{n}_r\} = \overline{g}_r(t) + \alpha_r a_3(t) + \beta_r b_3(t).$$

An initial condition at time t=0 is required to integrate this equation. In the case of photovoltage decay, the steady-state solution (5.41) applies until t=0 when the light source is switched off. One specifies that the initial carrier concentration n(x,0) is equal to the steady-state concentration of (5.41). However, if the solar cell is in the dark until a short pulse of light illuminates it at t=0, one specifies n(x,0) is zero. At this stage, it will be assumed that n(x,0) is known from the conditions before t=0, but these need not be specified at the moment. The transform of the concentration is therefore

$$\overline{n}_r(t) = \left[\int_0^d e^{-\xi_r t'}\{\overline{g}_r(t') + \alpha_r a_3(t') + \beta_r b_3(t')\}dt' + \overline{n}_r(0)\right]e^{\xi_r t},$$

where $\overline{n_r}(0)$ is the transform of n(x,0). The inverse SL transform

$$n(x,t) = \sum_{r=1}^{\infty} \overline{n}_r(t)\phi_r(x) \qquad (7.20)$$

provides the minority carrier concentration from the transformed solution, i.e.

$$n(x,t) = \sum_{r=1}^{\infty} \frac{2A_r e^{-fx+\xi_r t}\{a_2\mu_r \cosh\mu_r x + (a_2 f - a_1)\sinh\mu_r x\}\{G_r(t) + I_r(t) + \overline{n}_r(0)\}}{a_2(\mu_r + f) - a_1}. \qquad (7.21)$$

Here $\overline{n_r}(0)$ is given in Appendix D for a steady-state decay,

$$G_r(t) = \int_0^d \exp(-\xi_r t')\overline{g}_r(t')dt', \qquad (7.22)$$

and

$$I_r(t) = \int_0^t \exp(-\xi_r t')(\alpha_r a_3 + \beta_r b_3)dt'. \qquad (7.23)$$

If one defines constants c_r and d_r by

$$c_r = \frac{2A_r a_2 \mu_r}{a_2(\mu_r+f)-a_1}, \quad d_r = \frac{2A_r(a_2 f-a_1)}{a_2(\mu_r+f)-a_1}, \qquad (7.24,7.25)$$

the minority carrier density is displayed in its simplest form, showing the sinh and cosh terms,

$$n(x,t) = \sum_{r=1}^{\infty} \{c_r \cosh\mu_r x + d_r \sinh\mu_r x\}\{G_r(t)+I_r(t)+\bar{n}_r(0)\}\exp(\xi_r t - fx). \quad (7.26)$$

This result (7.26) shows the excess electron concentration as an infinite sum of sinh and cosh terms with the dependence on the boundary conditions transferred to the parameters c_r, d_r, μ_r and to the functions $G_r(t)$, $I_r(t)$ and $n_r(0)$. The nature of the constants μ_r depends on the solutions of the transcendental equation (7.10) and for sufficiently large negative eigenvalues ξ_r, the constants μ_r will be imaginary (see Appendix C). Consequently the eigenfunctions will be trigonometric functions for all but a few eigenvalues. The result (7.26) lends itself to further consideration of solar cell problems which are insensitive to individual boundary conditions.

7.3 Application of the transient solution to lifetime measurements.

In the voltage decay methods (Dhariwal et al, 1977) for lifetime measurements, an excess of minority carriers is created by current injection or by illumination. The lifetime is measured by following the decay in time of the natural modes of excitation (ξ_1, ξ_2, ξ_3, ...). In these methods $G_r(t)$, $I_r(t)$ or $\bar{n}_r(0)$ represent the amplitude of the disturbance. Usually only one of these functions is involved in the decay and the other two functions are zero. For example, in the method of open-circuit voltage decay (Dhariwal and Vasu, 1981) $\bar{n}_r(0)$ is non-zero and G_r and I_r are both zero at all times. When a delta pulse of light (Dhariwal

and Vasu, 1981) is used to illuminate the device, G_r is non-zero, but I_r and $\overline{n_r}(0)$ are both zero throughout the experiment. The general solution (7.26) developed above is used to examine and compare the open-circuit voltage decay methods following both the decay of steady-state illumination and the decay after a short pulse of light (Tyagi et al, 1982).

(a) The method of open-circuit voltage decay from the steady-state.

In the method of open-circuit voltage decay (OCVD) a steady-state excess minority carrier concentration is produced in the solar cell by either illumination or by carrier injection. The steady-state conditions are halted abruptly at time t=0 and the subsequent decay of the open-circuit voltage is measured. At the junction, x=0, the excess carrier density is given by

$$n(0,t) = n_0\{\exp(eV/k_BT)-1\} \qquad (7.27)$$

where n_0 is the equilibrium electron concentration and V is the junction voltage. Since there is no current flow across the junction, the open-circuit voltage decays according to

$$V(t) = (k_BT/e)\ln(1+n(0,t)/n_0); \qquad (7.28)$$

the excess electron density is measured from the above equation as a function of the voltage.

Regarding equation (7.26) for the minority carrier concentration, the parameters $a_3(t)$ and $b_3(t)$, hence $I_r(t)$ also, are zero because there is no current flow after t=0. The integral of the transformed generation rate, $G_r(t)$ (equation (7.22)), is zero since there is no light after t=0. Thus, the excess carrier density is given by

$$n(x,t) = \sum_{r=1}^{\infty}\{c_r\cosh\mu_r x+d_r\sinh\mu_r x\}\overline{n}_r(0)\exp(\xi_r t-fx) \qquad (7.29)$$

where

$$\bar{n}_r(0) = \int_0^d \frac{2A_r n(x) e^{fx} dx\{(a_1-a_2 f)\sinh\mu_r x - a_2\cosh\mu_r x\}}{D\{a_1-(\mu_r+f)a_2\}}$$

in which n(x) is the excess carrier density in the steady-state up to t=0. From equation (5.41) the steady-state excess carrier density is

$$n(x) = N_1 e^{-fx}\chi\Big((a_1-a_2\alpha)\{(b_1-b_2 f)\sinh\mu(d-x)+b_2\mu\cosh\mu(d-x)\} +$$

$$\{b_1-b_2\alpha\}e^{(f-\alpha)d}\{(a_1-a_2 f)\sinh\mu x - a_2\mu\cosh\mu x\}\Big) - N_1 e^{-\alpha x}$$

where the following parameters are used: χ from equation (5.40), a_3 and b_3 are both zero because there is no current flow across the junction and

$$N_1 = \alpha N_0/[D(\alpha-2f)-1/\tau] \quad , \quad \mu = \left(f^2+1/L^2\right)^{\frac{1}{2}}.$$

The evaluation of the integral in (7.29) is performed in Appendix D, and the result is

$$n(x,t)= \sum_{r=1}^{\infty} N_1 e^{\xi_r t - fx} C_r\left[\frac{1}{\mu^2-\mu_r^2} - \frac{1}{(f-\alpha)^2-\mu_r^2}\right]\{(a_1-a_2 f)\sinh\mu_r x - a_2\mu_r\cosh\mu_r x\} \tag{7.30}$$

where C_r is defined by

$$C_r \equiv \frac{2\left[(a_1-a_2\alpha)\mu_r+(b_1/b_2-\alpha)e^{(f-\alpha)d}\{(a_1-a_2 f)\sinh\mu_r d - a_2\mu_r\cosh\mu_r d\}\right]}{\left(a_2\mu_r\{\mu_r d+\tfrac{1}{2}\sinh\mu_r d\}+a_2(a_2 f-a_1)(\cosh 2\mu_r d-1)+(a_2 f-a_1)^2\{\sinh 2\mu_r d/2\mu_r - d\}\right)^{\frac{1}{2}}} . \tag{7.31}$$

The open-cicuit voltage, at x=0, is therefore by (7.28),

$$V(t) = (k_B T/e)\ln\left\{\frac{N_1}{n_0}\sum_{r=1}^{\infty}\left(C_r e^{\xi_r t} a_2\mu_r\left[\frac{1}{(f-\alpha)^2-\mu_r^2} - \frac{1}{\mu^2-\mu_r^2}\right]\right)+1\right\}. \tag{7.32}$$

Equation (7.32) allows direct measurement of the lifetime from the decay of the open-circuit voltage, V. The lifetime is interpreted from the eigenvalues ξ_r and equation(7.32) which allows the lifetime to be written

as

$$1/\tau = (\mu_r^2 - f^2)D - \xi_r. \qquad (7.33)$$

The higher terms of the series in equation (7.32) have large negative eigenvalues, these terms decay rapidly after the steady-state light source is switched off. Thus, the first few terms dominate the decay and the lifetime is interpreted from these (see section 7.3(c)).

(b) The method of voltage decay following a short pulse of light.

By this method, the lifetime is measured from the open-circuit voltage decay following a square pulse of light. At all other times, the solar cell is unilluminated and there is no current to supply minority carriers to the base of the solar cell. Thus the functions $I_r(t)$ and $\overline{n_r}(0)$ are both equal to zero . The amplitude of the excess carrier distribution generated by the light pulse is $G_r(t)$ of equation (7.22) and the excess carrier density is given by equation(7.21).

An assumption is made here that the light pulse is square in shape and lasts for t_1 seconds after t=0. The photogeneration rate of equation (5.22) then becomes

$$g(x,t) = \alpha N_0 \exp(-\alpha x)\{H(t)-H(t-t_1)\} \qquad (7.34)$$

where H(t) is the Heaviside function,

$$H(t) = \begin{cases} 1, & t \geq 0, \\ 0, & t < 0. \end{cases}$$

In practice the duration of the pulse is considerably less than the lifetime of carriers, the shape of the pulse is not square and the incident number of photons, N_0, is very high. This has led previous authors (Dhariwal and Vasu, 1981) to call the light pulse a delta pulse

because that is the limiting case as t_1 tends to zero and as N_0 tends to infinity.

Equations (7.22), (7.34) and the SL transform (7.4) of g(x,t) show the function $G_r(t)$ as a double integral

$$G_r=\int_0^t e^{-\xi_r t'}\{H(t')-H(t'-t_1)\}dt'\int_0^d \frac{2A_r\alpha N_0 e^{fx-\alpha x}\{(a_1-a_2f)\sinh\mu_r x-a_2\mu_r\cosh\mu_r x\}dx}{D\{a_1-a_2(\mu_r+f)\}} \qquad (7.35)$$

Utilising results from Appendix D, namely H_5 and H_{10} of Table D.1, the integrals above are evaluated, yielding for $t > t_1$,

$$G_r(t) = \left\{\frac{1-e^{-\xi_r t_1}}{\xi_r}\right\}\frac{2A_r\alpha N_0}{D\{a_1-a_2(\mu_r+f)\}}[(a_1-a_2f)H_{10}-a_2\mu_r H_5] \qquad (7.36)$$

The results from Appendix D for H_5 and H_{10} give the square bracket term of equation (7.36) as

$$\frac{(a_1-a_2f)\{e^{fd-\alpha d}[(f-\alpha)\sinh\mu_r d-\mu_r\cosh\mu_r d]+\mu_r\}+a_2\mu_r e^{fd}\{(f-\alpha)\cosh\mu_r d-\mu_r\sinh\mu_r d\}e^{-\alpha d}}{(f-\alpha)^2-\mu_r^2}$$

$$-(f-\alpha)a_2\mu_r/\{(f-\alpha)^2-\mu_r^2\} \quad .$$

The contents of the square bracket are rearranged to yield

$$\frac{e^{fd-\alpha d}[\{a_2(\mu_r^2-f^2)+a_1 f+\alpha(a_2 f-a_1)\}\sinh\mu_r d-(a_1-a_2\alpha)\mu_r\cosh\mu_r d]+\mu_r(a_1-a_2\alpha)}{(f-\alpha)^2-\mu_r^2} \quad .$$

Multiplying inside the braced term by b_2, so that the transcendental equation (7.10) may be used to eliminate terms, the square bracket is

$$\frac{e^{fd-\alpha d}[\{a_2b_2(\mu_r^2-f^2)+a_1b_2 f+\alpha b_2(a_2 f-a_1)\}\sinh\mu_r d-(a_1b_2-a_2b_2\alpha)\mu_r\cosh\mu_r d]-b_2\mu_r(a_1-a_2\alpha)}{b_2\{(f-\alpha)^2-\mu_r^2\}}$$

which becomes

$$\frac{e^{fd-\alpha d}[\{a_1b_1-a_2b_1 f-a_1b_2\alpha+a_2b_2 f\alpha\}\sinh\mu_r d-(b_1-b_2\alpha)a_2\mu_r\cosh\mu_r d]-\mu_r(a_1-a_2\alpha)b_2}{b_2\{(f-\alpha)^2-\mu_r^2\}} \quad .$$

Hence using (7.35), $G_r(t)$ is given by

$$G_r(t) = \frac{2A_r\alpha N_0\left[1-e^{-\xi_r t_1}\right]\left[(b_1-b_2\alpha)e^{fd-\alpha d}\{(a_1-a_2f)\sinh\mu_r d-a_2\mu_r\cosh\mu_r d\}+b_2\mu_r(a_1-a_2\alpha)\right]}{\xi_r b_2 D\{a_1-a_2(\mu_r+f)\}\{(f-\alpha)^2-\mu_r^2\}}$$

Equation (7.21) shows the excess carrier density with $G_r(t)$ above as

$$n(x,t)=\sum_{r=1}^{\infty}\frac{\alpha N_0 C_r e^{\xi_r t-fx}\left(1-e^{-\xi_r t_1}\right)\{(a_1-a_2f)\sinh\mu_r x-a_2\mu_r\cosh\mu_r x\}}{\xi_r\{(f-\alpha)^2-\mu_r^2\}} \qquad (7.37)$$

where equation (7.31) has been used for C_r. Note that equation (7.37) applies for $t>t_1$. For $t<0$, $n(x,t)$ is zero and for $t<t_1$, the first integral in $G_r(t)$ of equation (7.35) is given by

$$\{1-\exp(-\xi_r t)\}/\xi_r.$$

Thus for $0<t<t_1$, the excess carrier density is

$$n(x,t) = \sum_{r=1}^{\infty}\frac{\alpha N_0 C_r e^{-fx}\left(e^{\xi_r t}-1\right)\{(a_1-a_2f)\sinh\mu_r x-a_2\mu_r\cosh\mu_r x\}}{\xi_r\{(f-\alpha)^2-\mu_r^2\}} . \qquad (7.38)$$

The eigenvalues ξ_r of the SL equation (7.2) are predominantly large and negative (see the following section), thus one finds the excess electron density increases rapidly during the pulse (by equation (7.38)) and then falls off exponentially (by equation(7.37)) after the pulse is finished.

(c) Some numerical results.

Some sample calculations are performed by utilising the boundary conditions of Table 5.1, case 4. This is equivalent to making the substitutions

$$a_1 = 2fD, \quad a_2 = D, \quad a_3 = 0, \quad b_1 = 2fD+s, \quad b_3 = 0,$$

in equations (7.30), (7.31) and (7.37). The excess minority carrier concentration for the decay of a steady-state profile using the boundary conditions of case 4 of Table 5.1 is

$$n(x,t) = \sum_{r=1}^{\infty} N_1 C_r e^{\xi_r t - fx}\left\{(\mu^2-\mu_r^2)^{-1} - \{(f-\alpha)^2-\mu_r^2\}^{-1}\right\}\{f\sinh\mu_r x - \mu_r \cosh\mu_r x\} \quad (7.39)$$

where equation (7.31) yields

$$C_r = \frac{2e^{fd-\alpha d}(f-\alpha+s/D)\{f\sinh\mu_r d - \mu_r\cosh\mu_r d\} + 2(f-\alpha)\mu_r}{\left[\mu_r^2(d+\sinh 2\mu_r d/2\mu_r)+f(1-\cosh 2\mu_r d)+f^2(\sinh 2\mu_r d/2\mu_r - d)\right]^{1/2}} . \quad (7.40)$$

A similar expression to equation (7.39) is found for the response of the solar cell to a short light pulse, the excess electron density of equation (7.37) is

$$n(x,t) = \sum_{r=1}^{\infty} \frac{\alpha N_0 C_r e^{\xi_r t - fx}\left(1-e^{\xi_r t_1}\right)}{\xi_r\{(f-\alpha)^2-\mu_r^2\}}\{f\sinh\mu_r x - \mu_r\cosh\mu_r x\} \quad (7.41)$$

with C_r as given by equation (7.40).

The parameters μ_r and hence the eigenvalues ξ_r are obtained from the transcendental equation (7.10) when the boundary conditions of case 4 of Table 5.1 are imposed on it, i.e.

$$\{f(f+s/D)-\mu_r^2\}\tanh\mu_r d - s\mu_r/D = 0. \quad (7.42)$$

Taking the limit as the surface recombination velocity tends to zero, the transcendental equation becomes

$$(f^2-\mu_r^2)\tanh\mu_r d = 0 \quad (7.43)$$

which has roots

$$\mu_r = -f,\ 0,\ f;\ \pi i,\ 2\pi i,\ 3\pi i,\ \ldots$$

The root μ_r=0is excluded because it gives rise to an eigenfunction equal to zero. Another limit of interest is the limit of s tending to infinity, then the transcendental equation is

$$f\tanh\mu_r d - \mu_r = 0 \qquad (7.44)$$

and has roots

$$\mu_r = 0,\ f,\ 1.2263i,\ 4.6174i,\ 7.7975i. \qquad (7.45)$$

Here the data of Table 5.2 has been used. Again the root μ_r equals zero is excluded because the eigenfunction it corresponds to is zero. The root μ_r=f occurs in the limit as fd tends to infinity (Sharma and Tewary, 1982), but this also gives rise to the zero eigenfunction because the term $f\sinh\mu_r d - \mu_r\cosh\mu_r d$ is zero in the numerator of C_r in equation (7.40) by the transcendental equation. In their equations (A34) and (A35) Sharma and Tewary (1982) suggest that this the root μ_r=f dominates the decay of their experiments, but since the corresponding eigenfunction is zero, the first imaginary root is the important root.

Some sample results of numerical calculations using the data of Table 5.2 are given in Figures 7.1 to 7.3. Figure 7.1 shows the rapid convergence of the infinite sum (7.39) at t=0 to the steady-state excess electron density of (5.42) where in both cases s is infinite. Good agreement is reached after only three terms in the series have been calculated (curve (c)). As the time proceeds from t=0, the decay of the higher terms is so rapid that after 0.5τ only one term dominates the series. The larger imaginary roots of the transcendental equation (7.43) play a part for a much longer period when s is zero, about six terms in the series are needed in (7.39) to gain agreement with the steady-state distribution at t=0, but this is not shown in Figure 7.1. The initial decay following t=0 for s=0 is more rapid until the more slowly decaying first term dominates the sum.

A sample time decay is given in Figure 7.2, curve (a) for the decay of the carrier concentration at open-circuit using equation (7.39), the data of Table 5.2 and an infinite s. The initial stages have many time constants giving rise to the slight curvature before $t=10^{-7}$ secs. For later times, a single exponential dominates the decay and corresponds to the least negative of the eigenvalues, ξ_1 say. The response of the excess carrier density of equation (7.41) to a short pulse of light of duration t_1 secs ending at t=0 is shown in Figure 7.2, curve (b). The curve is lower than curve (a) because the short pulse generates fewer carriers than when steady-state is reached. However, both curve (a) and (b) have the same rate of decay because the same boundary conditions with s=0 have been used.

Curve (c) shows the effect of a short pulse of light when the back surface recombination velocity, s, is zero, which may occur when a p^+-region at the back of the device blocks the minority carriers from reaching the contact. The initial concentration is enhanced relative to the case of infinite s, an effect noticed in chapter 5 in the steady-state also, since high surface recombination acts as a sink for minority carriers. Curve (c) shows a rapid non-exponential decay as the higher terms in the series fall off rapidly. After 10^{-6} secs, a single exponential dominates, but the curve decays more slowly than curve (b) where s is infinite. This is again due to the high recombination sink for minority carriers at the back surface in curve (b). From curves (b) and (c), the high surface recombination velocity has an effect similar to degrading the lifetime of the solar cell.

Curve (d) indicates the rate of decay following the termination of a steady-state light source is the same as following a short light pulse in curve (c). However, the carrier density is enhanced at t=0 over the short pulse because the steady-state concentration is higher.

The development in time of the excess carrier profile is shown in

Figure 7.3 at various times. The recombination rate is proportional to n/τ and so is faster in the region of higher concentration near the junction, x=0. The carrier concentration is low at all times near the back surface, x=d, because the surface recombination velocity is infinite.

7.4 Conclusions.

A solution to the minority carrier diffusion equation has been obtained with general linear boundary conditions. This has enabled a single treatment of the diffusion equation to encompass the results of a number of previous authors (Dhariwal et al, 1977; Dhariwal and Vasu, 1981; Von Roos, 1981; Sharma and Tewary, 1982). This method has shown in Figure 7.2 that the lifetime measured from the decay rate following a short light pulse or the termination of a steady-state light source is independent of the method of excitation. The rate of decay is however dependent on the chosen boundary conditions at the junction and at the back of the solar cell. These boundary conditions change with different operating conditions for the solar cell, for example case 2 of Table 5.1 boundary conditions represent short circuit operation and case 3 boundary conditions represent open-circuit operation. A single treatment of the diffusion equation using general linear boundary conditions yields a solution which fulfils all of the operating conditions of a solar cell and this is why it is useful.

This work is indebted to the work of Sharma and Tewary (1982) which drew attention to Sturm-Liouville transforms as a way of solving the electron diffusion equation. Through equations (7.39) and (7.40) a simplification of their results (A20) to (A32) was made. Also, some inaccuracy in their interpretation of roots of the transcendental equation for the eigenvalues of the Sturm-Liouville problem has been clarified. The work of Sharma and Tewary (1982) was extended to explain

the carrier density decay following a short pulse of high intensity illumination through equation (7.41).

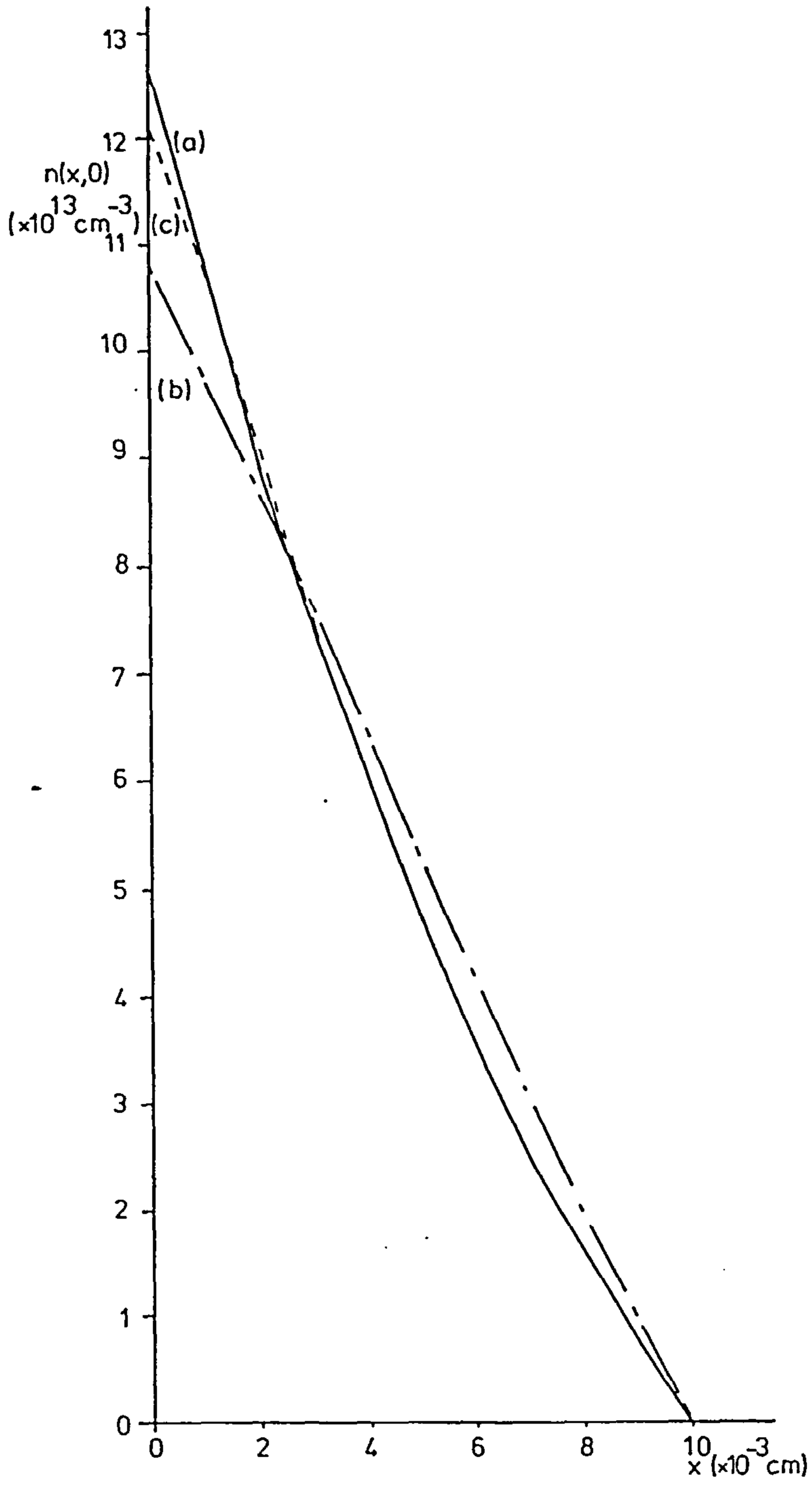

Figure 7.1 Convergence of the infinite series (7.39) at time t=0, to the steady-state excess carrier concentration (5.62) using Table 5.2 data for Si but with infinite s. Curve(a) shows n(x,0), (b) shows the first term only and (c) shows three terms in the series.

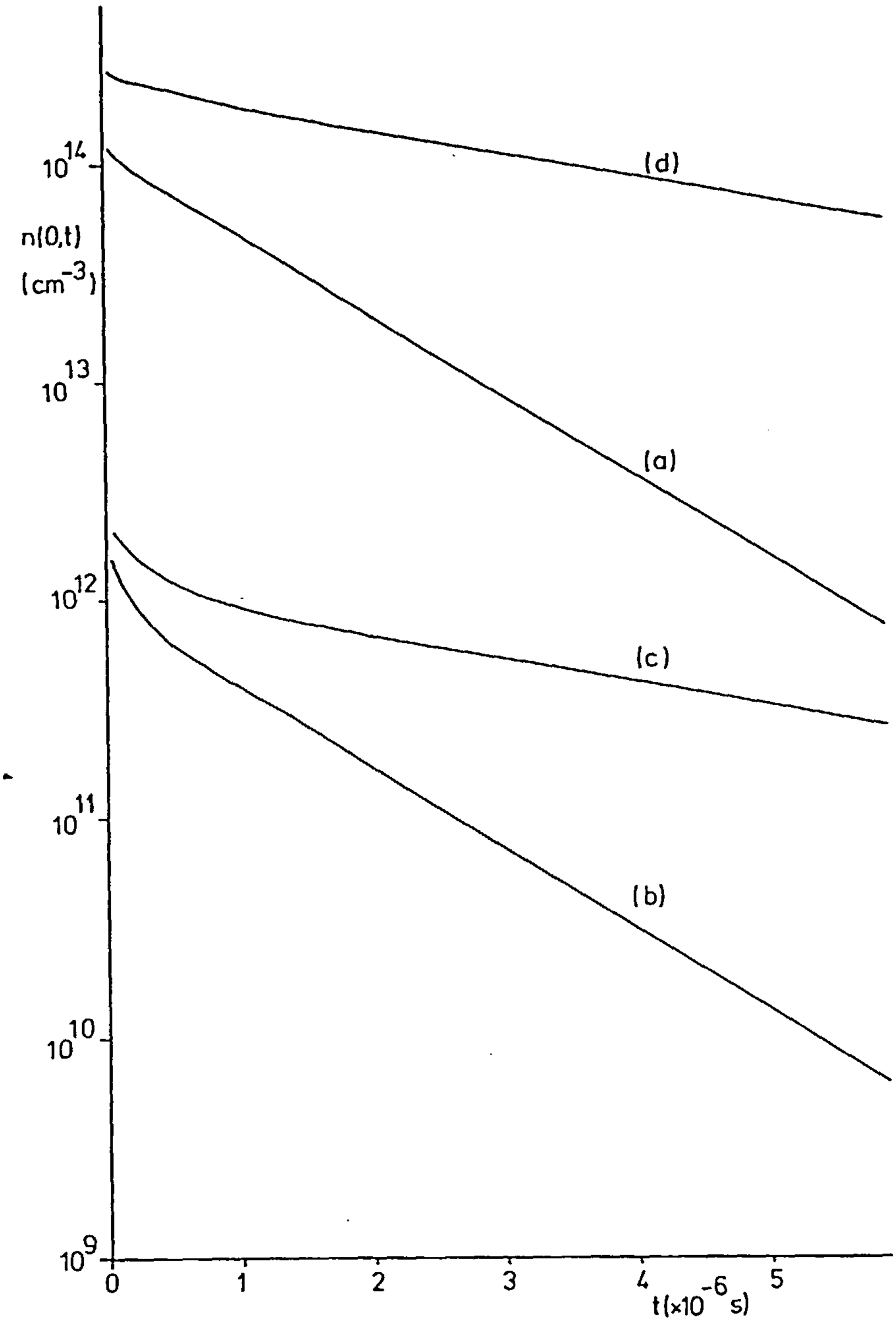

Figure 7.2 Decay of the excess carrier concentration at x=0 using the data of Table 5.2. In the curve (a), equation (7.39) with infinite s is used; in curve (b), equation (7.41) with s=∞ is used and in curve (c) equation (7.41) with s=0 is used. In curve (d), equation (7.39) with s=0 is used.

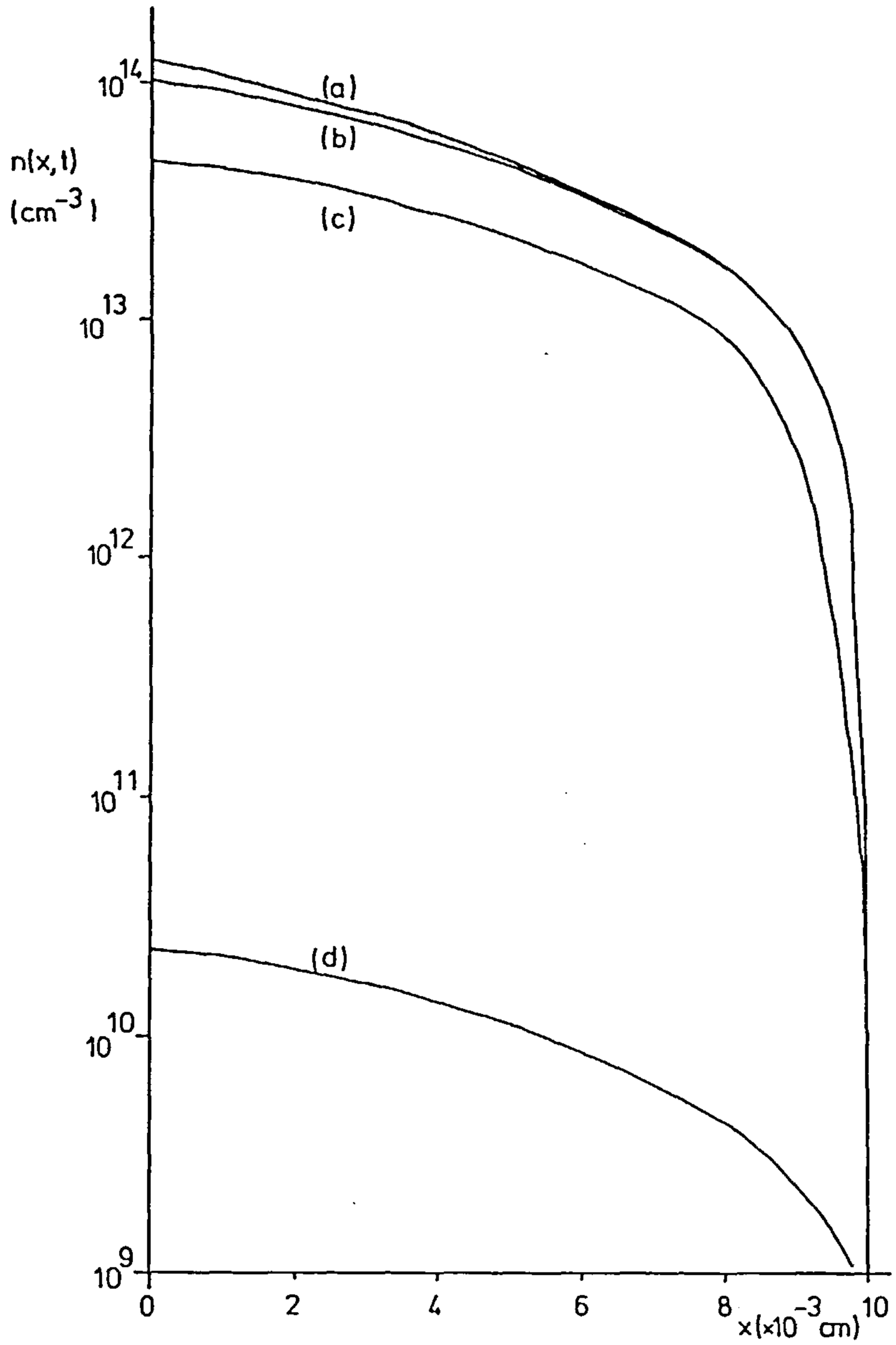

Figure 7.3 Decay of the excess carrier concentration profile using equation (7.39) and Table 5.2 data with s=∞; (a) at t=0, (b) at t=10^{-7} secs, (c) at t=10^{-6} secs and (d) at t=10^{-5} secs.

CHAPTER 8

THE STEADY-STATE MINORITY CARRIER DIFFUSION EQUATION OF A POLYCRYSTALLINE SOLAR CELL

8.1 Introduction

Recent theoretical interest (Bohm et al, 1982 and Bohm et al, 1984) in the minority carrier diffusion equation has centred on its use within the bulk region of a single grain of a polycrystalline solar cell. Historically, Shockley (1950) was the first author to describe a similar problem; a thin filament of semiconductor whose carrier density varied in three dimensions was treated without the effects of illumination. Later work has sought solutions where illumination affects the carrier concentrations and the problem has been simplified to two dimensions. This simplification was achieved by regarding the grain as an infinite region between two parallel recombination planes (Bohm et al, 1982 and Bohm et al, 1984) or as the interior of a circular cylinder surrounded by a curved recombination surface (Fossum and Sundaresan, 1982). In the circular cylinder study, an approximate numerical solution was performed.

An alternative way (Card and Yang, 1977; Ghosh et al, 1980) of looking at the problem is based on a transformation of grain boundary traps into a uniform distribution of states throughout the bulk of the grain. The polycrystalline semiconductor region is treated as though it was monocrystalline but with an effective lifetime due to the surface recombination.

Here, it is assumed that the solar cell or diode is made out of columnar grains which run from the front of the device to the back contact with an n-p junction part way along the columnar grain as in Figure 8.1. A circular cylinderical region is used to model the grain and the diffusion equation for the minority carriers in the steady-state is solved. The grain boundary occupies the curved surface ($r=\ell$) of the

cylinder, the junction is at the top of the cylinderical region (z=0) and the back contact is at the bottom (z=d) of the cylinder. The Sturm-Liouville transform (Sneddon, 1972 and Appendix A) is used to reduce the two dimensional problem in a cylinder into the one dimensional diffusion equation familiar in solar cell analysis. Two new parameters influence the minority carrier concentration:

(i) the recombination velocity, s_{gb}, at the surface of the cylinder, r=ℓ, representing the grain boundary and

(ii) the size of the grain, ℓ, which is equal to the radius of the cylinder.

The grain size, ℓ, also influences (Ghosh et al, 1980) the diffusion length, L, in polycrystalline material.

The assumptions (Sharma and Tewary, 1982) made for single crystal devices will again be used here to apply the minority carrier diffusion equation. These assumptions are (i) that p-n coupling may be neglected and (ii) that the space-charge region has negligible effect on the regions which lead to the lifetime. Three further assumptions will be necessary in the polycrystalline material, (iii) no current flows across the grain boundary surface, (iv) the recombination rate, U_{gb}, at the grain boundary can be displayed as

$$U_{gb} = s_{gb} n \tag{8.1}$$

where s_{gb} is the constant surface recombination velocity. Also, (v) an assumption is made that the grain size, ℓ, is larger than one diffusion length, L.

8.2 Solution of the diffusion equation in cylinderical polar coordinates with a Sturm-liouville transform.

The most general form of the diffusion equation was given by equation (5.15) in chapter 5. This will be solved here with some simplifications: (i) steady-state will be assumed, i.e.

$$\frac{\partial n}{\partial t} = 0, \tag{8.2}$$

where n is the number of excess carriers per unit volume; (ii) the excess carriers, in this case electrons in the p-type base, are distributed axisymmetrically in the cylinder, i.e.

$$n = n(r,z) \tag{8.3}$$

and (iii) the electric field, $\underline{E}$, acts only in the direction of the z-axis. Hence, the diffusion equation to be examined is

$$D\left\{ \frac{\partial^2 n}{\partial z^2} + \frac{\partial^2 n}{\partial r^2} + \frac{1}{r}\frac{\partial n}{\partial r} \right\} + 2fD\frac{\partial n}{\partial z} + g(z) - \frac{n}{\tau} = 0, \tag{8.4}$$

where

$$f \equiv e|\underline{E}|/k_B T \ . \tag{8.5}$$

The appropriate generalised boundary conditions are similar to case 6 of Table 5.1 of chapter 5,

$$a_1 n(r,0) + a_2 \frac{\partial n(r,z)}{\partial z}\bigg|_{z=0} = a_3(r) \tag{8.6}$$

at the junction plane z=0,

$$b_1 n(r,d) + b_2 \frac{\partial n(r,z)}{\partial z}\bigg|_{z=d} = b_3(r) \tag{8.7}$$

at the back surface of the solar cell z=d, together with

$$c_1 n(\ell,z) + c_2 \frac{\partial n(r,z)}{\partial r}\bigg|_{r=\ell} = 0 \tag{8.8}$$

at the grain boundary surface $r=\ell$. In order to solve the diffusion equation (8.4) with the boundary conditions given by (8.6) to (8.8), the Sturm-Liouville transform will be used. As before, solutions to an eigenvalue problem are sought with which one produces a basis of orthonormal eigenfunctions. In this case, the eigenvalue problem is

$$\frac{\partial^2 \phi}{\partial r^2} + \frac{\partial \phi}{\partial r} - \frac{\phi}{L^2} = \xi\phi. \tag{8.9}$$

Equation (8.9) is Bessel's equation of order zero, this has the general solution (Watson, 1944)

$$\phi = AJ_0(\lambda r) + BY_0(\lambda r),$$

where λ is given by

$$\lambda^2 \equiv -1/L^2 - \xi^2 \tag{8.10}$$

and L is the diffusion length ($\sqrt{D\tau}$). Since $Y_0(\lambda r)$ tends to minus infinity as r tends to zero, one sets B=0 because ϕ is expected to be continuous at r=0. The boundary condition at $r=\ell$ (8.8) is used to determine the constants λ,

$$c_1 J_0(\lambda\ell) + c_2 J_0'(\lambda\ell) = 0.$$

From Watson (1944) or Sneddon (1972, p.513, (A25)) one has the following formula relating the derivative of the Bessel function of order zero to a Bessel function of order one,

$$\frac{dJ_0}{dr} = -\lambda J_1(\lambda r) \tag{8.11}$$

and hence,

$$c_1 J_0(\lambda \ell) - c_2 \lambda J_1(\lambda \ell) = 0, \tag{8.12}$$

Equation (8.12) is a transcendental equation with infinitely many roots $\lambda=\lambda_m$(m= 1, 2, 3, ...). These roots yield the eigenfunctions

$$\phi_m = A_m J_0(\lambda_m r) \tag{8.13}$$

to (8.9). The inner product of two functions is defined by

$$(\phi_m . \phi_n) \equiv \int_0^{\ell} \phi_m \phi_n r dr = \delta_{mn} \tag{8.14}$$

where r is the weight function in this case (like e^{2fx}/D in chapter 7). This allows one to find the constants A_m which normalise the eigenfunctions of (8.13),

$$\int_0^{\ell} A_m^2 \{J_0(\lambda_m r)\}^2 r dr = 1$$

Integrating by parts and using (8.12),

$$\tfrac{1}{2} A_m^2 \ell^2 |J_0(\lambda_m \ell)|^2 + \int_0^{\ell} A_m^2 r^2 J_0(\lambda_m r) \lambda_m J_1(\lambda_m r) dr = 1.$$

Also from Sneddon (1972, p.513, (A24)),

$$\frac{\partial}{\partial r}\left\{ r J_1(\lambda r) \right\} = \lambda r J_0(\lambda r) \tag{8.15}$$

thus,

$$\tfrac{1}{2}A_m^2\ell^2 J_0(\lambda_m\ell)^2 + \tfrac{1}{2}A_m^2\ell^2 J_1(\lambda_m\ell)^2 = 1,$$

and finally

$$A_m = (\sqrt{2}/\ell)\{J_1^2(\lambda_m\ell) + J_0^2(\lambda_m\ell)\}^{-\frac{1}{2}}. \tag{8.16}$$

The eigenfunctions of (8.9) are therefore,

$$\phi_m(r) = \frac{2J_0(\lambda_m r)}{J_0(\lambda_m\ell)}\left\{1 + \left\{\frac{c_1}{c_2\lambda_m}\right\}^2\right\}^{-\frac{1}{2}} \tag{8.17}$$

where (8.12) has been used. The Sturm-Liouville transform is defined by

$$n(r,z) = \sum_m \bar{n}_m(z)\phi_m(r), \quad \bar{n}_m(z) = \mathcal{J}[n;m] \equiv \int_0^\ell n\phi_m r\,dr. \tag{8.18,8.19}$$

Using equation (8-4-23) of Sneddon (1972, p.450), which is

$$\mathcal{J}\left[\frac{\partial^2 n}{\partial r^2} + \frac{1}{r}\frac{\partial n}{\partial r}\ ;\ m\right] = -\lambda_m^2\bar{n}_m(z),$$

equation (8.4) is transformed and becomes

$$\frac{d^2\bar{n}_m(z)}{dz^2} + 2f\frac{d\bar{n}_m(z)}{dz} + \xi_m\bar{n}_m(z) + \frac{g_m(z)}{D} = 0 \tag{8.20}$$

Also, it is necessary to transform the boundary conditions given in equations (8.6) and (8.7), and these are

$$a_1\bar{n}_m(0) + a_2\left.\frac{d\bar{n}_m(z)}{dz}\right|_{z=0} = \bar{a}_{3m}\ , \tag{8.21}$$

$$b_1\bar{n}_m(d) + b_2\left.\frac{d\bar{n}_m(z)}{dz}\right|_{z=d} = \bar{b}_{3m} \tag{8.22}$$

The transform, $\overline{g_m}(z)$, of the generation function, $g(z)$, will be given

here for the regular exponential decay of photons as in equation (5.22). The transform of g(z) by equation (8.19) is

$$\bar{g}_m(z) = \alpha N_2 e^{-\alpha z} \tag{8.23}$$

where

$$N_2 = N_0\sqrt{2}/\{\lambda_m[(c_2\lambda_m/c_1)^2+1]^{\frac{1}{2}}\}. \tag{8.24}$$

The diffusion equation given in (8.20) is almost the same as the one dimensional steady-state diffusion equation (5.21) solved in chapter 5. The solution (5.42) was obtained with the usual generation function (5.22) and thus one needs only to make the replacements

$$N_0 \to N_2, \quad (-1/D\tau) \to \xi_m, \quad \mu \to \mu_m$$

in equation (5.21) and the solution to (8.20) is then given by

$$\bar{n}_m(z) + N_3 e^{-\alpha z} = \tag{8.25}$$

$$\left[\{\bar{a}_{3m}+N_3(a_2\alpha-a_1)\}[(b_1-b_2f)\sinh\mu_m z+b_2\mu_m\cosh\mu_m z]\right.$$

$$\left.+\{b_{3m}+N_3(b_2\alpha-b_1)e^{-\alpha d}\}e^{fd}[(a_1-a_2f)\sinh\mu_m z-a_2\mu_m\cosh\mu_m z]\right]$$

$$\div\left[e^{fz}\{(a_1b_1-[a_1b_2+a_2b_1]f+a_2b_2\xi_m)\sinh\mu_m d+(a_1b_2-a_2b_1)\mu_m\cosh\mu_m d\}\right]$$

where

$$N_3 = \alpha N_2/[D\{\alpha(\alpha-2f)+\xi_m\}]$$

and

$$\mu_m = \left\{f^2+1/L^2+\lambda_m^2\right\}^{\frac{1}{2}} \tag{8.26}$$

The complete solution to the two dimensional equation (8.4) requires the inverse transform (8.18), together with (8.13) for the eigenfunctions,

$$n(r,z) = \sum_{m=1}^{\infty} \bar{n}_m(z)A_m J_0(\lambda_m r),$$

hence,

$$n(r,z) = \sum_{m=1}^{\infty} \left[\frac{\sqrt{2}J_0(\lambda_m r)e^{-fz}}{aJ_0(\lambda_m \ell)\{1+(c_1/c_2\lambda_m)^2\}^{\frac{1}{2}}} \left\{ -N_3 e^{(f-\alpha)z} + \right.\right.$$

$$\left.\left. \frac{a_4\{(b_1-b_2f)\sinh\mu_m(d-z)+b_2\mu_m\cosh\mu_m(d-z)+b_4\{(a_1-a_2f)\sinh\mu_m z-a_2\mu_m\cosh\mu_m z\}}{\{a_1b_1-(a_1b_2+a_2b_1)f+a_2b_2\xi_m\}\sinh\mu_m d+(a_1b_2-a_2b_1)\mu_m\cosh\mu_m d} \right] \right. \quad (8.27)$$

where $a_4=\bar{a}_{3m} + N_3(a_2\alpha-a_1)$, $b_4=e^{fd}\{\bar{b}_{3m} + N_3e^{-\alpha d}(b_2\alpha-b_1)\}$.

This is the excess minority carrier density in a single grain of polycrystalline semiconductor due to the effect of illumination or current injection.

8.3 The current-voltage relationship.

The current along the axis of the cylinder at the juction plane (z=0) is calculated using the boundary conditions of case 1 of Table 5.1. That is,

$$n(r,0) = n_0\{\exp(eV/k_BT)-1\} \quad (8.28)$$

at z=0 where V is the applied voltage, k_B is Boltzmann's constant, T is the temperature, e is the modulus of the electronic charge and n_0 is the equilibrium electron concentration. At the back contact, z=d, one has

$$(2fD+s)n(r,d) + D\frac{\partial n}{\partial z}\Big|_{z=d} = 0, \quad (8.29)$$

and also on the curved surface ($r=\ell$) of the cylinder

$$\tfrac{1}{2}s_{gb}n(\ell,z) + D\frac{\partial n}{\partial r}\Big|_{r=\ell} = 0. \quad (8.30)$$

The factor of one half arises because carriers are supplied to the surface from grains on either side. The parameters of the general linear boundary conditions become

$a_1=1$, $a_2=0$, $a_3=n_0(e^{eV/k_BT}-1)$, $b_1=s+2fD$, $b_2=D$, $b_3=0$, $c_1=\frac{1}{2}s_{gb}$, $c_2=D$.

Note that in Appendix B it was shown that $a_2=0$ was not permitted except when $a_3=0$ if the linear boundary conditions (B.1) and (B.2) are used to determine the eigenfunctions of the Sturm-Liouville transform. Here the boundary condition (8.30) is the only boundary condition necessary to calculate the eigenvalues and eigenfunctions because the Sturm-Liouville equation (8.9) is a function of the radial coordinate, r. One can use equations (8.28) and (8.29) here because these equations are subsidiary boundary conditions which apply to the transformed diffusion equation (8.19).

The transformed parameters $\bar{a}_{3m}$ and $\bar{b}_{3m}$ are given by

$$\bar{a}_{3m}=\int_0^{\ell} n_0\left(e^{eV/k_BT}-1\right)A_mJ_0(\lambda_m r)rdr = \lambda_m^{-1}n_0\ell A_mJ_1(\lambda_m\ell)\left(e^{eV/k_BT}-1\right) \qquad (8.31)$$

where equation (8.14) has been used and of course since $b_3=0$,

$$\bar{b}_{3m} = 0.$$

Utilising equations (8.12) and (8.16),

$$\bar{a}_{3m} = \frac{n_0s_{gb}\{\exp(eV/k_BT)-1\}}{\sqrt{2}D\lambda_m^2\{1+(s_{gb}/\sqrt{2}D\lambda_m)^2\}^{\frac{1}{2}}}.$$

Hence, from equation (8.27) the minority carrier concentration is

$$n(r,z) = \sum_{m=1}^{\infty}\left\{\frac{s_{gb}J_0(\lambda_m r)e^{-fz}}{\ell DJ_0(\lambda_m\ell)\{\lambda_m^2+s_{gb}^2/4D^2\}}\right\}\left\{-N_1^*e^{(f-\alpha)z} + \frac{a_4^*[(f+s/D)\sinh\mu_m(d-z)+\mu_m\cosh\mu_m(d-z)]-(\alpha-2f-s/D)N_1^*e^{(f-\alpha)d}\sinh\mu_m z}{(f+s/D)\sinh\mu_m d + \mu_m\cosh\mu_m d}\right\}, \qquad (8.32)$$

where

$$a_4^* = N_1^* + n_0\left(e^{eV/k_BT} - 1\right), \qquad N_1^* = \alpha N_0/D\{\alpha(\alpha-2f)+\xi_m\}. \tag{8.33}$$

The current density of the minority electrons passing across the junction plane, where the current direction is towards negative z, is given by

$$J(r,0) = eD\frac{\partial n(r,0)}{\partial z} + e2fDn(r,0). \tag{8.34}$$

Thus, the electron current density using equation (8.32) is

$$J(r,0) = \sum_{m=1}^{\infty} \frac{es_{gb}J_0(\lambda_m r)}{\ell J_0(\lambda_m \ell)\{\lambda_m^2 + s_{gb}^2/4D^2\}} \left\{ fa_4^* + \alpha N_1^* - 2fN_1^* - \right.$$

$$\left. \frac{a_4^*\{(f+s/D)\cosh\mu_m d + \mu_m \sinh\mu_m d\} + N_1^*(\alpha-2f-s/D)\exp\{(f-\alpha)d\}}{\mu_m^{-1}(f+s/D)\sinh\mu_m d + \cosh\mu_m d} \right\}. \tag{8.35}$$

The total current across the junction plane is obtained by integrating the current density over the area of the junction. One can then obtain an averaged current density, $\bar{J}$, by dividing by the area of the junction, $\pi\ell^2$, i.e.

$$\bar{J} = 2/\ell^2 \int_0^{\ell} J(r,0) r dr \tag{8.36}$$

Using equations (8.15) and (8.12) to intgrate (8.35), one has

$$\bar{J} = \sum_{m=1} \frac{eN_1^* s_{gb}^2}{\ell^2 D\lambda_m^2\{\lambda_m^2 + s_{gb}^2/4D^2\}} \left\{ f\left[n_0\{\exp(eV/k_BT)-1\} - N_1^*\right] + \alpha N_1^* - \right.$$

$$\left. \frac{\left[n_0\{\exp(eV/k_BT)-1\} + N_1^*\right]\left[(f+s/D)\cosh\mu_m d + \mu_m \sinh\mu_m d\right] + N_1^*(\alpha-2f-s/D)\exp\{(f-\alpha)d\}}{\mu_m^{-1}(f+s/D)\sinh\mu_m d + \cosh\mu_m d} \right.$$

The usual form of the current-voltage relationship is obtained here by

writing for the polycrystalline solar cell,

$$|\overline{J}| = \overline{J}_0\{\exp(eV/k_BT)-1\} - \overline{J}_L \tag{8.37}$$

where the dark current is

$$\overline{J}_0 = \sum_{m=1}^{\infty} \frac{en_0s_{gb}^2}{\ell^2 D\lambda_m^2\{\lambda_m^2+s_{gb}^2/4D^2\}}\left\{\frac{(f+s/D)\cosh\mu_m d+\mu_m\sinh\mu_m d}{\mu_m^{-1}(f+s/D)\sinh\mu_m d+\cosh\mu_m d} -f\right\} \tag{8.38}$$

and the light current is

$$\overline{J}_L = \sum_{m=1}^{\infty} \frac{eN_1^*s_{gb}^2}{\ell^2 D\lambda_m^2\{\lambda_m^2+s_{gb}^2/4D^2\}}\left\{\alpha-f-\frac{(f+s/D)\cosh\mu_m d+\mu_m\sinh\mu_m d+(\alpha-2f-s/D)e^{(f-\alpha)d}}{\mu_m^{-1}(f+s/D)\sinh\mu_m d+\cosh\mu_m d}\right\}. \tag{8.39}$$

The form of the single crystal solar cell current-voltage relationship is contained within the square bracketed terms of equations (8.38) and (8.39), but with the diffusion length L replaced by μ_m^{-1}. The effect of the grain boundary recombination velocity, s_{gb}, and the grain size, ℓ, is introduced by the parameters λ_m, μ_m and N_1^* in the prefactors of equations (8.38) and (8.39). The parameter μ_m is an inverse diffusion length given by equation (8.26).

The electron concentration n(r,z) can be averaged in the same way over the radius, r, from equations (8.32) and (8.36),

$$\overline{n(r,z)} = \sum_{m=1}^{\infty}\int_0^{\ell} \frac{2J_0(\lambda_m r)r dr s_{gb}e^{-fz}}{\ell^3 J_0(\lambda_m\ell)D\{\lambda_m^2+s_{gb}^2/4D^2\}}\left\{ - N_1^*\exp\{(f-\alpha)z\} + \frac{a_4^*\{(f+s/D)\sinh\mu_m(d-z)+\mu_m\cosh\mu_m(d-z)\}+(\alpha-2f-s/D)N_1^*e^{(f-\alpha)d}\sinh\mu_m z}{(f+s/D)\sinh\mu_m d + \mu_m\cosh\mu_m d}\right\}.$$

Using equations (8.12) and (8.15), the averaged minority carrier density is

$$n(r,z) = \sum_{m=1}^{\infty} \frac{e^{-fz}}{\ell^2\lambda_m^2\{\lambda_m^2 D^2/s_{gb}^2 + \frac{1}{4}\}} \Bigg[- N_1^* e^{(f-\alpha)z} + \frac{a_4^*\{(f+s/D)\sinh\mu_m(d-z)+\mu_m\cosh\mu_m(d-z)\}+(\alpha-2f-s/D)N_1^* e^{(f-\alpha)d}\sinh\mu_m z}{(f+s/D)\sinh\mu_m d + \mu_m\cosh\mu_m d} \Bigg] . \quad (8.40)$$

Again, the form of the single crystal result (equation (5.42)) is contained in the square bracketed term, but with μ_m^{-1} replacing the the diffusion length. The effect of surface recombination velocity, s_{gb}, and grain size, ℓ, is contained in the prefactor of equation (8.40).

Considerable simplification of these results (8.37) to (8.40) is achieved by assuming that the back contact of the solar cell is Ohmic, i.e. the back surface recombination velocity, s, tends to infinity and also assuming the electric field, $\underline{E}$, is zero, then f is zero. Hence, the averaged dark current density is

$$\overline{J}_O = \sum_{m=1}^{\infty} (en_O D\mu_m \coth\mu_m d)/\left[\ell^2\lambda_m^2\{\lambda_m^2 D^2/s_{gb}^2 + \tfrac{1}{4}\}\right], \quad (8.41)$$

and the averaged light current density is

$$\overline{J}_L = \sum_{m=1}^{\infty} eN_1^* D\left[\alpha+\mu_m e^{-\alpha d}-\mu_m\coth\mu_m d\right]/\{\ell^2\lambda_m^2(\lambda_m^2 D^2/s_{gb}^2 + \tfrac{1}{4})\} \quad (8.42)$$

where the current-voltage relationship is given by equation (8.37). The radially averaged minority carrier concentration is

$$\overline{n(r,z)} = \sum_{m=1}^{\infty} \frac{\left[n_O\left\{e^{eV/k_B T}-1\right\}+N_1^*\right]\sinh\mu_m(d-z)+N_1^* e^{-\alpha d}\sinh\mu_m z - N_1^* e^{-\alpha z}\sinh\mu_m d}{\ell^2\lambda_m^2\{\lambda_m^2 D^2/s_{gb}^2 + \tfrac{1}{4}\}\sinh\mu_m d} . \quad (8.43)$$

The diffusion coefficient, D, is a function of the grain size in polycrystalline semiconductors (Ghosh et al, 1980). The Einstein relation is

$$D = \upsilon k_B T/e \quad (8.44)$$

and it gives the diffusion coefficient in terms of the bulk mobility, υ_0, and the grain boundary space-charge region, u_{gb}, via the polycrystalline mobility (Orton and Powell, 1980), υ,

$$\upsilon^{-1} = \upsilon_0^{-1} + \upsilon_{gb}^{-1} \quad . \tag{8.45}$$

The space-charge region mobility is given by thermionic emission (Seager and Castner, 1978) in chapter 3 as

$$\upsilon_{gb} = e\ell\exp(-e\phi_{BO}/k_BT)(2\pi m_c k_B T)^{\frac{1}{2}} \tag{8.46}$$

where ϕ_{BO} is the potential barrier height at the grain boundary and m_c is the effective mass of electrons in polycrystalline material. Hence, putting these results together, the diffusion coefficient is given by

$$D = \frac{\upsilon_0 \ell \exp(-e\phi_{BO}/k_BT)(k_BT/2\pi m_c)^{\frac{1}{2}}}{\upsilon_0 + e\ell\exp(-e\phi_{BO}/k_BT)(2\pi m_c k_B T)^{\frac{1}{2}}} \quad . \tag{8.47}$$

Note that the diffusion coefficient tends to the bulk value for large grain sizes or when the barrier height is very small. For small grains or for a large barrier at the grain boundary, the diffusion coefficient is proportional to the grain size.

Using equations (8.37), (8.41), (8.42) and (8.47) some numerical results for polycrystalline silicon are presented in Figures 8.2 to 8.5. In addition to the data of Table 5.2, the following data is used:
τ=1.0μs, D=34cm^{2}s^{-1}, d=500μm, eϕ_{BO}=0.18eV, m_c=0.19m_0,
where m_0 is the free electron rest mass.

8.4 Discussion of the figures.

In Figure 8.2 there is a general decrease in the light generated current, $\bar{J}_L$, with the reducing grain size, ℓ, and with increasing surface recombination velocity. For small recombination velocities (s_{gb}<10ms^{-1}),

the effect is slight because there are few centres available for trapping minority carriers. As the number of surface states is increased, so more minority carriers recombine at the grain boundary. This leaves fewer of them to reach the junction plane in order to contribute to the current. For high surface recombination velocities, the grain boundary acts as an infinite sink for the minority carriers. The recombination rate is then limited by how rapidly the carriers can diffuse from the bulk into the grain boundary. This effect has also been observed for point and line defects in silicon (Wight et al, 1981). Thus, the light generated current tends to fall to a fairly constant minimum value with further increase in the surface recombination velocity.

For smaller grain sizes, $\overline{J}_L$, is smaller because there are more grain boundaries at which minority carriers are trapped, an effect also noted by Ghosh, Fishman and Feng (1980).

The effect of increasing grain boundary recombination velocity on the reverse saturation current, $\overline{J}_0$, is like reducing the lifetime. One finds in effect, that $\overline{J}_0$ increases with larger recombination velocities (Hovel, 1975, p.105). Using equation (8.37), the open-circuit voltage as shown in Figure 8.3 is given by

$$\overline{V}_{oc} = (k_B T/e)\ln(1+\overline{J}_L/\overline{J}_0). \qquad (8.48)$$

Thus in Figure 8.3, the open-circuit voltage tends to decrease with larger surface recombination velocity because of the tendency of $\overline{J}_L$ to fall and for J_0 to rise. Again for high surface recombination velocities, $\overline{V}_{oc}$ reaches a constant minimum because the recombination rate is limited by carrier diffusion to the traps in the grain boundary surface. By the nature of the dependence of $\overline{V}_{oc}$ on $\overline{J}_L$ and $\overline{J}_0$ through equation (8.48), the change in $\overline{V}_{oc}$ is smaller than the change in $\overline{J}_0$ or $\overline{J}_L$.

For smaller grains, the diffusion coefficient is less by equation (8.47). Thus the reverse saturation current of (8.41) becomes smaller in

smaller grains. However the light generated current of (8.42) is less affected by the reducing diffusion coefficient because N_1^* is proportional to 1/D by equation (8.33). Hence for small surface recombination velocities at the grain boundary, the open-circuit voltage increases slightly with reducing grain size. This effect has been noted in experiments by Neugroschel and Mazer (1982), but Fossum and Lindholm (1980b) found that the open-circuit voltage reduced with smaller grains. The results of Fossum and Lindholm (1980b) may be interpreted from Figure 8.3 if a larger surface recombination velocity is assumed at the grain boundary.

The aspects of Figures 8.2 and 8.3 are combined in Figures 8.4 and 8.5. The flat region of the current-voltage characteristic near short-circuit conditions is strongly affected by grain boundary recombination in small grains in Figure 8.4, but for larger grains in Figure 8.5, it is less strongly affected. There is also a wider variation in the open-cicuit voltage in the smaller grain material in Figure 8.4 than in a larger grain in Figure 8.5.

8.5 Conclusions.

The minority carrier diffusion equation has been solved in a cylindrical region representing the bulk region of a columnar grain (see Figure 8.1) in a polycrystalline solar cell. The effects of changes in the grain size and the surface recombination velocity at the grain boundary on the light generated current and the open-circuit voltage were examined.

Larger surface recombination velocities reduced the light generated current and to a lesser extent, reduced the open-circuit voltage. For large surface recombination velocities, increasing the grain size improved both $\overline{J}_L$ and $\overline{V}_{oc}$. The effect of surface recombination on $\overline{J}_L$ was

smaller in large grains because the recombination rate is probably limited by how fast carriers can diffuse towards the grain boundary.

The results obtained here are in agreement with the work of Bohm et al (1984) and their work is extended here by including the shrinkage of the diffusion length (Ghosh et al, 1980) observed in polysilicon to be a function of the grain size. Also, the more realistic model of a cylinderical grain has been adopted here instead of the infinite region sandwiched between two flat recombination planes (Bohm et al, 1982).

It has been shown that in principle one can include the effects of a small constant electric field in the grain and a finite back surface recombination velocity; these effects were considered in chapter 5 for single crystal semiconductors and were not repeated since they were of secondary importance in polycrystalline devices.

For small recombination velocity at the grain boundary, the open-cicuit voltage increased in smaller grains. This result was in agreement with the experimental work of Neugroschel and Mazer (1982). However for large recombination rate at the grain boundary, the open-circuit voltage was smaller in all grain sizes, see section 8.4 or Fossum and Lindholm (1980b).

A slight loss of generality in the model explained here lay in the choice of boundary condition (8.28) at the junction. This boundary condition was adopted from the single crystal study, but an implicit assumption was made that grain boundary recombination in the junction space-charge region had a negligible effect on the quasi-Fermi level separation. Techniques for grain boundary removal by laser recrystallization (Young et al, 1980) and passivation of grain boundaries (Seager et al, 1980) are likely to make this a plausible assumption. If this is not the case, Bohm et al (1982) took an alternative approach by using a simple radial function for the voltage, V. Their reduction of V near the grain boundary accounted for recombination and grain size.

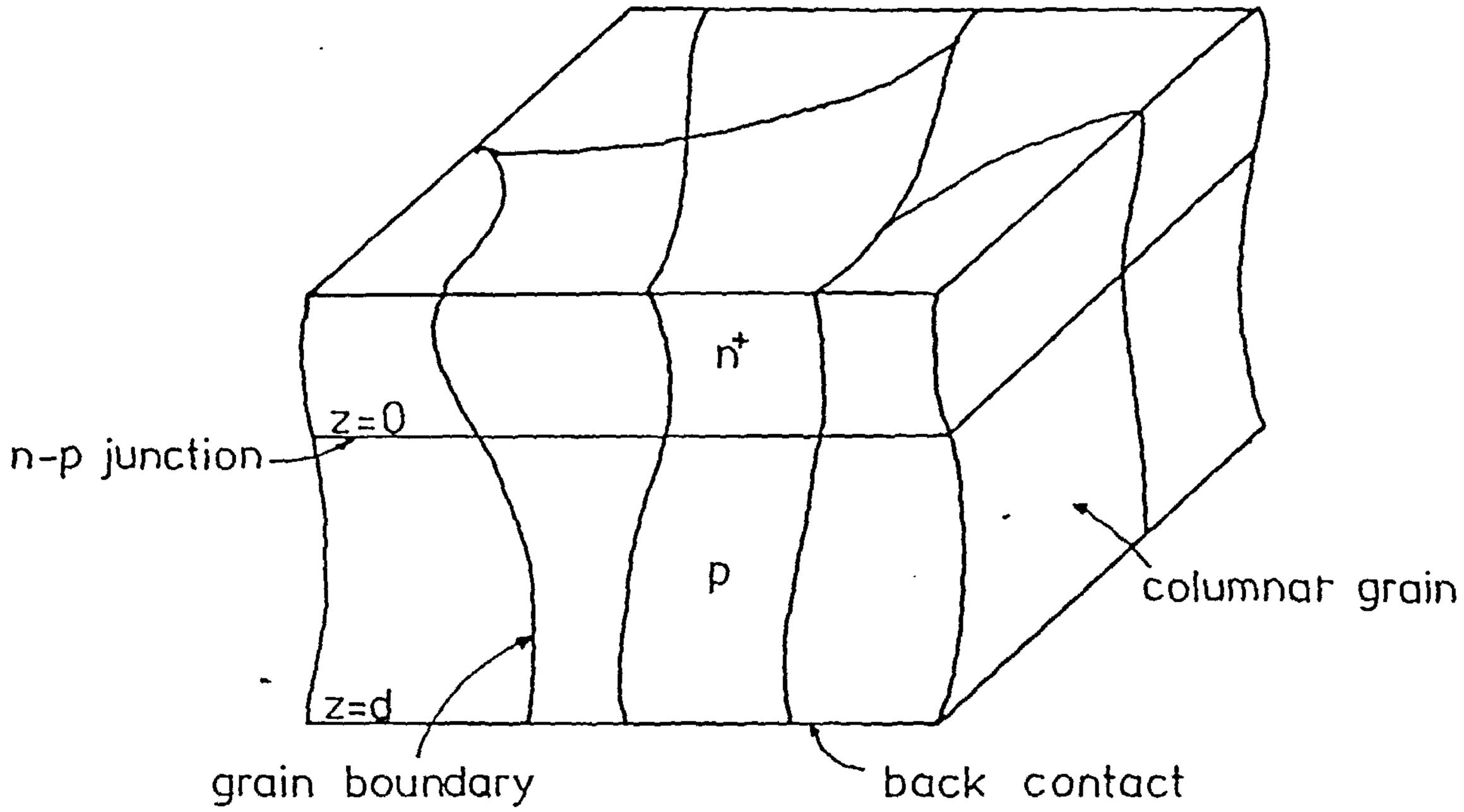

Figure 8.1 A polysilicon n-p junction solar-cell with columnar grains.

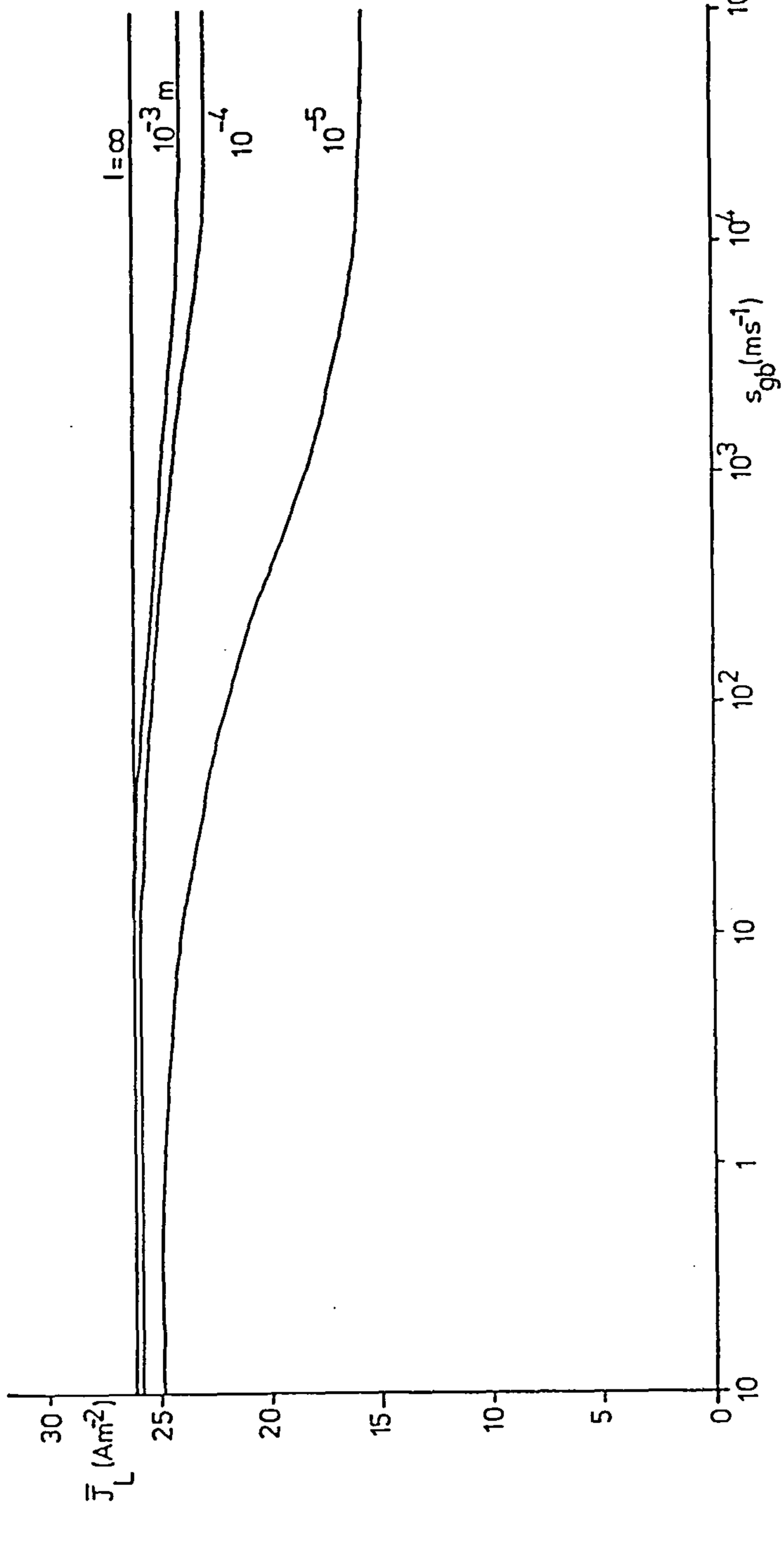

Figure 8.2 The light generated current, $\bar{J}_L$, as a function of grain boundary recombination velocity, s_{gb}, and grain size, ℓ, using equation (8.42), Table 5.2 data and extra data given in the text.

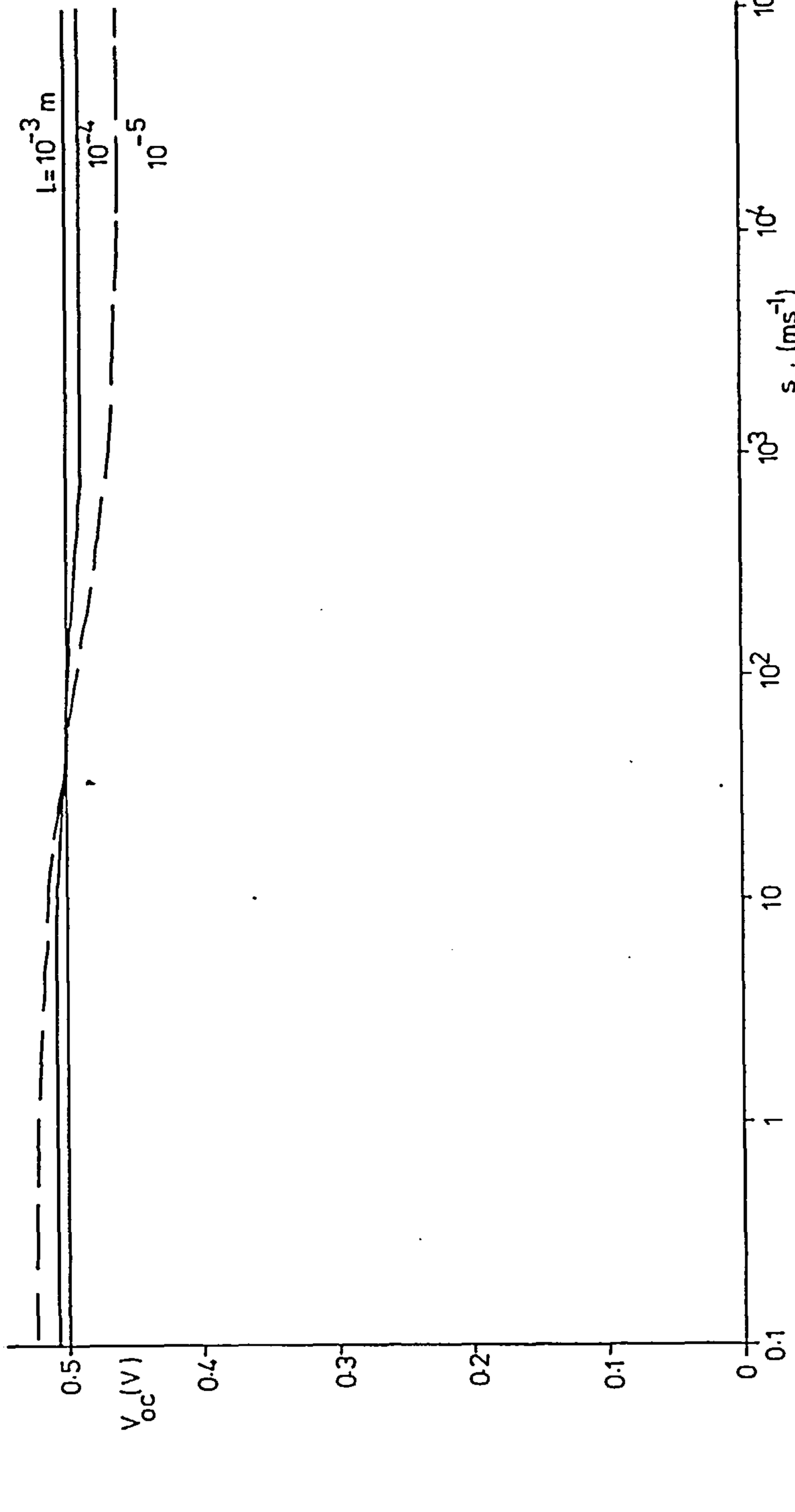

Figure 8.3 The open circuit voltage, V_{oc}, as a function of grain boundary recombination velocity, s_{gb}, and grain size, ℓ, using equation (8.48) , Table 5.2 data and extra data given in the text.

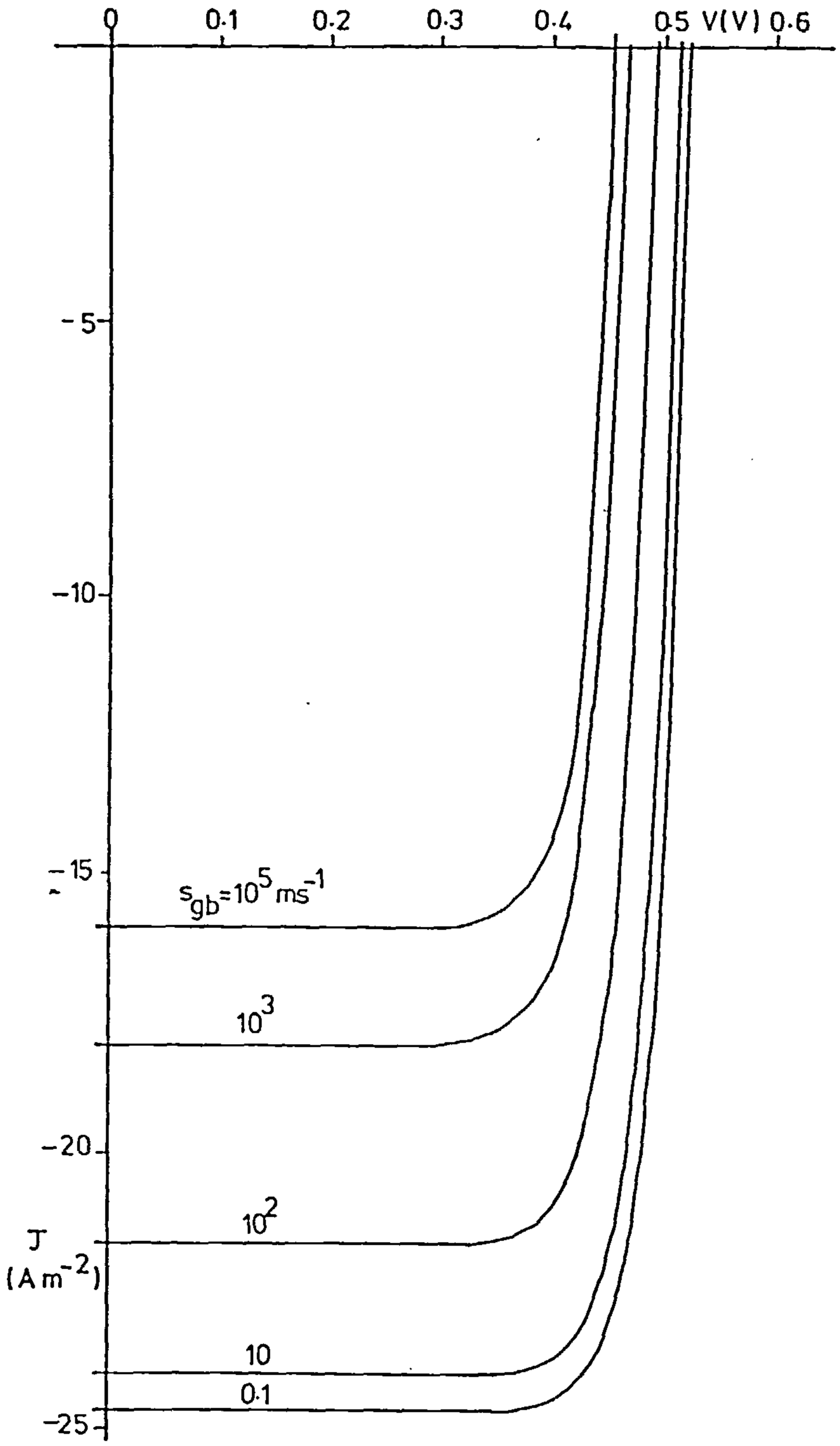

Figure 8.4 The current-voltage characteristic of a polysilicon solar cell with a grain size of 10 μm. Equation(8.37), Table 5.2 data and extra data given in the text are used.

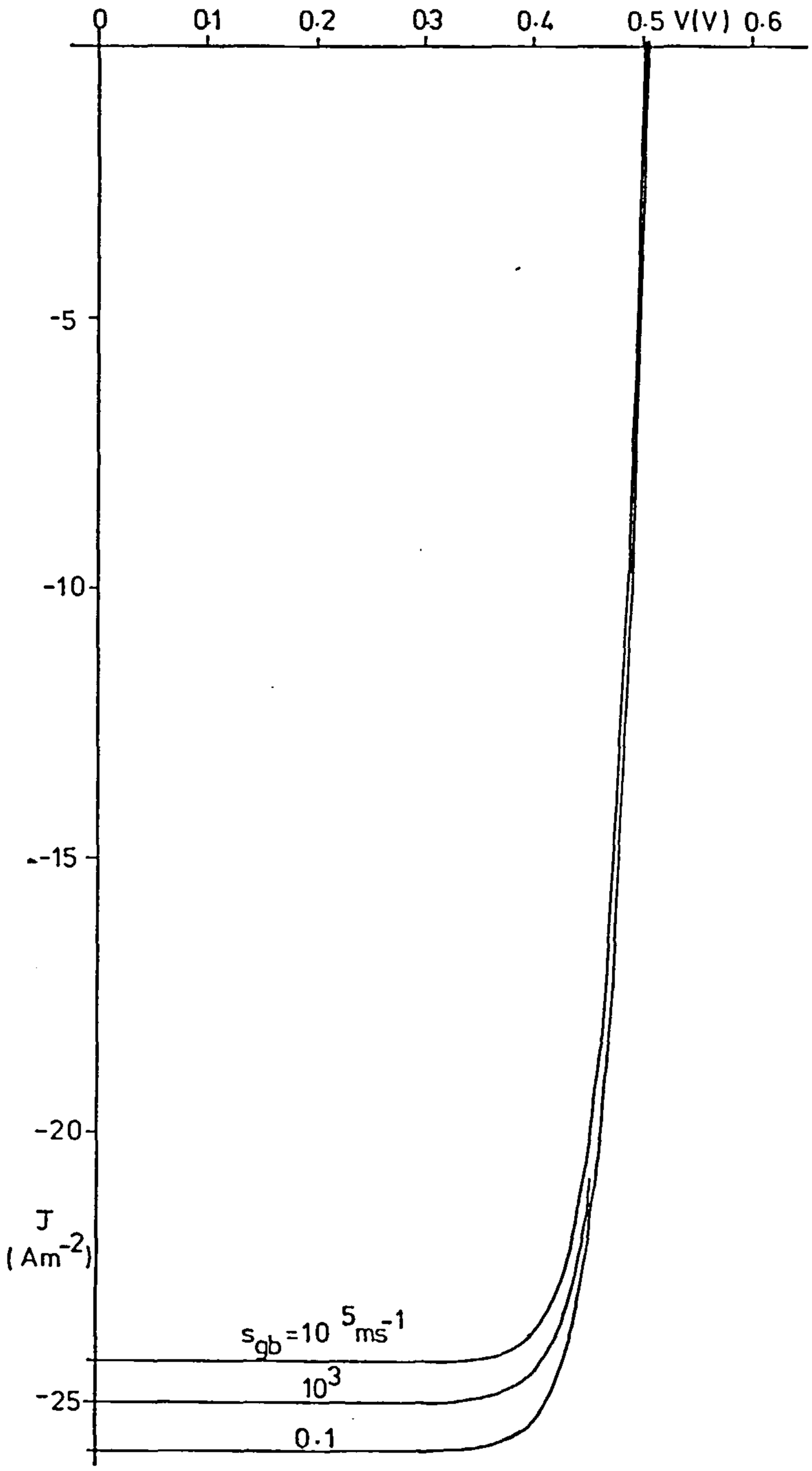

Figure 8.5 The current-voltage characteristic of a polysilicon solar cell with a grain size of $10^3 \mu m$. Equation (8.37), Table 5.2 data and extra data given in the text are used.

CHAPTER 9

SUMMARY OF CONCLUSIONS AND TOPICS FOR FUTURE RESEARCH

The purpose of this chapter is to summarise the main points of the conclusions which were given in detail with the appropriate chapters and to outline a few research topics that might either enhance or follow on from this project.

9.1 Summary of conclusions.

In chapter 2, the Shockley-Read statistics was generalised to include Auger effects, trap relaxation times, extra carriers from the neighbouring material and was applied to two simple surface trap distributions. The recombination velocity at the surface tended to fall to a minimum for near intrinsic material because the traps were largely occupied and there were insufficient electrons left in the conduction band to recombine with every hole that was trapped. When the equilibrium Fermi level lay close to one of the energy bands because of a large doping concentration, the recombination velocity rose by virtue of extra Auger transitions. Away from equilibrium, the recombination velocity increased with the excess carrier concentration because of Auger effects until a maximum was reached. Then the recombination velocity decreased because of trap saturation. A simple trap spectrum increased all of these tendencies when it was used in place of a single level at mid-gap.

The surface recombination statistics developed here was employed in chapter 3 to calculate the potential barrier height at a grain boundary. Poisson's equation was solved for the barrier potential with the assumption of flat, parallel quasi-Fermi levels and this model led to good agreement with experimental results. The Shockley-Read statistics was displayed as a generalisation of the Fermi-Dirac statistics. A single treatment was then possible for both equilibrium and steady-state conditions using only the Shockley-Read statistics. The equilibrium barrier height displayed a maximum with respect to doping in the bulk and

this was found to occur when the Fermi level lay approximately at the same energy as the surface state.

In addition, the recombination rate at a grain boundary, the resistivity and capacitance in equilibrium were investigated in polysilicon.

The radiative recombination rate in quantum well laser diodes was studied in chapter 4. Good agreement of the experimental gain curves and a theory based on complete relaxation of k-selection rules was found. One cannot rule out the possibility of the gain curves being fitted equally well by a model based on partial k-selection, involving intraband relaxation times (Yamada, 1983). Until now, it has been argued that strict k-selection rules should be obeyed even in highly doped structures (Sugimura, 1983), but a possible explanation of our results may be due to the strong carrier-carrier interaction. Since experimental work on single and multi-quantum well structures is very active, in time gain curves may be obtained which no longer resemble the simple no k-selection model and a more detailed theoretical investigation may be needed.

In the model of a quantum well structure described here, the effect of band-gap shrinkage has been included because of the large carrier concentrations present during laser operation. Also, a more detailed calculation than before was made of the energy levels in a multi-quantum well laser to take account of the shifted levels in the asymmetric quantum wells at the end of the structure.

General solutions to the minority carrier diffusion equation in the steady-state and time-dependent cases were derived in chapters 5 to 8 for a simple p-n junction solar cell. These solutions allowed one to calculate the excess carrier densites in low injection and therefore to obtain the current or the voltage for most of the operating conditions of the solar cell. The use of a general photogeneration rate in the steady-state solution enabled a new function (Hsieh et al, 1980) to represent the variation with distance of the solar spectrum inside the solar cell

in chapter 6. An advantage of the new function for the generation rate was that fewer terms were involved in the solution than when the conventional exponential decay (Dunbar and Hauser, 1976) was used. However, this new representation of the solar spectrum was independent of the wavelength of the incident light and was not available for more than the AM1 and AM2 spectra.

The use of transient photovoltage decay from the steady-state to measure lifetimes in solar cells has been examined here in chapter 7. The work of Sharma and Tewary (1982) on open-circuit voltage decay was confirmed and extended to more general current flow conditions. Also, the carrier density decay following a short pulse of light was studied and it was shown that the same lifetime can be inferred from the results as would be obtained from the steady-state decay. Some confusion over the eigenvalues of the Sturm-Liouville problem and their use in the transform in the work of Sharma and Tewary (1982) was clarified here by considering the amplitudes of the concomitant eigenfunctions.

The effect of the electrons in the p-type base of an n-p solar cell on the current was considered here. The contribution to the current by holes in the n-type emitter was neglected purely to simplify the mathematics, but the effect of the hole current could easily be included because the diffusion equations for electrons and holes are very similar. However, the effect of high injection either by a large electrical current passing through the solar cell or by a concentration of the incident light is more complicated and necessitates computer solutions of the carrier transport equations (see for example Fossum, 1976).

In a polycrystalline solar cell grown with columnar grains running from the front to the back of the cell and passing through the junction, the diffusion equation for electrons in the p-type base was solved in the steady-state. A finite Sturm-Liouville transform was employed to transform the two dimensional electron diffusion equation into a one dimensional

equation of the type studied in chapter 5. Then, the current-voltage characteristic was obtained and the effects on it of variation in the grain size and recombination velocity at the grain boundary were examined. It was found that for large grain boundary recombination velocity, the light current and therefore the open-circuit voltage were both reduced. This effect has been noted in experiments with polysilicon solar cells (Fossum and Lindholm, 1980b). For large recombination velocities, smaller grain sizes further reduced the open-circuit voltage. However, for smaller recombination velocities at the grain boundary, reducing the grain size had the unexpected effect of improving the open-circuit voltage. This effect was found in experiments by Neugroschel and Mazer (1982).

9.2 Topics for future research

(i) A comparitive study of the recombination rate using a single trap state and a simple distribution of surface states would yield valuable information concerning the distribution of surface traps when compared with similar experimental results, both for a simple surface and for a grain boundary.

(ii) Experimental curves which correspond to the theoretical curves of Figures 2.5 and 2.7 would give valuable insight into the magnitude of Auger effects, trap saturation because of the finite time of relaxation and to the validity of a constant recombination velocity used in low injection conditions in chapters 5 to 8.

(iii) The study of the potential barrier at a grain boundary showed that it was important to know the concentration of donor and acceptor-like traps in the surface. The sign of the trapped charge determines whether the barrier blocks the flow of the majority or minority carriers. Previous studies of the grain boundary surface state distribution have been made (Shyu and Cheng, 1982; Srivastava et al, 1982), but these

have not yielded the donor or acceptor-like nature of the traps. Such information would be very useful to the application of the theory given here.

(iv) A calculation of over the barrier current at a grain boundary was not attempted here because that requires jettisoning the assumption of flat quasi-Fermi levels away from equilibrium. This calculation is however necessary to understand the behaviour of polysilicon emitter transistors and thin-film resistors.

(v) Results have been gathered (Shyu and Cheng, 1982) of the variation with temperature of grain boundary capacitance in polysilicon. Another check on the theory given here could be made by examining the temperature variation of the capacitance obtained in section 3.9(b).

(vi) The nature of radiative recombination in AlGaAs quantum wells will be made clear as gain curves are made available for doped and undoped active layers and for polarized or unpolarized emissions. Further experiments are necessary before either strict k-selection rule or no k-selection rule models are rejected for quantum well lasers.

(vii) For a complete understanding of the rate of radiative transition in quantum wells, a calculation of the matrix element in a two dimensional structure for TE and TM polarizations is required.

(viii) In chapters 5, 6 and 8, the diffusion equation for electrons in the p-type base of a solar cell was given in the steady-state. For a complete understanding of the operation of the solar cell shown in Figure 5.1, a calculation of the much smaller contribution to the current by holes in the emitter is desirable, especially when the emitter is quite wide or when the doping in the emitter is low.

(ix) A new function representing the AM1 and AM2 spectra was given in chapter 6. This function would be more useful if data for it was available for other spectra, for example for the AM0 spectrum.

(x) This new function (Hsieh et al, 1980) for the photogeneration

rate in a solar cell has no wavelength dependence, but this would be desirable if one wishes to understand fully the way in which the sunlight is absorbed by a solar cell.

REFERENCES

Abramowitz,M., and I.A.Stegun, eds., 1970, "Handbook of Mathematical Functions" (Dover Publications Inc, New York).

Adams, M.J., and P.T.Landsberg, 1969, "The theory of the injection laser", in "Gallium Arsenide Lasers", ed. C.H.Gooch (Wiley, Chichester), Ch.2, pp.5-79.

Agarwal,S.K., S.C.Jain and S.Harsh, 1982, "Variation of minority carrier lifetime with level of injection in p-n junction devices", Electron. Lett., 18, pp.298-299.

Ando,T.,A.B.Fowler and F.Stern, 1982, "Electronic properties of two-dimensional systems", Reviews of Modern Physics, 54, pp.437-672.

Baccarani,G., M.Impronta, B.Riccò and P.Ferla, 1978a, "The I-V characteristics of polycrystalline silicon resistors", Rev. de Phys. Appl., 13, pp.777-782.

Baccarani,G., B.Riccò and G.Spadini, 1978b, "Transport properties of polycrystalline silicon films", J. Appl. Phys., 49, pp.5565-5570.

Barrett,C., and A. Vappaille, 1976, "Interfacial states spectrum of a metal-silicon junction", Solid-State Electron., 19, pp.73-75.

Blakemore,J.S., 1962, "Semiconductor Statistics", Vol III of International series of monographs on semiconductors (Pergamon Press, London).

Blakemore,J.S., 1982, "Semiconducting and other properties of Gallium Arsenide", J. Appl. Phys., 53, pp.R123-R181.

Bohm,M., R.Kern and H.G.Wagemann, 1982, "The influence of grain boundary recombination and grain size on the I-V characteristic of polycrystalline silicon solar cells", in proc. of 4th. E.C. photovoltaic solar energy conf., 10-12th. May 1982, Stresa, Italy (Reidel, Dordrecht, Netherlands) pp.516-521.

Bohm,M., H.C.Scheer and H.G.Wagemann, 1984, "A two-dimensional model for polysilicon solar cells", submitted to Solar Cells.

Brown,D.M., and P.V.Gray, 1968, "Si-SiO_2 fast interface state measurements", J. Electrochem. Soc., 115, pp.760-766.

Burt,M.G., 1983, "Gain spectra of quantum well lasers", Electron. Lett., 19, pp.210-211.

Burt,M.G., 1984, private communication.

Card,H.C., and E.S.Yang, 1977, "Electronic processes at grain boundaries in polycrystalline semiconductors under optical optical illumination", IEEE Trans. on Electron Devices, ED-24, pp.397-402.

Card,H.C., J.G.Shaw, G.C.McGonigal, D.J.Thompson, A.W.de Groot and K.C. Cao, 1982, "Carrier transport at grain boundaries in silicon", in proc. of 16th. Photovoltaic specialist's conference,27-30th. September, San Diego, CA (IEEE , New York) pp.633-639.

Casey,H.C.,Jr., and M.B.Panish, 1978, "Heterostructure lasers, part A: Fundamental principles" (Academic Press, New York).

Cheng,L.J., and C.M.Shyu, 1981, "Electrical properties of grain boundaries in silicon bicrystals", in "Semiconductor silicon/1981", eds. H.R.Huff, R.J.Kreigler, Y.Takeishi (The Electrochem. Soc., Pennington, NJ) pp.390-399.

Condit,H.R., and F.Grum, 1964, "Spectral energy distribution of daylig-ht", J. Opt. Soc. Am., 54, pp.937-944.

Courant,R., and D.Hilbert, 1955, "Methods of Mathematical Physics", Vol.1., 2nd. ed'n. (Interscience, New York, NY).

Cummerow,R.L., 1954, "Photovoltaic effect in p-n junctions", Phys. Rev., 95, pp.16-21.

Dhariwal,S.R., L.S.Kothari and S.C.Jain, 1977, "Theory of transient photovoltaic effects used for measurements of lifetimes of carriers in solar cells", Solid-State Electronics, 20, pp.297-304.

Dhariwal,S.R., L.S.Kothari and S.C.Jain, 1981, "On the recombination of electrons and holes at traps with finite relaxation times", Solid-State Electronics, 24, pp.749-752.

Dhariwal,S.R., and N.K.Vasu, 1981, "A generalised approach to lifetime measurement in p-n junction solar cells", Solid-State Electronics, 24, pp.915-927

Dingle,R., 1975, "Confined carrier quantum states in ultrathin semi-conductor heterostructures", in Festkörperprobleme-Advances in solid-

state physics, ed. H-J.Queisser (Pergamon-Vieweg, Braunschweig),Vol.XV, pp.21-48.

Dixon,E.R., 1978, "Spectral composition of Australian daylight", J. Opt. Soc. Am., 68, pp.437-449.

Dunbar,P.M., and J.R.Hauser, 1976, "A study of efficiency in low resistivity solar cells", Solid-State Electronics, 19, pp.269-277.

Dutta, N.K., 1982, "Calculated threshold current of GaAs quantum well lasers", J. Appl. Phys., 53, pp.7211-7214.

Dutta, N,K., R.L.Hartman and W.T.Tsang, 1983, "Gain and carrier life-time measurements in AlGaAs single quantum well lasers", IEEE. J. Quant. Electron., QE-19, pp.1243-1246.

Ellis, B., and T.S.Moss, 1970, "Calculated efficiencies of practical GaAs and Si solar cells including the effect of built-in electric fields", Solid-State Electronics, 13, pp.1-24.

Evans, D.A., and P.T.Landsberg, 1963, "Recombination statistics for Auger effects with applications to p-n junctions", Solid-State Electron., 6, pp.169-181.

Fossum, J.G., 1976, "Computer aided numerical analysis of silicon solar cells", Solid-State Electronics, 19, pp.269-277.

Fossum, J.G., and F.A.Lindholm, 1980a, "Theory of grain boundary and intragrain recombination currents in polysilicon p-n junction solar cells", IEEE Trans. on Electron Devices, ED-27, pp.692-700.

Fossum, J.G., and F.A.Lindholm, 1980b, "Effects on the open-circuit voltage of grain boundaries within the junction space-charge region of polycrystalline solar cells", IEEE Electron Device Letters, EDL-1, pp.267-269.

Fossum, J.G., and R.Sundaresan, 1982, "Analysis of minority-carrier transport in polysilicon devices", IEEE Trans. on Electron Devices, ED-29, pp.1185-1197.

Garrett, C.G.B., and W.H.Brittain, 1955, "Physical theory of semi-conductor surfaces", Phys. Rev., 99, pp.376-387.

Ghosh, A.K., C.Fishman, and T.Feng, 1980, "Theory of the electrical and photovoltaic properties of polycrystalline silicon", J. Appl. Phys., 51, pp.446-454.

Goldstein, L., Y.Horikoshi, S.Tarucha and H.Okamoto, 1983, "Effect of well size fluctuation on photoluminescence spectrum of AlAs-GaAs super-lattices", Jap. J. Appl. Phys., 22, pp.1489-1492.

de Graaff, H.C., M.Huybers, and J.G. de Groot, 1982, "Grain boundary states and the characteristics of lateral polysilicon diodes", Solid-State Electronics, 25, pp.67-71.

Gradshteyn, I.S., and I.M.Ryzhik, 1980, "Tables of integrals, series and products", 4th. ed'n., Ed. Alan Jeffrey (Academic Press, New York).

Hakki, B.W., and T.L.Paoli, 1975, "Gain Spectra in GaAs double hetero-structure injection lasers", J. Appl. Phys., 46, pp.1299-1306.

Hall, R.N., G.E.Fenner, J.D.Kingsley, T.J.Soltys and R.O.Carlson, 1962, Coherent light emission from GaAs junctions", Phys. Rev. Lett., 9, pp.366-368.

Haug, A., 1981, "Auger recombination with deep impurities in indirect band-gap semiconductors", Physica Status-Solidi, (b)108, pp.443-448.

Henderson, S.T., and D.Hodgkiss, 1964, "The spectral energy distribution of daylight", Br. J. Appl. Phys., 15, pp.947-952.

Herman, F., and R.V.Kazowski, 1981, "Electronic structure of defects at Si/SiO_2 interfaces", J. Vac. Sci. Tech., 19, pp.395-401.

Hess, E., I.Topol, K.-R. Schulze, H.Neumann and K.Unger, 1973, "Band structure and pseudopotential form factors for AlAs", Phys. Stat. Sol., (b)55, pp.187-192.

Hess, K., B.A.Vojak, N.Holonyak Jr., R.Chin, and P.D.Dapkus, 1980, "Temperature dependence of threshold current for a quantum-well hetero-structure laser", Solid-State Electronics, 23, pp.585-589.

Holonyak, N., Jr., R.M.Kolbas, R.D.Dupuis, and P.D.Dapkus, 1980, "Quantum well heterostructure lasers", IEEE. J. Quantum Electronics, QE-16, pp.170-186.

Holonyak, N.,Jr., W.D.Laidig, M.D.Camras, K.Hess, M.S.Burroughs, J.J. Coleman, and P.D.Dapkus, 1981, "Size fluctuations and high energy laser operation of $Al_xGa_{1-x}As$-AlAs-GaAs quantum well hetrostructures", J. Appl. Phys., 52, pp.6777-6782.

Hovel, H.J., 1975, "Solar Cells", Vol. 11 of "Semiconductors and Semimetals", Ed's R.K.Willardson and A.C.Beer (Academic Press, New York).

Hsieh, H.C., C.Hu and C.I.Drowley, 1980, "A new method of analyzing the short circuit current of silicon solar cells", IEEE Trans. on Electron Devices, ED-27, pp.883-885.

In kson, J.C., 1976, "The effect of electron interaction on the bandgap of extrinsic semiconductors", J. Phys. C.: Solid-State Physics, 9, pp. 1177-1183.

Iwamura, H., T.Saku, H. Kobayashi and Y.Horikoski, 1983, "Spectrum studies on a GaAs-AlGaAs multi-quantum-well laser diode grown by molecular beam epitaxy", J. Appl. Phys., 54, pp.2692-2695.

Kasemset, D., C.-S.Hong, N.B.Patel and P.D.Dapkus, 1983, "Graded barrier single quantum well lasers - theory and experiment", IEEE J. Quantum Electronics, QE-19, pp.1025-1030.

Kazmerski, L.L., 1980, "Polycrystalline and amorphous thin-films and devices", (Academic Press, New York) Chapter 3.

Kingston, R.H. and S.F.Neustadter, 1955, "Calculation of the space charge, electric field and free carrier concentration at the surface of a semiconductor", J. Appl. Phys., 26, pp.718-720.

Kittel, C., 1976, "Introduction to Solid-State Physics", 5th. ed'n. (Wiley,New York), pp.191-192.

Klimpke, C.M.H. and P.T.Landsberg, 1979, "An improved analysis of the

n-type Schottky barrier solar cell", in 2nd. European Photovoltaic solar energy conference, 23-26th. April, Berlin (Reidel,Dordrecht,Netherlands) pp.678-681.

Klimpke, C.M.H. and P.T.Landsberg, 1981, "An improved analysis of the Schottky barrier solar cell", Solid-State Electronics, 24, pp.401-406.

Kobayashi, H., H.Iwamura, T.Saku and T.Otsuka, 1983, "Polarization-dependent gain-current relationship in GaAs-AlGaAs multi-quantum-well laser diodes", Electron. Lett., 19, pp.166-168.

Kreider, D.L., R.G.Kuller, D.R.Ostberg and F.W.Perkins, 1966, "An introduction to linear analysis" (Addison Wesley Publ. Co. Inc., Reading, Mass.).

Landsberg, P.T., 1956, "Defects with several trapping levels in semiconductors", Proc. Phys. Soc., B69, pp.1056-1059.

Landsberg, P.T., 1957, "A contribution to the recombination statistics of excess carriers in semiconductors", Proc. Phys. Soc., B70, pp.282-296.

Landsberg, P.T., 1960, "Solid-State Physics in electronics and telecommunications" (Academic Press, London) Vol. 1, pp.436-455.

Landsberg, P.T., ed., 1969, "Solid-State Theory: Methods and Applications", (Wiley Interscience, London), pp.264-270.

Landsberg, P.T., 1978, "Thermodynamics and Statistical Mechanics", (Oxford University Press, Oxford).

Landsberg, P.T., and C.M.H.Klimpke, 1980, "Surface recombination effects in an improved theory of a p-type MIS solar cell", Solid-State Electron., 23, pp.1139-1145.

Landsberg, P.T., 1982a, "Some general recombination statistics for semiconductor surfaces ", IEEE Trans. on Electron devices, ED-29, pp. 1284-1286.

Landsberg, P.T., 1982b, "Semiconductor Statistics", in "Handbook of semiconductors", Vol. 1, ed. W.Paul (North-Holland, Amsterdam) pp.359-449.

Lane, C.H., 1968, "Stress at the Si-SiO_2 interface and its relationship to the interface states", IEEE Trans. on Electron Devices, ED-15, pp.998 -1003.

Lasher, G., and F.Stern, 1964, "Spontaneous and stimulated recombination radiation in semiconductors", Phys. Rev., 133A, pp.553-563.

Lennox, S.C., and M. Chadwick, 1970, "Mathematics for engineers and applied scientists" (Heinemann, London).

Lineberger, W.C., 1976, "Atomic electron affinities", IEEE Trans. on Nuclear Science, NS-23, pp.934-935.

Look, D.C., 1981, "Statistics of multicharge centres in semiconductors: Applications", Phys. Rev., B24, pp.5852-5862.

Ma, Y.Y., and R.H.Bube, 1977, "Properties of CdS films prepared by spray pyrolysis", J. Electrochem. Soc., 124, pp.1430-1435.

Mallinson, J.R., and P.T.Landsberg, 1977, "Meteorological effects on solar cells", Proc. Roy. Soc. Lond., A355, pp.115-130.

Marinelli, F., 1965, "Approximate calculation of the spectral function for the stimulated recombination radiation in semiconductors", Solid-State Electronics, 8, pp.939-942.

Martin, W.C., 1959, "Atomic energy levels and spectra of neutral and singly ionized phosphorus (PI and PII)", J. Opt. Soc. Am., 49, pp.1071-1085.

NASA, 1971, "Solar electromagnetic radiation", NASA Bull. SP-8005, revised May 1971 and also in M.P.Thekaekara, Solar Energy, 14, p.109, 1973.

Neugroschel, A., and J.A.Mazer, 1982, "Effects of grain boundaries on the current-voltage characteristics of polycrystalline silicon solar cells", IEEE Trans. on Electron Devices, ED-29, pp.225-236.

Nicollian, E.H., 1977, "Electrical properties of the Si-SiO_2 interface and its influence on device performance and stability", J. Vac. Sci. Tech., 14, pp.1112-1121.

Nimtz, G., 1980, "Recombination in narrow-gap semiconductors", Phys. Reports, 63, pp.265-300.

Orton, J.W., and M.J.Powell, 1980, "The Hall effect in polycrystalline and powdered semiconductors", Rep. Prog. in Phys., 43, pp.1263-1307.

Panayotatos, P., and H.C.Card, 1980, "Recombination velocity at grain boundaries in polycrystalline silicon under illumination", Electron Device Letters, EDL-1, pp.263-266.

Pilkuhn, M.H., 1968, "The injection laser", Phys. Stat.-Sol., 25, pp.9-62.

Pimpale, A., and P.T.Landsberg, 1982, "Extrema of majority and minority carrier quasi-Fermi levels in p-n junction solar cells", in Proc. of 4th. European Photovoltaic Solar Energy Conference, 10-12th. May, Stresa, Italy (Reidel, Dordrecht, Netherlands), pp.516-521.

Robbins, D.J., and P.T.Landsberg, 1980, "Impact ionization and Auger recombination involving traps in semiconductors", J. Phys. C: Solid-State Physics, 13, pp.2425-2439.

Russer, P., 1980, "Evaluation of the stimulated emission rate of semiconductors with no k-selection rule", Wiss Ber AEG-Telefunken, 53, pp. 167-169.

Sah, C.T., 1976, "Origin of interface states and oxide charges generated by ionizing radiation", IEEE Trans. on Nucl. Sci., NS-23, pp. 1563-1568.

Sah, C.T., and W. Shockley, 1958, "Electron-hole recombination statistics in semiconductors through flaws with many charge conditions", Phys. Rev., 109, pp.1103-1115.

Schiff, L.I., 1955, "Quantum Mechanics", 3rd. ed'n. (McGraw-Hill, Kogakusha, Tokyo), pp.37-44.

Schmid, W., and J.Reiner, 1982, "Minority carrier lifetime in gold-diffused silicon at high carrier concentrations", J. Appl. Phys., 53, pp. 6250-6252.

Seager, C.H., 1981, "Grain boundary recombination: Theory and experiment in silicon", J. Appl. Phys., 53, pp.3960-3968.

Seager, C.H., and T.G.Castner, 1978, "Zero-bias resistance of grain boundaries in neutron-transmutation-doped polycrystalline silicon", J. Appl. Phys., 49, pp.3879-3889.

Seager, C.H., D.S.Ginley and J.D.Zook, 1980, "Improvement of polycrystalline silicon solar cells with grain-boundary hydrogenation techniques", Appl. Phys. Lett., 36, pp.831-833.

Seto, J.Y.W., 1975, "The electrical properties of polycrystalline silicon films", J. Appl. Phys., 46, pp.5247-5254.

Sharma, S.K., and V.K.Tewary, 1982, "Theory of open-circuit photovoltage decay in a finite base solar cell with drift field", J. Phys. D: Appl. Phys., 15, pp.1077-1087.

Shockley, W., 1950, "Electrons and holes in semiconductors" (Van Norstrand, Princeton, NJ).

Shockley,W., and W.T.Read Jr., 1952, "Statistics of the recombination of electrons and holes", Phys. Rev., 87, pp.835-842.

Shyu, C.M., and L.J.Cheng, 1982, "Electronic states associated with grain

boundaries in silicon", in "Grain boundaries in semiconductors", ed's G.E. Pike, C.H.Seager and H.J.Leamy (Elsevier Science, New York), pp.131-136.

Singh, R.J., and R.S.Srivastava, 1983, "Si-SiO_2 interface states based on optically activated conductance techniques", Solid-State Electronics, 26, pp.319-323.

Sneddon, I.N., 1972, "The use of integral transforms" (Tata-McGraw-Hill, New Delhi).

Spencer, M.G., W.J.Schaff and D.K.Wagner, 1983, "Electrical characterization of grain boundaries in GaAs", J. Appl. Phys., 54, pp.1429-1440.

Sreedhar, A.K., B.L.Sharma and R.K.Purohit, 1969, "Efficiency calculations of heterojunction solar energy converters", IEEE Trans. on Electron Devices, ED-16, pp.309-312.

Srivastava, P.C., J.C.Bourgoin, F.Rabajo and J.Mimila-Arroya, 1982, "Transient capacitance spectroscopy in polycrystalline silicon", J. Appl. Phys., 53, pp.8633-8638.

Sugimura, A., 1983, "Structure-dependent threshold current density in InGaAsP quantum well lasers", Appl. Phys. Lett., 42, pp.17-19.

Sze, S.M., 1969, "Physics of semiconductor devices", 2nd. ed'n. (Wiley Interscience, New York).

Taylor, W.E., N.H.Odell and H.Y.Fan, 1952, "Grain boundary effects in germanium", Phys. Rev., 88, pp.867-875.

Tyagi, M.S., J.F.Nijs and R.J.Van Overstraeten, 1982, "Effect of surface recombination on the transient decay of excess carriers produced by short wavelength laser pulses", Solid-State Electronics, 25, pp.411-415.

Unger, K., 1967, "Spontaneous and stimulated emission in junction lasers. I. Bands with parabolic state densities", Zeitschrift fur Physik, 207, pp.322-331.

Von Roos, O., 1978, "Recombination-generation currents in degenerate semiconductors", Solid-State Electronics, 21, pp.633-636.

Von Roos, 1981, "Analysis of the photovoltage decay (PVD) method for measuring minority carrier lifetimes in p-n junction solar cells", J. Appl. Phys., 52, pp.5833-5837.

de Vos, A., and H.J.Pauwels, 1977, "Collection efficiency of hetero-junction solar cells", IEEE Trans. on Electron Devices, ED-24, pp.388-391.

Watson, G.N., 1944, "A treatise on the theory of Bessel functions", 2nd. ed'n. (Cambridge University Press, London).

Werner, J., W.Jantsch, K.H.Froener and H.-J.Queisser, 1982, "Transport across grain boundaries in semiconductors", ed's H.J.Leamy, G.E.Pike and C.H.Seager (Elsevier Science, New York), pp.99-104.

Wight, D.R., I.D.Blenkinsop, W.Harding and B.Hamilton, 1981, "Diffusion limited lifetime in semiconductors", Phys. Rev., B23, pp.5495-5510.

Wu, C.H., and R.H.Bube, 1974, "Thermoelectric and photothermoelectric

effects in semiconductors: Cadmium sulfide films", J. Appl. Phys., 45, pp.648-660.

Yamada, M., 1983, "Transverse and longitudinal mode control in semiconductor injection lasers", IEEE J. Quantum Electronics, QE-19, pp. 1365-1380.

Young, R.T., R.F.Wood, J.Narayan, C.W.White and W.H.Christie, 1980, "Pulsed laser techniques for solar cell processing", IEEE Trans. on Electron Devices, ED-27, pp.807-815.

APPENDIX A

FINITE STURM-LIOUVILLE TRANSFORMS

The eigenfunctions of the Sturm-Liouville (SL) problem are utilised as an orthonormal basis to transform problems involving a self-adjoint operator, $\underline{L}$, in an inhomogeneous or time-dependent differential equation. One first obtains the eigenvalues, ξ_r, and eigenfunctions, ϕ_r, of the SL equation

$$\underline{L}\phi - \xi\phi = 0 \tag{A.1}$$

together with the boundary conditions

$$a_1\phi(0) + a_2\left(\frac{d\phi}{dx}\right)\Big|_{x=0} = 0 \tag{A.2}$$

and

$$b_1\phi(0) + b_2\left(\frac{d\phi}{dx}\right)\Big|_{x=0} = 0. \tag{A.3}$$

The self-adjoint operator, $\underline{L}$, is defined by

$$\underline{L} = \frac{1}{p(x)}\frac{d}{dx}\left(q(x)\frac{d}{dx}\right) + r(x).$$

The finite SL transform of a function, f, is given by the inner product of f with one of the eigenfunctions, ϕ_r, of the SL problem defined by equations (A.1,A.2,A.3) where a weight function, p(x), is used,

$$\mathcal{I}[f;\xi_r] \equiv \bar{f}_r = \int_0^d p(x)\phi_r(x)f(x)dx \ . \tag{A.4}$$

Applying this formula to the operator, $\underline{L}$, acting on f, one has

$$\mathcal{I}[\underline{L}f;\xi_r] = \int_0^d p(x)\phi_r(x)\left\{\frac{1}{p(x)}\frac{d}{dx}\left(q\frac{df}{dx}\right) + rf\right\}dx.$$

Integration by parts yields

$$J[\underline{L}f;\xi_r]=\int_0^d\left\{-\left[\frac{d}{dx}\phi_r(x)\right]q(x)\frac{df}{dx}+p(x)\phi_r(x)r(x)f\right\}dx+\left[\phi_r(x)q(x)f'\right]_0^d,$$

and after a second integration,

$$J[\underline{L}f;\xi_r] = \int\left\{\frac{d}{dx}\left[q(x)\frac{d}{dx}\phi_r(x)\right]\frac{1}{p(x)}+r(x)\phi_r(x)\right\}p(x)f(x)dx$$

$$+\left[\phi_r(x)q(x)f'(x)-\phi_r'(x)q(x)f(x)\right]_0^d$$

Therefore, using equation (A.1)

$$J[\underline{L}f;\xi_r] = \xi_r J[f;\xi_r]+q(d)[\phi_r(d)f'(d)-\phi_r'(d)f(d)]$$

$$-q(0)[\phi_r(0)f'(0)-\phi_r'(0)f(0)].$$

Providing $a_2\neq 0$,

$$\phi_r'(0)f(0)-\phi_r(0)f'(0) = a_2^{-1}\left[f(0)\{a_2\phi_r'(0)+a_1\phi_r(0)\}-\phi_r(0)\{a_1f(0)+a_2f'(0)\}\right]$$

using (A.2)one has

$$\phi_r'(0)f(0)-\phi_r(0)f'(0) = -a_2^{-1}\phi_r(0)\{a_1f(0)+a_2f'(0)\}$$

and similarly providing $b_2\neq 0$,

$$\phi_r'(d)f(d)-\phi_r(d)f'(d) = -b_2^{-1}\phi_r(d)\{b_1f(d)+b_2f'(d)\}.$$

On the other hand, if $a_2=0$,

$$\phi_r'(0)f(0)-\phi_r(0)f'(0) = -a_1^{-1}\{f'(0)a_1\phi_r(0)-\phi_r'(0)a_1f(0)\}$$

$$= a_1^{-1}\phi_r(0)\{a_1f(0)\},$$

and similarly if $b_2=0$,

$$\phi_r'(d)f(d)-\phi_r(d)f'(d) = b_1^{-1}\phi_r'(d)\{b_1 f(d)\}.$$

Finally, the SL transform of $\underline{L}f$ is given by

$$\mathcal{I}[\underline{L}f;\xi_r] = \xi_r \mathcal{I}[f;\xi_r] + b_2^{-1}\phi_r(d)q(d)\{b_1 f(d)+b_2 f(d)\}$$
$$- a_2^{-1}\phi_r(0)q(0)\{a_1 f(0)+a_2 f'(0)\} .$$

Taking into account the possibility of $a_2=0$ or $b_2=0$, parameters α_r and β_r are defined by

$$\alpha_r = \begin{cases} -a_2^{-1}\phi_r(0)q(0), & a_2\neq 0, \\ a_1^{-1}\phi_r'(0)q(0), & a_2=0, \end{cases} \tag{A.5}$$

and

$$\beta_r = \begin{cases} b_2^{-1}\phi_r(d)q(d), & b_2\neq 0; \\ -b_1^{-1}\phi_r'(d)q(d), & b_2\neq 0; \end{cases} \tag{A.6}$$

then one has

$$\mathcal{I}[\underline{L}f;\xi_r] = \xi_r \bar{f}_r + \alpha_r\{a_1 f(0)+a_2 f'(0)\} + \beta_r\{b_1 f(d)+b_2 f'(d)\}.$$

In the case of interest here, one takes the SL transform of the minority carrier density and so the formula above yields

$$\mathcal{I}[\underline{L}n(x,t);\xi_r] = \xi_r \bar{n}_r(t) + \alpha_r a_3(t) + \beta_r b_3(t) \tag{A.7}$$

using the boundary conditions of case 6 of Table 5.1. The function $n(x,t)$ is represented using the transform of n and the basis of SL eigenvectors,

$$n(x,t) = \sum_{r=1}^{\infty} \langle n(y,t).\phi_r(y)\rangle \phi_r(x)$$

where

$$\langle n(y,t).\phi_r(y)\rangle = \int_0^d p(y)n(y,t)\phi_r(y)dy$$

is the inner product of n with one of the eigenfunctions, ϕ_r. Thus, the inverse SL transform is given by

$$n(x,t) = \sum_{r=1}^{\infty} \bar{n}_r(t)\phi_r(x). \qquad (A.8)$$

Equations (A.5, A.6, A.7, A.8) are used to transform the inhomogeneous and time-dependent diffusion equation and to obtain its solution in chapters 7 and 8.

APPENDIX B

THE USE OF INHOMOGENEOUS BOUNDARY CONDITIONS WITH FINITE STURM-LIOUVILLE TRANSFORMS

The eigenfunctions ($\phi_r(x)$, r= 1, 2, 3, ...) are developed for the Sturm-Liouville (SL) problem of equation(7.2) of chapter 7 where linear homogeneous boundary conditions of the form

$$a_1\phi_r(0) + a_2\phi_r'(0) = 0 \qquad (B.1)$$

and

$$b_1\phi_r(d) + b_2\phi_r'(d) = 0 \qquad (B.2)$$

are utilised. The eigenfunctions form an orthonormal basis of infinite dimension for the Euclidean space of continuous functions on the interval $[0,d]$, thus the carrier concentration is represented (Kreider et al, 1966) by

$$n(x,t) = \sum_{r=1}^{\infty} \langle n(y,t).\phi_r(y)\rangle\phi_r(x). \qquad (B.3)$$

However, the boundary conditions of case 6 of Table 5.1 which are applied to the diffusion equation are not homogeneous. That the method may be used with inhomogeneous boundary conditions is not obvious at first sight. Equation (B.3) may also be applied to the derivative of the minority carrier density and this gives

$$n'(x,t) = \sum_{r=1}^{\infty} \langle n'(y,t).\phi_r(y)\rangle\phi_r(x),$$

hence one finds the boundary condition of Table 5.1, case 6 at x=0 yields

$$a_3(t)=a_1\sum_{r=1}^{\infty}\int_0^d n(y,t)\phi_r(y)p(y)dy\phi_r(0)+a_2\sum_{r=1}^{\infty}\int_0^d n'(y,t)\phi_r(y)p(y)dy\phi_r(0).$$

Defining a function h(x,t) by

$$h(x,t) = a_1 n(x,t) + a_2 n'(x,t)$$

one has

$$a_3(t) = h(0,t) = \sum_{r=1}^{\infty} \{\langle h(y,t).\phi_r(y)\rangle \phi_r(0)\}$$

or alternatively using the notation of the SL transform

$$a_3(t) = h(0,t) = \sum_{r=1}^{\infty} \bar{h}_r(t)\phi_r(0). \qquad (B.4)$$

Providing $\phi_r(0)$ is not zero for at least one value of r then one needs no restriction on $a_3(t)$ since the right hand side of (B.4) is not automatically zero. Similarly at x=d, one finds

$$b_3(t) = k(d,t) = \sum_{r=1}^{\infty} \bar{k}_r(t)\phi_r(d)$$

where

$$k(x,t) = b_1 n(x,t) + b_2 n'(x,t)$$

and again if $b_3(t) \neq 0$ then one must have $\phi_r(d) \neq 0$.

Note that the boundary condition at x=0 for case i of Table 5.1 sets

$$a_1 = 1,\ a_2 = 0,\ a_3 = n_0\{\exp(eV/k_BT)-1\},$$

and one may not use this boundary condition with the method of finite SL transforms. This is because $a_2=0$ and the homogeneous boundary condition (B.1) at x=0 implies $\phi_r(0)=0$ for all values of r and hence $a_3(t)=0$ by (B.4).

APPENDIX C

SOLUTIONS OF THE TRANSCENDENTAL EIGENVALUE EQUATION FOR THE STURM-LIOUVILLE PROBLEM

In this appendix, the nature of the real and complex roots of the transcendental equation (7.10) of chapter 7 will be examined. The transcendental equation in its general form,

$$\{a_1b_1-(a_1b_2+a_2b_1)f+a_2b_2(f^2-\mu_r^2)\}\sinh\mu_r d + (a_1b_2-a_2b_1)\mu_r\cosh\mu_r d = 0,$$

has the obvious root, $\mu_r=0$; however, equation (7.11) shows that the eigenfunction, $\phi_r(x)$, corresponding to the eigenvalue

$$\xi_r = -f^2D - 1/\tau$$

is everywhere zero. Thus, the solution $\mu_r=0$ of the transcendental equation is excluded from the set of parameters μ_r which lead to eigenfunctions.

The boundary conditions of case 4 of Table 5.1 have been widely used in the numerical examples of section 7.3, using them, equations (7.8) and (7.9) defining the constants A_r and B_r become

$$(f+\mu_r)A_r + B_r(f-\mu_r) = 0 \qquad (C.1)$$

and

$$\{f+ s/D +\mu_r\}A_r\exp(\mu_r d) + \{f+ s/D -\mu_r\}B_r\exp(-\mu_r d) = 0. \qquad (C.2)$$

Supposing $\mu_r=f$ is a solution of the transcendental equation in this case, as it is in equations (7.43),for s=0,and (7.44),for s=∞, then equations (C.1) and (C.2) yield

$$\mu_r=f \Rightarrow \{A_r=0,\ (s/D)B_r\exp(-fd)=0\}.$$

Thus for all positive surface recombination velocities the root $\mu_r=f$,

when it occurs, yields an eigenvector equal to zero. When the surface recombination velocity is zero, the roots $\mu_r = (f,-f)$ give the same eigenvalue

$$\xi_r = -1/\tau$$

and they give the same eigenvector as a consequence. One of the roots is excluded, $\mu_r = -f$ say, and the other root, $\mu_r = f$, is included in the set of parameters $\{\mu_r\}$ yielding eigenvalues $\{\xi_r\}$.

For non-zero back surface recombination velocities a further real root of the transcendental equation,

$$\{f(f+s/D)-\mu_r^2\}\tanh\mu_r d - s\mu_r/D = 0, \qquad (C.3)$$

formed from the equations (C.1) and (C.2) at the boundaries x=0 and x=d, exists as follows: From Figure C.1, if the gradient of the first term on the left hand side of equation (C.3) is larger than s/D at $\mu_r = 0$, the lines cross at a real root , μ_1. Since the curve is symmetric in negative μ_r the negative root $-\mu_1$ yields the same eigenvalue. That is, if one has

$$\{[f(f+s/D)-\mu_r^2]d\,\mathrm{sech}^2\mu_r d - 2\mu_r\tanh\mu_r d\}\Big|_{\mu_r=0} = f(f+s/D)d \geq s/D$$

then a real root exists. In the limit as s tends to infinity the requirement is that $fd \geq 1$, but the root $\mu_r = f$ is then given by (C.3) which as before gives an eigenvector of zero.

All other roots of the transcendental equation are imaginary, i.e. they are real roots of the following equation:

$$\{a_1b_1-(a_1b_2+a_2b_1)f+a_2b_2(f^2+\nu_r^2)\}\tan\nu_r d + (a_1b_2-a_2b_1)\nu_r = 0 \qquad (C.4)$$

where $i\nu_r \equiv \mu_r$.

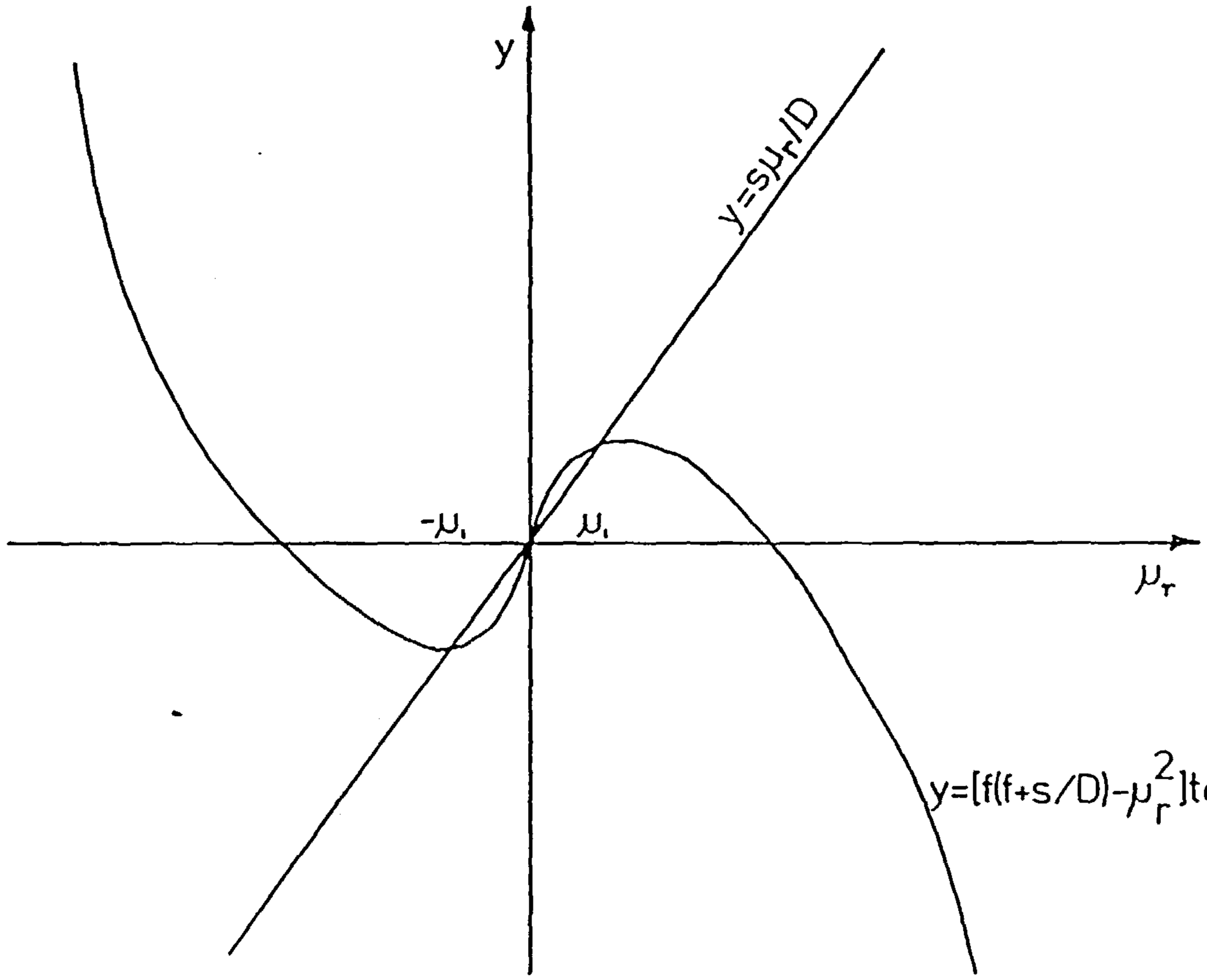

Figure C1 Graphical solution for real roots of the transcendental equation (C.3).

APPENDIX D

THE STURM-LIOUVILLE TRANSFORM OF THE STEADY-STATE EXCESS MINORITY CARRIER DENSITY

The Sturm-Liouville (SL) integral transform of the excess minority carrier density in the steady-state as defined by equation (5.41) is used in equation (7.29) to calculate the decay of the carrier concentration once the light source is switched off. The integral $\bar{n}_r(0)$ is given by

$$\bar{n}_r(0) = \int_0^d \frac{2A_r e^{fx} n(x)\{(a_1-a_2 f)\sinh\mu_r x - a_2\mu_r \cosh\mu_r x\}dx}{D\{a_1 - a_2(\mu_r+f)\}} \qquad (D.1)$$

where $n(x)$ is the steady-state carrier density (5.41) and A_r is given by equation (7.13). The most general form of $\bar{n}_r(0)$ to be used here is

$$\bar{n}_r(0) = \int_0^d \frac{2A_r e^{fx}\{(a_1-a_2 f)\sinh\mu_r x - a_2\mu_r \cosh\mu_r x\}}{D\{a_1 - a_2(\mu_r+f)\}} \times$$

$$\left[\frac{\{a_3+(a_1-a_2\alpha)N_1\}\{(b_1-b_2 f)\sinh\mu(d-x)+b_2\mu\cosh\mu(d-x)\}e^{-fx}}{\{a_1b_1-(a_1b_2+a_2b_1)f-a_2b_2/L^2\}\sinh\mu d+(a_1b_2-a_2b_1)\mu\cosh d} + \right.$$

$$\left. \frac{\{b_3+(b_1-b_2\alpha)N_1 e^{-\alpha d}\}e^{f(d-x)}\{(a_1-a_2 f)\sinh\mu x - a_2\mu\cosh\mu x\}}{\{a_1b_1-(a_1b_2+a_2b_1)f-a_2b_2/L^2\}\sinh\mu d+(a_1b_2-a_2b_1)\mu\cosh\mu d} - N_1 e^{-\alpha x}\right] dx.$$

The parameters a_3 and b_3 are of course constants in the steady-state. It is possible to define constants θ_1, θ_2, θ_3, and θ_4, which simplify the integral, i.e.

$$\theta_1 = \left[\frac{\{a_3 + N_1(a_1-a_2\alpha)\}(b_1-b_2 f)}{\{a_1b_1-(a_1b_2+a_2b_1)f-a_2b_2/L^2\}\sinh\mu d+(a_1b_2-a_2b_1)\mu\cosh\mu d}\right], \qquad (D.2)$$

$$\theta_2 = \left[\frac{\{a_3+N_1(a_1-a_2\alpha)\}b_2\mu}{\{a_1b_1-(a_1b_2+a_2b_1)f-a_2b_2/L^2\}\sinh\mu d+(a_1b_2-a_2b_1)\mu\cosh\mu d}\right], \qquad (D.3)$$

$$\theta_3 = \left[\frac{\{b_3+(b_1-b_2\alpha)N_1e^{-\alpha d}\}e^{fd}(a_1-a_2f)}{\{a_1b_1-(a_1b_2+a_2b_1)f-a_2b_2/L^2\}\sinh\mu d+(a_1b_2-a_2b_1)\mu\cosh\mu d}\right] \qquad (D.4)$$

and

$$\theta_4 = \left[\frac{\{b_3+(b_1-b_2\alpha)N_1e^{-\alpha d}\}e^{fd}(-a_2\mu)}{a_1b_1-(a_1b_2+a_2b_1)f-a_2b_2/L^2\ \sinh\mu d+(a_1b_2-a_2b_1)\mu\cosh\mu d}\right] . \qquad (D.5)$$

Hence, the integral becomes

$$\bar{n}_r(0) = \int_0^d \{c_r\cosh\mu_r x+d_r\sinh\mu_r x\}\left[\theta_1\sinh\mu(d-x)+\theta_2\cosh\mu(d-x)+\right.$$

$$\left.\theta_3\sinh\mu x+\theta_4\cosh\mu x-N_1e^{(f-\alpha)x}\right]dx \qquad (D.6)$$

where also

$$c_r = 2A_ra_2\mu_r/D\{a_2(\mu_r+f)-a_1\}, \qquad (D.7)$$

and

$$d_r = 2A_r(a_1-a_2f)/D\{a_1-a_2(\mu_r+f)\}. \qquad (D.8)$$

Multiplying out the factors contained within the integral (D.6) and performing the separate integrals one has

$$\bar{n}_r(0) = c_r\theta_1H_1 + c_r\theta_2H_2 + c_r\theta_3H_3 + c_r\theta_4H_4 - c_rN_1H_5 +$$

$$d_r\theta_1H_6 + d_r\theta_2H_7 + d_r\theta_3H_8 + d_r\theta_4H_9 - d_rN_1H_{10}, \qquad (D.9)$$

where the H_i {i= 1, 2, 3,...,10} are the simple integrals of the product of two hyperbolic functions and are performed by repeated integration by parts, for example

$$H_1 = \int_0^d \cosh\mu_r x\sinh\mu(d-x)dx = (\mu/\mu_r)\int_0^d \sinh\mu_r x\cosh\mu(d-x)dx.$$

A second integration by parts yields

$$H_1 = (\mu/\mu_r^2)\left[\cosh\mu_r x\cosh\mu(d-x)\right]_0^d + (\mu/\mu_r)^2 H_1 ,$$

and finally,

$$H_1 = \frac{1}{\mu_r^2-\mu^2}\left[\mu\cosh\mu_r d - \mu\cosh\mu d\right] .$$

Likewise, H_2 to H_{10} are calculated by repeated integration by parts or are obtained from standard integral tables (Gradshteyn and Ryzhik, 1980). The results are collected in Table D.1.

From the integrals H_1 to H_{10}, the parameters θ_1 to θ_4 and c_r and d_r, the transform of the steady-state carrier density is obtained using equation (D.9). The two factors $c_r\theta_1 H_1$ and $d_r\theta_1 H_6$ combine to give the following result:

$$\frac{2A_r\theta_1\{\mu[(a_1-a_2f)\sinh\mu_r d-a_2\mu_r\cosh\mu_r d]-\mu_r[(a_1-a_2f)\sinh\mu d-a_2\mu\cosh\mu d]\}}{D(\mu_r^2-\mu^2)\{a_1-a_2(\mu_r+f)\}},$$

where equations (D.7), (D.8) and Table D.1 were used. Similarly addition of $c_r\theta_2 H_2$ to $d_r\theta_2 H_7$ yields,

$$\frac{2A_r\theta_2\{\mu_r[(a_1-a_2f)\cosh\mu_r d-a_2\mu_r\sinh\mu_r d]-\mu_r[(a_1-a_2f)\cosh\mu d-a_2\mu\sinh\mu d]\}}{D(\mu_r^2-\mu^2)\{a_1-a_2(\mu_r+f)\}},$$

Using the expressions (D.2) and (D.3) for θ_1 and θ_2, the two factors above are combined and one obtains

$$\left\{(b_1-b_2f)\mu[(a_1-a_2f)\sinh\mu_r d-a_2\mu_r\cosh\mu_r d]+b_2\mu_r\mu[(a_1-a_2f)\cosh\mu_r d-a_2\mu_r\sinh\mu_r d]\right.$$

$$\left.-b_2\mu_r\mu[(a_1-a_2f)\cosh\mu d-a_2\mu\sinh\mu d]-(b_1-b_2f)\mu_r[(a_1-a_2f)\sinh\mu d-a_2\mu\cosh\mu d]\right\}\times$$

$$\frac{2A_r\{N_1(a_1-a_2\alpha)+a_3\}}{D(\mu_r^2-\mu^2)\{a_1-a_2(\mu_r+f)\}[\{a_1b_1-(a_1b_2+a_2b_1)f-a_2b_2/L^2\}\sinh\mu d+(a_1b_2-a_2b_1)\mu\cosh\mu d]} .$$

The first two square bracketed terms in the above expression combine to give an expression which is the same as the left hand side of the transcendental equation (7.10) and that is equal to zero. The third and fourth square bracketed factors combine to yield an expression the same as the square bracketed term in the denominator. Thus, the above expression simplifies to

$$(c_rH_1+d_rH_6)\theta_1+(c_rH_2+d_rH_7)\theta_2 = \frac{2A_r\mu_r\{a_3+(a_1-a_2\alpha)N_1\}}{D(\mu_r^2-\mu^2)\{a_1-a_2(\mu_r+f)\}} \qquad (D.10)$$

The next four terms of (D.9) are

$$c_r(\theta_3H_3+\theta_4H_4) + d_r(\theta_3H_8+\theta_4H_9)$$

using Table D.1 for H_3, H_4, H_8 and H_9, together with (D.4), (D.5), (D.7) and (D.8) for θ_3, θ_4, c_r and d_r the above terms yield

$$\frac{\{b_3+(b_1-b_2\alpha)N_1e^{-\alpha d}\}e^{fd}2A_r(\mu_r^2-\mu^2)^{-1}}{D\{a_1-a_2(\mu_r+f)\}[\{a_1b_1-(a_1b_2+a_2b_1)f-a_2b_2/L^2\}\sinh\mu d+(a_1b_2-a_2b_1)\mu\cosh\mu d]} \times$$

$$[\sinh\mu_r d\{(a_1-a_2f)a_2(\mu^2-\mu_r^2)\sinh\mu d+a_2^2\mu_r^2\mu\cosh\mu d-\mu(a_1-a_2f)^2\cosh\mu d +$$

$$\mu_r\cosh\mu_r d\{(a_1-a_2f)^2\sinh\mu d-a_2^2\mu^2\sinh\mu d\}] \ . \qquad (D.11)$$

Here, the contents of the square brackets have been rearranged into multiples of $\cosh\mu_r d$ and $\sinh\mu_r d$. One adds the left hand side of the transcendental equation (7.10), multiplied by

$$-(1/b_2)\{(a_1-a_2f)\sinh\mu d-a_2\mu\cosh\mu d\},$$

to the square bracketed term. This is possible because the right hand side of (7.10) is zero, and the result of the addition inside the square bracket is

$$[\sinh\mu_r d\{\mu\cosh\mu d(a_1a_2b_1/b_2-a_1^2-a_1a_2f-a_2^2b_1f/b_2)-(a_1-a_2f)/b_2\sinh\mu d \times$$

$$(a_1b_1-(a_1b_2+a_2b_1)f+a_2b_2(f^2-\mu^2))\}+\mu_r/b_2\cosh\mu_r d\{a_2\mu\cosh\mu d(a_1b_2-a_2b_1)+$$

$$\sinh\mu d(a_1^2b_2-2a_1a_2b_2f+a_2^2b_2f-a_2b_2\mu^2-a_1^2b_2+a_1a_2b_2f+a_1b_1a_2-a_2^2b_1f)\}] \ .$$

Addition of the $\sinh\mu d$ and $\cosh\mu d$ terms above yields the square bracket term of the denominator of (D.11) and so (D.11) becomes

$$\frac{2A_re^{fd}\{b_3+(b_1-b_2\alpha)N_1e^{-\alpha d}\}\{(a_1-a_2f)\sinh\mu_r d-a_2\mu_r\cosh\mu_r d\}}{Db_2(\mu^2-\mu_r^2)\{a_1-a_2(\mu_r+f)\}} \ . \qquad (D.12)$$

The last two terms of (D.9) are $-N_1c_rH_5$ and $-N_1d_rH_{10}$ and equation (D.7) and (D.8) with H_5 and H_{10} from Table D.1 gives

$$\frac{\{(f-\alpha)^2-\mu_r^2\}^{-1}A_r}{D\{a_1-a_2(\mu_r+f)\}}\Big[\Big[(f-\alpha)\{(a_1-a_2f)\sinh\mu_r d-a_2\mu_r\cosh\mu_r d\}+\{a_2\mu_r\sinh\mu_r d$$

$$-(a_1-a_2f)\cosh\mu_r d\}\mu_r\Big]e^{(f-\alpha)d}+\mu_r(a_1-a_2\alpha)\Big](-2N_1)$$

Expanding the square bracket term only, one obtains

$$\{(a_1-a_2f)(f-\alpha)\sinh\mu_r d+a_2\mu_r^2\sinh\mu_r d+(a_2\mu_r\mu-a_1\mu_r)\cosh\mu_r d\} \ ,$$

adding to it the the transcendental equation divided by b_2, i.e.

$$\{a_1b_1/b_2-(a_1+a_2b_1/b_2)f-a_2(\mu_r^2-f^2)\}\sinh\mu_r d+(a_1-a_2b_1/b_2)\mu_r\cosh\mu_r d,$$

reduces the square bracket term to

$$(b_1/b_2-\alpha)\{(a_1-a_2f)\sinh\mu_r d-a_2\mu_r\cosh\mu_r d\}.$$

The last two terms of (D.9) are therefore given by

$$-2A_rN_1\left[\frac{e^{(f-\alpha)d}(b_1/b_2-\alpha)\{(a_1-a_2f)\sinh\mu_r d-a_2\mu_r\cosh\mu_r d\}+\mu_r(a_1-a_2\alpha)}{D\ \{a_1-a_2(\mu_r+f)\}\{(f-\alpha)^2-\mu_r^2\}}\right] \qquad (D.13)$$

Combining the results (D.10), (D.12) and (D.13), the transform of the steady-state excess carrier density is

$$\bar{n}_r(0)=\frac{2A_r}{Db_2}\left[\frac{\{a_3+(a_1-a_2\alpha)N_1\}b_2\mu_r+\{b_3+(b_1-b_2\alpha)N_1e^{-\alpha d}\}e^{fd}\{(a_1-a_2f)\sinh\mu_r d-a_2\mu_r\cosh\mu_r d\}}{\{a_1-a_2(\mu_r+f)\}(\mu^2-\mu_r^2)}\right.$$

$$\left.-\frac{(a_1-a_2\alpha)N_1b_2\mu_r+(b_1-b_2\alpha)N_1e^{(f-\alpha)d}\{(a_1-a_2f)\sinh\mu_r d-a_2\mu_r\cosh\mu_r d\}}{\{a_1-a_2(\mu_r+f)\}\{(f-\alpha)^2-\mu_r^2\}}\right]. \quad (D.14)$$

In the method of open-circuit voltage decay, there is no current flow across the junction, x=0, or across the back surface, x=d, i.e.

$$a_3 = b_3 = 0,$$

and therefore the transform of the initial (steady-state) excess carrier density becomes

$$\bar{n}_r(0) = \frac{2A_rN_1}{D\{a_1-a_2(\mu_r+f)\}}\left[\frac{1}{(\mu^2-\mu_r^2)}-\frac{1}{(\mu^2-\mu_r^2)}\right] \times$$

$$[(a_1-a_2\alpha)\mu_r+(b_1/b_2-\alpha)e^{(f-\alpha)d}\{(a_1-a_2f)\sinh\mu_r d-a_2\mu_r\cosh\mu_r d\}]. \quad (D.15)$$

the expression (D.14) is used in section 7.2(a) of chapter 7 as the transform of the steady-state carrier density which applies until time, t=0, when the light source is switched off. The integrals H_5 and H_{10} of Table D.1 are used also in chapter 7, section 7.2(b) to obtain the transform of the photogeneration rate after a short light pulse at time, t=0.

Table D.1 Integrals of hyperbolic functions and exponentials used in the Sturm-Liouville transform of the steady-state carrier density.

Integral	Result
$H_1 = \int_0^d \cosh\mu_r x \sinh\mu(d-x)dx$	$= (\mu_r^2-\mu^2)^{-1}\mu[\cosh\mu_r d-\cosh\mu d]$
$H_2 = \int_0^d \cosh\mu_r x \cosh\mu(d-x)dx$	$= (\mu_r^2-\mu^2)^{-1}[\mu_r \sinh\mu_r d-\mu\sinh\mu d]$
$H_3 = \int_0^d \cosh\mu_r x \sinh\mu x dx$	$= (\mu_r^2-\mu^2)^{-1}[\mu_r \sinh\mu_r d\sinh\mu d+\mu(1-\cosh\mu_r d\cosh\mu d)]$
$H_4 = \int_0^d \cosh\mu_r x \cosh\mu x dx$	$= (\mu_r^2-\mu^2)^{-1}[\mu_r \sinh\mu_r d\cosh\mu d-\mu\cosh\mu_r d\sinh\mu d]$
$H_5 = \int_0^d e^{(f-\alpha)x}\cosh\mu_r x dx$	$= \dfrac{(f-\alpha)(e^{(f-\alpha)d}\cosh\mu_r d-1)-\mu_r e^{(f-\alpha)d}\sinh\mu_r d}{\{(f-\alpha)^2-\mu_r^2\}}$
$H_6 = \int_0^d \sinh\mu_r x \sinh\mu(d-x)dx$	$= (\mu_r^2-\mu^2)^{-1}[\mu\sinh\mu_r d-\mu_r \sinh\mu d]$
$H_7 = \int_0^d \sinh\mu_r x \cosh\mu(d-x)dx$	$= (\mu_r^2-\mu^2)^{-1}\mu_r[\cosh\mu_r d-\cosh\mu d]$
$H_8 = \int_0^d \sinh\mu_r x \sinh\mu x dx$	$= (\mu_r^2-\mu^2)^{-1}[\mu_r \cosh\mu_r d\sinh\mu d-\mu\sinh\mu_r d\cosh\mu d]$
$H_9 = \int_0^d \sinh\mu_r x \cosh\mu x dx$	$= (\mu_r^2-\mu^2)^{-1}[\mu_r(\cosh\mu_r d\cosh\mu d-1)-\mu\sinh\mu_r d\sinh\mu d]$
$H_{10} = \int_0^d \sinh\mu_r x e^{(f-\alpha)x}dx$	$= \dfrac{e^{(f-\alpha)d}\{(f-\alpha)\sinh\mu_r d-\mu_r\cosh\mu_r d\}+\mu_r}{\{(f-\alpha)^2-\mu_r^2\}}$